The application of click reactions in the synthesis of modified oligonucleotides

A thesis submitted to the
Board of the Faculty of Physical Sciences
in partial fulfilment of the requirements for the degree of

Doctor of Philosophy

Jieqiong Qiu

St Edmund Hall, University of Oxford, Michaelmas Term 2015

Supervisor: Professor Tom Brown

Declaration

I, Jieqiong Qiu, declare that the thesis entitled ‘The application of click reactions in the synthesis of modified oligonucleotides’ and the work presented in this thesis was carried out under the supervision of Prof. Tom Brown. All the work presented is my own, except where otherwise stated, and has not been submitted in full or in part for any other degree at this or any other university.

Jieqiong Qiu

November 2015

Genius only means hard-working all one’s life.

Dmitri Mendeleev (1834–1907), Russian chemist

Abstract

'Click' chemistry has been widely applied in nucleic acid studies, the most common reactions being the copper-catalysed and strain-promoted alkyne-azide cycloadditions (CuAAC and SPAAC respectively). This thesis describes the use of these complementary reactions in the synthesis of modified oligonucleotides. Both reactions are used to ligate alkyne- and azide-modified oligonucleotides together to form larger strands on the solid phase. The CuAAC reaction can produce ODNs containing a biocompatible triazole linkage that mimics the DNA phosphodiester linkage, however its use *in vivo* is limited by the cytotoxicity of Cu(I). In contrast, the SPAAC reaction does not require catalysis, but more chemically complex cyclooctynes are needed. Multiple sequential ligations by the SPAAC reaction can be carried out on solid-phase without a template oligonucleotide, allowing the efficient synthesis of oligonucleotides up to *ca.* 190 bases in length, and greatly simplifying purification. Click chemistry was used to synthesize novel nucleic acid fluorescent probes. Using the SPAAC reaction, fluorescently labelled oligonucleotides were ligated to obtain permanently cross-linked stable duplexes, which were evaluated for their FRET properties. A new nucleic acid probe system was developed containing thiazole orange (TO) or benzothiazole orange (BO), and a second fluorophore was directly attached to the same nucleobase by CuAAC. The thermal stability and steady state fluorescence of the oligonucleotides containing these modifications were studied. These probes can be multiplexed for detection of point mutations in DNA. This was exemplified by targeting R516G mutation in the CFTR gene by simultaneously monitoring two channels in real-time PCR.

Contents

Acknowledgements

I would like to firstly thank my supervisor, Professor Tom Brown, for giving me this great opportunity to work on such a varied and interesting research project. I would also like to thank him for all his help, knowledge, patience and encouragement throughout my PhD, it would have been impossible without him.

Secondly, I would like to thank Dr. Afaf El-Sagheer and all at ATDBio Ltd. for their help in synthesising all my many oligonucleotides. I would also like to thank the NMR and mass spectrometry staff for all their advice and help over the years.

I express my gratitude to past and present members of the Brown research group that have created a pleasurable working environment; I have enjoyed working with you all, especially all the tea breaks. I would like to say a special thanks to Dr. Adam Wilson, Dr. Arun Shivalingam, Dr. Joanna McGouran and Dr. Sara DeOrnellas for the extensive knowledge and expertise they have shared with me. I would also like to say a massive thank you to Dr. Afaf El-Sagheer for helping me so much during my PhD, with her expertise and scope of ideas for my research during the good and bad. Thank you to those who have proof read this thesis.

Thank you to all my friends for supporting me throughout my PhD. In particular, Xiaomei Ren, Rachel Gao, Meng Han, Agnes Tyburn, Anna Dysko and Pietro Marafini, thank you for being there for a chat whenever I needed it, through the good and the bad, I could not have gone through it without you all.

Finally, I would like to say the biggest thank you of all to my mum and dad, for their unconditional love, support, patience, motivation and encouragement throughout my PhD. I would also like to thank all my family, particular my cousins Qiqing Qiu and Lufang Qiu.

List of abbreviations

A	adenine/adenosine
AAC	copper-free Huisgen [3+2] azide-alkyne reaction
app.	apparent
APS	ammonium persulfate
aq.	aqueous
BARAC	biarylazacyclooctynone
BCN	bicyclo[6.1.0]nonyne
BO	benzothiazole orange
bp	base pair
br	broad (IR/NMR)
C	cytosine / cytidine
calc.	calculated
CFTR	cystic fibrosis transmembrane conductance regulator
COSY	^{1}H-^{1}H correlation spectroscopy
CPG	controlled pore glass (solid support)
C_T	cycle threshold (number of cycles required to generate fluorescent signal
CuAAC	copper-catalysed azide-alkyne 1,3-dipolar cycloaddition
Cy3	trimethine cyanine dye
Cy5	pentamethine cyanine dye
δ	chemical shift in parts per million
d	doublet
dd	double doublet
ds	double-stranded

dT	2′-deoxythymidine
DCA	dichloroacetic acid
DEPT	distortionless enhancement through polarization transfer
DIBAC	aza-dibenzocyclooctyne
DIBO	4-dibenzocyclooctynol
DIC	diisopropylcarbodiimide
DIFBO	difluorobenzocyclooctyne
DIFO	difluorinated cyclooctyne
DIMAC	dimethoxy azacyclooctyne
DIPEA	diisopropylethylamine, Hünig's base
DMAP	4-dimethylamino pyridine
DMF	*N*,*N*′-dimethylformamide
DMSO	dimethyl sulfoxide
DMT	4,4′-dimethoxytrityl
DMTrCl	4,4′-dimethoxytrityl chloride
DNA	deoxyribonucleic acid
dNTP	deoxyribonucleotide triphosphate
EDC	*N*-(3-dimethylaminopropyl)-*N*′-ethylcarbodiimide hydrochloride
EDTA	ethylenediamine tetra acetate/acetic acid
EI	electron ionisation
em	emission
eq.	equivalent
ESI	electrospray ionisation
ex	excitation
FAM	carboxyfluorescein

Fmoc	fluorenylmethyloxycarbonyl (protecting groups of DNA)
FRET	fluorescence resonance energy transfer
G	guanine / guanosine
HEX	6-hexachloro-fluorescein
HMBC	heteromultinuclear bond correlation, long-range $^{1}H–^{13}C$ COSY
HMQC	heteromultinuclear quantum correlation, $^{1}H–^{13}C$ COSY
HOBt	hydroxybenzotriazole
HPLC	high-performance liquid chromatography
HRMS	high resolution mass spectrometry
Hz	hertz
IC	internal conversion
ISC	inter-system crossing
J	coupling constant (Hz)
k	reaction rate constant
kcal mol^{-1}	kilocalorie per mole
LCAA	long chain alkylamine
LRMS	low resolution mass spectrometry
M	molar concentration
m	multiplet (NMR)
MHz	megahertz
mM	millimolar concentration
MOFO	monofluorinated cyclooctyne
MBs	molecular beacons
MPPS	macroporous polystyrene (solid support)
MS	mass spectrometry

M^{-1} s^{-1}	unit of a second order rate constant
MT	mutant type (DNA sequence)
m/*z*	mass to charge ratio
NAP	nucleic acid purification
nmol	nanomole
NHS	*N*-hydroxysuccinimide
μM	micromolar concentration
NMR	nuclear magnetic resonance
OCT	cyclooctyne
OD	optical density
ODN	oligonucleotide
PAGE	polyacrylamide gel electrophoresis
PCR	polymerase chain reaction
PEG	polyethylene glycol
pH	potential of hydrogen (negative logarithm of the positive hydrogen ion concentration)
PNA	phosphomolybdic acid
ppm	parts per million
q	quartet (NMR)
R_f	retention factor
RNA	ribonucleic acid
ROX	6-carboxy-X-rhodamine
RT	room temperature
s	singlet (NMR)
SNPs	single nucleotide polymorphisms

SPAAC	ring-strain promoted [3+2] alkyne-azide cycloaddition
SPNOC	strain-promotion nitrile oxide cycloaddition
ss	single-stranded
STRs	short tandem repeats
T	thymine / thymidine
t	triplet (NMR)
TAMRA	carboxytetramethylrhodamine
TBE	tris/borate/EDTA buffer
TBTA	tris(benzyltriazolylmethyl)amine
TCA	trichloroacetic acid
TEA	triethylamine (Et_3N)
TEAA	triethylammonium acetate (HPLC buffer)
TEAB	triethylammonium bicarbonate (HPLC buffer)
TEMED	*N*,*N*,*N*′,*N*′-tetramethylethylene diamine
TFA	trifluoroacetic (protecting groups of DNA)
THPTA	tris(3-hydroxypropyltriazolylmethyl)amine
THF	tetrahydrofuran
TLC	thin layer chromatography
T_m	DNA melting temperature
TO	thiazole orange
tz	triazole linkage
U	uracil
UV	ultra-violet radiation of the electromagnetic spectrum
WT	wild-type (DNA sequence)

CHAPTER 1

Introduction

Chapter 1 - Introduction

1.1 Nucleic acids

1.1.1 Primary structure of nucleic acids

DNA, or 2′-deoxyribonucleic acid, carries the biological instructions that make each species unique. It is a large polymeric molecule composed of many subunits, each of which contains a phosphate, pentose sugar and heterocyclic base. These subunits are referred to as nucleotides and possess one of four bases – purines adenine (A) and guanine (G), and pyrimidines cytosine (C) and thymine (T) (Figure 1.1).

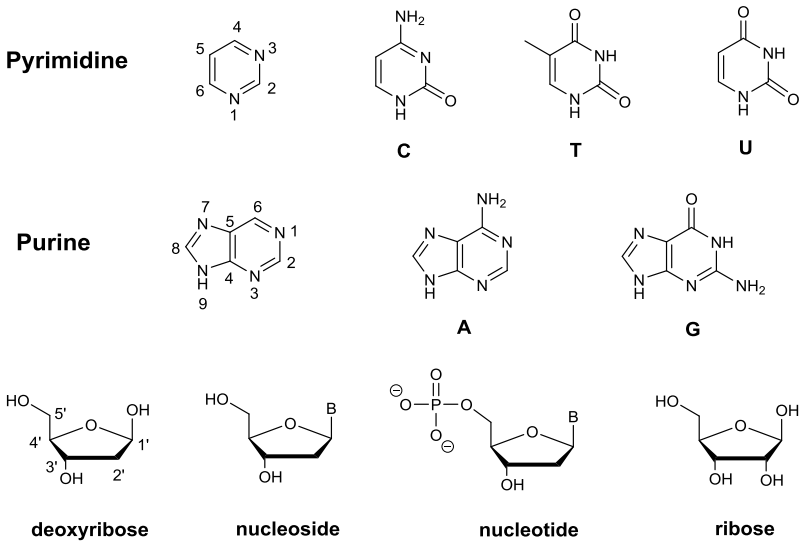

Figure 1.1. Structures of the pyrimidine and purine heterocyclic bases present in nucleic acids, and a nucleoside and nucleotide, where B is any of the heterocyclic bases. Pyrimidine: cytosine (C), thymine (T), uracil (U); purine: adenine (A), guanine (G).

The heterocyclic base is attached to the 1′ carbon atom of the sugar *via* the nucleobase N(1) atom for pyrimidines and N(9) for purines. The pentose sugar in DNA is 2′-deoxy-D-ribose, while in RNA – a "temporary copy" of DNA – the sugar is D-ribose. The purines A and G and the pyrimidine C are found in DNA and RNA, while thymine is replaced by uracil in RNA. If the nucleotide lacks a phosphate group it is referred to as a nucleoside (Figure 1.1).

The rotation around the glycosidic bond allows the nucleoside to have an essentially infinite number of possible conformations, with *anti* and *syn* being at the extremes (Figure 1.2). The *anti*-conformation is predominant in natural double stranded DNA for base pairing and steric reasons.[1]

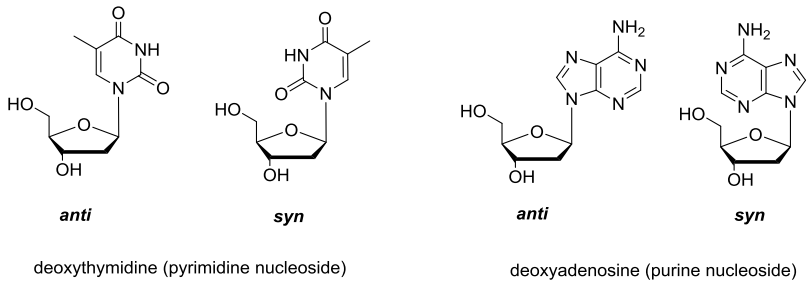

Figure 1.2. *anti* and *syn* conformations of a pyrimidine nucleoside (T) and a purine nucleoside (A).

The primary structure of DNA is the specific sequence of nucleotides found in a single strand of nucleic acid (Figure 1.3). By convention this is written from the 5′-hydroxyl (primary OH) side to the 3′-hydroxyl (secondary OH) group.

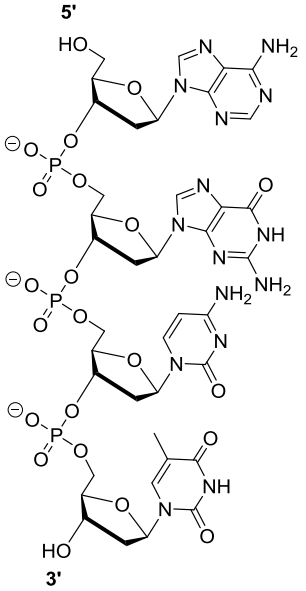

Figure 1.3. Primary structure of DNA. The structure shown here is an example of oligonucleotide 5′-AGCT-3′.

1.1.2 Secondary structure of nucleic acids

Two strands of nucleic acids can combine to form a DNA double helix – a concept that originated from a combination of ideas and discoveries by Erwin Chargaff,[2,3] Rosalind Franklin,[4,5] James Watson and Francis Crick.[6] The B-DNA helical secondary structure shown in Figure 1.4 is the canonical form adopted by DNA. The phosphodiester groups run down the backbone of the helix and are anionic at neutral pH, enabling the DNA helix to exist in a stable and soluble form under physiological conditions. The nucleobases are located in the centre of the double helix and form a hydrophobic environment. A interacts with T *via* two hydrogen bonds and C interacts with G *via* three hydrogen bonds (Figure 1.4). As a result, the ratio of purines to pyrimidines is equal in duplex DNA.[2,3] The stability of this secondary structure is determined by base pairing between complementary strands and base stacking between adjacent bases.[7] This structure can be disrupted under alkaline conditions or high temperature, resulting in denaturation to single-stranded nucleic

acids.[8] DNA and RNA are chemically unstable under acidic conditions and RNA is chemically unstable under alkaline conditions.

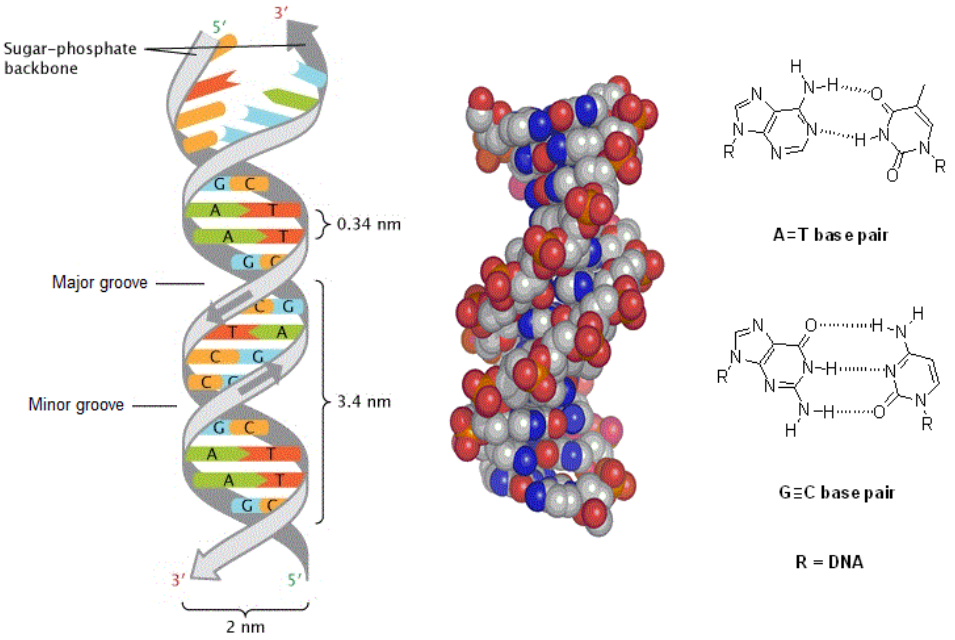

Figure 1.4. The schematic double helix structure of DNA, and the three-dimensional as determined by X-ray crystallography (PDB: 1BNA).[9] The B-DNA helix has a diameter of around 20 Å (2 nm), and a helical turn of 34 Å (3.4 nm).[10]

DNA can also adopt an A-form secondary structure. This form is favoured at low humidity, and is wide and compact, with a narrow and deep major groove, and a wide and shallow minor groove. B-DNA is favoured at high humidity; it is slimmer and more elongated because the bases are perpendicular and closer to the helix axis; it has a wide major groove and a narrow minor groove. Both grooves have approximately equal depth in the B-DNA duplex. It is worth mentioning that although the B-form is the canonical secondary structure of DNA, the energetic barrier to the A-form is sufficiently low that it can also be readily formed.[11]

1.2 Solid phase oligonucleotide synthesis

Nucleic acids are enzymatically produced *in vivo*. However, to facilitate their study *in vitro*, methods have been sought to prepare them on a large scale by chemical synthesis. To this end, the solid-phase approach has been developed. The solid-phase technique has a large number of advantages over conventional chemical synthesis for oligomeric molecules in terms of efficiency. Solid phase synthesis overcomes the technical difficulties associated with poor solubility and complicated purification encountered in solution phase synthesis, as the desired product is linked to the solid support by covalent bonds, facilitating removal of excess reactants and by-products by filtration.[12] In addition, the product is synthesised step-by-step, and is controlled automatically and precisely by computer.[13] After the synthesis is complete, the product can be cleaved from the solid support. This revolutionary methodology was originally reported by Merrifield in 1963 for solid phase peptide synthesis.[14-16] The scope of solid phase synthesis was then expanded and applied for the efficient synthesis of oligonucleotides.[17,18]

The original solid support reported by Merrifield[13] and optimized by Letsinger *et al.*[19] was an organic polymer. Later, the inorganic matrix controlled pore glass (CPG) and silica gel were used by Caruthers *et al.*[20] to solve the resin swelling problem caused by the polymer support, which may cause a physical barrier to reaction.[21,22] CPG and macroporous polystyrene (MPPS) supports have been found to be ideal for oligonucleotide synthesis.[23] They are rigid and display negligible swelling in common organic solvents. Reagents and solvents can be rapidly removed by solvent washes after the various synthesis steps. CPG beads are defined by the pore sizes (e.g. 500, 1000, 1500, 2000, or 3000 Å resin), with the largest 3000 Å resin typically used for preparation of 100–200 nucleotide long oligonucleotides. Conversely, highly cross-linked polystyrene beads (e.g. MPPS) allow

efficient oligonucleotide synthesis on an extremely small scale (10 nmol) due to enhanced moisture exclusion. The solid supports are functionalised to introduce reactive sites. A long chain alkylamine linker (LCAA) is commonly attached to CPG resins by silylation, and the nucleoside is attached to CPG *via* a succinyl linker to an amino group (i.e. an amide bond). The loading of amino groups on the solid support is kept within 30–80 μmol g^{-1} due to steric crowding issues at higher loading.[1] For highly efficient synthesis, the oligonucleotide loading is controlled within 20–30 μmol g^{-1}.

Oligonucleotides can be synthesised by the phosphoramidite approach, as first described by Beaucage and Caruthers in 1981.[18] Later, methyl phosphoramidite monomers[24] were replaced by the more user-friendly 2-cyanoethyl phosphoramidite monomers.[25] This approach found widespread adoption and is still used in oligonucleotide synthesis today. As opposed to nature, solid phase phosphoramidite oligonucleotide synthesis normally proceeds in the 3′ to 5′ direction.[26,27] An important feature of this chemistry is that the functionally reactive groups must be protected. The 5′-position of the sugars are protected with an acid-labile DMT (4,4′-dimethoxytrityl) group (Figure 1.5); the nucleobases thymidine (DNA) and uridine (RNA) do not require any nucleobase protection;[28] guanine is protected to improve solubility in acetonitrile;[29] adenine and cytosine both have exocyclic primary amino groups on the heterocyclic base that are protected.[30] The most commonly used protecting groups for the heterocyclic bases are shown in Figure 1.5. However, some chemical groups that are used in chemically modified oligonucleotides (e.g. some fluorescent dyes) are extremely sensitive to aqueous ammonia, and require much milder conditions. For this reason, "ultramild" protected monomers (Figure 1.6) have also been designed which can be removed quickly at room temperature by treatment with ammonia or milder reagents.

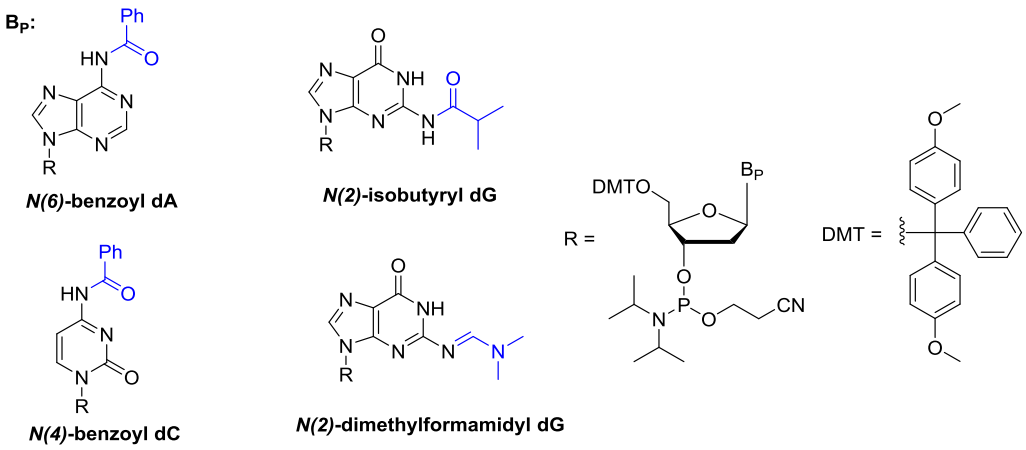

Figure 1.5. DNA base protecting groups. Structures of protecting groups commonly employed for the protection of adenine, cytosine and guanine bases during phosphoramidite DNA oligonucleotide synthesis.

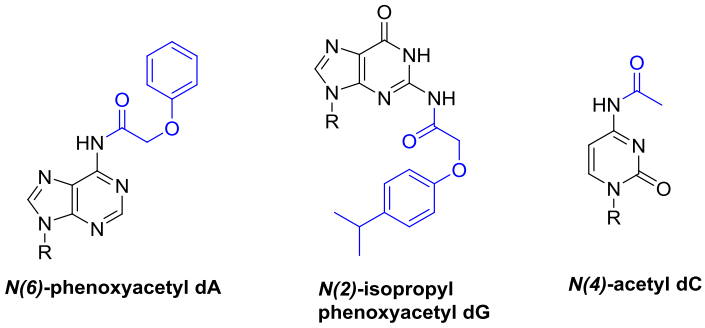

Figure 1.6. Ultramild protecting groups. Structures of heterocyclic base protecting groups designed for removal under "ultramild" conditions after phosphoramidite DNA oligonucleotide synthesis.

A cycle of oligonucleotide synthesis consists of four steps: 5′-OH deprotection, phosphoramidite coupling, capping, and oxidation (Figure 1.7).[31] The first monomer is attached to a solid support (CPG or polystyrene) and every synthetic cycle involves coupling a nucleotide residue to the growing oligonucleotide chain to assemble the required oligonucleotide sequence. The efficiency of each cycle (typically 99.5%) can be monitored during the detritylation by UV or conductivity measurement of the liberated

4,4′-dimethoxytrityl group (DMT) as a cation. The resultant oligonucleotides can be cleaved from the solid support and deprotected by treating with ammonia solution, and then purified by a variety of methods such as desalting or reversed-phase HPLC.

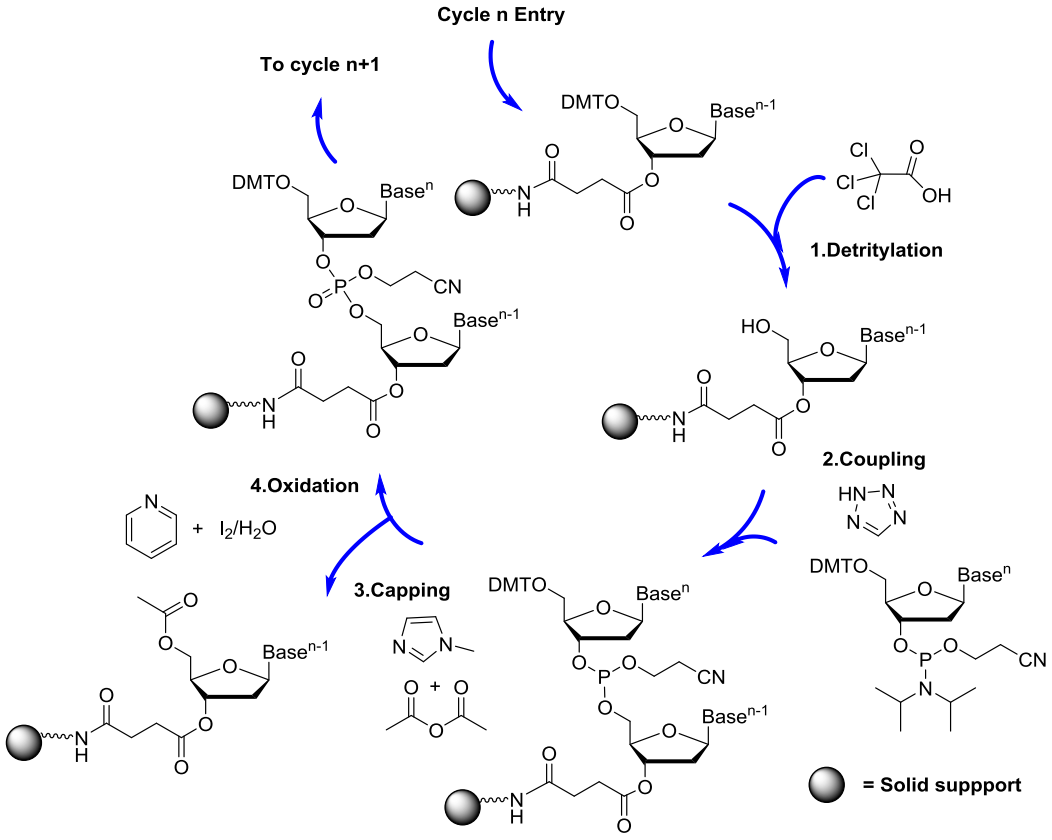

Figure 1.7. Synthetic cycle for the preparation of oligonucleotides by the phosphoramidite method.

1.3 Click chemistry

1.3.1 Cu(I)-catalysed azide-alkyne cycloaddition reaction (CuAAC)

Nucleic acids are responsible for some of the most important activities in living cells, including information storage, information transfer, modulation of gene expression and primitive immune responses. Therefore it is important to understand their properties

through biophysical and biochemical studies. To this end, 'Click' chemistry has become an important tool. The concept of click chemistry was first introduced by Meldal[32] and Sharpless[33] in 2001 to describe reactions in which two organic molecules are joined together with high selectivity and efficiency under mild conditions.[34] The premier example of click chemistry is the extremely fast, stereospecific and efficient Cu(I)-catalysed azide-alkyne cycloaddition reaction (CuAAC). As opposed to the uncatalysed Huisgen [3+2] azide-alkyne cycloaddition (AAC), which proceeds at elevated temperatures up to 100 °C and produces an equal mixture of 1,4- and 1,5-triazole regioisomers (Figure 1.8 A),[35] the CuAAC reaction gives only the 1,4-disubstituted triazole product in high yields at room temperature under mild conditions (Figure 1.8 B).[36]

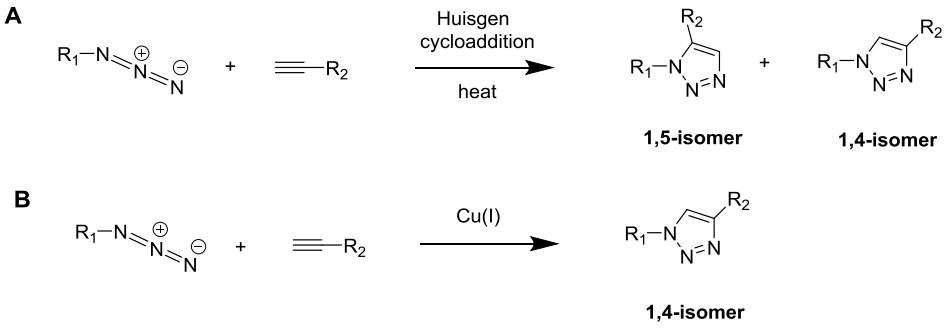

Figure 1.8. Thermal and Cu(I)-catalysed azide-alkyne cycloaddition reactions and product distribution. A: the thermal reaction between an azide and an alkyne; B: the Cu(I)-catalysed reaction; R_1 and R_2: substituents.

There is a dramatic improvement in both rate and regioselectivity with Cu(I)-catalysis.[37] The reaction is very tolerant of other functional groups, gives rise to few side reactions, and performs best in aqueous systems over a broad temperature (0 °C – 160 °C) as well as pH range (4–12).[38] In addition, the 1,2,3-triazole derivatives that are formed are chemically stable and inert to severe hydrolytic, oxidizing and reducing conditions, even at

elevated temperatures. As a consequence, the CuAAC reaction has already found a wide range of applications in diverse fields including the synthesis of catenane and rotaxanes,[39] metal ligands,[40] oligonucleotides[41] and proteins.[42]

To determine the role of copper in the reaction, mechanistic studies were conducted by Sharpless *et al.*[36,38] As shown in Figure 1.9 A, copper forms the Cu(I) acetylide, then reacts with azide to form a six-membered Cu-containing intermediate. Later, Fokin *et al.*[43] demonstrated that two different copper atoms are involved in the cycloaddition steps (Figure 1.9 B). Cu(I) plays a vital role in accelerating the CuAAC reaction. However, the free Cu(I) ion is unstable in aqueous solution where it can form Cu(0) and Cu(II) by exchanging electrons through disproportionation. For this reason, sodium ascorbate is used as a reducing agent to regenerate Cu(I) from Cu(II).

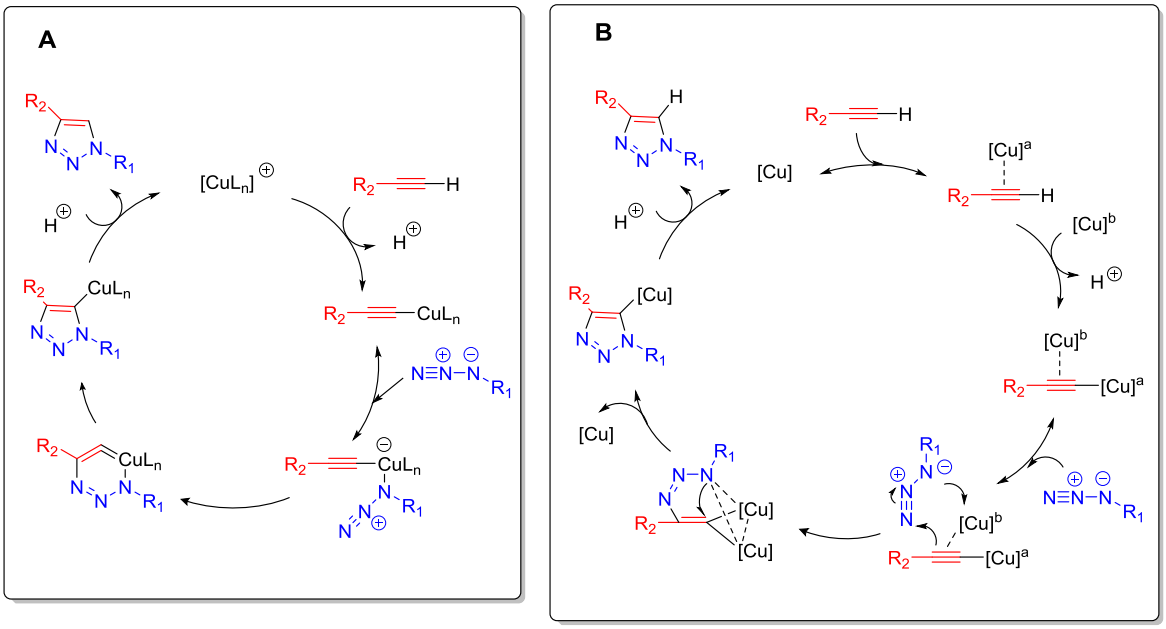

Figure 1.9. The first catalytic cycle (A)[36] proposed and the second two copper atoms catalytic cycle (B)[43] proposed for CuAAC. R_1 and R_2: substituents.

Also, tris(benzyltriazolylmethyl)amine (TBTA) (Figure 1.10) is used as a ligand to bind and stabilise Cu(I), thereby preventing disproportionation and reducing oxygen-promoted side reactions.[44] However, the limited solubility of TBTA in water restricts its use to organic solvent systems. Consequently, the water-soluble ligand tris(3-hydroxypropyltriazolylmethyl)amine (THPTA) (Figure 1.10) was developed.[45] Furthermore, the CuAAC reaction must be carried out in the absence of oxygen since ascorbate ($C_6H_7O_6^-$) can react with Cu(II) in the presence of oxygen to form H_2O_2. This in turn generates reactive radical species, such as hydroxyl radicals ($^{\cdot}OH$), that play a crucial role in the cleavage of the oligonucleotide backbone.[46]

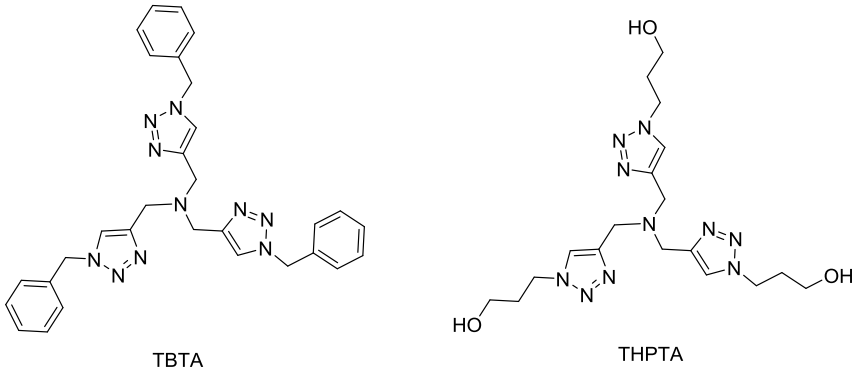

Figure 1.10. Polytriazole ligands for the CuAAC reaction. Tris(benzyltriazolylmethyl)amine (TBTA) and tris(3-hydroxypropyltriazolylmethyl)amine (THPTA).

1.3.2 Metal-free click chemistry

As discussed above, oligonucleotides are unstable in the presence of Cu(I) and oxygen, which cause oligonucleotide backbone degradation. In addition, the cytotoxicity of Cu(I) restricts the *in vivo* applications of nucleic acids,[47] or experiments involving living cells.[48] However, the Huisgen [3+2] azide-alkyne reaction (AAC) is usually very slow and

inefficient in the absence of Cu(I)-catalysis.[49] In view of this limitation, there is significant interest in developing a metal-free click chemistry that retains all the beneficial properties of the CuAAC click reaction. The key criteria of this chemistry are high efficiency and yields; the reactants are also required to be non-toxic, with no by-products, or only inoffensive ones. One of the most well developed methods is the Staudinger ligation, developed by Bertozzi *et al.*[48] In addition, the ring strain-promoted alkyne-azide [3+2] cycloaddition (SPAAC) reaction is a highly promising and simple method for nucleic acid applications.

1.3.3 Staudinger ligation

In the classical Staudinger reduction,[50-52] a phosphine reacts with an azide to produce an aza-ylide intermediate, which is then converted to a primary amine and phosphine oxide in the presence of H_2O (Figure 1.11 A). Interestingly, a modified Staudinger reaction occurs when the unstable aza-ylide can rearrange to yield a stable covalent adduct. For example, methyl ester (Figure 1.12 B) can act as an electrophilic trap and capture the nucleophilic aza-ylide by intramolecular cyclization to form an amide linkage.[53] Although this reaction hinders the introduction of azides during oligonucleotide synthesis, it can be exploited as a labelling method.[54] For example, FAM-tethered triphenylphosphine and azide-labelled oligonucleotide can be efficiently and site selectively linked together.[55] Indeed, the Staudinger reaction was the first biorthogonal reaction applied in living cells.[56] However, the electron-rich phosphine is prone to oxidation in air, which increases the background signal in live cell imaging;[57] the reaction also has relatively slow kinetics ($k \approx 2 \times 10^{-3}$ M^{-1} s^{-1}),[58] which further limits its ability to probe fast biological processes.

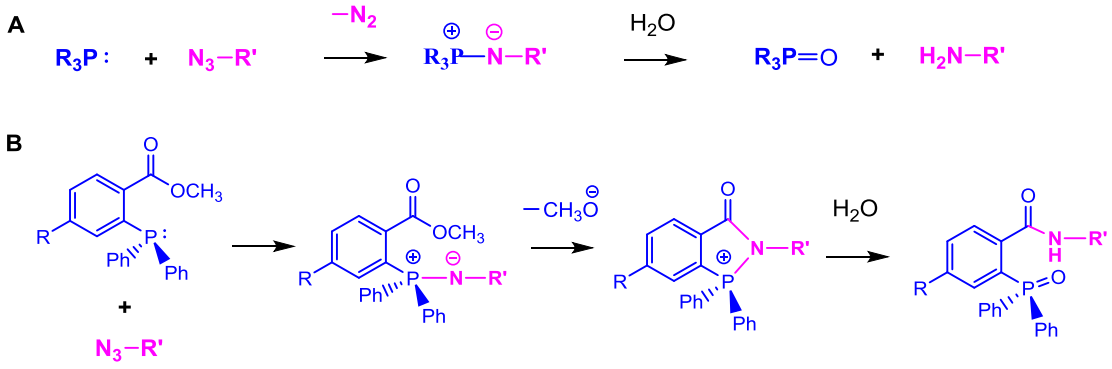

Figure 1.11. Comparison of classical and modified Staudinger reactions. A: The classical Staudinger reaction of phosphines and azides. Hydrolysis of the aza-ylide produces an amine and a phosphine oxide. B: The modified Staudinger ligation that produces a stable covalent adduct by amide bond formation.[53] R and R′: substituents.

1.3.4 Strain-promoted alkyne-azide cycloaddition reaction (SPAAC)

Due to the limitation of the slow reaction kinetics of the Staudinger ligation, the ring strain-promoted alkyne-azide [3+2] cycloaddition (SPAAC) reaction has been developed to avoid the use of copper and initiate spontaneous AAC. Instead of terminal alkynes, SPAAC makes use of internal alkynes in cyclic systems such as cyclooctyne. The bond angle of the *sp*-hybridised carbons in cyclooctyne is *ca.* 160° (Figure 1.12 B, C), significantly lower than the ideal angle for alkynes (180°) (Figure 1.12 A). Therefore, upon reaction to form the triazole, significant ring strain is released. Interestingly, SPAAC should be kept Cu(I) free as Cu(I) actually inhibits the reaction by forming a Cu(I)-cyclooctyne complex (Figure 1.12 D).[59,60]

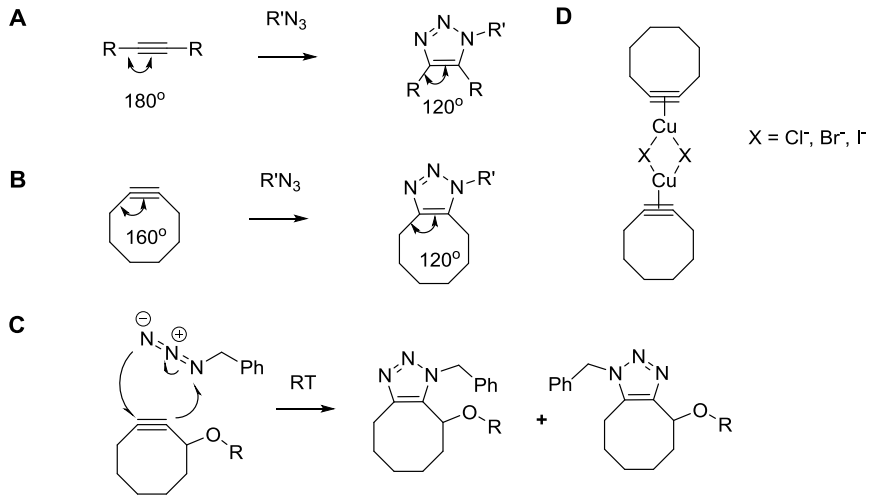

Figure 1.12. The Cu-free reaction of alkynes and azides. A: a comparison of bond angles between a linear alkyne and the corresponding triazole product; B: a comparison between a strained cyclooctyne and its corresponding triazole product; C: example of a SPAAC reaction between an azide and cyclooctyne (OCT) under Cu-free condition and with no additional reagents, both regioisomers of the cyclooctyl triazole are shown;[48] D: a Cu(I)-cyclooctyne complex.[60] R and R′: substituents.

The first generation cyclooctyne OCT (Figure 1.13 A) was reported by Agard *et al.* for live cell labelling ($k = 1.3 \times 10^{-3}$ M^{-1} s^{-1}).[61,62] It was found that OCT based SPAAC proceeds as fast as the Staudinger ligation with no apparent toxicity. Subsequent efforts aimed to modify cyclooctynes in order to enhance reactivity. For example, adding one or two fluorine atoms to the ring system (Figure 1.13 B, C) was found to increase the reaction rate by 3- or 60-fold due to withdrawal of electron density compared to OCT.[62] For the difluoro DIFO, however, its low hydrophilicity decreased its bioavailability. This was addressed by the synthesis of hydrophilic DIMAC (Figure 1.13 D, $k = 3.0 \times 10^{-3}$ M^{-1} s^{-1}).[63]

Aromatic rings were introduced to the cyclooctyne system (DIBO, $k = 5.7 \times 10^{-2}$ M^{-1} s^{-1})[64] (Figure 1.13 E) by Boons *et al.*[65] to enhance ring strain and boost reactivity. The reactivity of cyclooctyne can also be enhanced by augmenting additional ring strain through the

addition of a cyclopropyl ring, as demonstrated by BCN (*endo*: k = 0.14 M^{-1} s^{-1}; *exo*: k = 0.11 M^{-1} s^{-1})[66] (Figure 1.13 F), which is *ca.* 100-fold faster than the parent cyclooctyne. Highly reactive cyclooctynes were designed to make use of a combination of activating factors. DIFBO[67] (Figure 1.13 G), for example, combines the favourable kinetics of DIFO (Figure 1.13 C) with strain enhancement through the fused aromatic ring of DIBO (Figure 1.13 E). DIFBO (k = 0.22 M^{-1} s^{-1}) reacts rapidly with respect to either parent compound, but also undergoes spontaneous trimerization in solution to form two asymmetric products.

Various other aromatic analogues have been synthesised, including the further addition of one more sp^2-like centre to the dibenzocyclooctyne ring as reported by Debets *et al.*[68] in the study of aza-dibenzocyclooctyne (Figure 1.13 H), which has an exocyclic amide linkage and a rate constant of 0.31 M^{-1} s^{-1}. Jewett *et al.*[69] developed a cyclooctyne with an amide within the ring, BARAC (Figure 1.13 I). To date, BARAC is the most reactive cyclooctyne reported, with a second-order rate constant of 0.96 M^{-1} s^{-1}, over 7-fold higher that the rate constant for BCN. But the most readily accessible cyclooctyne analogue is bicycle[6.1.0]nonyne (BCN), which is synthesised in four steps.[66]

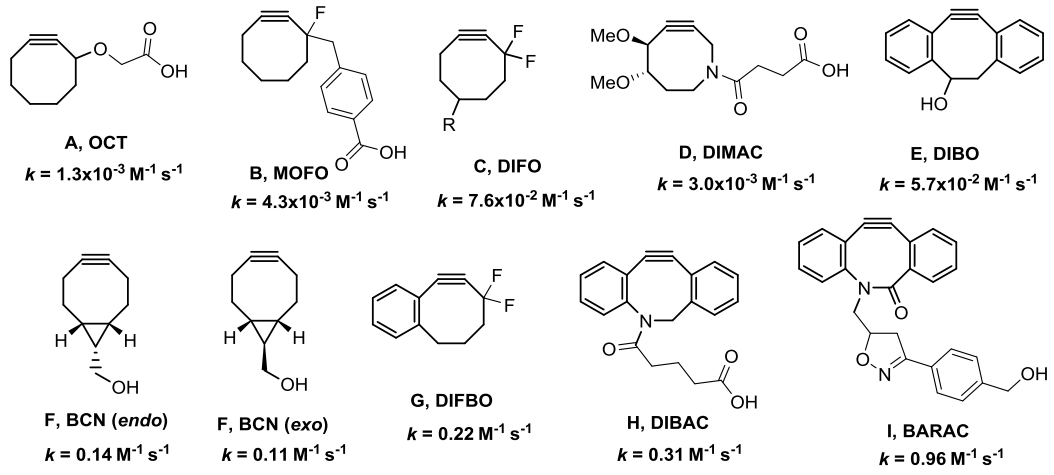

Figure 1.13. Strained cycloalkynes.[62-69]

1.4 Long oligonucleotides synthesis

DNA synthesis techniques play a pivotal role in the field of modern molecular biology and synthetic biology. One limitation of gene synthesis is the cost of assembling long highly pure oligonucleotides. Oligonucleotide synthesis on a DNA microchip[70] reduces cost due to the greatly increased throughput compared with the current column-based synthesis, as described in Section 1.2. However, microchip-based synthesis is relatively inefficient and gives complex mixtures of oligonucleotides, which can make it difficult to obtain pure oligonucleotides. The polymerase chain reaction (PCR) does allow the amplification of specific oligonucleotides up to a total of *ca.* 35 kilo-base pairs,[71] but PCR-based DNA synthesis does not allow the incorporation of different modifications at specific loci, and as such limits the scope of biological studies, e.g. epigenetics. Alternatively, enzymatic ligation of oligonucleotides can be carried out to produce large fragments, but this is best used in a small scale, and some modified nucleobases are not tolerated by ligase enzymes. Therefore, it would be valuable to develop a purely chemical method for the assembly of long oligonucleotides, especially, with the aim of achieving wider scalability and flexibility.

For solid phase synthesis, the length of oligonucleotides is limited to around 150 bases due to imperfect coupling efficiency and chemical lesions caused by side-reactions during the chemical synthesis. Thus it is necessary to design inexpensive and simple methods to conjugate shorter oligonucleotides on a large scale. To this end, previous work in the Brown group has focused on triazole linkages using CuAAC.[72,73] The first unnatural triazole linkage (Figure 1.14 B) was prepared using a 5′-propargylamido-modified oligonucleotide and a 3′-azide labelled oligonucleotide.[72] The linkage did not severely impede normal or modified polymerases during polymerase chain reaction (PCR).

However, sequencing of the PCR product revealed that one base around the ligation site was skipped during replication. In 2011, Brown *et al.* published a second generation triazole linkage (Figure 1.14 C) that more effectively mimicked the natural phosphodiester linkage (Figure 1.14 A), and as a result could be read through accurately by DNA polymerases in *Escherichia coli* and for the first time in live human cells.[73] The same group has also reported that the templated DNA strand ligation can be carried out using the ring-strain promoted alkyne–azide [3+2] cycloaddition reaction (SPAAC), and that the reaction can be completed in 1 minute.[59]

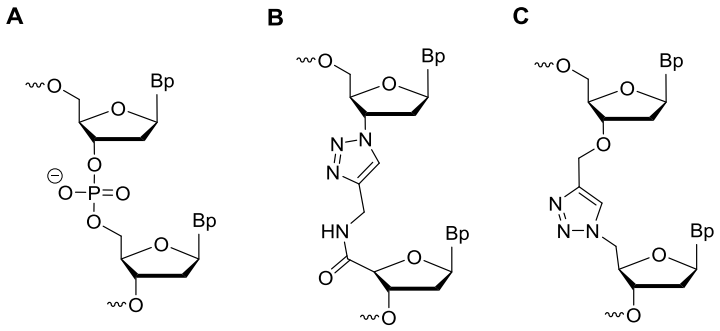

Figure 1.14. DNA linkage structures. A: canonical DNA; B: first triazole DNA analogue; C: biocompatible triazole analogue. Bp = protected base.

Furthermore, the CuAAC reaction has been successfully used on the solid phase to synthesise oligonucleotides with triazole instead of phosphodiester linkages. Bi-functionalised azide alkyne monomers, where the alkyne is protected using a trimethylsilyl group, were coupled to the resin-bound nucleoside and then deprotected. After two coupling reactions, a 3-mer oligonucleotide was obtained in 84% yield; however, the overall yield was just 0.61% after 9 reactions (10-mer).[74] The solid phase ligation of oligonucleotides *via* the CuAAC reaction was also employed by Eritja *et al*. to obtain oligonucleotides carrying 5′-5′ linkages.[75] In neither case did the assembly of long

oligonucleotides proceed with good yields. The challenge remains to achieve a clean and efficient method for chemical ligation of oligonucleotides.

1.5 Nucleic acid labelling

For nucleic acid detection in DNA diagnostics, labelling methods are essential. One of the most important examples of oligonucleotide labelling involves the use of fluorescent dyes. The resulting fluorescent nucleic acids are of vital importance in probes for DNA detection and diagnostics due to their abilities to discriminate between different DNA targets.

In order to generate these probes, there are two main routes – fluorophore attachment during solid phase oligonucleotide synthesis, or post-synthetic labelling. The first approach requires the corresponding phosphoramidite monomers (Figure 1.15), in which the dyes are attached to the nucleobase, sugar or an artificial backbone; the modified monomers must be compatible with oligonucleotide synthesis.

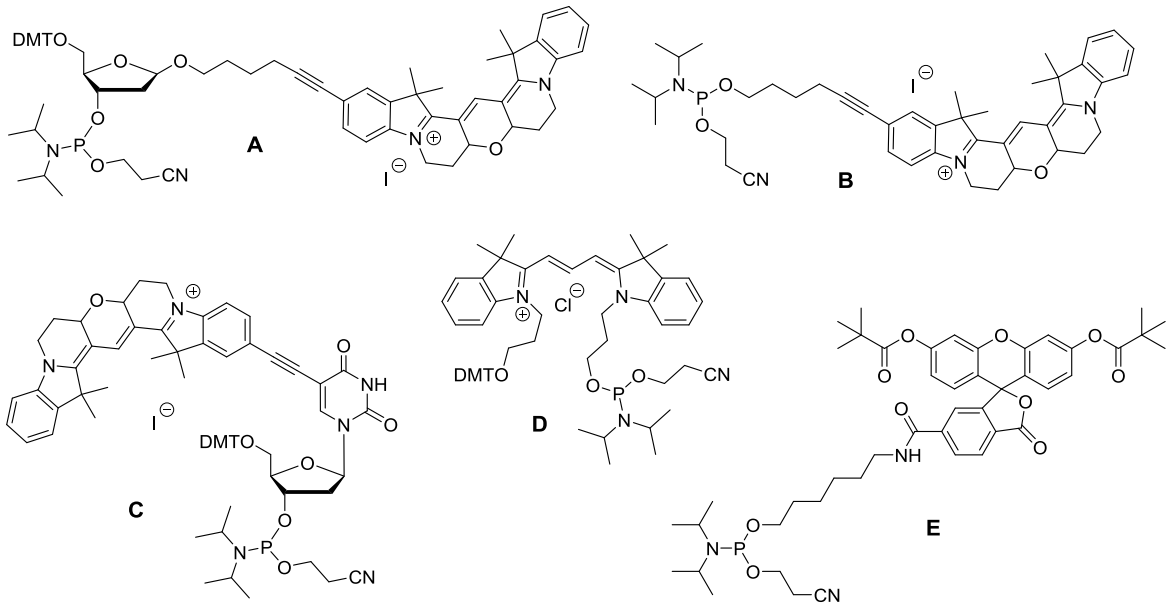

Figure 1.15. Examples of phosphoramidite monomers of fluorescent dyes. A: Cy3B-dR phosphoramidite (β-anomer);[76] B: ethynyl Cy3B phosphoramidite;[76] C: 5-Cy3B dT phosphoramidite;[76] D: Cy3 phosphoramidite; E: FAM phosphoramidite (6-regioisomer). (D, E: are commercially available.) DMT: 4,4′-dimethoxytrityl group (Figure 1.5).

This method is high yielding and has good selectivity, allowing for efficient multiple and mixed dye additions at both terminal and internal positions.[76] However, phosphoramidite monomers of fluorescent dyes can be challenging to synthesise and expensive. As a result, relatively few are commercially available. For some dyes that are unstable during oligonucleotide synthesis or ammonia treatment for cleavage from resin and deprotection (e.g. Cy5), post-synthetic labelling is required, as described below.

1.5.1 Post-synthetic labelling of oligonucleotides *via* amino group

One of the most common post-synthetic strategies for dye-labelling of oligonucleotides involves the use of *N*-hydroxysuccinimide (NHS) activated esters (Figure 1.16). A diverse range of amino-modified phosphoramidite monomers (Figure 1.17) can be incorporated into DNA during solid phase oligonucleotide synthesis, either internally or at the termini. The amino group can be attached to the nucleobase, which subsequently localises in the major groove (Figure 1.17 A, B), or it can be placed at the 2′-position of the sugar, which orientates the group to the minor groove (Figure 1.17 C). 5-Amino-modified C6-dT and 5-amino-modified C2-dT phosphoramidite monomers are commercially available; 5′-TFA-amino-modified C6 phosphoramidite (Figure 1.17 D) and 3′-amino-modified C7 CPG 1000 Å (Figure 1.17 E) are also commercially available; 2′-amino-modified dT phosphoramidite (Figure 1.17 C) can be readily synthesised.[77] NHS esters are not stable in buffer, particularly above pH 8, which is required for the labelling reaction, and are sensitive to moisture/decomposition during storage. Therefore, the development of alternative labeling strategies is of importance.

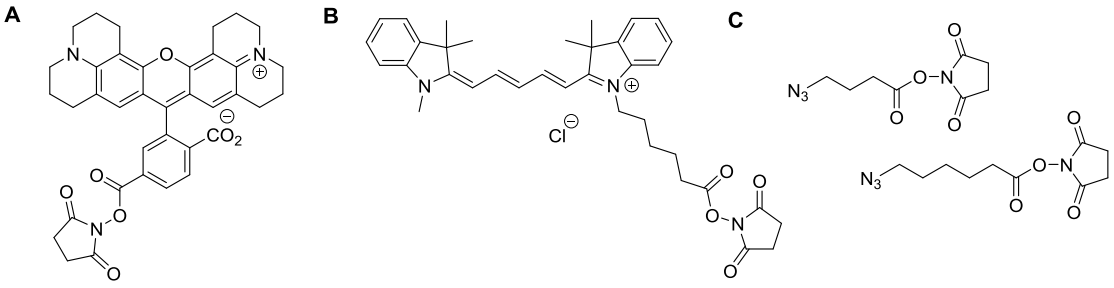

Figure 1.16. Examples of *N*-hydroxysuccinimide (NHS) activated esters. A: ROX NHS ester; B: Cy5 NHS ester; C: 4-azidobutyric acid NHS ester and 6-azidohexanoic acid NHS ester.[78]

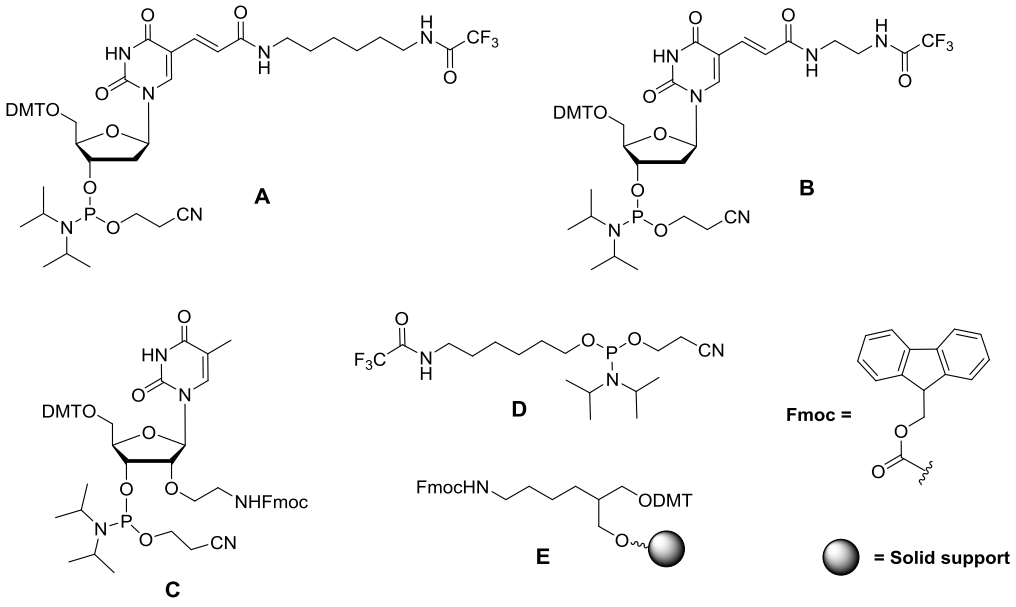

Figure 1.17. Aminoalkyl monomers can be used for introduction of the reactive amino groups for post-synthetic labelling of oligonucleotides (all are commercially available except C). A: 5-amino-modified C6-dT phosphoramidite (5-position labelling); B: 5-amino-modified C2-dT phosphoramidite (5-position labelling); C: 2′-amino-modified C2-dT phosphoramidite (2′-labelling);[77] D: 5′-TFA-amino-modified C6-CE phosphoramidite (5′-labelling); E: 3′-amino-modified C7 CPG 1000 Å (3′-labelling). DMT: 4,4′-dimethoxytrityl group (Figure 1.5).

1.5.2 Labelling *via* the CuAAC reaction

The CuAAC click reaction, as one of the most efficient chemical reactions, has attracted a great deal of attention for oligonucleotide labelling and has been investigated by a large group of workers. Seela *et al.*[79] introduced a large variety of alkynyl residues into nucleobases (Figure 1.18 A, B, C, F and G) and found that whilst these groups can be used for click chemistry, their lipophilic characters also enhanced DNA duplex stabilities by 1–2 °C per modification. Carell *et al.*[80] developed the Cu(I)-catalysed click reaction for the multiple post-synthetic labelling of alkyne-modified oligonucleotides, which contain up to six consecutive alkyne-modifications (Figure 1.18 A, B). The click chemistry was

performed using azide-modified fluorescein and coumarin (Figure 1.18 H, I); complete high-density conversion of six click sites was obtained. In addition, coumarin azide only becomes fluorescent after triazole formation,[81] providing the added benefit of being a fluorogenic click dye. Wagenknecht *et al.*[82] introduced alkyne groups using two alternative approaches: (i) as a nucleobase modification at the 2′-position of uridine (Figure 1.18 D) and (ii) as a nucleotide substitution using (*S*)-(–)-3-amino-1,2-propanediol as an artificial linker (Figure 1.18 E). It is worth noting that by coupling the azide-modified coumarin dye (Figure 1.18 J) to the 2′-position of uridine (Figure 1.18 D), a significant Stokes' shift of *ca.* 100 nm and good quantum yields were obtained which may potentially be useful for fluorescent nucleic acid probe applications.

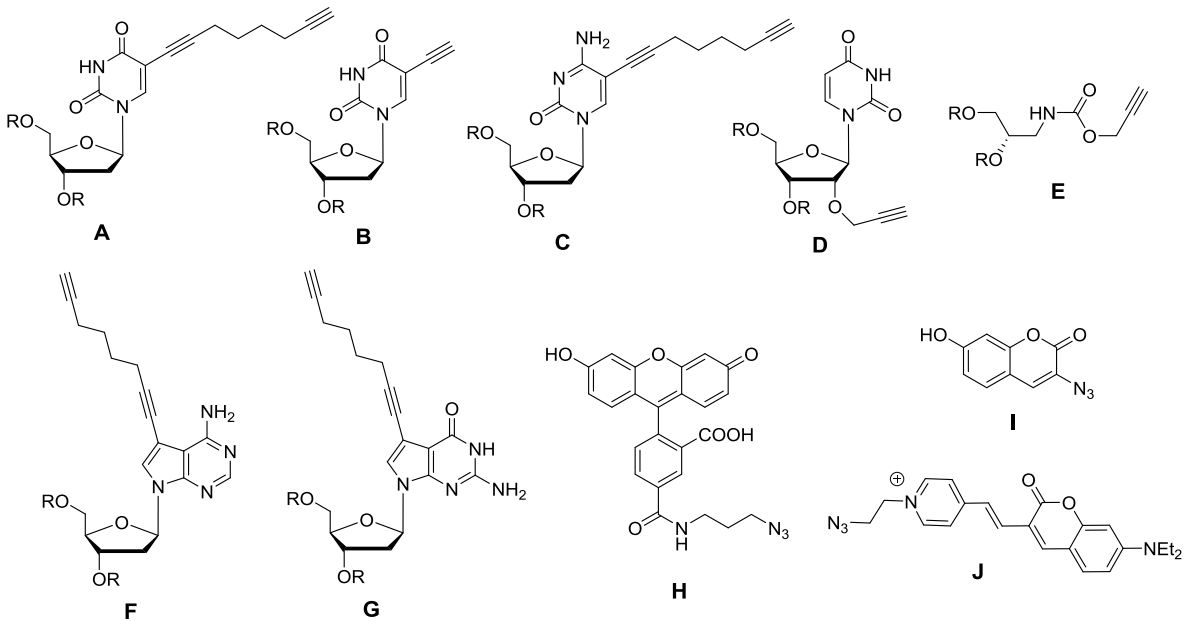

Figure 1.18. Structures of alkyne-modified nucleosides incorporated into oligonucleotides by solid phase synthesis (A–G) and azide-modified monomers (H–J) that used in the CuAAC reactions. A: 5-octadiynyl-deoxyuridine;[79,80] B: 5-ethynyl-deoxyuridine;[79,80] C: 5-octadiynyl-deoxycytidine;[79] D: 2′-*O*-propargyl-uridine;[82] E: (*S*)-(–)-3-amino-1,2-propanediol;[82] F: 7-octadiynyl-7-deazadeoxyadenosine;[79] G: 7-octadiynyl-7-deazadeoxyguanosine;[79] H: fluorescein azide;[80] I: coumarin azide-1;[80] J: coumarin azide-2.[82] R: DNA.

The click reaction was also carried out with reversed coupling partners, such that the azide-modified oligonucleotides clicked with alkyne-labelled fluorescent dyes or other reporters. However, the azide functional group is incompatible with solid phase oligonucleotide synthesis due to the Staudinger ligation (Section 1.3.3). Therefore, the simplest method of introducing azide group is by post-synthetically labelling amino-modified oligonucleotides with 4-azidobutyric or 6-azidohexanoic acid NHS activated ester (Figure 1.16 C).[78] Alternative approaches include introducing alkyl halide groups (Figure 1.19 A, B) during solid phase synthesis, which can then be converted to azides by treatment with NaN_3.[83,84] Furthermore, the azide group at 3′-ribose sugar of adenosine (Figure 1.19 C) was incorporated into oligonucleotides by standard RNA solid phase synthesis.[85] The monomer is stable because of the sterically hindered azide group, which limits the reaction with phosphoramidites.

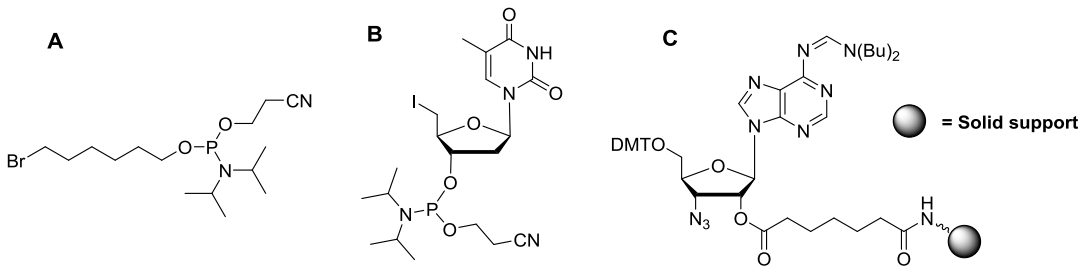

Figure 1.19. Structures of azide-precursory monomers incorporated into oligonucleotides during solid phase synthesis. A: 6-bromohexanol phosphoramidite;[83] B: 5′-iodo dT phosphoramidite;[84] C: 3′-azido-3′-deoxyadenosine-functionalised on solid phase.[85] DMT: 4,4′-dimethoxytrityl group (Figure 1.5).

The resulting fluorescent nucleic acids can be used as probes, which can be tailored to specifically bind targets with high affinity. These probes typically depend upon target hybridization *via* base pairing. In order to understand their mode of action, a brief summary of important fluorescence principles is initially described.

1.6 Fluorescence

1.6.1 Fluorescence theory

Upon absorption of a photon ($h\nu_A$), a fluorophore is excited from ground state (S_0) to one of the higher vibrational states of S_1 (or S_2, excited singlet states). This step is very fast and happens within 10^{-15} s. In the next 10^{-12} s, the molecule undergoes non-radiative relaxation to the lowest vibrational state of electronically excited states (S_1), a process called internal conversion (IC). The molecule then returns to a ground state (S_0) by emission of a photon ($h\nu_F$). This process is known as fluorescence. Emission only occurs from the lowest vibrational level of the excited singlet states (S_1) and is independent of the excitation wavelength based on Kasha's rule.[86] Emission (Figure 1.20, red) is of lower energy than absorption (Figure 1.20. blue) due to internal conversion (IC) and relaxation. Therefore, emission is observed at a longer wavelength than absorption. The difference between the maxima of the absorption and emission is called the Stokes' shift.[87]

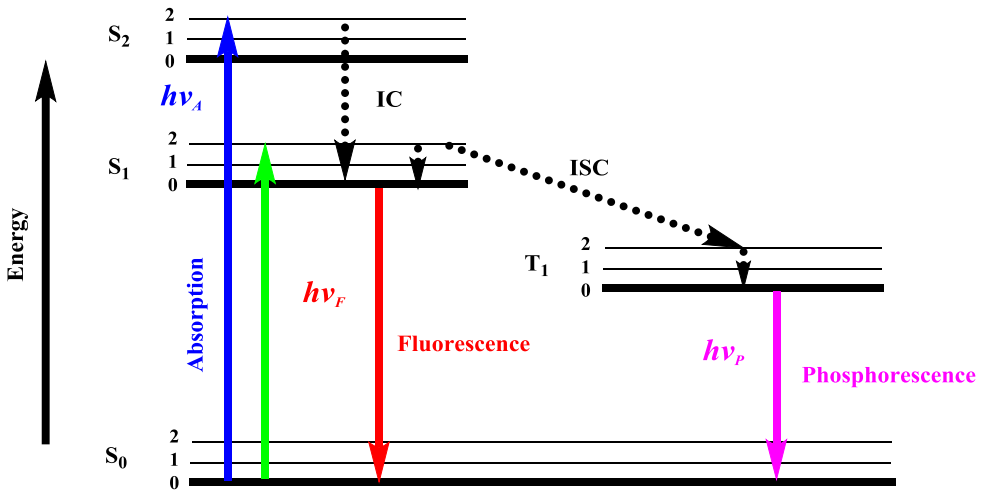

Figure 1.20. Jablonski energy level diagram illustrating the pathway of an excited electron. $h\nu_A$: photon absorption; $h\nu_F$: fluorescence emission; $h\nu_P$: phosphorescence; S_0: ground; S_1 and S_2: excited singlet states; T_1: an excited triplet state; 0, 1, 2: vibrational level; IC: internal conversion; ISC: intersystem crossing; all straight lines: involving photons; all dotted lines: involving vibrational or thermal transitions.

1.6.2 Fluorescence resonance energy transfer (FRET) and fluorescence quenching

a) Static quenching

Static quenching occurs when a complex is formed between a fluorophore and a quencher. This complex absorbs energy from light but fails to emit it upon relaxation of the excited state to the ground state (Figure 1.21 A). The mechanism is also referred to as "contact quenching" or "ground-state complex formation".[88] In contact quenching, the donor fluorophore and acceptor quencher interact by proton-coupled electron transfer *via* the formation of hydrogen bonds. This process is therefore controlled by electrostatic, steric and hydrophobic forces in aqueous solution. Contact quenched molecules display a change in the absorption spectra of the two molecules.

b) Collisional quenching

Another mechanism is called "collisional quenching" or "dynamic quenching" in which the fluorescence intensity of a fluorophore is reduced by intermolecular collisions with quenchers (Figure 1.21 B). This form of quenching depends on the spatial overlap of donor and acceptor molecular orbital, which is not strongly dependent on the excitation wavelength; however, it is only efficient at very short distances. Therefore it is particularly useful in hairpin loop oligonucleotide probes such as molecular beacons, which are described below (Section 1.7.1).

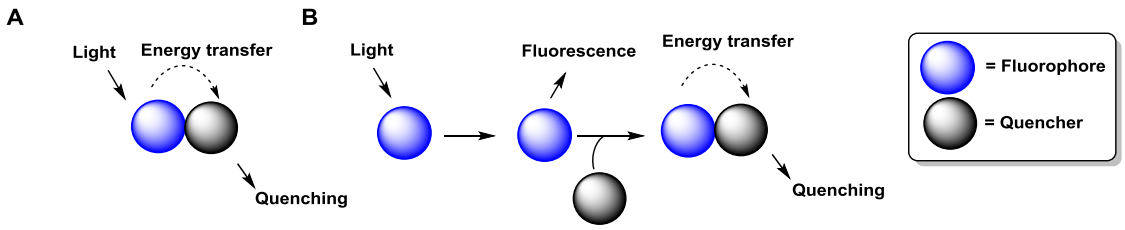

Figure 1.21. Illustration of static quenching (A) and collisional fluorescence quenching (B).

c) Förster (Fluorescence) resonance energy transfer (FRET)

Förster (Fluorescence) resonance energy transfer (FRET)[87] is the radiationless transmission of energy from a donor fluorophore to an acceptor molecule through dipole-dipole interactions without the emission of a photon. As a result, the donor's fluorescence intensity is reduced and the acceptor's emission intensity is increased simultaneously (Figure 1.22 A). For FRET to occur, the emission spectrum of the donor must overlap with the absorption spectrum of the acceptor (Figure 1.22 B). When the acceptor is also a fluorophore, the transmitted energy excites the acceptor, which then radiatively emits a photon. On the other hand, if the acceptor is non-fluorescent, only quenching of the donor emission is observed.

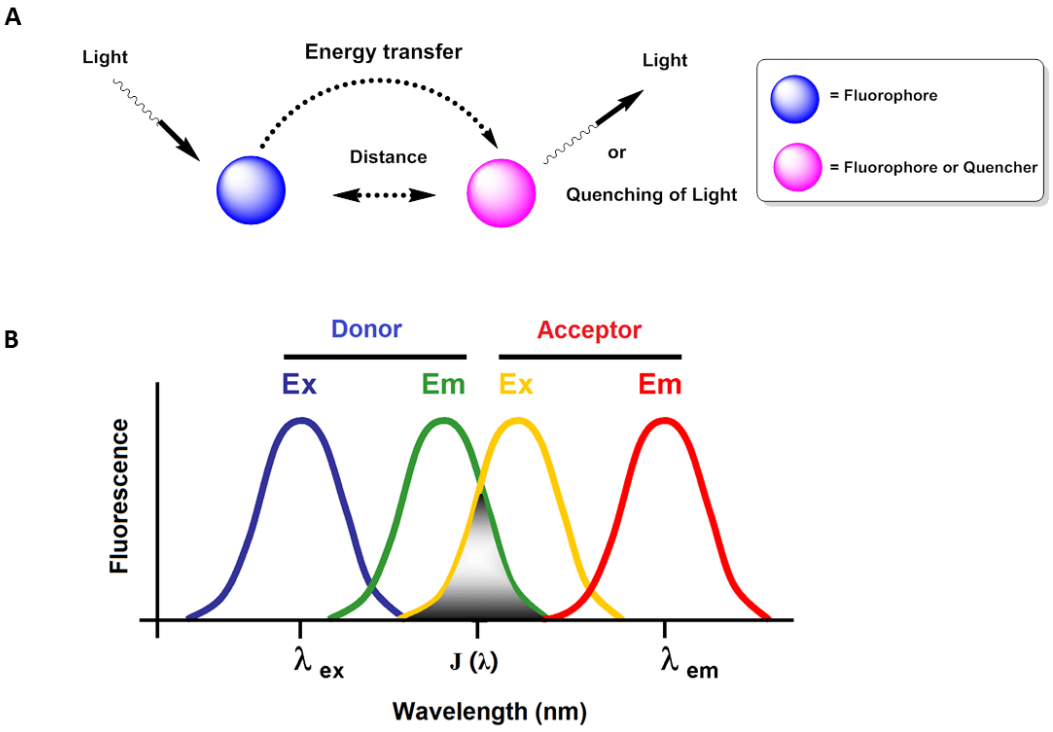

Figure 1.22. A: Illustration of fluorescence resonance energy transfer (FRET); B: Schematic representation of spectral overlap.

The efficiency of the energy transfer process depends strongly upon the donor-to-acceptor separation distance (r) and the Förster distance (R_0)[89] of the donor and acceptor pairs (equation 1). When the distance between the donor and acceptor is equal to the Förster distance (typically 10–100 Å, equation 2), the energy transfer efficiency is 50%. Consequently, the distance between two fluorophores can be quantitatively measured. However, it should be noted that FRET also depends on the relative orientation of the donor emission dipole and the acceptor absorption dipole (equation 3) and in particular the orientation factor (κ^2, Figure 1.23). If the fluorophores undergo isotropic reorientation in a time much shorter than the excited state lifetime of the donor, the average orientation κ^2 is generally assumed equal to 2/3. This is the case in most studies,[90] including those that involve double-stranded DNA.[91,92]

$$E = \frac{Ro^6}{Ro^6 + r^6}$$ equation 1[91]

$$R_o = 0.211 \left(\kappa^2 n^{-4} Q_D J(\lambda)\right)^{1/6} \text{ (in Å)}$$ equation 2[91]

$$\kappa^2 = (\cos\theta_A - 3\cos\theta_B \cos\theta_C)^2$$ equation 3[92]

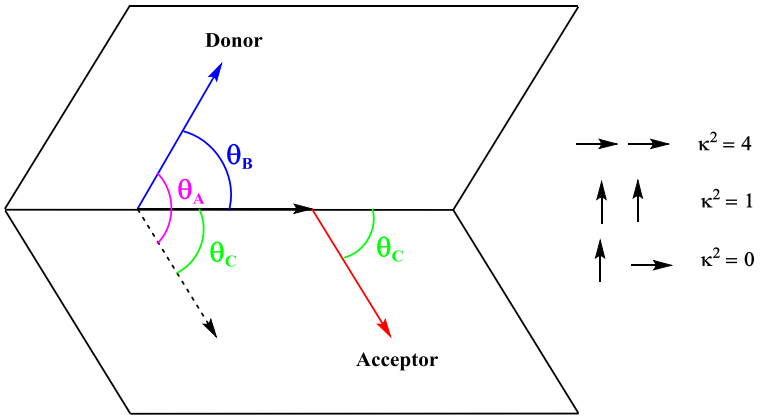

Figure 1.23. Schematic diagram of the dipole orientation angles in FRET between a donor (blue) and an acceptor (pink). E: the efficiency of FRET (equation 1). In equation 2, where Q_D is the fluorescence quantum yield of the donor in the absence of the acceptor, κ^2 is the dipole orientation factor, n is the refractive index of the medium and $J(\lambda)$ is the overlap integral of the donor emission and acceptor absorbance spectra. The orientation factor κ^2 (equation 3), θ_A is the angle between the emission transition dipole of the donor and the transition absorption dipole of the acceptor.

1.7 Fluorescent hybridization probes for nucleic acid detection

The basic properties of fluorescence described above play a key role in the design of nucleic acids probes, which are discussed in this section. Fluorescence is an extremely important means of detection in DNA sequencing, genetic analysis and DNA diagnostics.[93,94] Fluorescence has been widely used in biological studies of proteins and nucleic acids both *in vivo* and *in vitro* due to the high sensitivity of the technique.

Fluorescently labelled oligonucleotides have been used to detect genetic variations in DNA and to identify single nucleotide polymorphisms (SNPs).[93] For example, SNPs mutation can be detected using fluorescent hybridization probes in conjunction with fluorescence melting analysis and/or real-time polymerase chain reaction (PCR). As shown in Figure 1.24, the T_m value (melting temperature) of a fluorescent probe hybridised to a fully complementary target (green, WT) can be distinguished from its duplex with mutant target (peak, MT) due to the reduced stability caused by a single nucleobase substitution, insertion or deletion. This is because the mutant duplex contains a mismatched base pair.

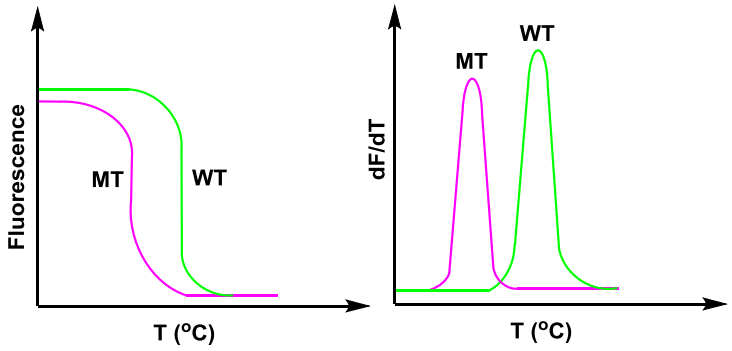

Figure 1.24. Idealised discrimination between wild-type (WT, green) and mutant (MT, pink) sequences during fluorescence melting analysis due to base pair mismatch formation.

Most of these oligonucleotide probes involve a fluorophore that is linked to a quencher. In the unhybridised state, the fluorophore is quenched by collisional or FRET mechanisms that are deactivated upon binding to the complementary strand. The general structures and mechanisms of action for some of these probes are discussed here (e.g. Molecular beacons (MBs)[88,95,96] and HyBeacons™ [77,97,98]).

1.7.1 Molecular beacons

Molecular beacons were first reported by Tyagi *et al.* in 1996.[95] The probes are single-stranded nucleic acids that are labelled with a fluorophore at one end and a quencher at the other. These probes are designed such that there is a loop portion (15–30 nucleotides long), which is complementary to the target sequence, and two arm sequences (5–7 nucleosides long) that are complementary to each other (but are not complementary to the target).[88,99] The sequence of the oligonucleotide enables an internal stem-loop structure to form[100,101] (Figure 1.25), thereby keeping the fluorophore and quencher in close proximity to each other and allowing efficient collisional quenching. Upon annealing to the complementary target, the stem-loop opens up, the fluorophore and quencher are separated, thereby generating strong emission.

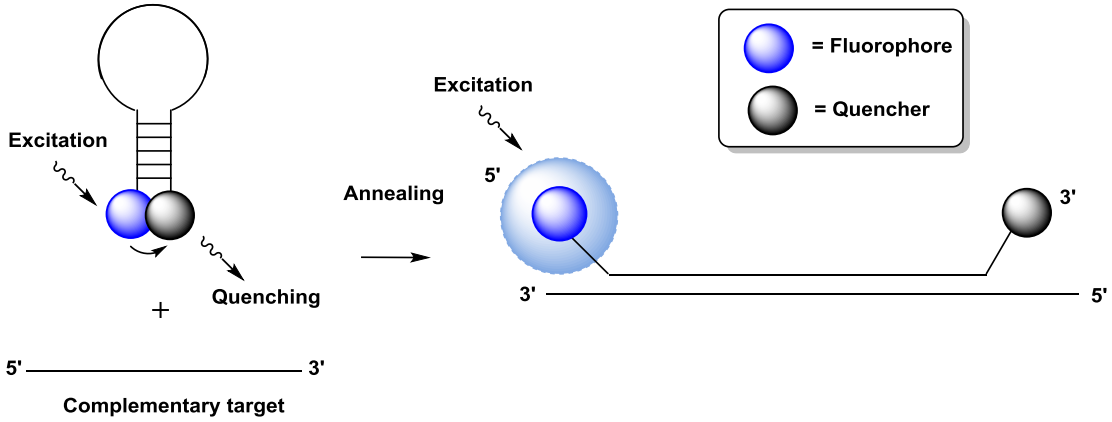

Figure 1.25. Schematic representation of molecular beacon interacting with the target sequence. On their own, molecular beacons are non-fluorescent due to fluorescence quenching. Once hybridised to the target, a rigid duplex is formed that separates the fluorophore and quencher, and restores fluorescence.

1.7.2 HyBeacon probes

HyBeacon probes are single-stranded oligonucleotides, containing two or more fluorophores covalently attached to one or more internal nucleotides, either on the nucleobase (major groove) or at the 2′-position of the sugar (minor groove). These probes show high fluorescence when hybridised to the complementary DNA target and low fluorescence in the unstructured single-stranded state due to inherent fluorescence quenching (Figure 1.26). Upon hybridization, the melting temperature of the duplex between a HyBeacon probe and a fully complementary target sequence is significantly higher than when it is bound to a mutant target (which contains a mismatched base pair). This provides a rapid method for detection and identification of single nucleotide polymorphisms (SNPs),[76] short tandem repeats (STRs),[97] as well as allele discrimination and mutation detection. HyBeacons have been employed in a variety of diagnostic applications *via* real-time PCR.[97,98] A combination of six HyBeacon probes has been used to simultaneously analyse mutations in a six-channel "one-color-per-locus" system for genetic analysis of cystic fibrosis mutations by DNA fluorescence melting analysis.[77]

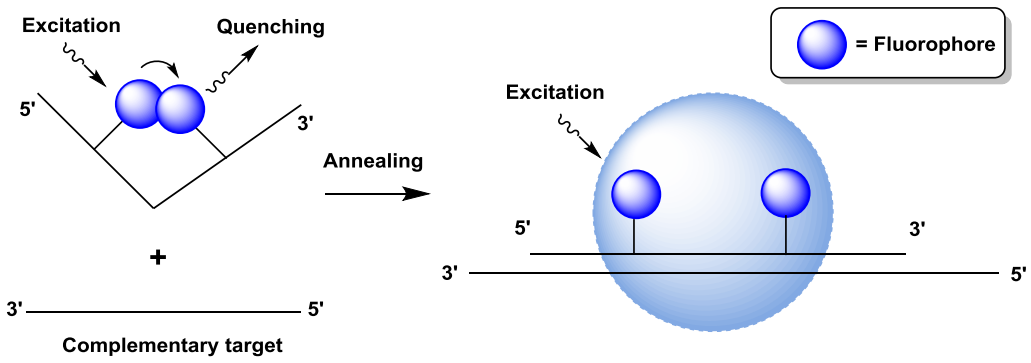

Figure 1.26. Schematic representation of HyBeacon probe interacting with the target sequence. On their own, the molecules are only weakly fluorescent due to internal fluorescence quenching. Once hybridised to the target, a rigid duplex is formed that separates the fluorophores, thereby restores fluorescence.

1.8 Asymmetric cyanine dyes

Whilst hybridization probes have found wide applications,[76,77] simple fluorescently-labelled nucleic acid probes can give strong fluorescent backgrounds, in part due to failed hybridization or excess probes binding to biological material non-specifically. The excess fluorescence can produce false-positive signals even at low concentrations, thus impeding highly sensitive measurements such as live cell imaging of RNA or genomic DNA. Therefore, it is necessary to develop new nucleic acid probes, and in particular fluorophores, to increase fluorescence sensitivity and selectivity. To this end, intercalating asymmetric cyanine dyes such as thiazole orange (TO) and benzothiazole orange (BO) are promising candidates since they are only fluorescent upon duplex formation and intercalation.

1.8.1 Thiazole orange (TO)

The asymmetric cyanine dyes are a valuable family of fluorophores, consisting of two different heteroaromatic fragments connected by one or more bonds that allow full conjugation.[102] An example of these dyes is thiazole orange (TO, Figure 1.27). It consists of a benzothiazole and quinoline moiety that are connected by a methine bridge. TO is an excellent photophysical probe for DNA binding since it is almost non-fluorescent in solution but its emission increases *ca.* 18,900-fold upon binding to DNA or RNA duplexes.[103-105] This is due to TO intercalation between the base pairs, reducing rotation around the methine bridge of the two aromatic systems to provide a planar fully conjugated system – In contrast, the unbound dye is not fully conjugated and when irradiated suffers from non-radiative decay.[106] Benzothiazole orange (BO, Figure 1.27) is

structurally related to TO, but has lower binding affinities to DNA duplexes, and also has lower absorbance.[107]

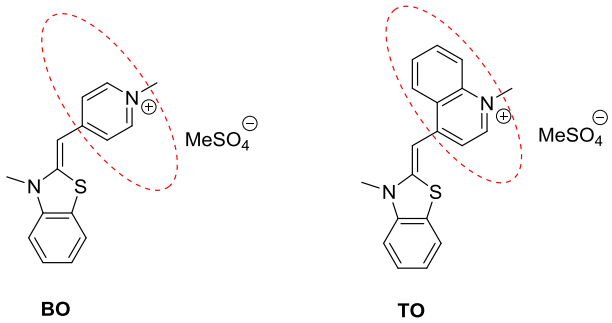

Figure 1.27. Examples of asymmetric cyanine dyes: benzothiazole orange (BO) and thiazole orange (TO).[107]

These interesting properties have prompted studies of their direct covalent attachment to nucleic acids. This can be achieved using TO derivatives TO_B and TO_Q (Figure 1.28), where attachment is *via* one of the two endocyclic nitrogens.[103] The nitrogen atom in quinoline is oriented to the DNA minor groove, while the nitrogen atom in benzothiazole is directed towards the major groove.[108] Privat *et al.*[109,110] have reported that the TO_Q-DNA conjugates gave higher stability and fluorescence when TO_Q was directed toward the minor groove of DNA duplexes. This result is consistent with an NMR study of TO dimer (i.e. TOTO) intercalating into the DNA duplex through the minor groove with the quinoline ring located between two purine bases.[111] Conversely, TO_B gave stronger fluorescence and greater stabilization when orientated towards the major groove.[103] This could be due to the different dihedral angle along methine bridge of the chromophore and linker; TO_B has a smaller dihedral angle (69.0°) while TO_Q has a dihedral angle around 170.7° and is less stable.[103] In addition, when TO_B was incorporated at the 5-postion of thymidine, the resulting oligonucleotide gave lower fluorescence in the absence of a complementary strand and higher fluorescence quantum yields than the TO_Q-DNA probes

upon hybridization to their targets. The emission was blue-shifted by 6 nm (530 to 524 nm) and the excitation was redshifted by 4 nm (511 to 515 nm).[112]

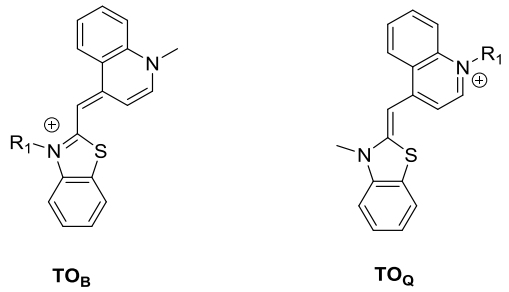

Figure 1.28. General structures of two thiazole orange (TO_B, TO_Q) analogues.[103] R_1: a hydrophobic alkyl $(-CH_2-)_{10}$ or a hydrophilic ethylene glycol chain $-CH_2$ $(-CH_2-O-CH_2-)_3$ CH_2-. TO_B: the linker is attached at the endocyclic nitrogen of the benzothiazole ring, TO_Q: the linker is attached at the endocyclic nitrogen of the quinoline ring.

1.8.2 Incorporation of TO into nucleic acids

TO can be attached to nucleic acids during solid phase oligonucleotide synthesis or post-synthetically on the sugar ring, nucleobase or phosphate backbone. For example, TO was attached to the central inter-nucleotidic phosphate group (Rp and Sp) of a pentadeca-2′-deoxyriboadenylate *via* a hydrophobic alkyl or a hydrophilic ethylene glycol chain by Privat *et al.* (Figure 1.29 A).[109,110] TO_B was coupled to the 5-position of 2′-deoxyuridine nucleosides with an alkyl linker (Figure 1.29 B) through the use of its phosphoramidite.[113] TO-DNA probes were also synthesised in which the TO served as an artificial DNA base (added *via* a phosphoramidite) (Figure 1.29 C).[114-116] It has no significant effect on the thermal stability when the "TO nucleotide" (Figure 1.29 D) is incorporated into the DNA strand, but displays up to 12-fold enhancement of fluorescence emission upon hybridization.[117] TO_B functionalised with an azide group can also be joined

post-synthetically to commercially available 2′-*O*-propargyl uridine *via* CuAAC (Figure 1.29 E).[118] Whilst the BO dye has attracted much interest due to its excellent nucleic acid staining properties,[119] there have been fewer reports of its use as a fluorescent "on-off" nucleic acid probe than for its analogue TO.

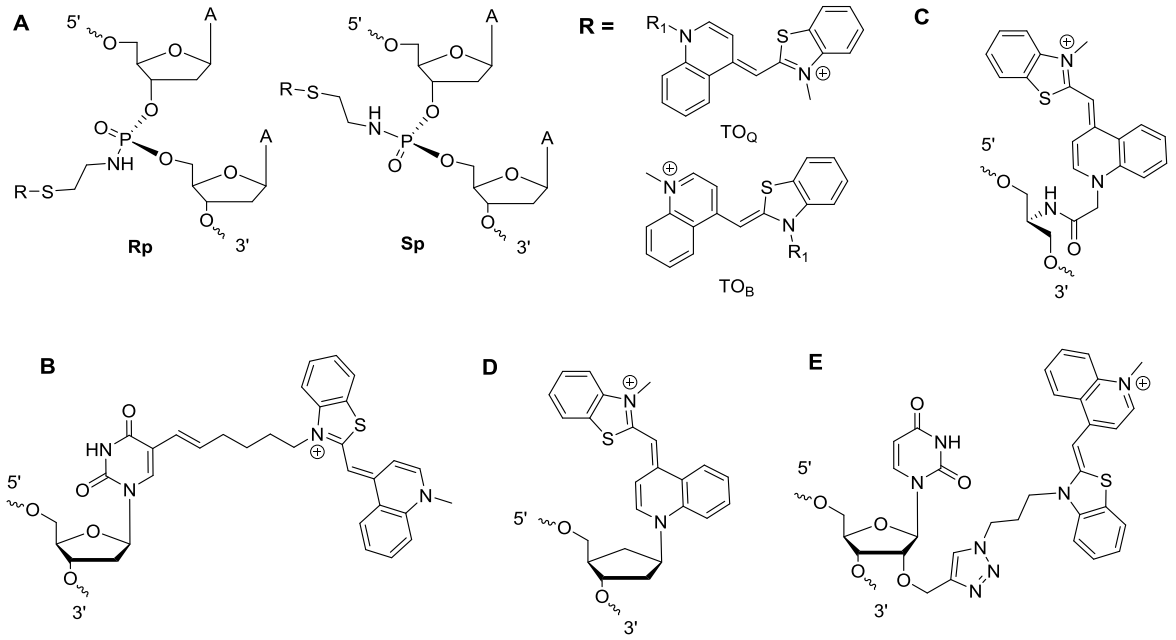

Figure 1.29. Examples of TO-modified DNA strands. A: TO was attached to the inter-nucleotidic phosphate. R_1: a hydrophobic alkyl $(-CH_2-)_{10}$ or a hydrophilic ethylene glycol chain $-CH_2(-CH_2-O-CH_2-)_3CH_2-$;[109,110,120] B: TO_B was attached to the 5-position of thymidine;[113] C: TO_Q as fluorescent universal nucleoside;[114] D: TO_Q as base surrogate;[117] E: TO_B was clicked to 2′-*O*-propargyl uridine.[118]

Recently, Okamoto *et al.* have developed hybridization probes where two TO dyes (Figure 1.30 A) were coupled to a double amino-modified pyrimidine base to obtain DNA and RNA TO-probes.[121-124] TO emission was suppressed before target hybridization due to an excitonic interaction produced by H aggregate formation between the dyes. This interaction was then disrupted after hybridization giving rise to strong fluorescence emission.[104,123,125,126] The same group designed another three intercalating fluorescent dyes

(Figure 1.30 B, C and D) by coupling methylquinoline to benzothiazole or benzoxazole with different bridges. These dyes were subsequently incorporated into DNA strands for further investigations of their fluorescence properties before and after hybridization to their complementary DNA targets.[127] The coloured probes showed good fluorescence intensities in their hybridised states, whilst their fluorescence was quenched in their unhybridised states. These probes were also used in multicolour RNA imaging in living cells.[128]

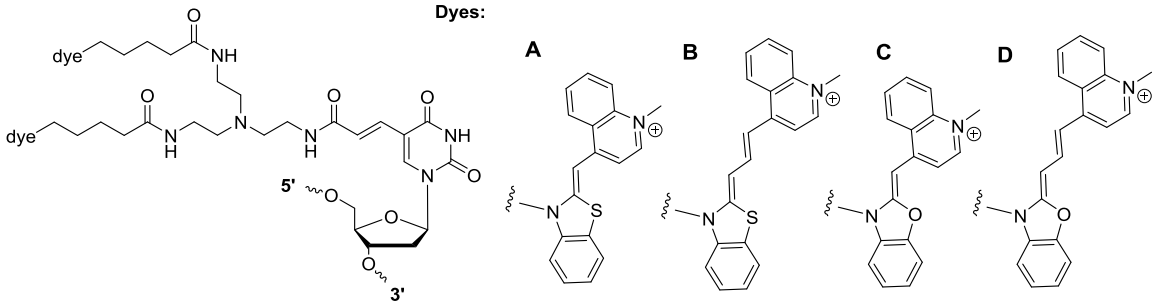

Figure 1.30. Structures of excitonic-interaction-controlled fluorescent probes for nucleic acid detection (doubly fluorescent dyes labelled nucleotides). A: TO ($\lambda ex_{max}/\lambda em_{max}$ = 511 nm/530 nm); B: TO-3 ($\lambda ex_{max}/\lambda em_{max}$ = 641 nm/659 nm); C: YO ($\lambda ex_{max}/\lambda em_{max}$ = 487 nm/506 nm). D: YO-3 ($\lambda ex_{max}/\lambda em_{max}$ = 608 nm/630 nm).

1.8.3 Applications of TO derivatives in nucleic acids

TOTO is a fluorescent bis-intercalating cyanine dye, with low fluorescence in solution. However, as with other cyanine dyes, when TOTO is bound to double strand DNA, its fluorescence is significantly enhanced, and has proven very useful for a variety of DNA applications.[129] TOTO has been widely applied in gel electrophoresis[105] as a high-performance nucleic acid stain, because it is stable during electrophoresis and has a large fluorescence enhancement (> 3000-fold) upon binding to double-stranded DNA.[130] The detection sensitivity of the TOTO-dsDNA complex is around 10 times higher than that

attained by ethidium homodimer (EthD), which is 50 times more sensitive than the conventional ethidium bromide. Rye *et al.* have reported F_{bound}/F_{free} values of 1100 for TOTO compared to 35 for EthD.[105] Furthermore, TO derivatives have been synthesised to label breast cancer cells,[131] and TO-DNA fluorescence hybridization probes have been known to be able to target the specific complementary RNA targets with 7-fold fluorescence enhancement.[113] This probe was used to detect very low levels of cyclin D1 mRNA, which is a marker for the diagnosis of breast cancer. The dye-modified DNA duplex featured multiple TO units, which were covalently attached to the DNA *via* triazole linkages. The intercalating dyes stabilized the duplex and gave strong fluorescence in the green region of the spectrum, which could be changed to the orange and red regions *via* FRET by addition of Cy3 and Cy5 dyes.[112] The dye-modified DNA duplex was then attached to a secondary antibody that was used in the centrosomes of *Drosophila* embryos for intracellular fluorescence imaging with a lower background signal. The double TO-labelled hybridization RNA probes showed high resistance against nucleases compared to the corresponding DNA probes in *in vivo* detection, and could be used for long-term monitoring of intracellular RNA based on inter-dye excitonic interactions.[123] These double labelled fluorescent "on-off" probes were also useful for quantitative and bioimaging assays, such as dot blotting assays. The fluorescence of the blot spots was read immediately at room temperature without the requirement for numerous washing or antibody and enzyme-treating steps.[121] Benzothiazole orange (BO) has also attracted much interest due to its significant fluorescent enhancement (400-fold) upon DNA binding.[102,119] Interestingly, BO has also been shown to be a fluorescent ligand that can bind to specific sites in DNA duplexes and DNA-RNA hybrids.[132] However, there are fewer reports of BO-modified nucleic acids used as fluorescent probes.

1.9 Research aims

There is a growing demand for very long and pure oligonucleotides – both natural and modified – for applications ranging from gene synthesis to live cell imaging.[133-135] With regards to length, oligonucleotide synthesis is limited by imperfect coupling efficiency and chemical lesions caused by side-reactions. Thus it would be beneficial to design an inexpensive and simple method to conjugate shorter oligonucleotide to form very large ones. Chapter 2 focuses on the use of the copper-catalysed azide-alkyne cycloaddition (CuAAC) reaction, whilst Chapter 3 discusses oligonucleotide ligation using the strain-promoted alkyne-azide cycloaddition (SPAAC) to synthesise long oligonucleotides on the solid phase.

This click chemistry is then exploited to label nucleic acids with fluorophores for use as probes.[136] Chapter 4 demonstrates labelling by SPAAC chemistry. DIBO- and BCN-thymidine monomers are incorporated into oligonucleotides for multiple labelling. In addition, the SPAAC methodology is used to join oligonucleotides together to obtain a permanently fixed, stable duplex without the risk of collisional quenching by fluorophores. FRET studies are carried out to evaluate these systems and the stability of the BCN monomer is also discussed in this chapter.

Due to the fluorescent backgrounds of traditional nucleic acid probes,[104,137] new probe systems are highly desirable. In this regard, TO-DNA (Chapter 5) and BO-DNA (Chapter 6) conjugates are developed and their fluorescence / thermal stabilities are discussed. They are then labelled with a different fluorophore by click chemistry (CuAAC). These modified probes are studied by fluorescence melting and room temperature fluorescence. Also, a two-probe system is designed to quantitatively and qualitatively

detect the CFTR R516G mutation by simultaneously monitoring two channels of CFX96^{TM} in real-time PCR.

CHAPTER 2

CuAAC-mediated click ligation of oligonucleotides on the solid phase

Chapter 2 – CuAAC-mediated click ligation of oligonucleotides on the solid phase

2.1 Introduction

There is considerable interest in producing long DNA constructs *in vitro* for use in gene synthesis[138,139] and nano-construct formation.[140,141] Methods have therefore been sought to prepare long oligonucleotides on a large scale by chemical synthesis or on a small scale by enzymatic synthesis. To this end, the solid phase phosphoramidite method has been developed, which is a highly efficient process for the synthesis of oligonucleotides up to *ca.* 150 nucleotides in length.[142,143] However, synthesis of longer oligonucleotides is limited by imperfect coupling efficiency and chemical modifications during oligonucleotide synthesis, as well as the associated difficulty in the purification of long oligonucleotides.[73,84] Alternatively, the polymerase chain reaction (PCR) allows the amplification of specific oligonucleotide templates, and the assembly of DNA fragments up to a total of *ca.* 35 kilo-base pairs.[71] However, PCR-based DNA synthesis[144,145] is normally used on a small scale, and does not allow the incorporation of different modifications at specific loci (e.g. methylated cytosine[146]), thus limiting its scope in biological applications. To solve this problem, enzymatic ligation of oligonucleotides[147] can be carried out to produce large DNA fragments, but some modified nucleobases are not tolerated by ligase enzymes. In addition, the scale of ligase-based DNA assembly is limited and ligases can produce misassembled DNA products. Therefore, it would be interesting and valuable to develop a purely chemical method to make large-scale chemically-modified DNA constructs.

Click chemistry has been widely applied in the nucleic acid field due to its high selectivity, remarkable efficiency and suitability for large-scale applications.[148,149] The most popular

click reactions are the Cu(I)-catalysed azide-alkyne cycloaddition (CuAAC) and strain-promoted alkyne-azide cycloaddition (SPAAC). The CuAAC reaction is one of the most efficient, chemoselective ligation reactions available, giving only 1,4-disubstituted 1,2,3-triazoles.[32,36] In previous studies, the CuAAC approach has been developed for the chemical ligation of oligonucleotides using 5′-alkyne and 3′-azide modified DNA strands. Whilst the reaction proceeds in near quantitative yield in the presence of a template oligonucleotide, the linkage is very long and cannot be read through by DNA polymerases.[45] Subsequent work focussed on shorter biocompatible triazole linkages, which are discussed in more detail in Section 1.4 (Chapter 1). The most promising of these linkages is **tz1** (Figure 2.1) that can be formed from the CuAAC reaction between 5′-azide and 3′-alkyne modified oligonucleotides. The CuAAC reaction requires a copper catalyst, prepared with the water-soluble tris(3-hydroxypropyltriazolylmethyl)amine ligand (THPTA, Figure 2.1, **2-1**) which binds to copper in its Cu(I) oxidation state. The **tz1** linkage mimics the natural phosphodiester linkage, and as a result can be read through accurately by DNA polymerases. It was the first example of a backbone modification that is biocompatible in *Escherichia coli* and in human cells.[73]

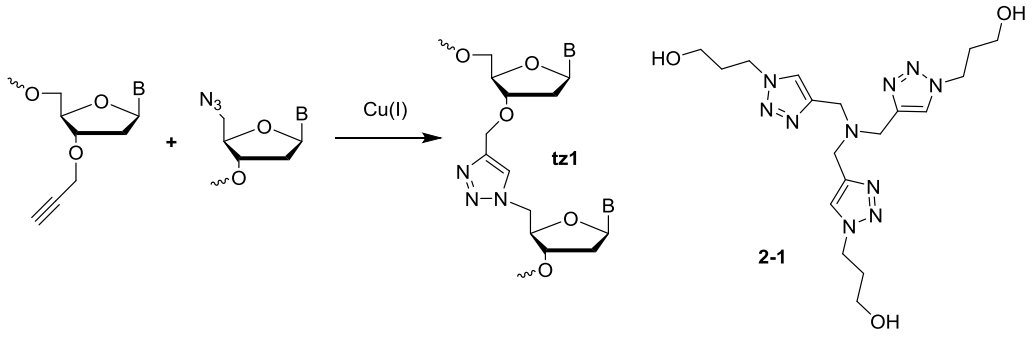

Figure 2.1. The structure of DNA triazole linkage (**tz1**) and the Cu(I)-binding ligand THPTA **2-1**.

This chapter describes the development of a simple and efficient method to conjugate two oligonucleotides on the solid phase. The kinetics of solid phase reactions are typically three orders of magnitude slower than the same reactions in solution, due to the limitation of diffusion of the reagents into the solid supports.[150] However, solid phase synthesis remains of interest because it overcomes the technical difficulties with solubility and purification associated with solution chemistry; it is also amenable to automation, especially for peptide synthesis[151,152] and oligonucleotide synthesis.[19,153] Importantly, a large excess of reagents can be used to drive the reactions to completion since the unwanted materials can be easily removed by filtration.

2.2 Synthesis of oligonucleotides

To assess the feasibility of CuAAC ligation of oligonucleotides on the solid phase, it was necessary to introduce the azide and alkyne functional groups. For synthetic reasons that are discussed in subsequent sections of this chapter, azides were placed at the 5′-position of oligonucleotides and left on the resin, whilst alkynes were placed at the 3′-position and were the solution phase component of the reaction. The oligonucleotides used in this study are listed in Table 2.1.

Types	Codes	Sequences	Mass found (calc.)
3′-alkyne ODNs (in solution)	ODN2-1	TTX3′	886 (888)
	ODN2-2	TTTTTTTTTTX3′	3321 (3321)
	ODN2-3	GCATTCATGTX3′	3359 (3359)
	ODN2-4	CCTATCTCGTTGTTGTTAGTGAATCTCTGTACTTTAGTGACCAGTTGGGATCTAGTGAAX3′	18534 (18535)
5′-azide ODNs (on the solid phase)	ODN2-5	5′ N_3-TTTTTTTTTTTT-500Å resin	3613 (3613)
	ODN2-6	5′ N_3-TCCCTTCCTCTTTTTTT-1000Å resin	5044 (5044)
	ODN2-7	5′ N_3-TCCCTTCCTCTTTTTTT-3000Å resin	5044 (5044)
	ODN2-8	5′ N_3-TCAGCATTCTATGTGTTAGTCCGGTGTTGATACTCGCATGACAGTGGAGAGGCATTTGCCT-3000Å resin	18872 (18872)
click-ligated ODNs	ODN2-9	ODN2-1-**tz1**-ODN2-5	4501 (4501)
	ODN2-10	ODN2-2-**tz1**-ODN2-5	6934 (6934)
	ODN2-11	ODN2-3-**tz1**-ODN2-5	6972 (6972)
	ODN2-12	ODN2-3-**tz1**-ODN2-6/7	8403 (8403)
	ODN2-13	ODN2-4-**tz1**-ODN2-7	23579 (23579)
	ODN2-14	ODN2-3-**tz1**-ODN2-8	22232 (22231)

Table 2.1. Oligonucleotides used in the CuAAC ligation reactions (mass spectra data in Appendix, Figure 9.1.1). 5′ N_3 = 5′-azido, prepared by converting a 5′-iodo group to azide (ODN2-6, ODN2-7, ODN2-8), or prepared by converting a 5′-OH group to a 5′-iodo group, then to azide (ODN2-5); X3′ = 3′-*O*-propargyl-5-methyl-deoxycytidine; click-ligated ODNs (ODN2-9–ODN2-14) with a linkage: **tz1** (Figure 2.1).

2.2.1 Synthesis of 3′-alkyne ODNs

To prepare 3′-alkyne ODNs, the alkyne-functionalised monomer 5′-*O*-(4,4′-dimethoxytrityl)-3′-*O*-propargyl-5-methyl-deoxycytidine **2-5** was first coupled to a polystyrene solid support, using standard conditons before use in solid phase oligonucleotide synthesis. The functionalised solid support was prepared in 4 steps from commercially available materials as shown in Scheme 2.1.[154]

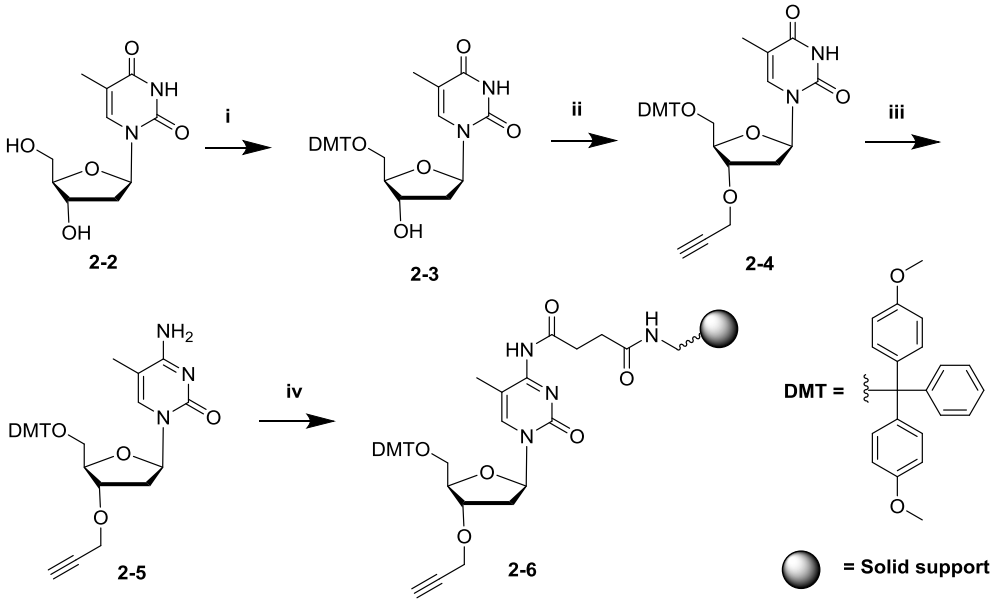

Scheme 2.1. Synthesis of 5′-*O*-(4,4′-dimethoxytrityl)-3′-*O*-propargyl-5-methyl-deoxycytidine on polystyrene solid support **2-6**. Reagents and conditions: (i) DMTrCl, pyridine, RT, 16 h, 47%; (ii) NaH, propargyl bromide, THF, RT, 12 h, 46%; (iii) *N*-methylimidazole, 0 °C, 15 min; phosphorus oxychloride, 0 °C, 30 min and RT, a further 30 min; aq. ammonia solution, RT, 19 h, 49%; (iv) diisopropylcarbodiimide (DIC), hydroxybenzotriazole (HOBt), succinylated aminoalkyl solid support, RT, 20 h.

Initially the 5′-hydroxyl group of thymidine was protected using 4,4′-dimethoxytrityl chloride (DMTrCl) to afford 5′-protected compound **2-3** in 47% yield. The 3′-hydroxyl group was then alkylated with propargyl bromide in the presence of sodium hydride in

THF to give compound **2-4** in a yield of 46%. Next, the thymine base was converted to 5-methylcytosine by treating **2-4** with *N*-methylimidazole, phosphorus oxychloride and aqueous ammonia solution affording **2-5** (49%). Finally the functionalised solid support was prepared by coupling nucleoside **2-5** to a succinylated aminoalkyl solid support (GE Healthcare custom primer support™ amino, 200) with diisopropylcarbodiimide (DIC) and hydroxybenzotriazole (HOBt). The loading of 5′-*O*-(4,4′-dimethoxytrityl)-3′-*O*-propargyl-5-methyl-deoxycytidine was determined from DMT group cleavage to be 22–24 μmol g^{-1}, which is ideal for efficient solid phase oligonucleotide synthesis (see Experimental, Section 8.2.2 for more details).

2.2.2 Synthesis of 5′-azide ODNs

Due to the incompatibility of the azide group with P(III) chemistry,[72] a modified strategy was developed for the synthesis of 5′-azide ODNs (Table 2.1). They were prepared on the resin by post-synthetic conversion of the 5′-hydroxyl group to an iodo moiety, which was then converted to a 5′-azide (Scheme 2.2). For the first of these steps, the oligonucleotides attached to the synthesis column, with a free 5′-OH, were treated with methyltriphenoxyphosphonium iodide in DMF at room temperature for 15 minutes. Alternatively, the commercially available 5′-iodo-dT phosphoramidite monomer (Glen Research) was used to avoid this additional manual hydroxyl to iodo conversion. Subsequent treatment with sodium azide in anhydrous DMF at 55 ºC for 4 h produced the desired 5′-azide functionalised oligonucleotides.

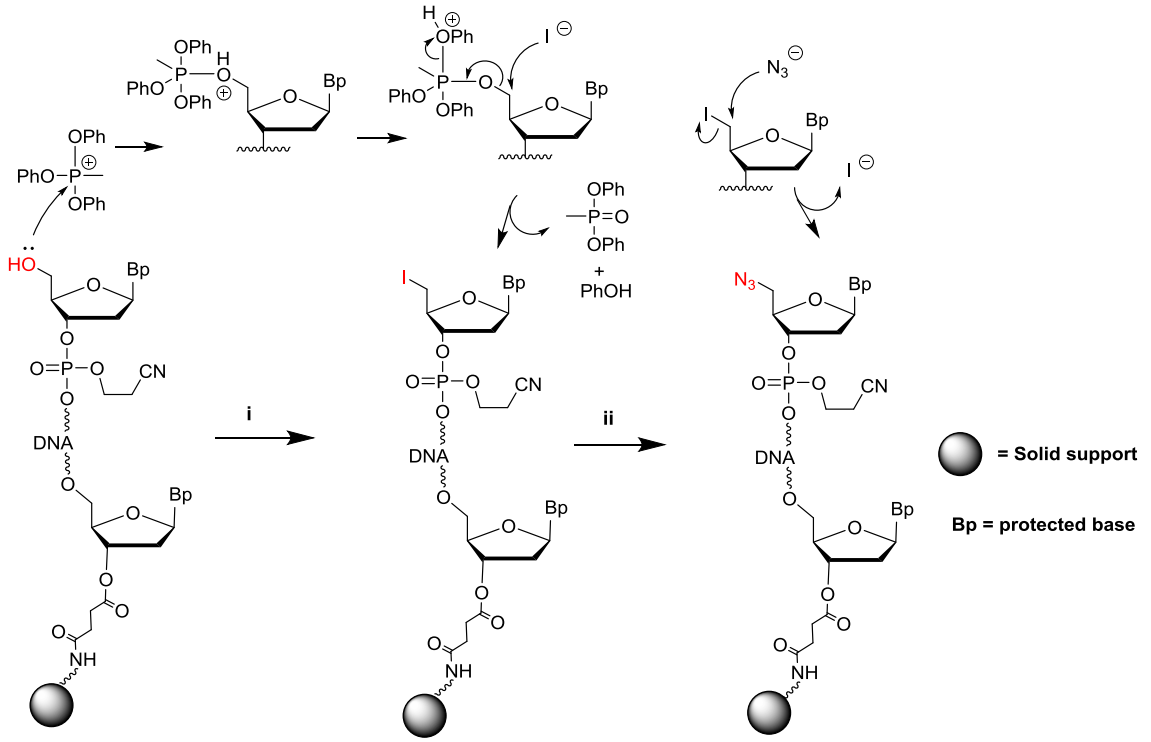

Scheme 2.2. Synthesis of the 5′-azide DNA strands and the mechanisms of the reactions. Reagents and conditions: (i) $[MeP(OPh)_3]^+I^-$, anhydrous DMF, RT, 15 min; (ii) NaN_3, anhydrous DMF, 55 ºC, 4 h.

2.2.3 Deprotection of 5′-azide ODNs

ODN2-5 is a 12-mer oligonucleotide containing only thymines, and therefore possesses no nucleobase protecting groups.[1] The significantly longer mixed bases ODN2-8 (61-mer) was also prepared and the protecting groups were not removed for the ligation reactions, its analysis after deprotection by mass spectrometry is shown in Figure 2.2. However, for ODN2-6 (17-mer on 1000 Å resin) and ODN2-7 (17-mer on 3000 Å resin) that contain cytosines and thymines, the cytosines were deprotected. This was to allow their use in the templated SPAAC reactions (discussed in Chapter 3). For these cytosines, the *N*(4) amine group was protected using Fmoc. This enabled deprotection of the oligonucleotides on the solid phase with 20% piperidine in DMF, which does not cause cleavage of the

oligonucleotide from the resin. To prepare the required Fmoc-protected dC phosphoramidite **2-8**, the 5′-DMT-*N*(4)-Fmoc-2′-deoxycytidine **2-7** nucleoside was phosphitylated as shown in Scheme 2.3.

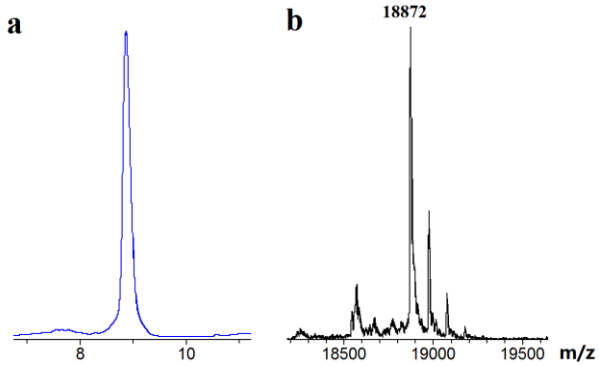

Figure 2.2. a: HPLC chromatogram of crude oligonucleotide ODN2-8 (61-mer), and b: mass spectrum (ESI^-) of ODN2-8 (calc.: 18872, found: 18872). In the mass spectrum, the main peak after the correct mass peak is the Et_3N adduct of the desired product.

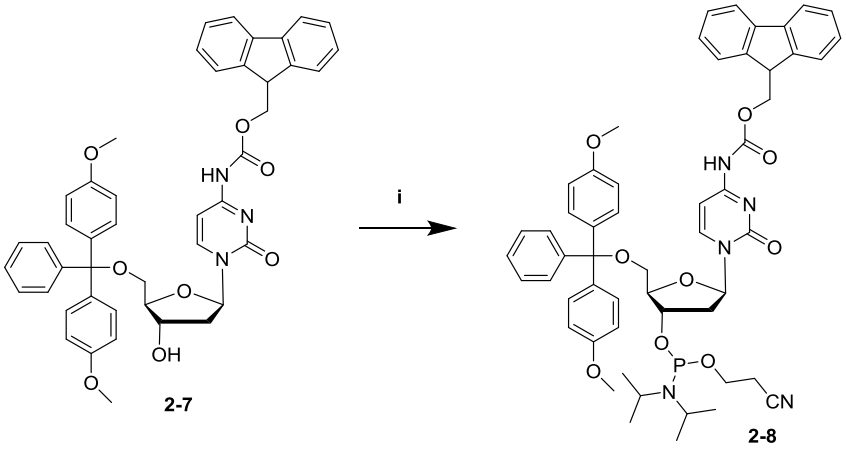

Scheme 2.3. Phosphitylation of 5′-DMT-*N*(4)-Fmoc-2′-deoxycytidine **2-7**. Reagents and conditions: (i) anhydrous DCM, DIPEA, 2-cyanoethyl *N*,*N*-diisopropylchlorophosphoramidite, RT, 1.5 h, 79%.

Two strategies were considered for the conversion of 5′-iodo to 5′-azide and cleavage of the Fmoc protecting group (Scheme 2.4). In method A, the 5′-iodo was first converted to the 5′-azide before deprotection of the cytosine bases. This afforded the 5′-azide oligonucleotide on the resin, which was then cleaved from resin for analysis by mass spectrometry (Figure 2.3). In method B, the cytosines were first deprotected before conversion of the 5′-iodo to the 5′-azide using sodium azide in DMF. However, more than two thirds of the 5′-iodo thymidines reacted with piperidine to form 5′-piperidine products as confirmed by mass spectrometry (Figure 2.4). Comparison of the two strategies shows that the desired 5′-azide oligonucleotides were obtained in higher purity and yield by method A.

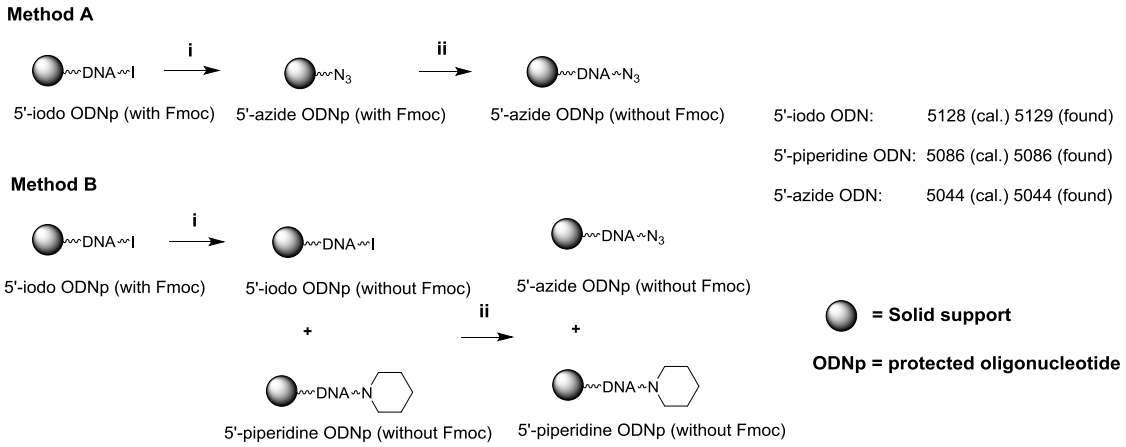

Scheme 2.4. Conversation of 5′-iodo to 5′-azide and deprotection of Fmoc-protected cytosines. Method A: (i) NaN_3, anhydrous DMF, 55 ºC, 4 h; (ii) 20% piperidine in DMF, RT, 20 min. Method B: (i) 20% piperidine in DMF, RT, 20 min; (ii) NaN_3, anhydrous DMF, 55 ºC, 4 h.

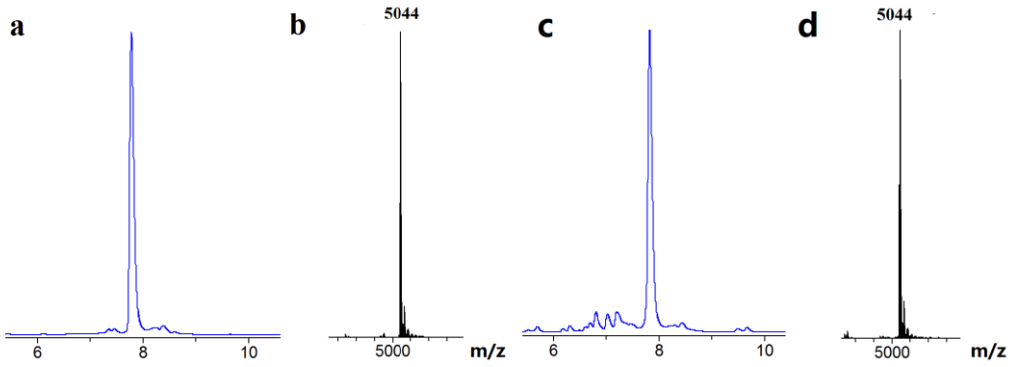

Figure 2.3. HPLC chromatogram of crude oligonucleotides ODN2-6 (17-mer, a) and ODN2-7 (17-mer, c) made by method A (Scheme 2.4), and mass spectra (ESI$^-$) of ODN2-6, b (calc.: 5044, found: 5044) and ODN2-7, d (calc.: 5044, found: 5044).

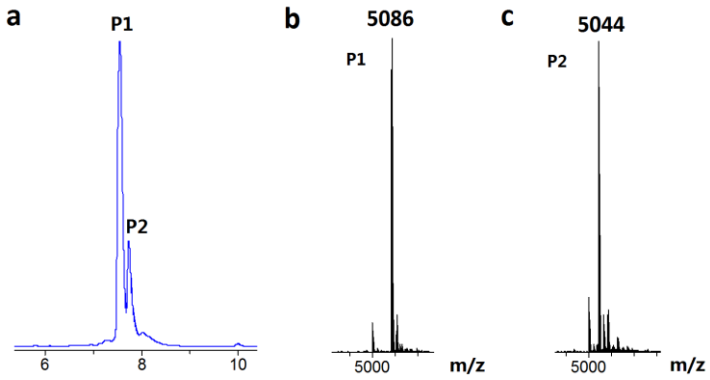

Figure 2.4. a: HPLC chromatogram of crude oligonucleotide ODN2-6 (17-mer) made by method B (Scheme 2.4); b: mass spectrum (ESI$^-$) of P1, the 5′-piperidine oligonucleotide (calc.: 5086, found: 5086); c: mass spectrum (ESI$^-$) of P2, the 5′-azide oligonucleotide (calc.: 5044, found: 5044).

2.3 DNA ligation by the CuAAC reaction on the solid phase

The CuAAC click reactions were carried out between the resin-bound 5′-azide ODNs and 3′-alkyne ODNs in solution, with the aim of preparing very long oligonucleotides containing the biocompatible artificial linkage **tz1** (Figure 2.1). Initially, DNA ligation conditions were optimised using short, simple sequences that contain only thymines (except the 5-methyl cytosine that contains the alkyne, i.e. 3′-alkyne ODN2-1 and

ODN2-2). 5′-azide ODN2-5 (12-mer on 500 Å resin) reacted with 5 eq. of 3′-alkyne ODN2-1 (3-mer, 0.3 mM, 40 µL, H_2O) at room temperature. The reaction time was varied from 3 to 22 h and a major product was clearly detected after the longest incubation time (22 h). The mass of the desired product was calculated to be 4501, but the mass of the main isolated product was 3946. This corresponds to an increase in molecular weight of starting OND2-5 of 333 (ODN2-5, calc.: 3613, found: 3613), indicating that a side reaction with a small molecule rather than ODN2-1 had occurred. As a result, the CuAAC reaction was repeated with 5′-azide ODN2-5 + 3′-alkyne ODN2-1 or 5′-azide ODN2-5 alone (i.e. omitting ODN2-1 from the reaction). In both cases, after 22 h the same product with a molecular weight of 3946 was found.

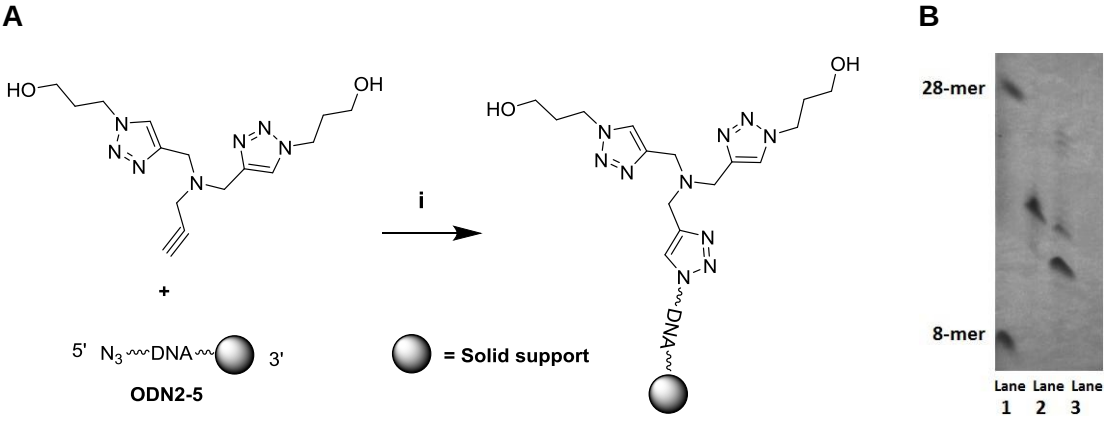

Figure 2.5. A: The CuAAC reaction between ODN2-5 and the bis(triazole). (i): $CuSO_4 \cdot 5H_2O$, sodium ascorbate, THTPA. B: 20% polyacrylamide gel. Lane 1: the marker dyes; lane 2: 22 h click reaction, mass of product = 3946; lane 3: 3 h click reaction, mass of product = 3613 (starting ODN2-5).

Given that the only small molecule involved in the reaction is the Cu(I)-binding ligand THPTA (provided by the Brown group), the purity of this compound was examined in greater detail. As reported by Jlalia *et al.*[155] the desired THPTA was obtained in 72% yield but could also be accompanied by mono- and bis(triazoles), with the molecular weight of

the bis(triazole) being 333 (Figure 2.5). Therefore, it was presumed that this alkyne impurity gave rise to the unexpected major product. To confirm this, the THPTA ligand was purified by column chromatography (Experimental, Section 8.2.1) and the reactions were repeated. As expected, the +333 molecular weight adduct was no longer obtained. This emphasizes the importance of using highly pure tris-triazole ligands in the CuAAC reaction.

The next variables that were altered were temperature and the concentration of 3′-alkyne ODNs. By simultaneously increasing both parameters, the reaction between ODN2-5 (12-mer on 500 Å resin) and 20 eq. of ODN2-1 (with only thymine bases, 3-mer) at 70 ºC for 21 h proceeded to completion, affording the ligated product ODN2-9 (Figure 2.6 a). This was repeated with ODN2-2 (with only thymine bases, 11-mer) giving *ca.* 90% conversion (Figure 2.6 c). When the temperature was decreased to 50 ºC for ODN2-1, the yield of the desired product ODN2-9 was reduced to 40% (Figure 2.6 b). The slightly higher yield with ODN2-1 suggests unsurprisingly that shorter ODNs are easier to couple to oligonucleotides on the resin, and higher temperature is beneficial for the reaction.

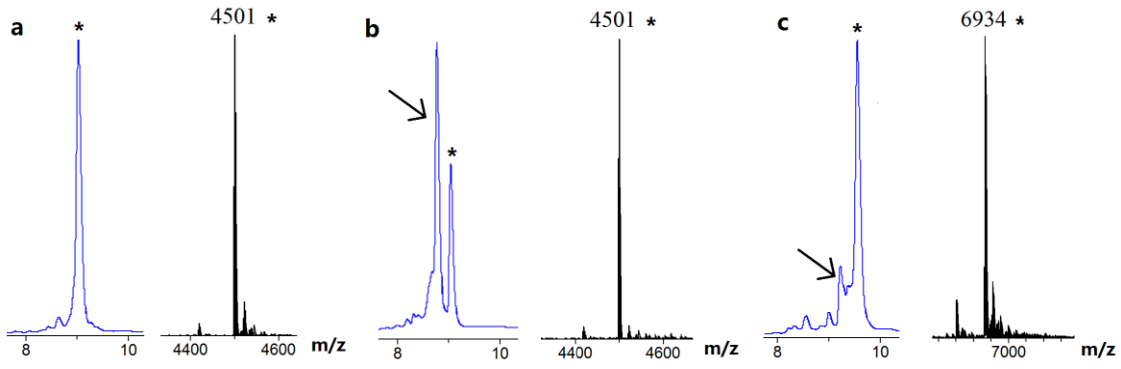

Figure 2.6. HPLC and MS characterisation of crude CuAAC-ligated products ODN2-9 (a, b) and ODN2-10 (c). a: ODN2-9 (70 ºC, 21 h), b: ODN2-9 (50 ºC, 21 h); c: ODN2-10 (70 ºC, 21 h). The arrows indicate starting material peaks (ODN2-5, calc.: 3613, found: 3613). The starred peaks correspond to the associated mass spectra (ESI⁻).

To further optimise these conditions, the effect of oligonucleotide concentration and reaction time were considered. The CuAAC reactions were carried out at 70 ºC for 5 or 21 h (Figure 2.7, Figure 2.8). The resin-bound 5′-azide ODN2-5 amount was kept constant (2.5 nmol), and 1, 3 or 10 eq. of 3′-alkyne ODN2-2 in 20 µL H_2O were used. Of these conditions, it was found that the best conversion (*ca.* 90%) from ODN2-5 to ODN2-10 was obtained using 10 eq. of ODN2-2 at 70 ºC for 21 h (Figure 2.7 c), and 3 eq. of ODN2-2 gave a slightly worse conversion (*ca.* 85%, Figure 2.7 b).

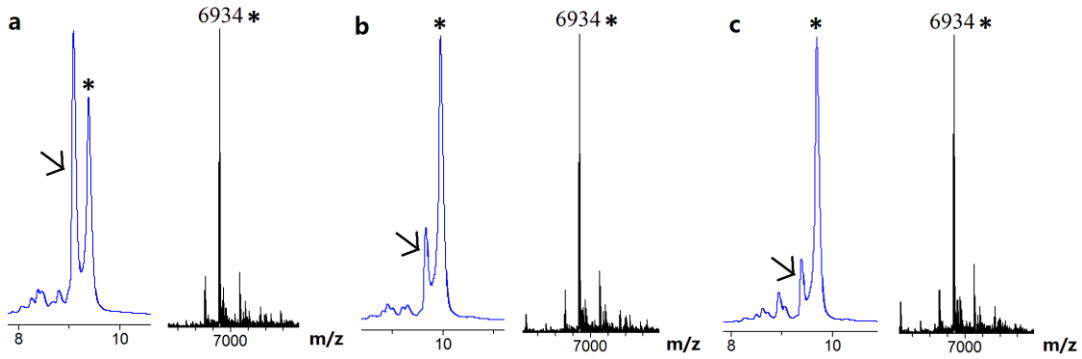

Figure 2.7. HPLC and MS characterisation of crude CuAAC-ligated product ODN2-10 (a, b, c: 70 ºC, 21 h). a: 1 eq. of ODN2-2; b: 3 eq. of ODN2-2; c: 10 eq. of ODN2-2. The arrows indicate starting material peaks (ODN2-5, calc.: 3613, found: 3613). The starred peaks correspond to the associated mass spectra (ESI^-).

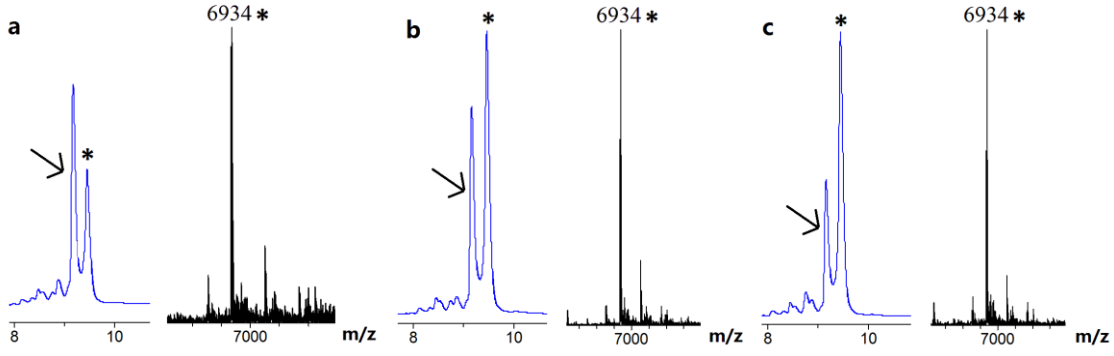

Figure 2.8. HPLC and MS characterisation of crude CuAAC-ligated product ODN2-10 (a, b, c: 70 ºC, 5 h). a: 1 eq. of ODN2-2; b: 3 eq. of ODN2-2; c: 10 eq. of ODN2-2. The arrows indicate starting material peaks (ODN2-5, calc.: 3613, found: 3613). The starred peaks correspond to the associated mass spectra (ESI^-).

In principle, it would be a good strategy if the reactions can be carried out at lower temperature or reduced reaction time, which reduces the chance of oligonucleotide degradation (e.g. acid-catalysed DNA depurination in unbuffered water, Scheme 2.5). However, the conversions had already been shown to be dependent on the reaction time and temperature.

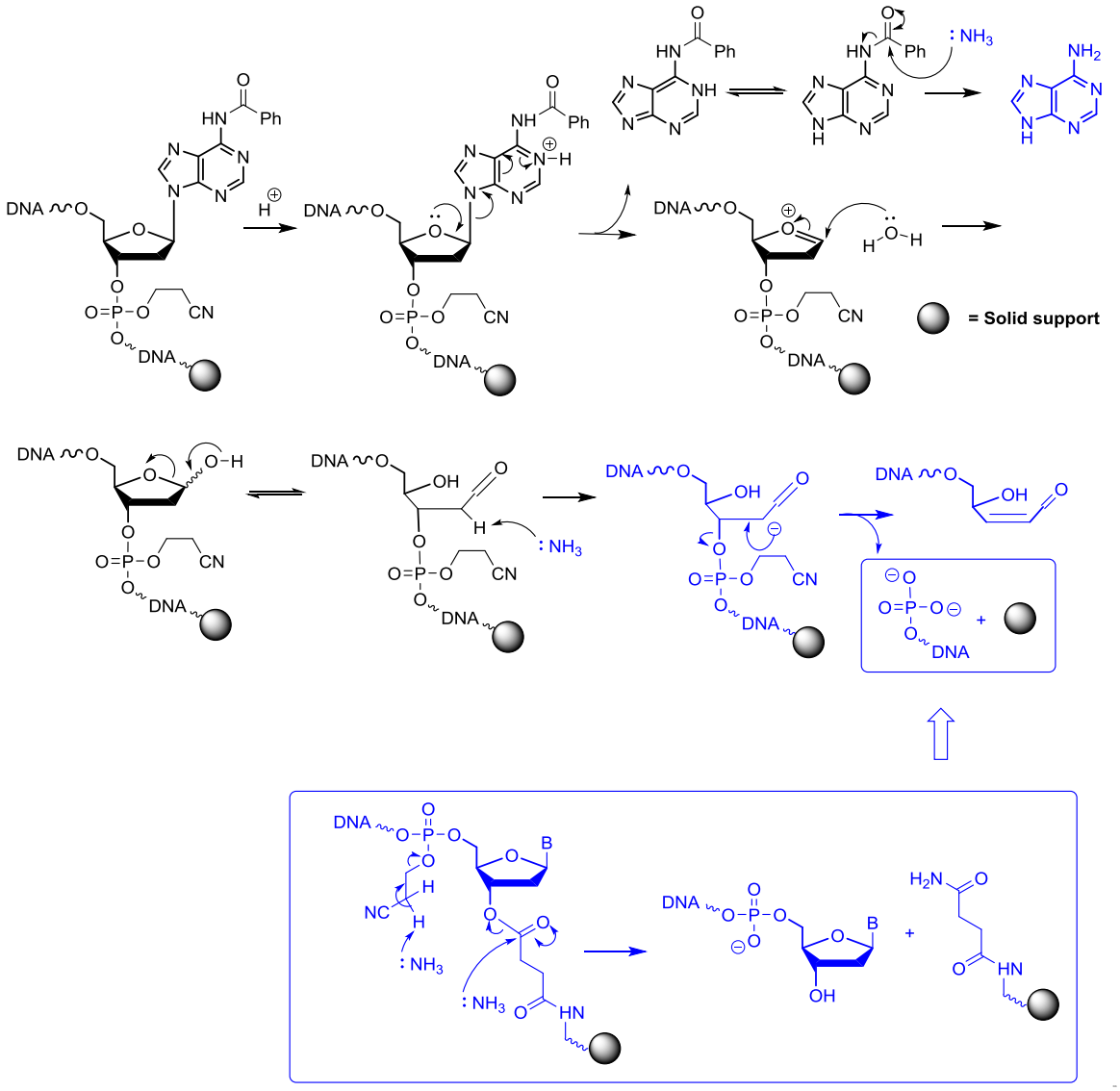

Scheme 2.5. Mechanism of acid-catalysed depurination and DNA chain cleavage.

Next, the optimization of reaction conditions was carried out using the solvents with different dielectric constants/dipole moments. The following combinations were used: 100% H_2O, 50% aqueous acetonitrile, 50% aqueous DMF and 50% aqueous THF. The reactions were carried out on ODN2-5 (12-mer on 500 Å resin) using the conditions (70 ºC, 21 h, 3′-alkyne ODNs: 0.75 mM, 15 µL), which were shown to be the best in the previous studies for solid phase DNA ligation by the CuAAC reaction.

Reaction in 50% aqueous acetonitrile at 70 ºC for 21 h produced unknown degradation products, resulting in less than 50% conversion to the desired product (Figure 2.9 b). This degradation could be due to acid-catalysed DNA depurination in unbuffered 50% aqueous acetonitrile, as mentioned above (Scheme 2.5). When the reactions were performed in 50% aqueous DMF or 50% aqueous THF at 70 ºC for 21 h, the best conversion to the desired product was obtained (> 95%), and almost no oligonucleotide degradation was detected by HPLC (Figure 2.9 c, d), whereas in H_2O, a small amount of starting material remained (> 90% conversion, Figure 2.9 a). This result indicates that 50% aqueous THF and 50% aqueous DMF are good choices for the solid phase CuAAC oligonucleotide ligation with minimal oligonucleotide degradation. In addition, the use of an organic co-solvent (50% aqueous THF or 50% aqueous DMF) helps to dissolve the support-bound DNA (ODN2-5) which has protecting groups, in particular the cyanoethyl phosphate protecting group which will reduce DNA solubility in water (phosphate-protected DNA is uncharged). It clearly helps to improve the reaction and reduce degradation. Therefore, 50% aqueous DMF and 50% aqueous THF were chosen for the further studies. To confirm this, subsequent reactions were carried out over a reduced reaction time (5–7 h) or at a lower temperature (i.e. 40 ºC).

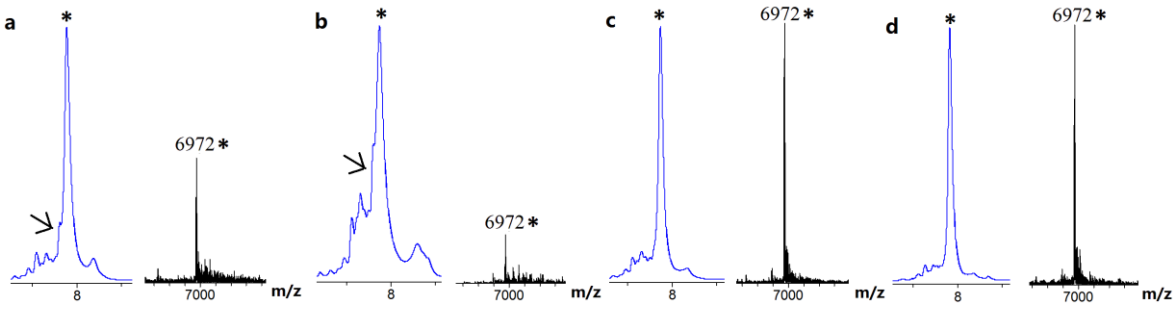

Figure 2.9. HPLC and MS characterisation of crude CuAAC-ligated product ODN2-11 (70 ºC, 21 h) using ODN2-5 (12-mer on 500 Å resin). a: H_2O, b: 50% aq. MeCN; c: 50% aq. DMF; d: 50% aq. THF. The arrows indicate starting material peaks (ODN2-5, calc.: 3613, found: 3613). The starred peaks correspond to the associated mass spectra (ESI^-).

As mentioned previously, shorter ODN2-1 (3-mer) gave higher yields of the desired product than longer ODN2-2 (11-mer). A potential reason for this could be that ligation efficiency is limited by the relatively small resin pore size. To study the effects of the resin pore size, the resin-bound 5′-azide ODN2-6 and ODN2-7 (17-mer) were treated with 3′-alkyne ODN2-3 (11-mer with mixed bases). Reactions were carried out at 40 ºC for 21 h or at 70 ºC for 7 h, and the crude CuAAC click-ligated products were analysed by mass spectrometry. In these two solvent systems (50% aqueous DMF and 50% aqueous THF), reactions on ODN2-6 (17-mer on 1000 Å resin) at 40 ºC for 21 h (Figure 2.10 a, c) or 70 ºC for 7 h (Figure 2.10 b, d) proceeded cleanly.

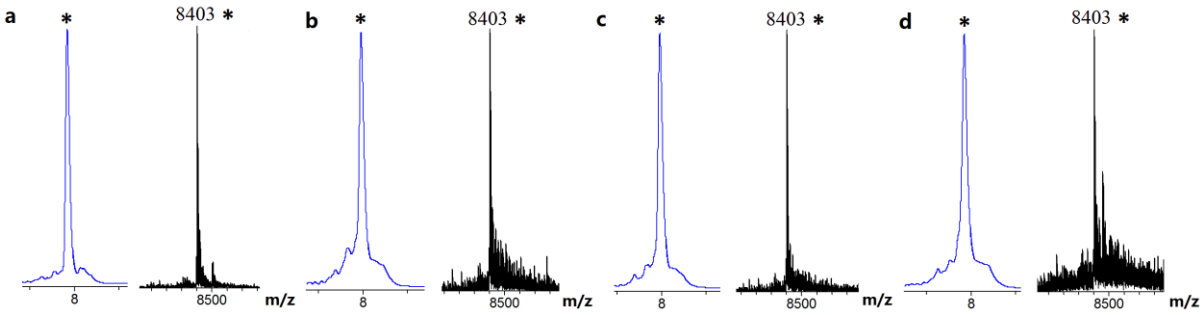

Figure 2.10. HPLC and MS characterisation of crude CuAAC-ligated product ODN2-12 using ODN2-6 (17-mer on 1000 Å resin). a: 40 ºC, 21 h, 50% aq. DMF; b: 70 ºC, 7 h, 50% aq. DMF; c: 40 ºC, 21 h, 50% aq. THF; d: 70 ºC, 7 h, 50% aq. THF. The starred peaks correspond to the associated mass spectra (ESI^-).

Also for ODN2-7 (17-mer on 3000 Å resin), HPLC analysis showed that the reactions at 40 ºC for 21 h or 70 ºC for 7 h in 50% aqueous DMF gave excellent conversion to product without major oligonucleotide degradation (*ca.* 95% conversion, Figure 2.11). It has to be acknowledged that the multiple small peaks around the main product peak on HPLC could indicate some degradation, possibly due to depurination caused by the lack of buffer in the solvent, or failed oligonucleotides from starting ODN2-7 (Figure 2.3 c).

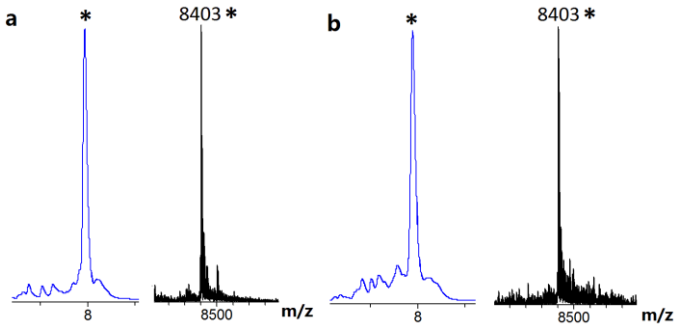

Figure 2.11. HPLC and MS characterisation of crude CuAAC-ligated product ODN2-12 using ODN2-7 (17-mer on 3000 Å resin). a: 40 ºC, 21 h, 50% aq. DMF; b: 70 ºC, 7 h, 50% aq. DMF. The starred peaks correspond to the associated mass spectra (ESI^-).

As anticipated, 50% aqueous DMF and 50% aqueous THF was found to be the best solvents for the CuAAC reaction on ODN2-6 (17-mer on 1000 Å resin). The reactions could be conducted at 40 ºC for 21 h or at 70 ºC for 7 h, and in both cases went to completion. Interestingly, no significant difference was observed between the reactions using different resin pore sizes. For ODN2-7 (17-mer on 3000 Å resin), the reactions in 50% aqueous DMF gave excellent conversion (*ca.* 95%), and ODN2-5 (12-mer on 500 Å resin) reacted as efficiently as ODN2-6 (17-mer on 1000 Å resin) or ODN2-7 (17-mer on 3000 Å resin) in 50% aqueous DMF and produced > 95% conversion (Figure 2.9 c). Similarly, when the reaction was performed in 50% aqueous THF, it was effectively complete within 21 h at 70 ºC.

2.4 Further studies of DNA ligation

Following the encouraging results presented in the section above, synthesis of longer oligonucleotides was attempted using CuAAC ligation. In view of the much longer oligonucleotides used in the subsequent reactions, the conditions were modified (e.g. increased reaction times), but were otherwise based on the optimized conditions described above. For example, 5′-azide ODN2-7 (17-mer on 3000 Å resin, 2.5 nmol) was reacted with 10 eq. of the long 60 nucleotides ODN2-4 at 70 °C and the reaction time was extended to 16 h, to give the ligated product ODN2-13 (Table 2.1). However, the reaction was not very clean, and was accompanied by partial degradation of the oligonucleotides (Figure 2.12). Attempts to decrease the reaction temperature and increase the reaction time, as well as increasing the amount of 3′-alkyne ODNs, did not improve the yield. A much longer resin-bound ODN2-8 (61-mer on 3000 Å resin) was then synthesised for further optimization of the reaction. ODN2-8 was allowed to react with 3 eq. of ODN2-3 (11-mer).

The reaction was complete in 21 h at 55 °C and the desired 72-base product ODN2-14 was isolated in good yield after cleavage from the resin and deprotection (Figure 2.13). It should be noted that at lower temperatures (40 °C) the reaction does not proceed to completion, even after 21 h (Figure 2.14). These results indicate that the CuAAC reaction can in principle be used for the efficient synthesis of very long oligonucleotides on the solid phase, but the reaction is not clean (i.e. oligonucleotide degradation occurs) when the reaction temperature is 70 °C and reaction time is long (> 7 h). This degradation might be caused by the depurination (Scheme 2.5) or copper-catalysed DNA backbone degradation, although, the CuAAC reactions were carried out under argon to exclude oxygen and avoid this. Further studies on the solid-phase CuAAC ligation need to be carried out in buffered solvents to prevent the possibility of DNA depurination. In addition, to exclude copper-catalysed degradation of DNA, copper-free solid-phase DNA ligation needs to be developed (and will be discussed in Chapter 3).

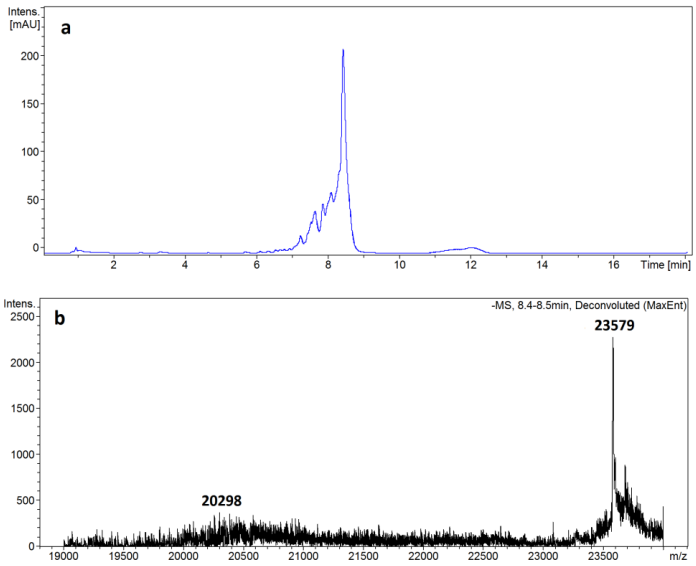

Figure 2.12. a: Reversed-phase HPLC chromatogram of crude CuAAC-ligated ODN2-13 (77-mer); and b: mass spectrum (ESI$^-$) of the ligated product ODN2-13 after 16 h at 70 ºC (calc.: 23579, found: 23579).

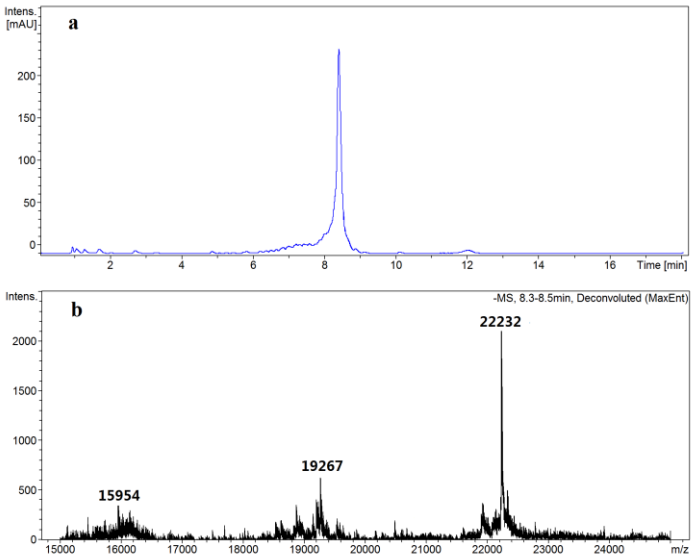

Figure 2.13. a: Reversed-phase HPLC chromatogram of crude CuAAC-ligated ODN2-14 (72-mer), and b: mass spectrum (ESI$^-$) of the ligated product ODN2-14 after 21 h at 55 ºC (calc.: 22231, found: 22232).

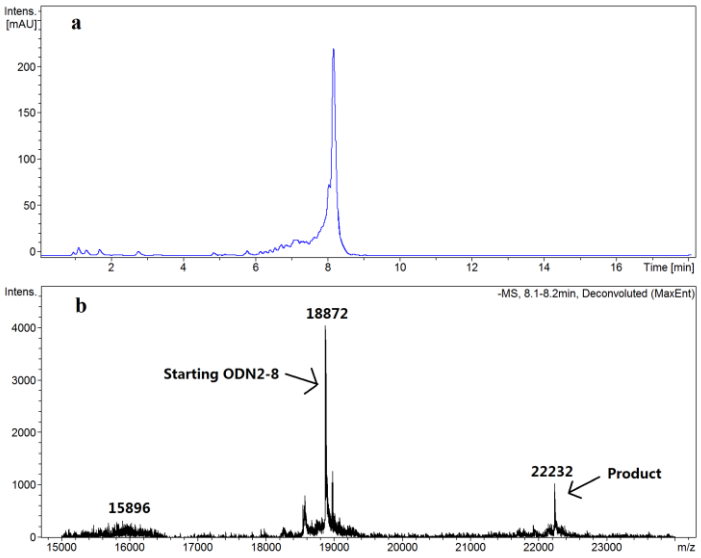

Figure 2.14. a: Reversed-phase HPLC chromatogram of incomplete crude CuAAC-ligated ODN2-14 (72-mer), and b: mass spectrum (ESI$^-$) of the ligated product after 21 h at 40 ºC showing the ligated product ODN2-14 (calc.: 22231, found: 22232) and starting ODN2-8 (calc.: 18872, found: 18872).

2.5 Conclusions

The alkyne functional group was incorporated into the 3′-end of ODNs during solid phase oligonucleotide synthesis, and the 5′-iodo-dT monomer was used to post-synthetically prepare 5′-azide labelled oligonucleotides *via* sodium azide displacement of iodide. This reaction proceeded cleanly and with a high conversion as confirmed by mass spectrometry. The support-bound 17-mer 5′-azide ODN2-6 (on 1000 Å resin) and ODN2-7 (on 3000 Å resin) were synthesised on CPG supports using 5′-DMT-*N(4)*-Fmoc-2′-deoxycytidine phosphoramidite monomer **2-8**. It was found that cleavage of the Fmoc protecting group using 20% piperidine in DMF for 20 minutes at room temperature gave the best results when performed after convertion of the 5′-iodo group into an azide.

In the CuAAC reaction, 3′-alkyne ODNs in solution were allowed to react with 5′-azide ODNs on the resin without template DNA in the presence of Cu(I) to form the biocompatible triazole analogue **tz1** (Figure 2.1). ODN2-6 (17-mer on 1000 Å resin) or ODN2-7 (17-mer on 3000 Å resin) were treated with 3′-alkyne ODN2-3 in 50% aqueous DMF. The reactions were complete within 7 h at 70 °C or 21 h at 40 °C to give the triazole product ODN2-12 in high purity (*ca.* 95%). Surprisingly, no significant difference was observed between the reactions using the two different resin pore sizes. ODN2-7 (17-mer on 3000 Å resin) was also treated with 60-mer ODN2-4 to give the 77-mer triazole product ODN2-13. In addition, when the much longer resin-bound 61-mer ODN2-8 was conjugated to 11-mer ODN2-3 under similar conditions, 72-mer oligonucleotide ODN2-14 was obtained in a good yield.

In summary, a simple method to efficiently conjugate two oligonucleotides on the solid phase by the CuAAC reaction has been established. These oligonucleotides are joined by the biocompatible triazole linker (**tz1**, Figure 2.1), which can mimic the natural

oligonucleotide phosphodiester backbone in biological or biochemical applications. The methodology described in this chapter could potentially be used to synthesise very long oligonucleotides on the solid support. However, high temperatures and/or long reaction times are necessary to promote the efficient solid-phase CuAAC ligation reactions on long oligonucleotides; these conditions frequently lead to partial degradation of the oligonucleotides. Hence, optimization of the reaction conditions is required. To avoid some of these problems, copper-free click reactions (e.g. SPAAC) were developed to assemble long oligonucleotides on the solid phase, as discussed in Chapter 3.

CHAPTER 3

SPAAC-mediated click ligation of oligonucleotides on the solid phase

Chapter 3 – SPAAC-mediated click ligation of oligonucleotides on the solid phase

3.1 Introduction

The Cu(I)-catalysed azide-alkyne 1,3-dipolar cycloaddition (CuAAC) click reaction has recently been applied to a wide range of applications in the field of nucleic acids,[148] especially for oligonucleotide ligation[45,149] and functionalization.[80,156] This wide utility is due to the extremely high efficiency afforded by the CuAAC reaction. As described in Chapter 2, it has been successfully used as a method of DNA ligation on the solid phase.[157] Expanding this methodology to long oligonucleotides would be advantageous for various nanotechnology and biology applications such as cloning and gene synthesis. However, it is challenging to synthesise long oligonucleotides due to copper mediated nucleic acid degradation.[47,158]

Due to oligonucleotide incompatibility with copper salts, there is a great demand to develop metal-free cycloaddition reactions in the nucleic acid field. It would be advantageous to use the click reaction in absence of Cu(I) and yet still achieve high yields and efficiency. The first observation of such a reaction, between cyclooctyne and azide was described more than 50 years ago by Wittig *et al.*[159,160] More recently, Gutsmiedl *et al.* reported that nitrile oxides react with norbornene-modified DNA efficiently and smoothly in high yields by the catalyst-free strain-promoted nitrile oxide cycloaddition (SPNOC).[161,162] The SPNOC reaction allows efficient functionalization of oligonucleotides on the solid phase with reporter groups such as fluorescent dyes.[163,164] Conjugation of a variety of ligands/labels bearing the azide functional group to cyclooctyne (OCT) modified solid-phase immobilised DNA/RNA has been also achieved by the strain-promoted alkyne-azide cycloaddition (SPAAC) click reaction.[165,166]

In terms of DNA-templated "click ligations", the SPAAC reaction has been reported to occur in solution within 1 minute when using 5′-dibenzocyclooctyne (DIBO) and 3′-azide modified ODNs.[59] The reason for this is steric strain; normally the bond angle for an alkyne is 180°, however in cyclooctyne this angle is reduced to *ca.* 160°. Therefore this strain is relieved (18 kcal mol^{-1}) upon triazole formation (Chapter 1, Figure 1.12).[167] The reactivity of the cyclooctyne moiety is further improved with the addition of extra ring strain and electron withdrawing groups as demonstrated by DIBO ($k = 5.7 \times 10^{-2}$ M^{-1} s^{-1})[64], which is *ca.* 50-fold faster than the parent cyclooctyne (OCT).[61,62] An achiral bicyclo[6.1.0]nonyne (BCN) cycloalkyne was extremely fast (*endo*: $k = 0.14$ M^{-1} s^{-1}; *exo*: $k = 0.11$ M^{-1} s^{-1})[66] in a DNA-templated crosslinking reaction compared to DIBO.[136] The DIBO/azide click reaction produces a mixture of stereoisomeric products (Figure 3.1), which originate from the two enantiomers of DIBO and the two triazole regioisomers, whilst BCN only gives two enantiomers upon reaction with an azide (Figure 3.1).[59] These and several other cyclooctyne derivatives (Figure 1.13) are discussed in Section 1.3.4 (Chapter 1).

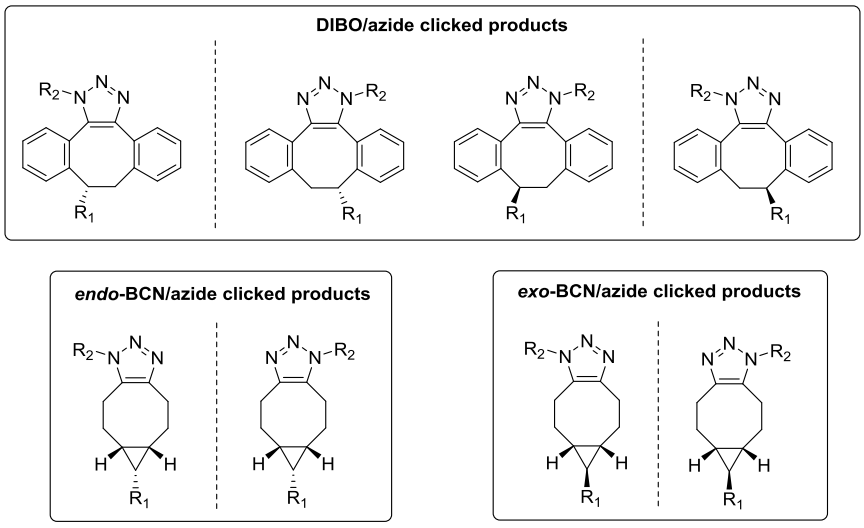

Figure 3.1. A mixture of stereoisomeric products from the DIBO/azide click reaction, and enantiomers from the *endo*-BCN/azide and *exo*-BCN/azide click reactions. R_1 and R_2: substituents.

The SPAAC-mediated ligation of oligonucleotides has not previously been reported using solid phase synthesis. This methodology could overcome technical difficulties associated with solubility and could simplify purification, since excess reactants and by-products can be removed by filtration.[12] It could be carried out on both small and large scale. In view of these benefits, the studies in this chapter focus on the solid phase ligation to form very long oligonucleotides by multiple SPAAC reactions (Figure 3.2). This work suggests a novel modular approach to the synthesis of large complex oligonucleotide analogues.

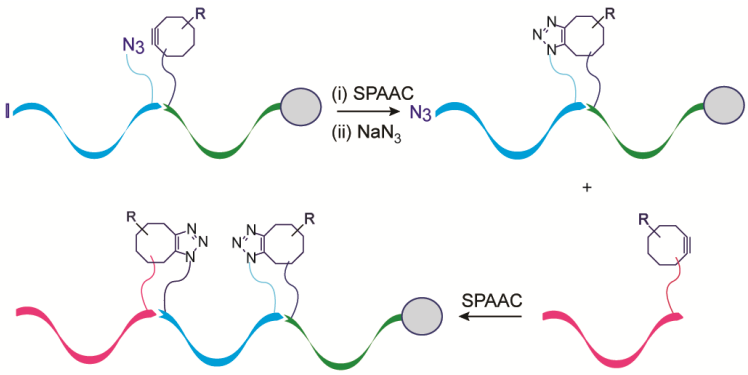

Figure 3.2. Sequential SPAAC ligation reactions on the solid phase using 5′-iodo as a masked 5′-azide to synthesise very long oligonucleotides.

3.2 Synthesis of functionalised ODNs

In this work, oligonucleotides were functionalised with azides and cyclooctynes on either the 3′ or 5′ end. The solid phase ligation was carried out using two oligonucleotide strands, one with a 5′-alkyne on the solid phase and the other with a 3′-azide in solution, to produce a DNA strand with a continuous 5′- to 3′- sequence and a triazole linkage at the ligation point. Alternatively, the reaction can also be performed using the resin-bound 5′-azide ODNs and 3′-alkyne ODNs. The general synthetic approach to these oligonucleotides will be discussed in this section.

Both SPAAC ligation reaction combinations (i.e. 5′-azide and 3′-alkyne, 5′-alkyne and 3′-azide) were evaluated for the synthesis of oligonucleotides. For 5′-modification of oligonucleotides, the functional groups were incorporated into ODNs as modified phosphoramidites during solid phase synthesis. For example, 5′-azide ODNs were prepared *via* nucleophilic substitution of 5′-iodo-dT by treatment with sodium azide (Scheme 3.1 A).[73] 5′-BCN ODNs were made by using a BCN phosphoramidite monomer at the 5′-terminus (Scheme 3.1 B). Regarding 3′-modifications, post-synthetic labelling of an incorporated primary amine with the corresponding activated ester or carbonate was the strategy used. This amino labelling process is widely used for the introduction of fluorescent labels[77,136] and functional groups.[64,168] 3′-DIBO ODNs, 3′-BCN ODNs and 3′-azide ODNs were synthesised by using 3′-amino-C7 modified ODNs (Scheme 3.2).

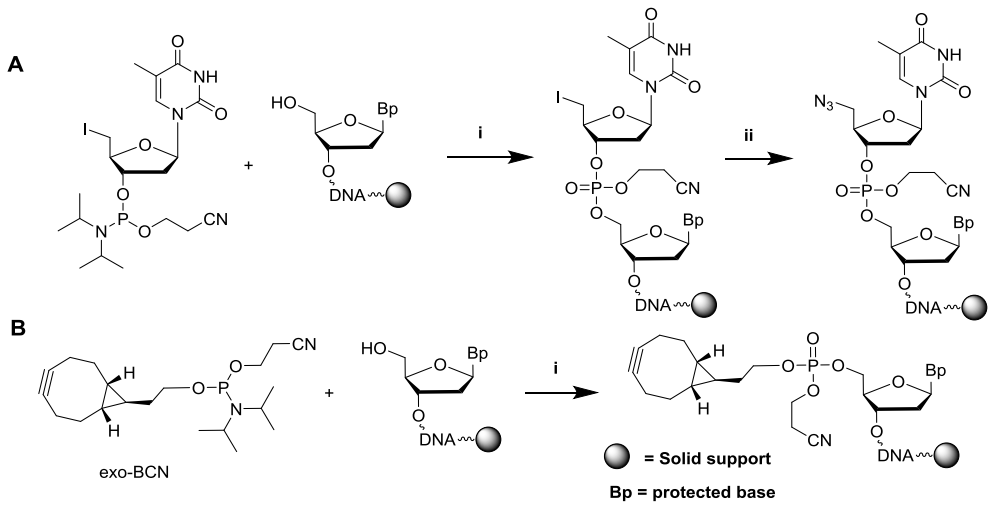

Scheme 3.1. Synthesis of 5′-modified ODNs on the solid support. A: 5′-azide ODNs; B: 5′-BCN ODNs. (i) Standard solid phase oligonucleotide synthetic conditions (Chapter 1, Figure 1.7); (ii) NaN_3, anhydrous DMF, 55 ºC, 4 h.

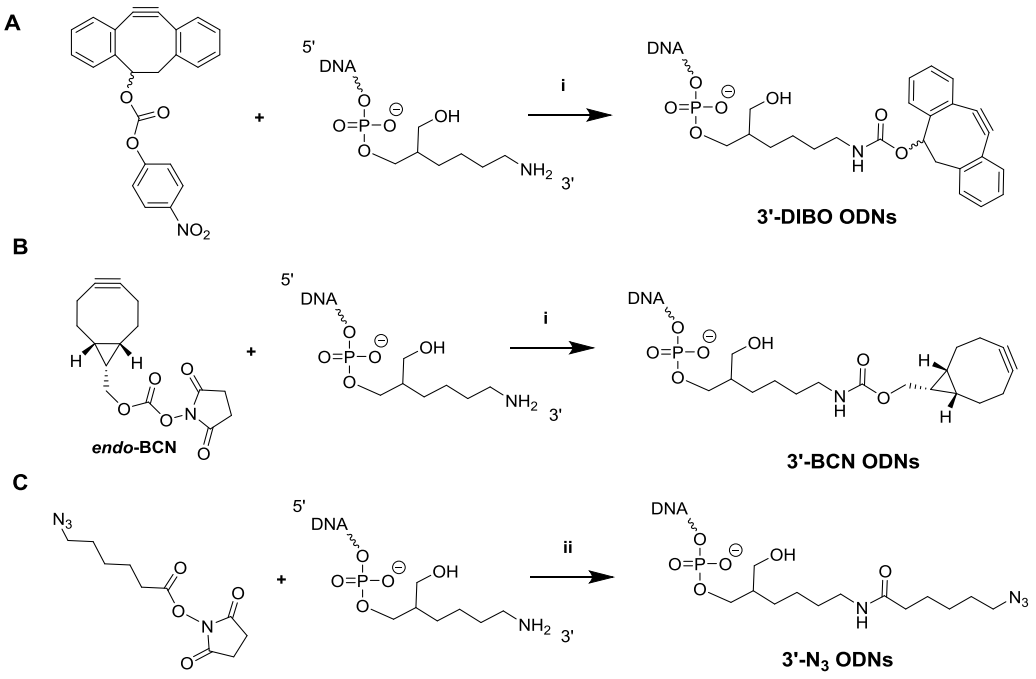

Scheme 3.2. Post-synthetic labelling of oligonucleotides with A: DIBO activated *p*-nitrophenyl carbonate;[59] B: BCN *N*-hydroxysuccinimide carbonate; C: 6-azidohexanoic acid NHS activated ester. (i) 0.5 M Na_2CO_3/$NaHCO_3$ buffer at pH 8.75, DMF, 55 °C, 4 h; (ii) 0.5 M Na_2CO_3/$NaHCO_3$ buffer at pH 8.75, DMSO, RT, 4 h.

3.3 Ligation of 3′-alkyne and 5′-azide ODNs

SPAAC click reactions were initially performed using 3′-alkyne ODNs in solution and 5′-azide ODNs on the solid phase. The oligonucleotides used in this study are listed in Table 3.1. All the functionalised oligonucleotides were synthesised as described above.

Types	Codes	Sequences	Mass found (calc.)
3′-alkyne ODNs (in solution)	ODN3-1	TTT-DIBO3′	1305 (1306)
	ODN3-2	TTTTTTTTTTT-DIBO3′	3739 (3739)
	ODN3-3	GCATTCATGTC-BCN3′	3692 (3692)
	ODN3-4	TCGACCGCCACCATGGTGAGCAAGGGCGAGGAGGATAACATGGCCATCATCAAGGAGTTCATGCGC-BCN3′	20803 (20802)
5′-azide ODNs (on the solid phase)	ODN3-5	5′ N_3-TTTTTTTTTTT-500Å resin	3613 (3613)
	ODN3-6	5′ N_3-TCCCTTCCTCTTTTTTT-1000 Å resin	5044 (5044)
	ODN3-7	5′ N_3-TCCCTTCCTCTTTTTTT-3000 Å resin	5044 (5044)
template ODNs	ODN3-8	AAAAAAAAAAAAAAAAAAA	5889 (5889)
	ODN3-9	AAGAGGAAGGGAGACATGAATGCT	7524 (7524)
click-ligated ODNs	ODN3-10	ODN3-1-**tz2**-ODN3-5	4919 (4919)
	ODN3-11	ODN3-2-**tz2**-ODN3-5	7352 (7352)
	ODN3-12	ODN3-3-**tz3**-ODN3-6/ODN3-7	8736 (8736)
	ODN3-13	ODN3-4-**tz3**-ODN3-6/ODN3-7	25846 (25846)

Table 3.1. Oligonucleotides used in the SPAAC reactions (mass spectra data in Appendix, Figure 9.1.2). 3′-alkyne ODNs were labelled with DIBO activated *p*-nitrophenyl carbonate or BCN *N*-hydroxysuccinimide carbonate using amino C7 linker at the 3′-end of the ODNs (Scheme 3.2 A, B); 5′ N_3 = 5′-azido, prepared by converting a 5′-iodo group to azide (ODN3-6, ODN3-7; Scheme 3.1, A), or prepared by converting a 5′-OH group to a 5′-iodo group, then to azide (ODN3-5; Chapter 2, Scheme 2.2); click-ligated ODNs with a linkage: **tz2** (3′-DIBO and 5′-azide, Scheme 3.3) or **tz3** (3′-BCN and 5′-azide, Scheme 3.4).

3.3.1 Ligation between 3′-DIBO and 5′-azide ODNs

The SPAAC reaction was carried out initially between 3′-DIBO ODNs and the resin-bound 5′-azide ODNs to form a triazole linkage (**tz2**) (Scheme 3.3). The two oligonucleotides were designed with thymine-only sequences in order to minimize the influence of protecting groups and non-canonical DNA secondary structures. To evaluate the effect of DIBO oligonucleotide length on the efficiency of the SPAAC reaction, ODN3-1 (3-mer) and ODN3-2 (11-mer) were synthesised.

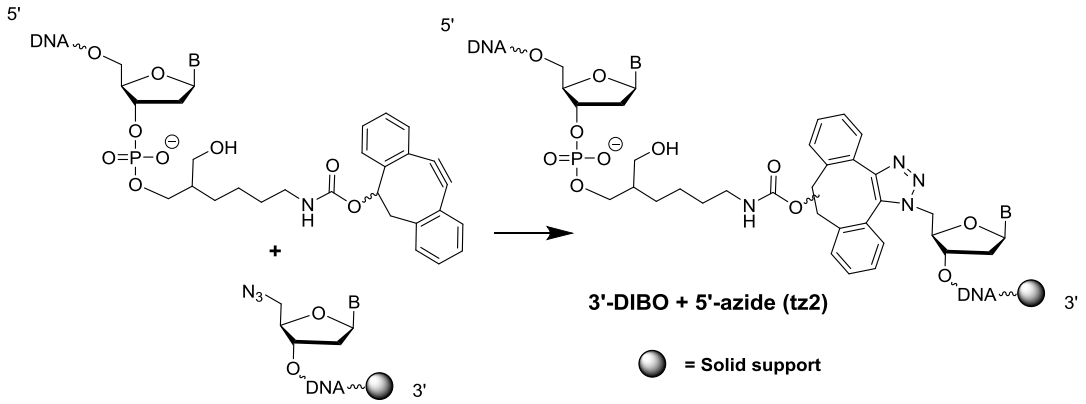

Scheme 3.3. The SPAAC ligation between the resin-bound 5′-azide ODNs and 3′-DIBO ODNs.

The SPAAC reactions between 5′-azide ODN3-5 (12-mer) and 3′-DIBO ODN3-1 (3-mer) or ODN3-2 (11-mer) were carried out in H_2O without a complementary template DNA strand. 5′-Azide ODN3-5 reacted with 20 eq. of 3′-DIBO ODN3-2 (11-mer) at room temperature and gave low yield of ODN3-11 product (10% conversion). The reaction gave a better conversion (*ca.* 50%) when using 3′-DIBO ODN3-1 (3-mer), but still did not reach completion. The reaction temperature was increased to 50 °C in the hope of boosting the conversion. The 3-mer ODN3-1 was reacted with ODN3-5 at 50 °C for 5 h to give *ca.* 95% of the desired product ODN3-10 (Figure 3.3 a). For the 11-mer ODN3-2 reacting with

ODN3-5 at 50 °C, > 95% conversion to ODN3-11 was observed after 20 h (Figure 3.3 b). The SPAAC ligations described above between DIBO and azide to form a triazole linkage **tz2** (Scheme 3.3), gave multiple peaks on HPLC due to the mixture of triazole stereoisomers formed in this reaction (Figure 3.1). Good conversion (> 95%) was obtained in the reaction of 5′-azide ODN3-5 (12-mer) and 3′-DIBO ODN3-2 (11-mer). However, the long reaction time and relatively high reaction temperature (20 h, 50 °C) might make this reaction unsuitable for more sensitive substrates, or for *in vivo* applications. For this reason, faster and milder conditions were investigated.

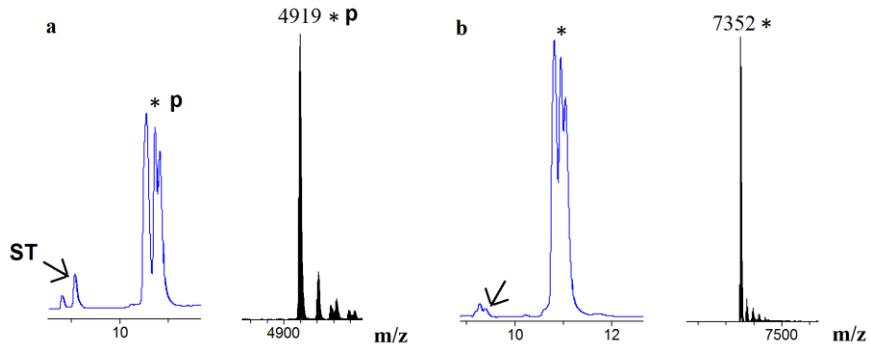

Figure 3.3. HPLC and MS characterisation of crude SPAAC-ligated products ODN3-10 (a: 50 °C, 5 h) and ODN3-11 (b: 50 °C, 20 h). The arrows indicate starting material peaks (ODN3-5, calc.: 3613, found: 3613). The starred clusters of peaks correspond to the associated mass spectra (ESI^-), which show the ligated products ODN3-10 (calc.: 4919, found: 4919) and ODN3-11 (calc.: 7352, found: 7352). In the HPLC chromatograms the clusters of peaks marked with an asterisk correspond to the different stereoisomers of the ligated product.

Since DNA templating has been shown to play an essential role in improving the efficiency of SPAAC-mediated DNA strand ligation in solution,[59] its role on solid phase DNA ligation was explored. The reactions were carried out in templated and non-templated modes for comparison (Figure 3.4).

In the templated version, two different orders of annealing were attempted. The first involved initial annealing of the resin-bound 5′-azide ODN3-5 to the template ODN3-8 in 0.2 M NaCl (Figure 3.4 d–f), and the other involved initial annealing of the 3′-alkyne ODN3-2 with the template ODN3-8 in 0.2 M NaCl. However, both annealing ways gave the same results. Reactions were carried out under non-templated and templated conditions at different temperatures (40 °C, RT and 4 °C) for 20 h. The non-templated reaction proceeded more efficiently than the templated one at 40 °C, giving > 95% conversion (Figure 3.4 a) in comparison to only 60–70% conversion in template mode (Figure 3.4 d). When the reactions were performed at 4 °C and RT, there was not an obvious difference between non-templated and templated ligations, and all the conversions were around 30–40% (Figure 3.4 b, c, e and f).

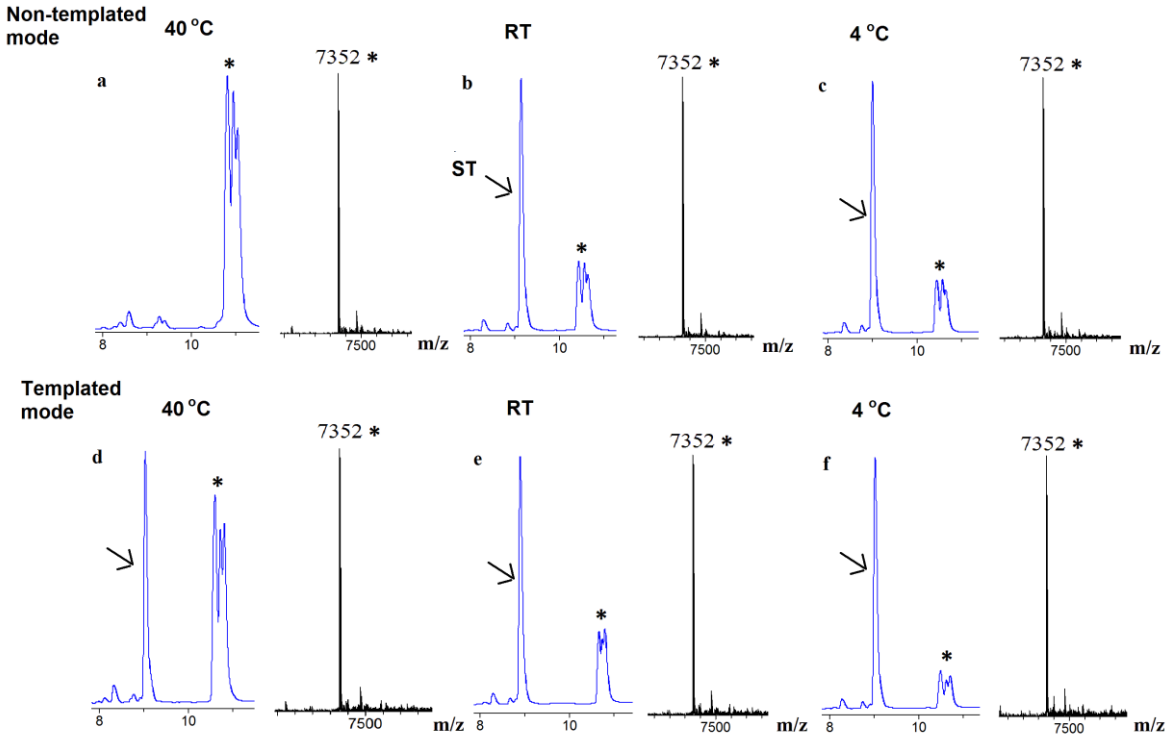

Figure 3.4. HPLC and MS characterisation of crude SPAAC-ligated product ODN3-11. Non-templated mode (a: 40 °C, b: RT, c: 4 °C); Templated mode (d: 40 °C, e: RT, f: 4 °C). The arrows indicate starting material peaks (ODN3-5, calc.: 3613, found: 3613). The starred clusters of peaks correspond to the associated mass spectra (ESI$^-$), which show the ligated product ODN3-11 (calc.: 7352, found: 7352). In the HPLC chromatograms, the cluster of peaks marked with an asterisk corresponds to the different stereoisomers of the ligated product.

3′-DIBO ODN3-2 (11-mer) was studied and gave > 95% conversion to the ligated product when reacted with the support-bound 5′-azide ODN3-5 at slightly elevated temperature (40 °C) under non-templated reaction conditions. In contrast the templated mode gave a more modest conversion of roughly 60–70%. This potentially suggests that the template blocked the reactions. This is probably due to sub-optimal hybridization caused by misalignment of reactants due to the repetitive nature of oligo-dT sequences ODN3-2 and ODN3-5 (with only thymines), which slowed the templated reaction. The conclusion from

these experiments is that templated ligation should not be attempted on homo-oligomeric sequences. To explore the templated ligation on the solid phase, subsequent study would be carried out on mixed-base sequences.

3.3.2 Ligation between 3′-BCN and 5′-azide ODNs

It was reasoned that the repetitive nature of the sequences of ODN3-2 and ODN3-5 led to sub-optimal annealing, decreasing reaction efficiency of the templated reaction in comparison to the non-templated mode. In view of this, two 5′-azide ODNs with the same sequences bound to 1000 Å and 3000 Å resin respectively were designed to study templated reactions. The sequences contained only T and C bases for ease of deprotection on the solid support (as described in Chapter 2). The C bases were Fmoc-protected allowing deprotection of the oligonucleotides on the solid support using 20% piperidine in DMF for 20 minutes at room temperature, whilst still retaining the ODNs on the resin. In addition, BCN was used instead of DIBO as a mixture of stereoisomeric triazoles was obtained using 3′-DIBO ODNs, whereas BCN will give only diastereomeric products (Figure 3.1), which will migrate as a single peak on HPLC and as a single band on gels. The templated reactions were carried out between 5′-azide ODN3-6/ODN3-7 and 3′-BCN ODN3-3 using template ODN3-9 to give enantiomeric ligated products with a **tz3** linkage (Scheme 3.4). CPG resin is the most common solid support for oligonucleotides synthesis, which is defined by the pore sizes. The bigger pore size CPG resin used, the longer oligonucleotides can be synthesised (e.g. 3000 Å resin can be used to synthesise oligonucleotides up to 200 bases). Therefore, two different pore sizes were used to synthesise 5′-azide ODN3-6 (17-mer on 1000 Å resin) and ODN3-7 (17-mer on 3000 Å resin), to assess the efficiency of the reaction on different solid supports.

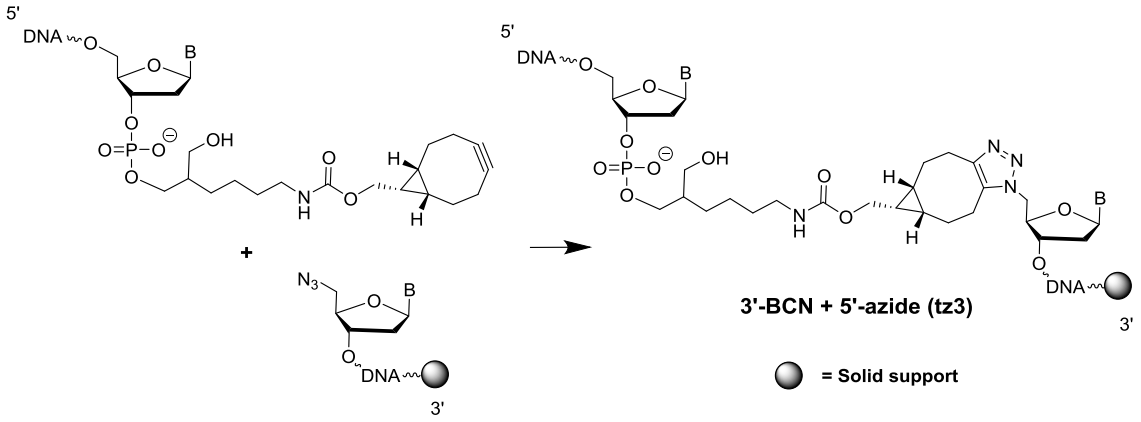

Scheme 3.4. The SPAAC ligation between the resin-bound 5′-azide ODNs and 3′-(*endo*) BCN ODNs.

ODN3-6 (17-mer on 1000 Å resin) gave > 95% conversion to desired product ODN3-12 under non-templated condition at 40 °C for 20 h (Figure 3.5 a). Two different orders of annealing in 0.2 M NaCl under templated condition were evaluated as discussed previously, both gave similar results (Figure 3.5 b, c) with conversions of approximately 70–80% based on reversed-phase HPLC chromatograms, as same as using homo-oligomeric sequences (3′-DIBO ODN3-2 and 5′-azide ODN3-5). Then 0.4 M NaCl and 1 M NaCl were used to promote the formation of duplexes for the templated reactions, but same results were observed as in 0.2 M NaCl. The ligations were also performed using ODN3-7 (17-me on 3000 Å resin); no significant difference was observed when using the two different pore sizes. These results indicated that DNA templating reduced SPAAC reaction rates on the solid phase. Therefore, subsequent reactions were carried out under non-templated conditions.

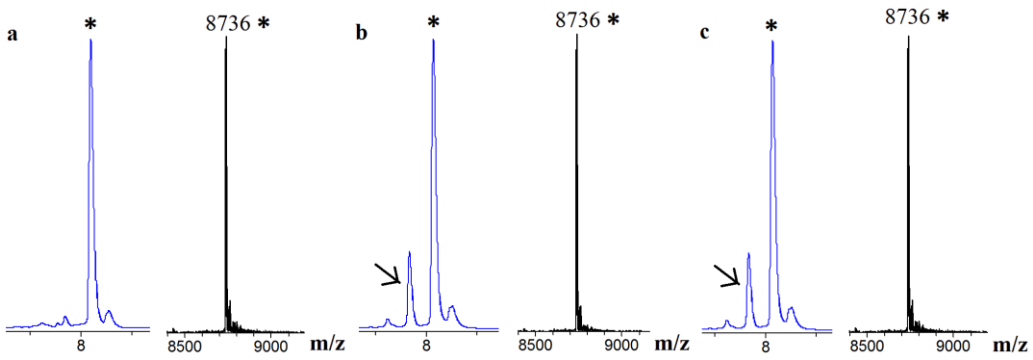

Figure 3.5. HPLC and MS characterisation of crude SPAAC-ligated product ODN3-12. a: under non-templated conditions; b, c: under templated conditions (b: annealing: 5′-azide ODN3-6 and template ODN3-9; c: annealing: 3′-BCN ODN3-3 and template ODN3-9). The arrows indicate starting material peaks (ODN3-6, calc.: 5044, found: 5044). The starred peaks correspond to the associated mass spectra (ESI$^-$), which is the ligated product ODN3-12 (calc.: 8736, found: 8736).

An excellent result (> 95% conversion) was obtained for the reaction between 3′-BCN ODN3-3 (11-mer) and 5′-azide DNA ODN3-6/ODN3-7 (17-mer) on the solid phase with a ratio of 1:1 at 40 °C for 20 h under non-templated conditions. A longer oligonucleotide 3′-BCN ODN3-4 (66-mer) was then designed and synthesised for use under the same conditions. Since ODN3-4 is a longer oligonucleotide (66-mer rather than the 11-mer previously tested), it presented a more challenging ligation. Therefore a slight excess of ODN3-4 (2 eq.) was used.

For comparison, 66-mer 3′-BCN ODN3-4 reacted with 5′-azide bearing ODNs on different resin types (ODN3-5 (12-mer on 500 Å resin), ODN3-6 (17-mer on 1000 Å resin) and ODN3-7 (17-mer on 3000 Å resin)) for 21 h at 40 °C and at 55 °C. The reaction at 40 °C was incomplete (*ca.* 40% conversion), while complete consumption of starting materials was observed at 55 °C. However, the reaction also gave unknown by-products or oligonucleotide degradation (Figure 3.6). This result indicated that the BCN moiety was

unstable in unbuffered water for 21 h at 55 °C (Scheme 3.5), although the milder conditions resulted in incomplete conversion. In addition, three types of CPG resin were used in the reactions, but no significant difference was observed. To explore the stability of BCN-modified oligonucleotides in solution and on the solid phase, the resin-bound 5′-BCN ODNs (60-mer on 3000 Å resin) were designed to replace the original 3′-BCN ODNs, and future SPAAC reactions would be carried out between 5′-BCN ODNs and 3′-azide ODNs (Scheme 3.6).

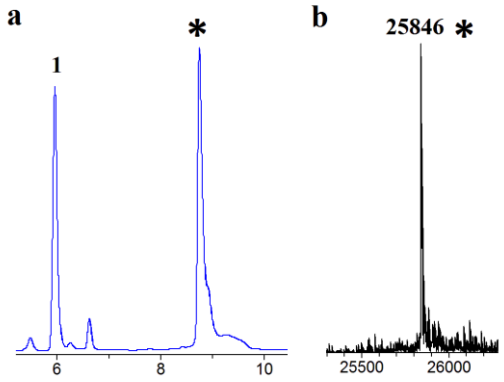

Figure 3.6. a: HPLC chromatogram of crude SPAAC-ligated product ODN3-13 (83-mer), and b: mass spectrum (ESI^-) of the ligated product ODN3-13 after 21 h at 55 °C. The starred peak corresponds to the associated mass spectrum (ESI^-), which shows the ligated product ODN3-13 (calc.: 25846, found: 25846). Peak-1: unknown by-product of the click reaction or oligonucleotide degradation (could not obtain a suitable mass spectrum).

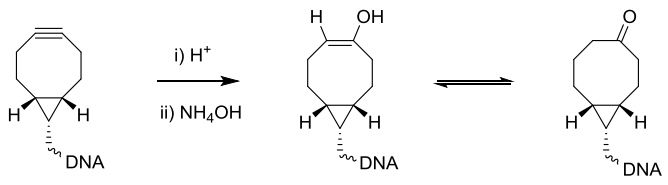

Scheme 3.5. Acid-catalysed instability of BCN-modified oligonucleotides.[169]

3.4 Ligation of 5′-BCN and 3′-azide ODNs

Next, SPAAC ligation reactions were studied between the resin-bound 5′-BCN ODNs and 3′-azide ODNs. The 5′-BCN modification was successfully incorporated into ODN3-14 (Figure 3.7) *via* a (*exo*) BCN phosphoramidite during solid phase oligonucleotide synthesis. The functionalised ODNs used for the SPAAC reaction in this study are listed in Table 3.2.

Types	Codes	Sequences	Mass found (calc.)
5′-alkyne ODNs (on the solid phase)	ODN3-14	5′ BCN-CAGCATTCTATGTGTTAGTCCGGTGTT GATACTCGCATGACAGTGGAGAGGCATTTGC CT-3000Å resin	18770 (18769)
3′-azide ODNs (in solution)	ODN3-15	CCTATCTCGTTGTTCTTAGTGAAACTCTGAAC TTTAGTGACCAGTTGGGATCTAGTGAAG-$N_3$3′	18849 (18849)
click-ligated ODNs	ODN3-16	ODN3-15-**tz4**-ODN3-14	37618 (37618)

Table 3.2. Oligonucleotides used in the SPAAC reactions (mass spectra data in Appendix, Figure 9.1.2). 5′ BCN: a BCN phosphoramidite monomer incorporated during oligonucleotide synthesis (Scheme 3.1 B); 3′ N_3: amino C7 linker was labelled with 6-azidohexanoic acid NHS activated ester (Scheme 3.2 C); click-ligated ODNs with a linkage: **tz4** (3′-azide and 5′-BCN, Scheme 3.6).

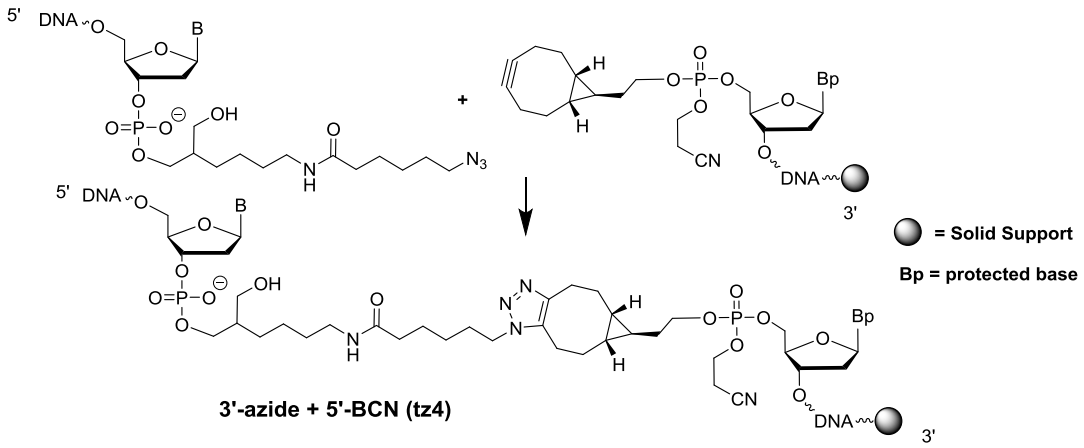

Scheme 3.6. The SPAAC ligation between the resin-bound 5′-BCN (*exo*) ODNs and 3′-azide ODNs.

The SPAAC click reaction was performed between the resin-bound 5′-BCN ODN3-14 and 3′-azide ODN3-15 to give a triazole linkage **tz4** (Scheme 3.6). When the reaction was performed at 40 °C for 7 h, it gave around 40% conversion (Figure 3.8). Longer reaction times (21 h) were tested to boost the reaction to reach completion. Next, 2 eq. of 3'-azide ODN3-15 was used for the reaction, and reaction time was increased to 21 h. The reaction proceeded efficiently to give the corresponding triazole derivatives in a very good conversion (estimated > 95%). All the starting oligonucleotide (ODN3-14, Figure 3.7) except the failed sequences (due to crude oligonucleotide on the solid phase) ligated to ODN3-15 to form 120-mer product ODN3-16 (Figure 3.9).

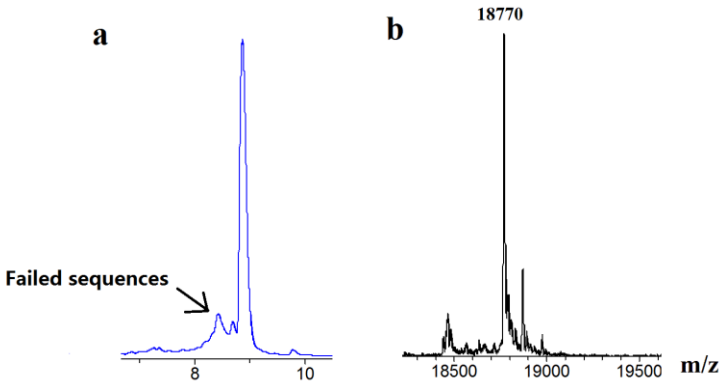

Figure 3.7. HPLC and MS characterisation of crude starting oligonucleotide ODN3-14 (60-mer). a: reversed-phase HPLC chromatogram, and b: mass spectrum (ESI$^-$) of crude ODN3-14 (calc.: 18769, found: 18770). The highlighted peak refers to failed sequences formed during solid phase oligonucleotide synthesis.

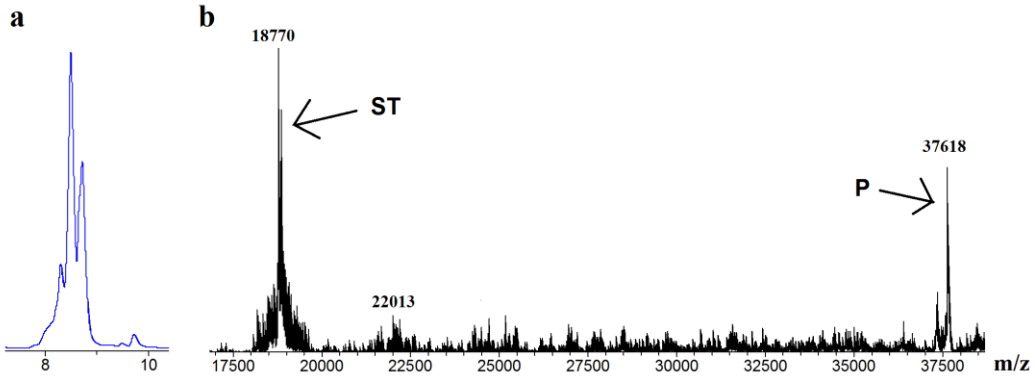

Figure 3.8. HPLC and MS characterisation of incomplete SPAAC ligation reaction between 5′-BCN ODN3-14 (60-mer) and 3′-azide ODN3-15 (60-mer). a: reversed-phase HPLC chromatogram and b: mass spectrum (ESI^-) of the ligated product after 7 h at 40 °C showing the ligated product (calc.: 37618, found: 37618) and starting oligonucleotide ODN3-14 (calc.: 18769, found: 18770).

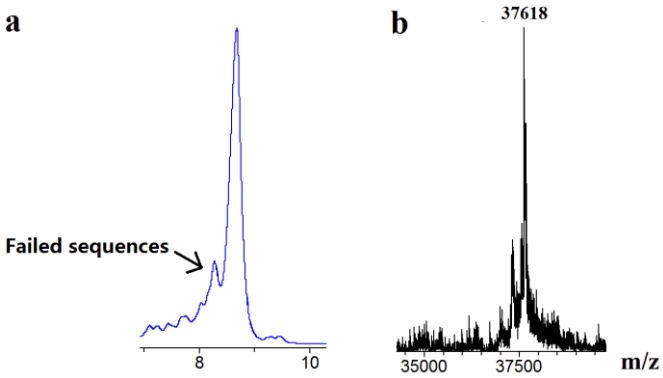

Figure 3.9. HPLC and MS characterisation of crude SPAAC ligation reaction between 5′-BCN ODN3-14 (60-mer) and 3′-azide ODN3-15 (60-mer). a: reversed-phase HPLC chromatogram and b: mass spectrum (ESI^-) of the ligated product ODN3-16 after 21 h at 40 °C (calc.: 37618, found: 37618). The highlighted peak refers to failed sequences formed during solid phase oligonucleotide synthesis ODN3-14 (Figure 3.7).

3.5 Multiple ligations

The clean and efficient chemical ligation of two long oligonucleotides on the solid phase by SPAAC click reaction suggested that multiple sequential ligation reactions might be possible (Figure 3.2). This approach requires the use of solution-phase oligonucleotides containing an azide at each end. To control the regioselectivity and avoid 5′-5′ ligation, a masked azide at the 5′-position (i.e. an iodide) was used. The functionalised ODNs used for the SPAAC reaction in this study are listed in Table 3.3.

Types	Codes	Sequences	Mass found (calc.)
5′-alkyne ODNs (on the solid phase)	ODN3-14	5′ BCN-CAGCATTCTATGTGTTAGTCCGGTGTTG ATACTCGCATGACAGTGGAGAGGCATTTGCCT-3000Å resin	18770 (18769)
3′-azide ODNs (in solution)	ODN3-17	5′ I-TCTACCTTGTTGTTCTTAGTGATACGCTGAC CTTTAGTGACCAGTTGTGATCTAGTGATG-$N_3$3′	18932 (18931)
	ODN3-18	5′ I-TCTACCAGTGACCAGTTCTAGTGAG-$N_3$3′	8114 (8114)
1st click-ligated ODNs	ODN3-19a/b	a = 5′I-ODN3-17-**tz4**-ODN3-14 b = 5′N_3-ODN3-17-**tz4**-ODN3-14	37615 (37615)[b]
	ODN3-20a/b	a = 5′I-ODN3-18-**tz4**-ODN3-14 b = 5′N_3-ODN3-18-**tz4**-ODN3-14	26798 (26798)[b]
3′-alkyne ODNs (in solution)	ODN3-4	TCGACCGCCACCATGGTGAGCAAGGGCGAGGA GGATAACATGGCCATCATCAAGGAGTTCATGC GC-BCN3′	20803 (20802)
2nd click-ligated ODNs	ODN3-21	ODN3-4-**tz3**-ODN3-19b	58418 (58417)
	ODN3-22	ODN3-4-**tz3**-ODN3-20b	47601 (47600)

Table 3.3. Oligonucleotides used in the SPAAC reactions (mass spectra data in Appendix, Figure 9.1.2). 5′ BCN: a BCN phosphoramidite monomer incorporated during oligonucleotide synthesis (Scheme 3.1 B); 5′ I: a 5′-iodo-dT phosphoramidite monomer incorporated during oligonucleotide synthesis, a: 5′-I ODNs, converted to b: 5′-N3 ODNs by treating with NaN_3 in DMF (Scheme 3.1 A); 3′ N_3: amino C7 linker was labelled with 6-azidohexanoic acid NHS activated ester (Scheme 3.2 C); 3′ BCN: amino C7 linker was labelled with BCN *N*-hydroxysuccinimide carbonate (Scheme 3.2 B); click-ligated ODNs with linkages: **tz3** (5′-azide and 3′-BCN, Scheme 3.4) or/and **tz4** (3′-azide and 5′-BCN, Scheme 3.6).

A SPAAC reaction was used to ligate 5′-iodo-3′-azide ODN3-17/ODN3-18 to the resin-bound 5′-BCN ODN3-14 in a 3:1 ratio, to give the ligated products ODN3-19a/ODN3-20a. The 5′-iodo group was then displaced on the solid phase by azide, treating with sodium azide in DMF (as described above), to give 5′-azide ODN3-19b/ODN3-20b, which were then reacted with 3′-BCN ODN3-4 (66-mer) at 40 °C. After cleavage from resin and deprotection, the crude ligated products were examined by PAGE analysis (Appendix, Figure 9.2.1). The desired product from two sequential SPAAC ligation reactions was observed on the gel but in both cases unwanted by-products and oligonucleotide degradation were also observed. Multiple sequential ligation reactions increased the ratio of degradation by-products that are caused by heating in H_2O. Normally unmodified oligonucleotides can be dissolved in H_2O and kept at 4 °C for several months and modified oligonucleotides are usually freeze-dried, stored at –18 °C, to prevent degradation. The two SPAAC reactions were carried out in H_2O at 40 °C for 42 h, which enhanced oligonucleotide degradation, especially oligonucleotides with the BCN-modification. In retrospect this degradation is not surprising, as acid-catalysed depurination and DNA chain cleavage can also occur in unbuffered water, as described in Chapter 2 (Scheme 2.5).

Optimization was carried out to minimise degradation of starting material 5′-BCN ODN3-14. Initially pH values from 7.0 to 8.0 using phosphate buffers were investigated. Different solvents including MeCN and DMF were also mixed with the phosphate buffer in 1:1 ratio. In addition, 0.2 M NaCl solution, 5% or 10% aqueous triethylamine (pH 12.50) and 5% or 10% aqueous pyridine (pH 9.70) were used to treat the starting material 5′-BCN ODN3-14 at 40 °C for 21 h. These buffers were chosen to prevent acid-catalysed depurination and potentially BCN degradation. The crude samples after cleavage from the resin were analysed by PAGE (Appendix, Figure 9.2.2). 5′-BCN ODN3-14 gave varying

degrees of degradation when treating with different buffers with the exception of 5% or 10% aqueous triethylamine and 5% or 10% aqueous pyridine. The best conditions were obtained in 10% aqueous triethylamine and 10% aqueous pyridine, and both were used in subsequent multiple ligations.

Next, multiple SPAAC reactions were conducted in 10% aqueous triethylamine (pH 12.5), and other conditions were kept constant as previously described (40 °C, 21 h). The crude SPAAC ligated products of sequential ligation reactions were monitored by PAGE. Unfortunately, all bands on the gel of ligated products were very weak. One possible reason is decomposition of the oligonucleotides. Another more likely explanation is that the oligonucleotide is cleaved from solid support in alkaline conditions during the SPAAC reaction, and removed by washing. With this in mind, the 1 M triethylammonium bicarbonate (TEAB) buffers with pH values varying from 9.7 to 11.2 were prepared for SPAAC click reactions. As pH value increased, the intensities of bands of ligated products reduced, and less starting material was observed (Figure 3.10). It was found that when the pH values from 9.7 to 10.5 were maintained, the ligation reactions proceed more efficiently.

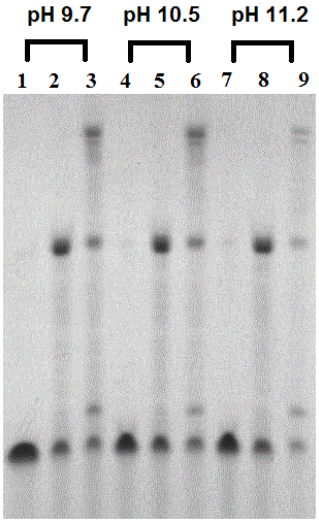

Figure 3.10. Denaturing polyacrylamide gel electrophoresis (PAGE) analysis of crude SPAAC ligated products of 1 M TEAB buffer with different pH. The crude click ligation reaction mixtures were analysed by 6% polyacrylamide/7 M urea gel electrophoresis at a constant power of 20 w for 1.5 h, using 1 × TBE buffer. Lane 1, 4 and 7: crude starting oligonucleotide ODN3-14 (60-mer); lane 2, 5 and 8: crude ligated product ODN3-19b (120-mer), produced by the ligation of ODN3-14 and ODN3-17, then treating with NaN_3 in DMF; lane 3, 6 and 9: crude ligated product ODN3-21 (186-mer), produced by the ligation of ODN3-14 and ODN3-17, and treating with NaN_3 in DMF, then ligating to ODN3-4.

The same reactions were also performed in 10% aqueous pyridine (pH 9.7) as a comparison. The final ligated products ODN3-21 and ODN3-22 (i.e. crude reaction mixture) were analysed by PAGE (Figure 3.11). The two SPAAC ligations were monitored by mass spectrometry (Figure 3.12 – Figure 3.15). Both reactions indicated that suitable conditions for the solid phase ligation of oligonucleotide by the SPAAC reaction have been developed, allowing the efficient assembly of oligonucleotides up to 186 bases in length. This is significant in the context of the standard solid phase phosphoramidite method, which is limited by accumulation of imperfect coupling and side-reactions, making it difficult to produce pure DNA longer than 100-mer in length. An added advantage of this approach is that the individual solution-phase ODNs can be purified

before ligation, and the desired product is therefore very different on PAGE gel than the starting materials and failure sequences. Therefore it is easy to purify. Naturally, this method is only useful if the application of the ligated ODN can tolerate a small number of artificial linkages in its backbone.

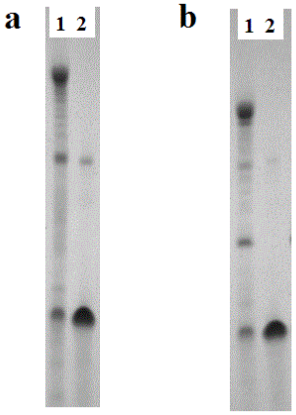

Figure 3.11. Denaturing polyacrylamide gel electrophoresis (PAGE) analysis of crude SPAAC ligated products. The crude ligation reaction mixtures were analysed by 6% polyacrylamide/7 M urea gel electrophoresis at a constant power of 20 w for 1.5 h, using 1 × TBE buffer. a) Lane1: crude ligated product ODN3-21 (186-mer), produced by the ligation of ODN3-14 and ODN3-17, and treating with NaN_3 in DMF, then ligating to ODN3-4; lane2: crude starting material ODN3-14 (60-mer). b) Lane1: ODN3-22 (151-mer), produced by the ligation of ODN3-14 and ODN3-18, and treating with NaN_3 in DMF, then ligating to ODN3-4; lane2: crude starting material ODN3-14 (60-mer).

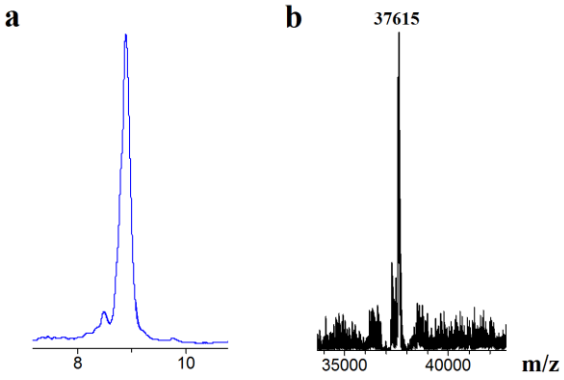

Figure 3.12. Monitoring formation of the SPAAC-mediated DNA ligation between ODN3-14 (60-mer) and ODN3-17 (60-mer). a: reversed-phase HPLC chromatogram and b: mass spectra (ESI^-) of crude ligated product ODN3-19b (120-mer) after 21 h at 40 °C (calc.: 37615, found: 37615).

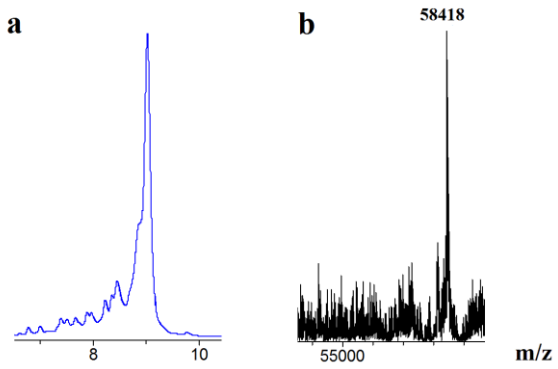

Figure 3.13. Monitoring formation of the SPAAC-mediated DNA ligation between ODN3-4 (66-mer) and ODN3-19b (120-mer). a: reversed-phase HPLC chromatogram and b: mass spectrum (ESI$^-$) of crude ligated product ODN3-21 (186-mer) after 21 h at 40 °C (calc.: 58417, found: 58418).

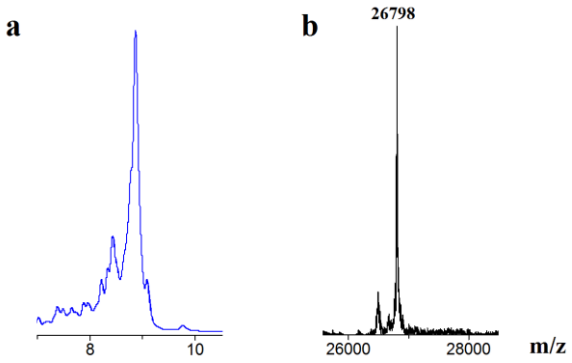

Figure 3.14. Monitoring formation of the SPAAC-mediated DNA ligation between ODN3-14 (60-mer) and ODN3-18 (25-mer). a: reversed-phase HPLC chromatogram and b: mass spectrum (ESI$^-$) of crude ligated product ODN3-20b (85-mer) after 21 h at 40 °C (calc.: 26798, found: 26798).

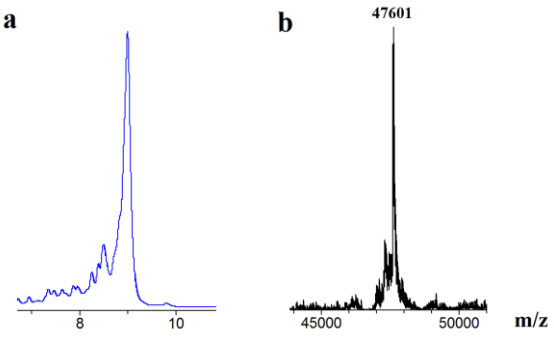

Figure 3.15. Monitoring formation of the SPAAC-mediated DNA ligation between ODN3-4 (66-mer) and ODN3-20b (85-mer). a: reversed-phase HPLC chromatogram and b: mass spectrum (ESI$^-$) of crude ligated product ODN3-22 (151-mer) after 21 h at 40 °C (calc.: 47600, found: 47601).

3.6 Ligation of 5′-BCN and 5′-azide ODNs

Oligonucleotides containing 5′-5′ or 3′-3′ inversion of polarity have been widely used in studying parallel stranded DNA[170], triplex-helices[171] and G-quaduplexes[172], also as probes for real-time PCR.[173] However, the ligation of two DNA fragments with opposite directionality to obtain 5′-5′ or 3′-3′ phosphate ester bonds by enzymatic ligation has not been utilised in nature. Hence this reaction cannot be carried out using ligase enzymes. We decided to evaluate the SPAAC reaction for the solid phase synthesis of a 5′-5′ linked oligonucleotide. The reaction was designed to ligate solution-phase 5′-BCN ODN3-14 to resin-bound 5′-azide ODN3-23; the ligated product ODN3-24 containing a triazole linkage **tz5** was obtained (Scheme 3.7). The functionalised ODNs used for the SPAAC reactions in this study are listed in Table 3.4.

Types	Codes	Sequences	Mass found (calc.)
5′-alkyne ODNs (in solution)	ODN3-14	5′ BCN-CAGCATTCTATGTGTTAGTCCGGTG TTGATACTCGCATGACAGTGGAGAGGCAT TTGCCT-3000Å resin	18770 (18769)
5′-azide ODNs (on the solid phase)	ODN3-23	5′ N_3-TCAGCATTCTATGTGTTAGTCCGGTG TTGATACTCGCATGACAGTGGAGAGGCAT TTGCCT-3000 Å resin	18872 (18872)
click-ligated ODNs	ODN3-24	ODN3-14-**tz5**-ODN3-23	37642 (37641)

Table 3.4. Oligonucleotides used in the SPAAC reactions (mass spectra data in Appendix, Figure 9.1.2). 5′ BCN: a BCN phosphoramidite monomer incorporated during oligonucleotide synthesis (Scheme 3.1 B); 5′ N_3 = 5′ azido, prepared by converting a 5′-iodo group to azide (Scheme 3.1 A); click-ligated ODNs with a linkage: **tz5** (5′-azide and 5′-BCN, Scheme 3.7).

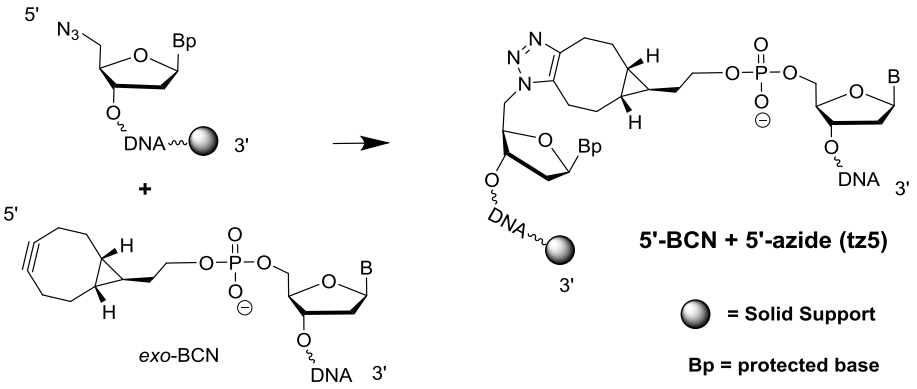

Scheme 3.7. The SPAAC ligation between the resin-bound 5′-azide ODNs and 5′-(*exo*) BCN ODNs.

The SPAAC reaction between ODN3-14 and ODN3-23 in a ratio of 1:1 was performed at 40 °C for 21 h yielding 50% product. After increasing the reaction temperature to 55 °C, the product ODN3-24 was obtained in 80% yield (Figure 3.16, confirmed by HPLC-MS analysis). However, attempts to push the reaction to completion by using 3 eq. of ODN3-14 resulted in failure. The reaction was limited by the difficulty in removing ODN3-14 from the reaction, even with multiple H_2O and acetonitrile washes. Further optimization will be required for ligation of 5′-azide and 5′-BCN ODNs. For example, efficiency could increase if the reaction would be carried out between the solution-phase 5′-azide ODN3-23 and resin-bound 5′-BCN ODN3-14, as observed for ligated product ODN3-16, produced by the resin-bound 5′-BCN ODN3-14 and 3′-azide ODN3-15 (Figure 3.9).

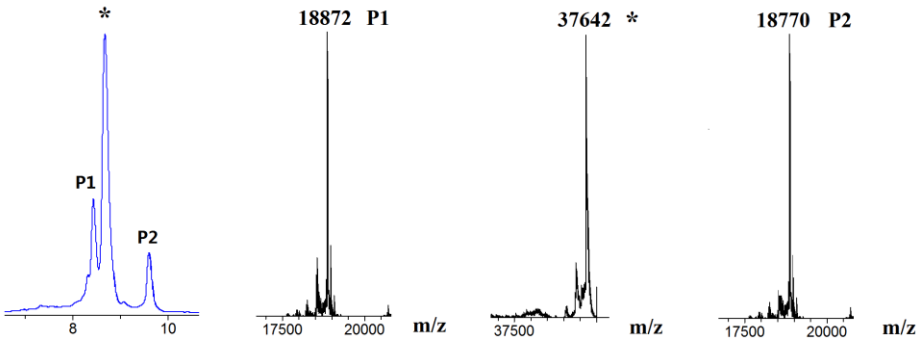

Figure 3.16. Monitoring formation of the SPAAC-mediated DNA ligation between ODN3-14 (60-mer) and ODN3-23 (61-mer). a: reversed-phase HPLC chromatogram and b: mass spectrum (ESI$^-$) of the ligated product ODN3-24 after 21 h at 55 °C (calc.: 37641, found: 37642, starred peak). P1: starting material ODN3-23 (calc.: 18872, found: 18872) and P2: 5′-BCN ODN3-14 (calc.: 18769, found: 18770).

3.7 Conclusions

5′-modified oligonucleotides were obtained by incorporating various functional groups during solid phase oligonucleotide synthesis (e.g. 5′-BCN ODNs, 5′-iodo ODNs). 5′-azide ODNs were created by treatment of the resin-bound 5′-iodo ODNs with sodium azide in DMF. The 3′-termini of oligonucleotides were modified by means of amino C7 linker, which was labelled by DIBO activated *p*-nitrophenyl carbonate, BCN *N*-hydroxysuccinimide carbonate and 6-azidohexanoic acid NHS activated ester post-synthetically, to obtain 3′-DIBO ODNs, 3′-BCN ODNs and 3′-azide ODNs respectively.

Conditions for the solid phase ligation of oligonucleotides by the SPAAC reaction have been developed which allow the efficient assembly of oligonucleotides up to 186 bases in length (ODN3-21). This has implications in terms of expanding the range of applications for oligonucleotides beyond what is possible with the standard solid phase phosphoramidite method, with its inherent length restrictions. Multiple sequential ligation reactions can be carried out by using a masked azide approach with no requirement for a template oligonucleotide, which simplifies oligonucleotide assembly (and reduces costs). DIBO was replaced by BCN, which reduced the number of stereoisomeric products and made the SPAAC reaction more rapid and clean. Due to the instability of the BCN moiety at high temperature (BCN stability is discussed further in Chapter 4), the SPAAC reactions are better carried out between the resin-bound 5′-BCN ODNs and solution-phase 3′-azide ODNs. In addition, the solid phase SPAAC reaction was also successfully used to synthesise long oligonucleotides with unnatural 5′-5′ linkages. The methodology described here may find uses in applications requiring artificial DNA nanostructures.

CHAPTER 4

SPAAC for oligonucleotide crosslinking and fluorescent labelling

Chapter 4 - SPAAC for oligonucleotide crosslinking and fluorescent labelling

4.1 Introduction

As discussed in Chapters 1 and 3, "click chemistry" has been widely applied in the field of nucleic acids.[174,175] The ring strain-promoted alkyne-azide [3+2] cycloaddition reaction (SPAAC) is a click reaction that proceeds with high efficiency in the absence of Cu(I), and therefore has the advantage of being compatible with *in vivo* applications.[61,62,66] The SPAAC reaction involves an azide and a strained alkyne such as a cyclooctyne. The use of a strained alkyne is necessary because the uncatalysed templated AAC reaction on DNA is exceedingly slow, as has been demonstrated on a hairpin loop system.[49] In contrast, templated SPAAC reactions on DNA can proceed to completion within 1 minute.[59] This reaction to form a triazole allows release of ring strain and gives a stable product. A variety of cyclooctyne derivatives have been used in nucleic acid applications.[64-66] For example, bicycle[6.1.0]nonyne (BCN)-modified deoxyuridine triphosphates have been multiply incorporated into DNA by enzymatic primer extension and polymerase chain reaction (PCR); the resultant products could then label with fluorescent dyes for use as fluorescent nucleic acid probes.[176] In addition, the 4-dibenzocyclooctynol (DIBO)-labelled phosphoramidite monomers Y_1 and Y_3 (Figure 4.1) have also been successfully used to synthesise oligonucleotides for DNA crosslinking and multiple labelling; the crosslinked duplexes were found to give much higher thermal stabilities than the uncrosslinked ones.[136] (More details of cyclooctyne derivatives are given in Chapter 1, Section 1.3.4.)

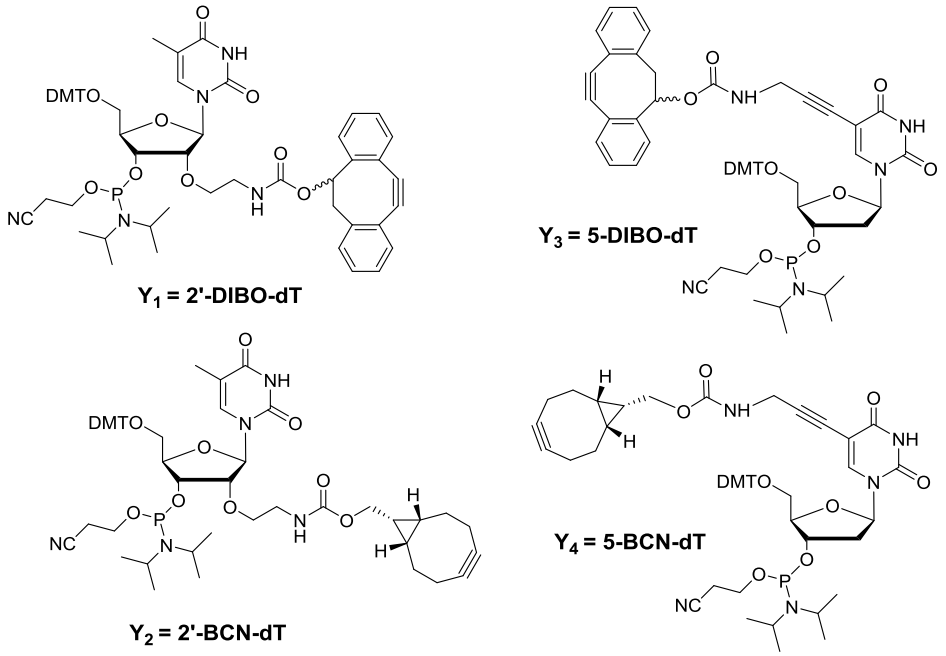

Figure 4.1. Phosphoramidite monomers for the insertion of DIBO and BCN into oligonucleotides.

This chapter describes the use of two BCN-functionalised thymidine phosphoramidites Y_2 and Y_4 (Figure 4.1), which were previously synthesised within the Brown Group (unpublished). Cycloalkyne BCN (*endo*, k = 0.14 M^{-1} s^{-1})[66] was chosen for its greater reactivity with azides compared to DIBO (k = 5.7 × 10^{-2} M^{-1} s^{-1}).[64] The achiral alkyne BCN gives two enantiomeric products (as described in Chapter 3, Figure 3.1) upon triazole formation (diastereomers when in DNA). In Y_2, the BCN moiety was attached to the 2′-oxygen of ribose *via* an aminoethoxy linker; in Y_4, the BCN moiety was joined to the 5-position of thymine *via* a propargyl linker. These phosphoramidite monomers allowed the BCN functional group to be placed within the oligonucleotide sequences, as well as at the 3′- and 5′- ends. In DNA duplexes, the 2′-BCN lies in the minor groove region; for the 5-BCN monomer, BCN extends into the major groove (Figure 4.2).

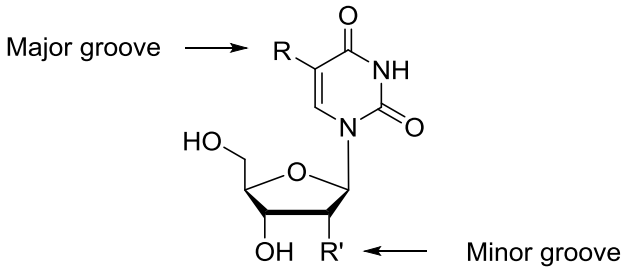

Figure 4.2. Position of attachment of the cycloalkyne modification to a thymidine nucleoside. R: 5-position of the base and R′: 2′-position of the sugar.

This chapter also presents studies on the chemical stability of the BCN monomers Y_2 and Y_4 (Figure 4.1) to oligonucleotide synthesis conditions, and the optimization of the synthesis of BCN-modified oligonucleotides. The BCN moiety was shown to be incompatible with 3% trichloroacetic acid (TCA) in DCM,[169] which is the typical reagent for DMT removal during solid phase oligonucleotide synthesis. Therefore other conditions were investigated, resulting in the selection of 10% dichloroacetic acid (DCA) in toluene as the preferred DMT deprotection system.

4.2 SPAAC-promoted DNA strand crosslinking

Crosslinking is of interest for its ability to stabilize the interaction of two DNA strands. Click chemistry has been used previously for inter-strand crosslinking,[78,136,177] leading to the formation of very stable DNA duplexes. In this chapter, the DIBO and BCN moieties (Figure 4.1, Y_1–Y_4) were incorporated into separate 14-mer oligonucleotides (OND4-1–ODN4-4, Table 4.1) with yields of up to 90% after purification by HPLC (10% DCA in toluene, was used for DMT removal, as described in Section 4.4). The azide-labelled complementary strand ODN4-5 was also synthesised (Table 4.1). 6-Azidohexanoic acid NHS activated ester was used to post-synthetically label an amino C6 linker at the 5-position of thymidine in DNA (Scheme 4.1). The azide functional group had to be introduced post-synthetically due to its incompatibility with phosphorus(III) during oligonucleotide synthesis (it is able to participate in the Staudinger reaction, as described in Section 1.3.3, Chapter 1).[50,51]

Codes	Sequences	Mass found (calc.)
ODN4-1	AATATGAY_1ATCTGT	4581 (4583)
ODN4-2	AATATGAY_2ATCTGT	4512 (4513)
ODN4-3	AATATGAY_3ATCTGT	4562 (4562)
ODN4-4	AATATGAY_4ATCTGT	4492 (4492)
ODN4-5	ACAGAZATCATATT	4539 (4539)

Table 4.1. Oligonucleotides used in the SPAAC DNA crosslinking reactions (mass spectra data in Appendix, Figure 9.1.3). Y_1 = 2′-DIBO-dT, Y_2 = 2′-BCN-dT, Y_3 = 5-DIBO-dT, Y_4 = 5-BCN-dT (Figure 4.1), and Z = amino-modified C6-dT labelled with 6-azidohexanoic acid NHS activated ester (Scheme 4.1).

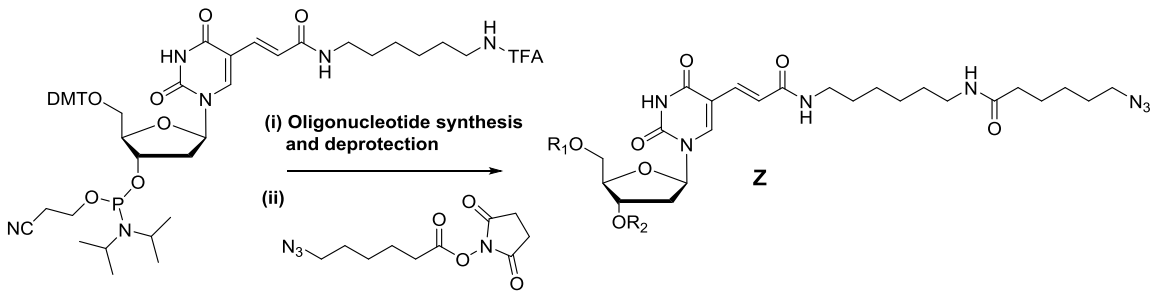

Scheme 4.1. Azide derivative of thymidine used in oligonucleotides for SPAAC crosslinking reactions. R_1 and R_2 = DNA.

The crosslinking reaction between the modified thymidines at TpA steps (to bring the reacting groups together) was used in this research to introduce crosslinks between ODN4-1–ODN4-4 and ODN4-5 at room temperature. SPAAC ligation reactions for minor to major groove crosslinking were carried out between ODN4-1 (2′-DIBO-dT) and ODN4-5 (Z) (Figure 4.3), as well as ODN4-2 (2′-BCN-dT) and ODN4-5 (Z) (Figure 4.4). The reactions for major to major groove crosslinking were conducted between ODN4-3 (5-DIBO-dT) and ODN4-5 (Z) (Figure 4.5), and ODN4-4 (5-BCN-dT) and ODN4-5 (Z) (Figure 4.6). All the reactions were carried out in 0.2 M NaCl to encourage duplex formation, were monitored at time points up to 1 h, and were analysed by mass spectrometry (Appendix, Figure 9.1.3) and 20% polyacrylamide gel electrophoresis (PAGE). The reactions were efficient, and were finished within 5 minutes in most cases. However, the crosslinking reaction between ODN4-3 (5-DIBO-dT) and ODN4-5 (Z) was slower, requiring 30 minutes.

Gel electrophoresis for crosslinking reactions

Minor to Major groove ligation (mM): DIBO

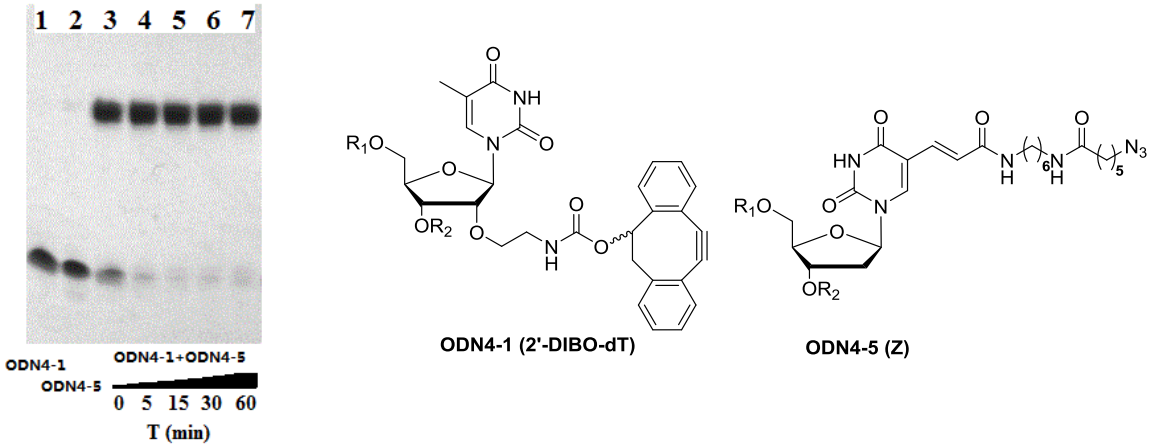

Figure 4.3. SPAAC ligation reactions for minor to major groove crosslinking between ODN4-1 (2′-DIBO-dT) and ODN4-5 (Z); lanes 1 and 2: control starting oligonucleotides ODN4-1 and ODN4-5 respectively; lanes 3–7: crude reaction mixtures after 0 min, 5 min, 15 min, 30 min and 1 h. R_1 and R_2 = DNA.

Minor to Major groove ligation (mM): BCN

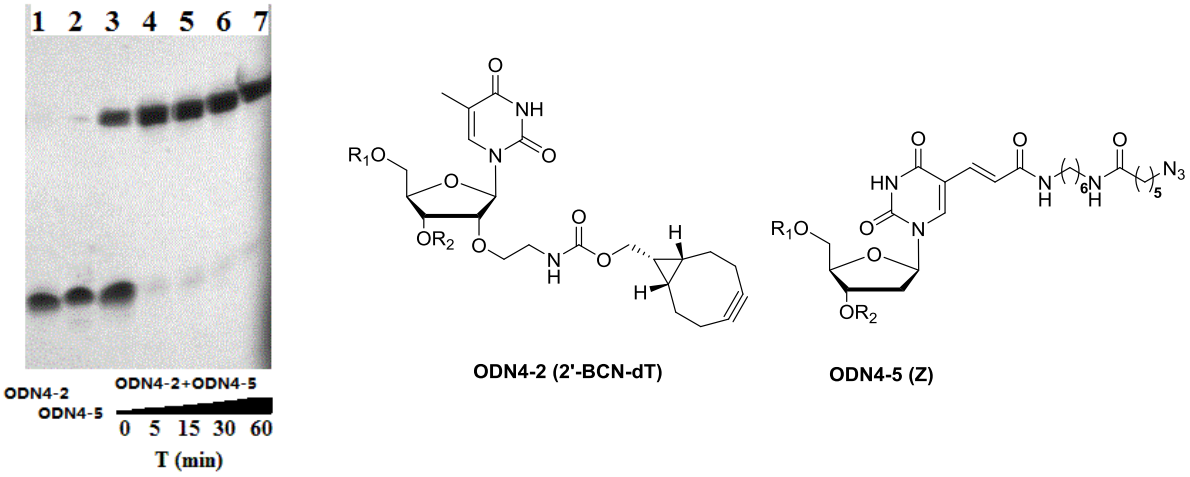

Figure 4.4. SPAAC ligation reactions for minor to major groove crosslinking between ODN4-2 (2′-BCN-dT) and ODN4-5 (Z); lanes 1 and 2: control starting oligonucleotides ODN4-2 and ODN4-5 respectively; lanes 3–7: crude reaction mixtures after 0 min, 5 min, 15 min, 30 min and 1 h. R_1 and R_2 = DNA.

Major to Major groove ligation (MM): DIBO

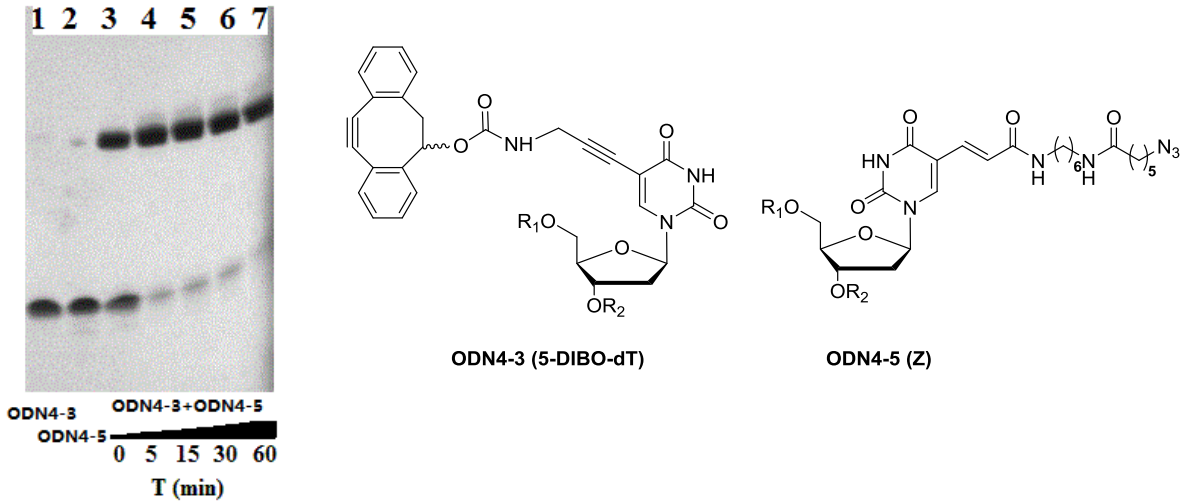

Figure 4.5. SPAAC ligation reactions for major to major groove crosslinking between ODN4-3 (5-DIBO-dT) and ODN4-5 (Z); lanes 1 and 2: control starting oligonucleotides ODN4-3 and ODN4-5 respectively; lanes 3–7: crude reaction mixtures after 0 min, 5 min, 15 min, 30 min and 1 h. R_1 and R_2 = DNA.

Major to Major groove ligation (MM): BCN

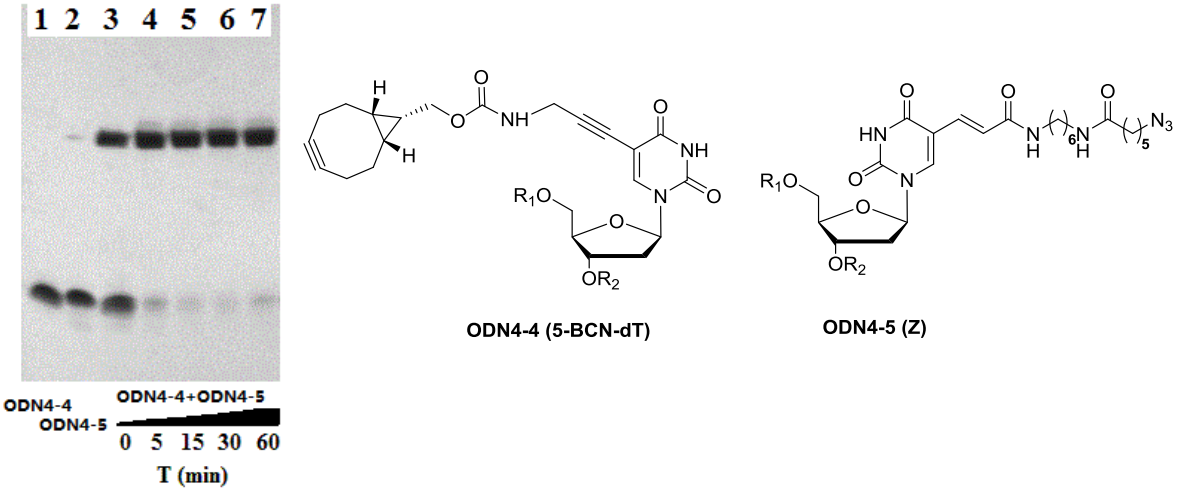

Figure 4.6. SPAAC ligation reactions for major to major groove crosslinking between ODN4-4 (5-BCN-dT) and ODN4-5 (Z); lanes 1 and 2: control starting oligonucleotides ODN4-4 and ODN4-5 respectively; lanes 3–7: crude reaction mixtures after 0 min, 5 min, 15 min, 30 min and 1 h. R_1 and R_2 = DNA.

In summary, the BCN and DIBO moieties were successfully incorporated into oligonucleotides using the corresponding phosphoramidite monomers during solid phase synthesis. The SPAAC reaction between BCN-modified oligonucleotides (ODN4-2, ODN4-4) and complementary azide-labelled oligonucleotide (ODN4-5) was found to be slightly faster than the SPAAC reaction for DIBO-modified oligonucleotides (ODN4-1, ODN4-3). All reactions were complete within 5 minutes, except the reaction between ODN4-3 (5-DIBO-dT) and ODN4-5 (Figure 4.5). These results of DNA crosslinking studies were consistent with previous work done in the Brown group on crosslinked duplexes, which unsurprisingly were found to be much more stable than non-crosslinked control duplexes.[136] This study shows that the SPAAC reaction is a powerful tool for building covalently crosslinked DNA constructs, and that the BCN and DIBO moieties (Figure 4.1) can be used for the synthesis of alkyne-modified oligonucleotides.

4.3 Multiple labelling (5-DIBO-dT, 5-BCN-dT) to produce fluorescent probes

As SPAAC is a reliable method for post-synthetic conjugation of DNA to reporter groups, it has the potential to be applied to the synthesis of multiply labelled fluorescent probes. To investigate this possibility, four multiply labelled probes were designed to target the R516G locus of the CFTR gene. Three additions of modified thymidine phosphoramidite monomers (Y_3 = 5-DIBO-dT and Y_4 = 5-BCN-dT, Figure 4.1) were incorporated into oligonucleotides to obtain ODN4-6 and ODN4-7 (Table 4.2). These two oligonucleotides were each labelled with two different fluorescent dyes (5-TAMRA azide and 5-sulforhodamine B azide, Figure 4.7), giving ODN4-8–ODN4-11.

code	Sequence	Mass found (calc.)
ODN4-6	CGCTTCY_3GTATCY_3ATATY_3CATCP	7619 (7619)
ODN4-7	CGCTTCY_4GTATCY_4ATATY_4CATCP	7409 (7409)
ODN4-8	ODN4-6 labelled with 5-TAMRA azide	9157 (9156)
ODN4-9	ODN4-6 labelled with 5-sulforhodamine azide	9542 (9540)
ODN4-10	ODN4-7 labelled with 5-TAMRA azide	8947 (8946)
ODN4-11	ODN4-7 labelled with 5-sulforhodamine azide	9332 (9330)

Table 4.2. Oligonucleotides used in the SPAAC reaction and fluorescence-clicked DNA probes (mass spectra data in Appendix, Figure 9.1.3). Y_3 = 5-DIBO-dT, Y_4 = 5-BCN-dT (Figure 4.1), P = 3′-propanol.

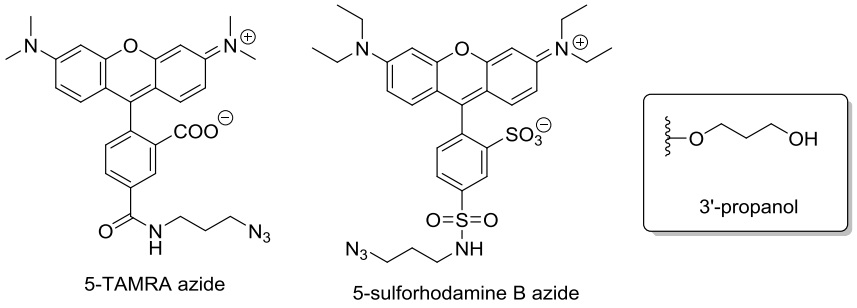

Figure 4.7. Modifications used in fluorescent probes.

The HPLC-MS analysis of two crude oligonucleotides ODN4-6 and ODN4-7 is presented in Figure 4.8. In both cases, three modified bases were successfully incorporated into the DNA strand. The desired oligonucleotides were accompanied by some failed sequences, which were present even when the optimized conditions for oligonucleotide synthesis were used (DMT removal by 10% DCA in toluene). The DIBO-modified ODN4-6 (Figure 4.8 a) gave fewer failed sequences compared to the BCN-modified ODN4-7 (Figure 4.8 b), presumably due to the instability of BCN (discussed in Section 4.4). The pure oligonucleotides were post-synthetically labelled with 5-TAMRA azide and 5-sulforhodamine B azide, separately. The HPLC-MS analysis of BCN-labelled

ODN4-7 after reaction with the dyes (i.e. ODN4-10, ODN4-11) are shown in Figure 4.9. However, because of the difficulty in purifing the labelled oligonucleotides, the purity of the fluorescent probes was limited. A study of the probe fluorescence properties was not deemed feasible. It was therefore necessary to assess the stability of the BCN moiety, and to optimize the conditions of oligonucleotide synthesis when using the BCN-modified monomers.

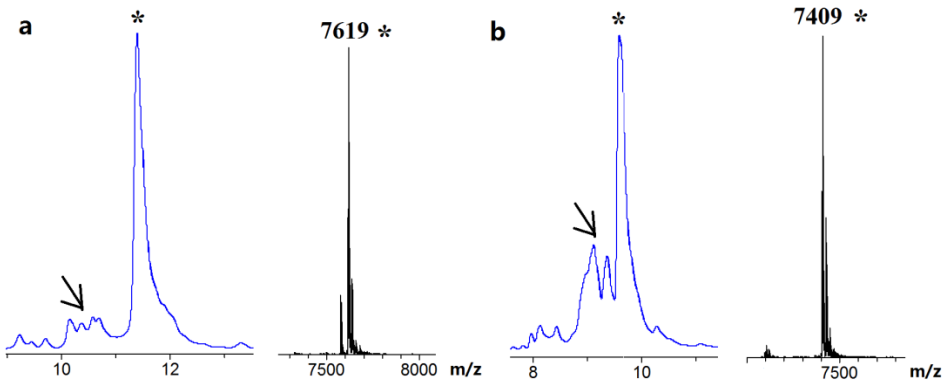

Figure 4.8. HPLC and MS characterisation of crude ODN4-6 (a) and ODN4-7 (b). The arrows indicate the failed sequence peaks. The starred peaks correspond to the associated mass spectra (ESI^-), which are the desired oligonucleotides.

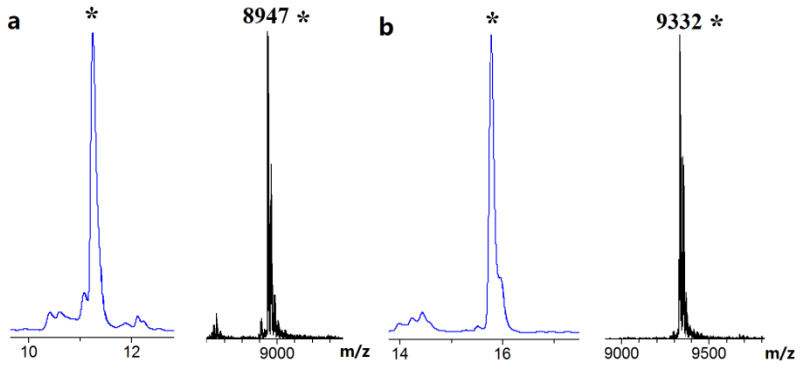

Figure 4.9. HPLC and MS characterisation of purified products ODN4-10 (a) and ODN4-11 (b). ODN4-10: ODN4-7 labelled with 5-TAMRA azide. ODN4-11: ODN4-7 labelled with 5-sulforhodamine B azide. The starred peaks correspond to the associated mass spectra (ESI^-), which are the desired products.

4.4 Stability of BCN-labelled oligonucleotides

The SPAAC reaction is a valuable tool for DNA labelling, and this makes it potentially useful in the synthesis of fluorescent nucleic acid probes. This section evaluates the stability of the BCN moiety; the used oligonucleotides are listed in Table 4.3.

Codes	Sequences	Mass found (calc.)
ODN4-12	AATATGAY_2ATCTGT	4512/4530 (4512)
ODN4-13	AATATGAY_4ATCTGT	4492/4510 (4492)
ODN4-14	ACAGAZATCATATT	4539 (4539)
ODN4-15	Y_2TCGATCTGCAT	3847/3865 (3846)

Table 4.3. Oligonucleotides used for testing the stability of the BCN moiety. Y_2 = 2′-BCN-dT, Y_4 = 5-BCN-dT, and Z = amino-modified C6-dT labelled with 6-azidohexanoic acid NHS activated ester (Scheme 4.1).

The stabilities of 2′-BCN-dT and 5-BCN-dT were studied by synthesising 14-mer oligonucleotides ODN4-12 and ODN4-13 (Table 4.2) containing a single BCN-T unit in the middle of their sequences. A solution of 3% TCA in DCM was used to remove the DMT protecting groups of ODN4-12 and ODN4-13. Unfortunately, the crude modified oligonucleotides contained a by-product whose molecular weight corresponded to the desired product plus 18 mass units. The ratio of the product to by-product was *ca.* 1:1, as analysed by HPLC-MS (Figure 4.10).

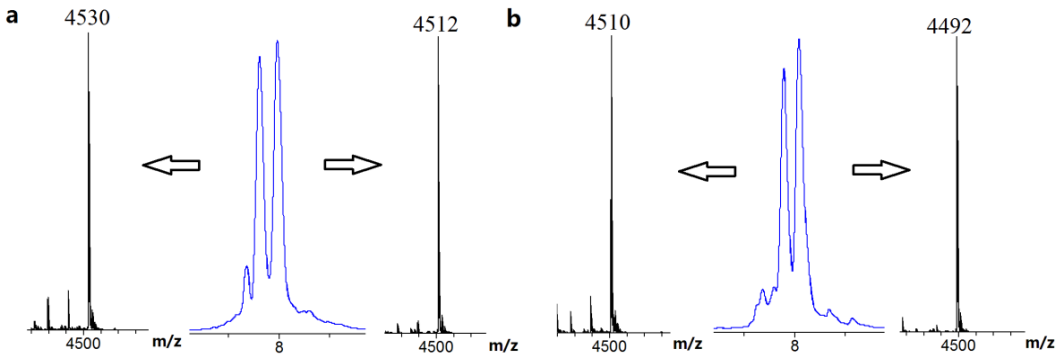

Figure 4.10. HPLC and MS characterisation of crude oligonucleotides. a: ODN4-12, b: ODN4-13.

There are several possibilities for the by-product at mass+18. One possibility is that aqueous ammonia solution reacts with the BCN alkyne functional group during oligonucleotide deprotection. Another hypothesis is hydrolysis of BCN, either during the synthesis of the BCN-modified dT monomers or during the synthesis of the oligonucleotides.

The purity of the 2′-BCN-dT and 5-BCN-dT phosphoramidite monomers was checked by MS and NMR; no degradation was detected. The two monomers were inserted into oligonucleotides ODN4-12 and ODN4-13. In both cases, a 1:1 ratio of product and by-product was obtained no matter what the position of BCN modification. In order to obtain pure samples of the correct mass and its derivative (mass+18), ODN4-13 was purified by HPLC. A portion of purified ODN4-13 was used in a click reaction. Reactions were carried out with ODN4-14, and the products were analysed by mass spectrometry and gel-electrophoresis.

Based on PAGE gel analysis (Figure 4.11), ODN4-13 reacted with ODN4-14 to form the expected ligation product within a few minutes, whereas ODN4-13 (mass+18) did not ligate with ODN4-14. This suggested that ODN4-13 (mass+18) did not have a functional

strained cyclooctyne and therefore was not able to react with the azide-labelled oligonucleotide. It was thought possible that the triple bond of ODN4-13's BCN moiety had reacted with one equivalent of H_2O to give the mass+18 impurity.

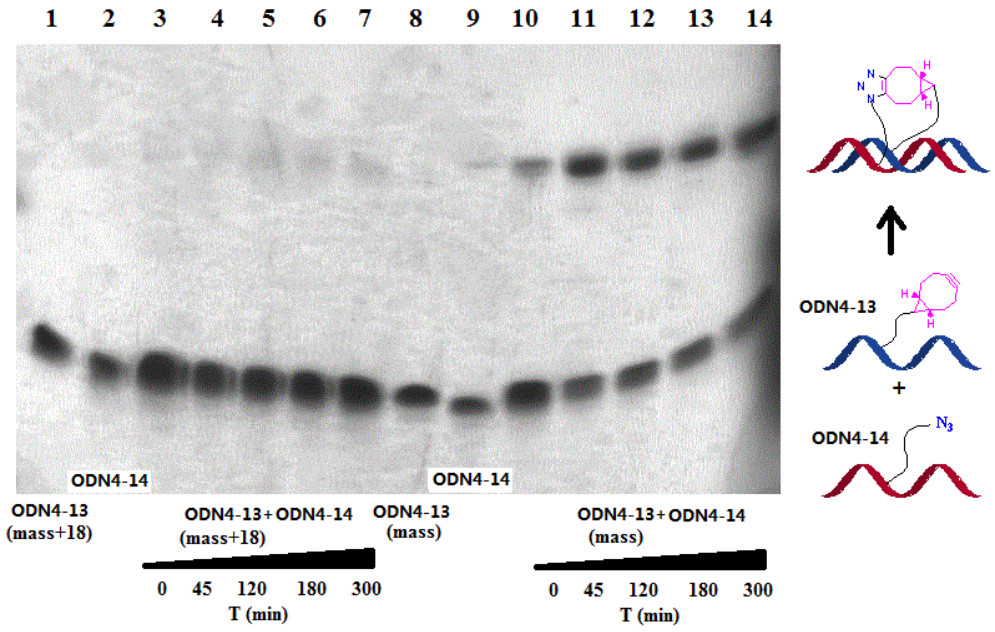

Figure 4.11. SPAAC ligation reactions for major to major groove crosslinking between ODN4-13 (mass+18) and ODN4-14, and between ODN4-13 (correct mass) and ODN4-14. Lane 1: ODN4-13 (mass+18); lane 2: ODN4-14; lanes 3–7: ODN4-13 (mass+18) and ODN4-14, the crude reaction mixtures after 0 min, 45 min, 2 h, 3 h and 5 h; lane 8: ODN4-13 (correct mass); lane 9: ODN4-14; lanes 10–14: ODN4-13 (correct mass) and ODN4-14, the crude reaction mixtures after 0 min, 45 min, 2 h, 3 h and 5 h.

Initially it was believed that the mass+18 impurity was the result of instability of ODN4-13 to the deprotection conditions of concentrated aqueous ammonia solution. To test this hypothesis, oligonucleotide ODN4-13 (correct mass) was divided into four portions: one was treated with concentrated aqueous ammonia solution overnight at room temperature, and the other three were treated with concentrated aqueous ammonia solution at 55 °C for 1 h, 3 h and 5 h respectively. Surprisingly, mass spectrometry analysis showed

that all the oligonucleotides were stable in ammonia solution. Another explanation for the appearance of the mass+18 impurity was needed.

Several solvents and reagents are used in oligonucleotide synthesis, including capping reagents (acetic anhydride in pyridine/THF and *N*-methylimidazole in THF), oxidizer solution (iodine in pyridine/THF/H_2O or tert-butyl hydroperoxide in DCM/decane) and deblock solution (3% TCA in DCM). The work described below was carried out to determine whether any of these reagents might cause the BCN to be unstable.

Initially, a synthesis of ODN4-15 with a 5′-addition of 2′-BCN-dT (Table 4.3) was carried out under standard conditions as a control (Figure 4.12 c). It was assumed that because BCN in this sequence was introduced as the final addition on the solid phase, ODN4-15 should contain a minimal amount of +18 by-product, as the BCN has been exposed to only one cycle of oligonucleotide synthesis and therefore only one treatment with the various reagents. Another synthesis of ODN4-15 was carried out separately, then subjected to oxidation with either a solution of 0.02 M iodine in pyridine/THF/H_2O for 15 minutes, or a solution of 1.0 M tert-butyl hydroperoxide in DCM/decane (4 : 1) for 15 minutes. After removal of the DMT protecting group, the oligonucleotides were cleaved from the resin by treatment with concentrated aqueous ammonia solution at 55 °C for 5 h. In all three cases, only a small amount (< 10%) of by-product (mass+18) was obtained (Figure 4.12). It may therefore be concluded that BCN is relatively stable to both oxidising agents for prolonged periods.

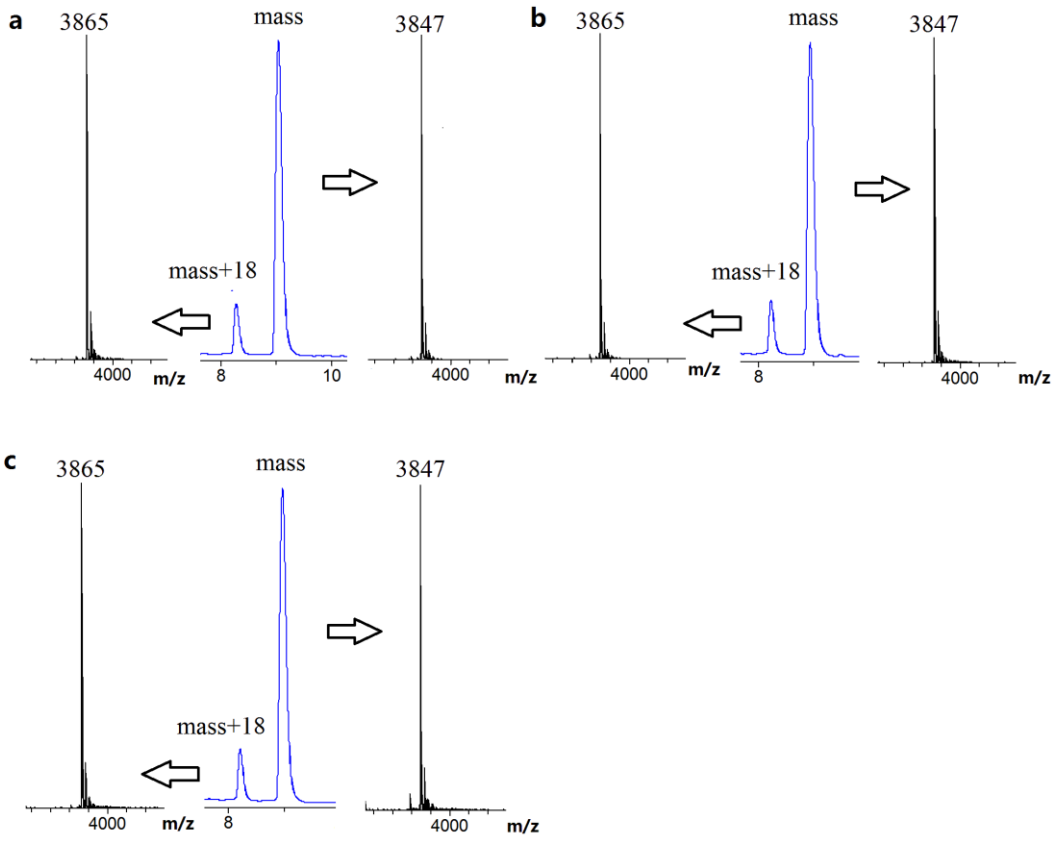

Figure 4.12. a: HPLC and MS characterisation of treatment of ODN4-15 with a solution of 0.02 M iodine in pyridine/THF/H_2O for 15 min, followed by treatment with $NH_3 \cdot H_2O$; b: HPLC and MS characterisation of treatment of ODN4-15 with a solution of 1.0 M tert-butyl hydroperoxide in DCM/decane (4 : 1) for 15 min, followed by treatment with $NH_3 \cdot H_2O$; c: HPLC and MS characterisation of synthesis of ODN4-15 under standard conditions (control).

A portion of ODN4-15 bound to the solid support was treated with the capping reagents (mixture of *N*-methylimidazole in THF and acetic anhydride in pyridine/THF, 1:1) and separately, with the deblock mixture (3% TCA in DCM). The BCN was found to be stable after treating with the capping reagents, i.e. the result (Figure 4.13 a) was as same as the control (Figure 4.12 c). However, when ODN4-15 was treated with TCA, the by-product of mass+18 was observed (Figure 4.13 b). This result suggests that TCA reacts with the

triple bond of BCN to form a TCA adduct, which can be hydrolysed by aqueous ammonia solution to give the mass+18 by-product.

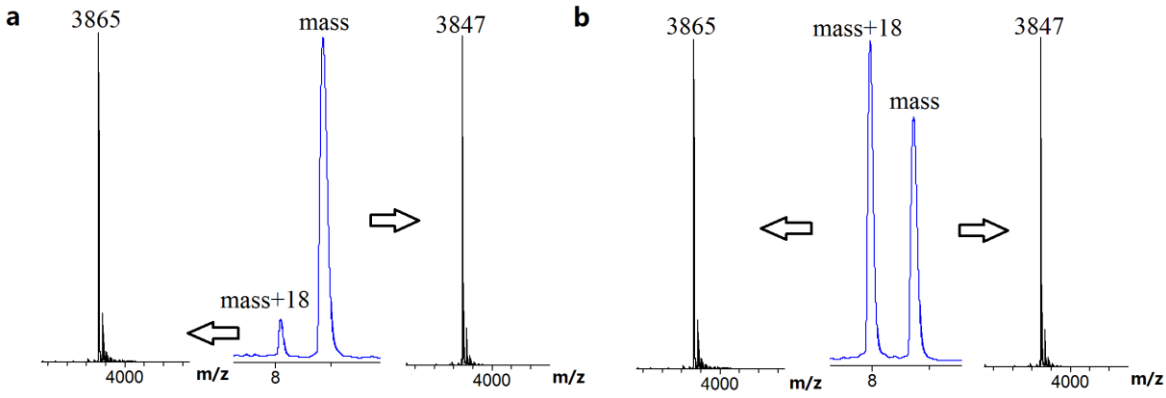

Figure 4.13. a: HPLC and MS characterisation of treatment of ODN4-15 with capping reagents (mixture of *N*-methylimidazole in THF and acetic anhydride in pyridine/THF, 1:1), followed by treatment with $NH_3 \cdot H_2O$; b: HPLC and MS characterisation of treatment of ODN4-15 with deblock solution (3% TCA in DCM), followed by treatment with $NH_3 \cdot H_2O$.

In oligonucleotide synthesis, detritylation is normally carried out in the presence of 3% TCA in DCM, but 10% DCA in toluene can also be used. ODN4-15 was treated with 3% TCA in DCM and 10% DCA in toluene for extended periods (15 minutes and 2 h), respectively, with results shown in Figure 4.14. After treating with TCA for 2 h, the product was completely converted to the by-product, but with DCA, the product and by-product were detected in an approximate ratio of 1:1.

As either TCA or DCA is required to deprotect the DMT protecting group, BCN stability remains an issue. However, using DCA to replace TCA, the required deprotection time in solid phase oligonucleotide synthesis is only slightly longer, so the DCA deblock mixture was chosen for all subsequent oligonucleotide synthesis involving BCN monomers.

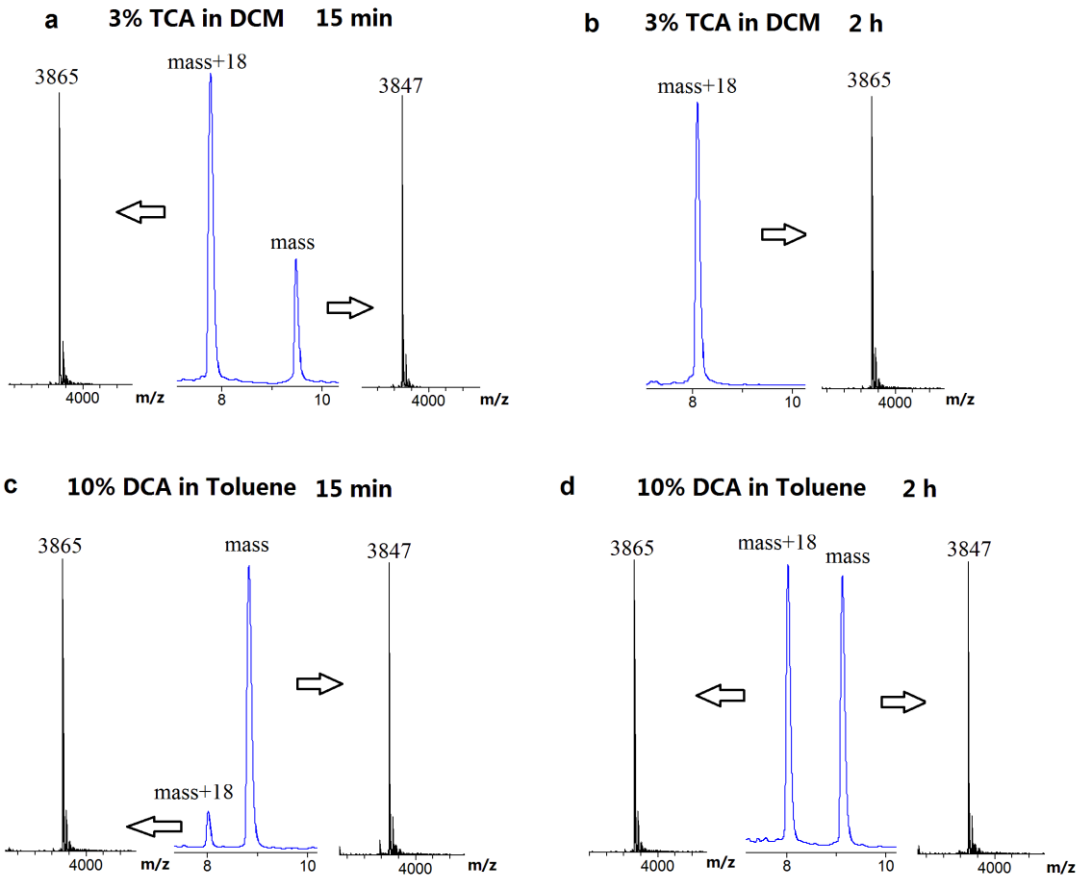

Figure 4.14. HPLC and MS characterisation of treatment of ODN4-15 with 3% TCA in DCM from 15 min (a), 2 h (b), followed by treating with $NH_3 \cdot H_2O$; HPLC and MS characterisation of treatment of ODN4-15 with 10% DCA in toluene from 15 min (c), 2 h (d), followed by treating with $NH_3 \cdot H_2O$.

During the course of this work, a paper on the instability of BCN to oligonucleotide synthesis conditions was published by Van Delft *et al.*[169] This paper reported that bicyclo[6.1.0]nonyne (BCN) had been hydrolysed to the corresponding cyclooctanone (Scheme 4.2) after treating with 3% TCA; as an alternative, 2.5% DCA in DCM was used as a mild 5′-DMT deblocking reagent. This is consistent with our findings.

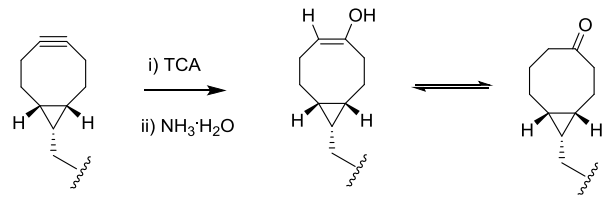

Scheme 4.2. Acid-catalysed instability of BCN-modified oligonucleotides.[169]

4.5 Fluorescent DNA nanoconstruct assembly

Fluorescent nucleic acid probes are important tools for imaging specific sequences of DNA *in vivo*. A wide range of fluorescent nanoconstructs have been developed.[178,179] For example, a three-fluorophore FRET system was designed by Bannwarth *et al.*[180] However, most fluorescent nanoconstructs lack structural stability; the fluorophores can be released from the nano-complex if the duplex denatures to form single strands. As a consequence, the flow of energy transfer in the nanoconstruct is disrupted. In addition, it is not possible to purify fluorescent nanoconstructs of this kind as the best purification strategies for large DNA constructs (such as PAGE) involve denaturing the DNA. Therefore, the assembly of fluorescent nanoconstructs which address the issues of stability and purification is of great importance. Such probes will have many applications in nanotechnology and biology.

The aim of this work is to make stable, differently coloured, highly fluorescent DNA nanoconstructs with readily distinguishable fluorescence characteristics. FRET interactions between fluorophores could be exploited by careful design of the DNA structure, with variation of the DNA length causing changes in biophysical properties. These nanoconstructs are to be used to visualise genomic DNA and various RNAs, with possible applications *in vivo*. Copper-free click ligation provides a direct and simple method for the generation of stable functionalised DNA nanoconstructs *via* inter-strand crosslinking

(Scheme 4.3). In consideration of the instability of the BCN moiety to acid during oligonucleotide synthesis, BCN was attached to oligonucleotides post-synthetically. In a model fluorescent nanoconstruct study, a 30-mer oligonucleotide ODN4-16 was prepared bearing three amino-modified C6-dT units. Three 5′-Cy5 oligonucleotides (ODN4-17–ODN4-19) with 2 or 3 amino-modified C6-dT units were synthesised and labelled with 6-azidohexanoic acid NHS activated ester, then crosslinked to the complementary 10-mers, each labelled with one BCN alkyne and a fluorescent dye (ODN4-20–ODN4-22, Table 4.4). This yielded 8 fluorescent nanoconstructs NS1–NS8 (Table 4.5).

Codes	Sequences	Mass found (calc.)
ODN4-16	AGCTGAZGCTAGCGGAZGATAGACGAZGCA	10200 (10200)
ODN4-17	Cy5-AGCGGAZGATTAGACGAZGCA	7638 (7638)
ODN4-18	Cy5-AGCTGAZGCTAGCGGAZGATAGACGAZGCA	10733 (10732)
ODN4-19	Cy5-AGCTGAZGCTTAGCGGAZGATTAGACGAZGCA	11342 (11341)
ODN4-20	FAM-TGCAY_5CGTCT	3861 (3861)
ODN4-21	Cy3-ATCAY_5CCGCT	3799 (3800)
ODN4-22	Cy5-AGCAY_5CAGCT	3874 (3875)
ODN4-23	ATCAY_5CCGCT	3293 (3293)

Table 4.4. Oligonucleotides used in the assembly of DNA fluorescent nanoconstructs (mass data spectra in Appendix, Figure 9.1.3). Z = amino-modified C6-dT, labelled with 6-azidohexanoic acid NHS ester; Y_5 = amino-modified C6-dT, labelled with BCN *N*-hydroxysuccinimide carbonate (Scheme 4.3).

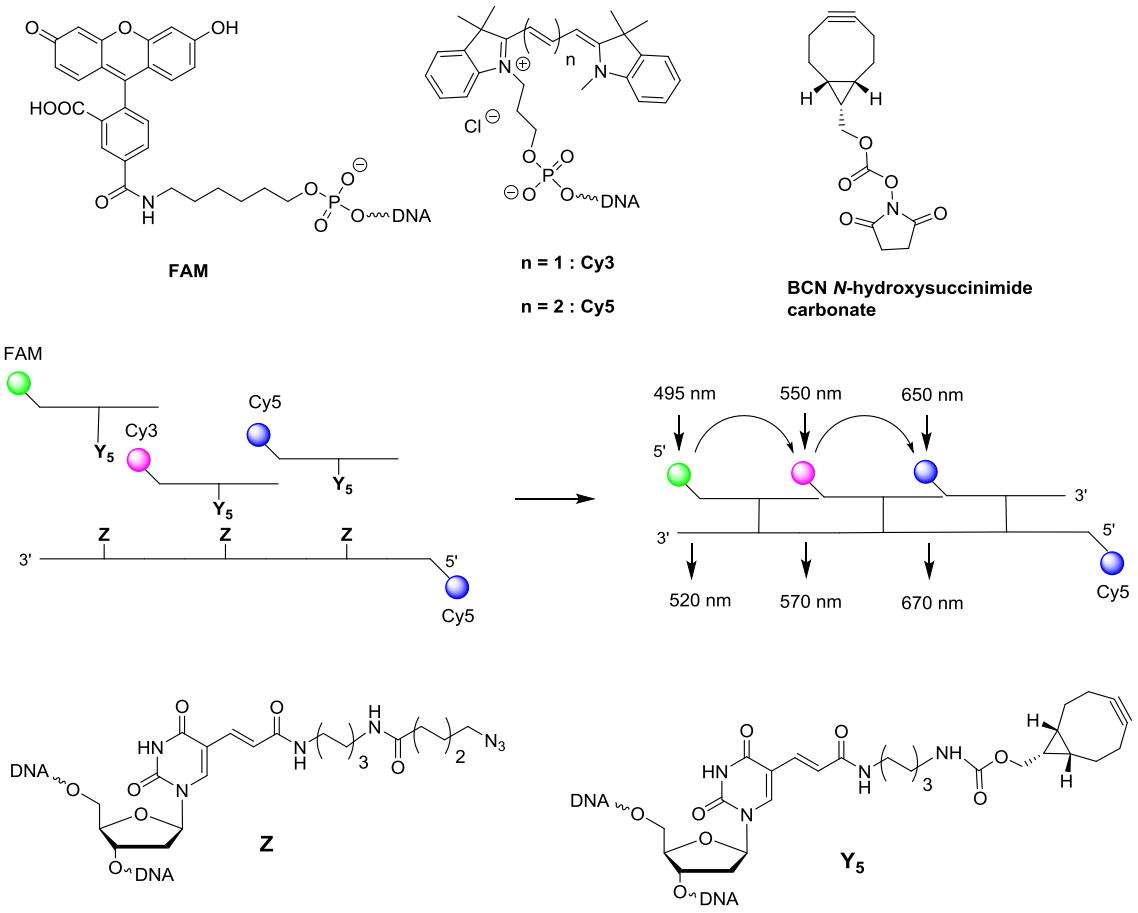

Scheme 4.3. Synthesis of fluorescent nanoconstructs. Z = amino-modified C6-dT, labelled with 6-azidohexanoic acid NHS activated ester; Y_5 = amino-modified C6-dT, labelled with BCN *N*-hydroxysuccinimide carbonate; FAM, Cy3 and Cy5 were incorporated into oligonucleotides using their corresponding phosphoramidite monomers, which are commercially available.

Codes	Sequences	Mass found (calc.)
NS1	ODN4-16+ODN4-20+ODN4-21+ODN4-22	21737 (21736)
NS2	ODN4-16+ODN4-20+ODN4-23+ODN4-22	21230 (21229)
NS3	ODN4-17+ODN4-20+ODN4-21	15300 (15299)
NS4	ODN4-17+ODN4-20+ODN4-23	14793 (14792)
NS5	ODN4-18+ODN4-20+ODN4-21+ODN4-22	22269 (22268)
NS6	ODN4-18+ODN4-20+ODN4-23+ODN4-22	21762 (21761)
NS7	ODN4-19+ODN4-20+ODN4-21+ODN4-22	22878 (22877)
NS8	ODN4-19+ODN4-20+ODN4-23+ODN4-22	22371 (22370)

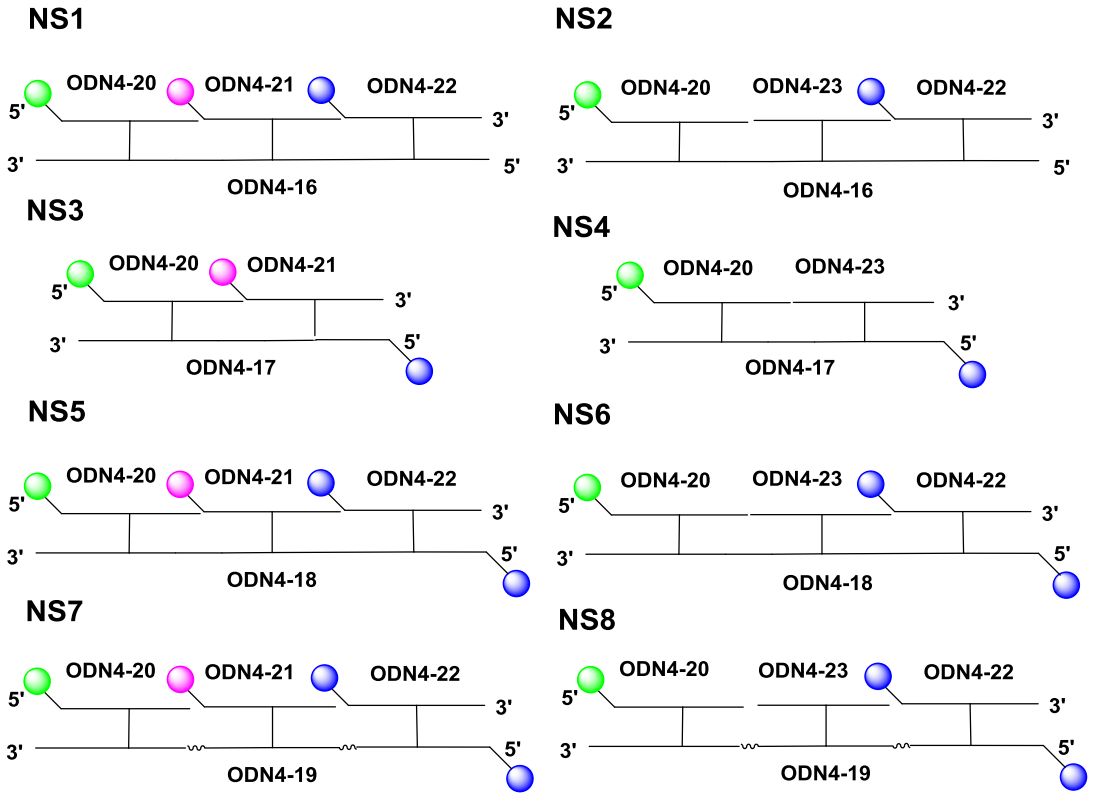

Table 4.5. The crosslinked fluorescent nanoconstructs (NS1–NS8) (mass data spectra in Appendix, Figure 9.1.3).

The synthesis of the fluorescent nanoconstruct NS1 (Table 4.5) proceeded remarkably smoothly (Figure 4.15). Each 10-mer fluorescent BCN-modified oligonucleotide (5′-FAM ODN4-20, 5′-Cy3 ODN4-21 and 5′-Cy5 ODN4-22) was added sequentially to the triple-azide-30-mer templated DNA (ODN4-16). The crosslinking click reaction was

carried out in 0.2 M NaCl at room temperature for 2 h. The covalent bonds formed in the crosslinking reaction are very important as they allow purification of the double-stranded structure NS1 by PAGE. This would not be possible if the strands were not covalently crosslinked. The control nanoconstruct NS2 (Table 4.5) was made by the same method, which consisted of crosslinking ODN4-16 to 5′-FAM ODN4-20, central unlabelled ODN4-23, and 5′-Cy5 ODN4-22. The PAGE analysis of crude crosslinked nanoconstructs NS1 and NS2 is shown in Figure 4.15. The desired nanoconstructs were observed together with traces of misassembled products, which could have arisen from non-templated SPAAC reactions. It is likely that the SPAAC reaction proceeded at a similar rate to duplex formation. It may be possible to optimise the process by carrying it out at a lower temperature, thereby reducing rate of the SPAAC reaction relative to the rate of duplex formation. However, it was found that the fluorescent crosslinked nanoconstructs could easily be obtained in high purity by PAGE, followed by reversed-phase HPLC. Further optimisation of the purification strategy was deemed unnecessary at this stage.

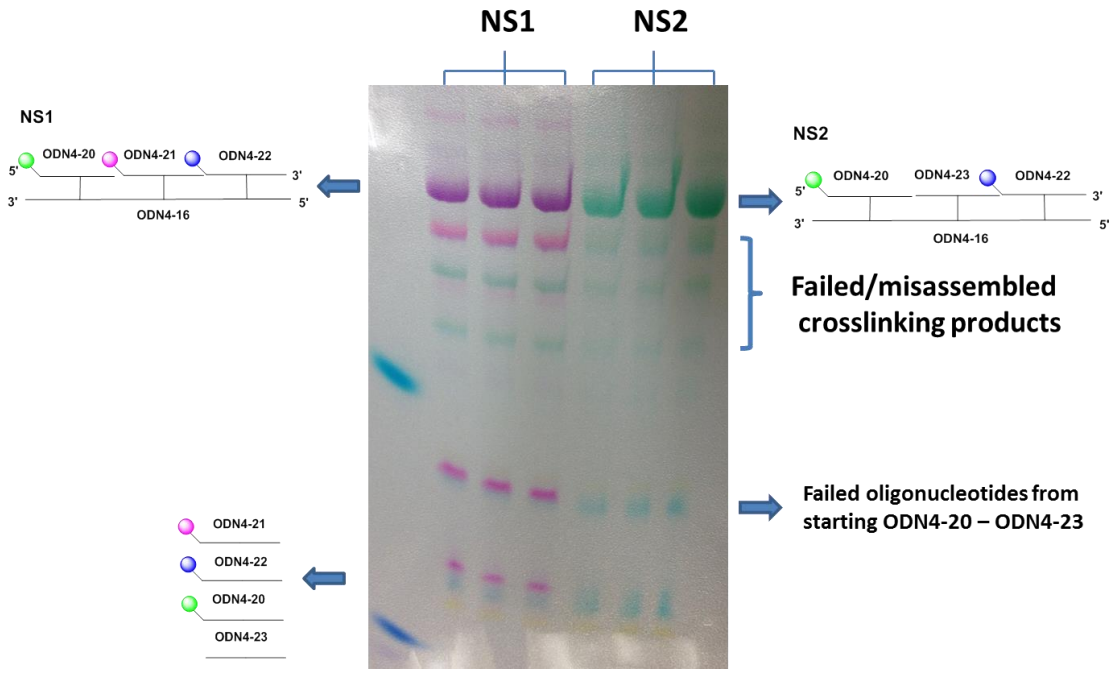

Figure 4.15. Denaturing polyacrylamide gel electrophoresis (PAGE) purification of crude SPAAC ligation reactions to synthesise the fluorescent nanoconstructs NS1 and NS2 (Table 4.5). The crude ligation reaction mixtures were analysed by 15% polyacrylamide/7 M urea gel electrophoresis at a constant power of 20 w for 2.5 h, using 1 × TBE buffer.

The nanoconstructs NS1 and NS2 were then used in fluorescence studies. The fluorescence emission of NS1, containing FAM and Cy3/5, was recorded by exciting at 495 nm (the excitation wavelength of FAM), and the fluorescence emission was measured to assess the transfer of energy from FAM to Cy3 to Cy5. The emission spectrum was dominated by the emission of Cy3 (Figure 4.16 A), with only a weak emission of Cy5, indicating that the energy transfer efficiency from Cy3 to Cy5 was low. This must be a consequence of the distance between the fluorophores and the relative orientations of the dyes, leading to only weak energy transfer from Cy3 to Cy5. However, the separation between Cy3 and Cy5 is only 10 bp, and as this is close to one helical turn, the dyes should both be on the same face of the duplex. As expected, NS2 did not give an intense fluorescence signal at 670 nm

(the emission wavelength of Cy5) when exciting at 495 nm (the excitation wavelength of FAM) (Figure 4.16 B) due to the longer distance (20 bp) and inefficient FRET between the FAM and Cy5 dyes; i.e. the overlap integral between the emission of FAM and excitation of Cy5 is very small.

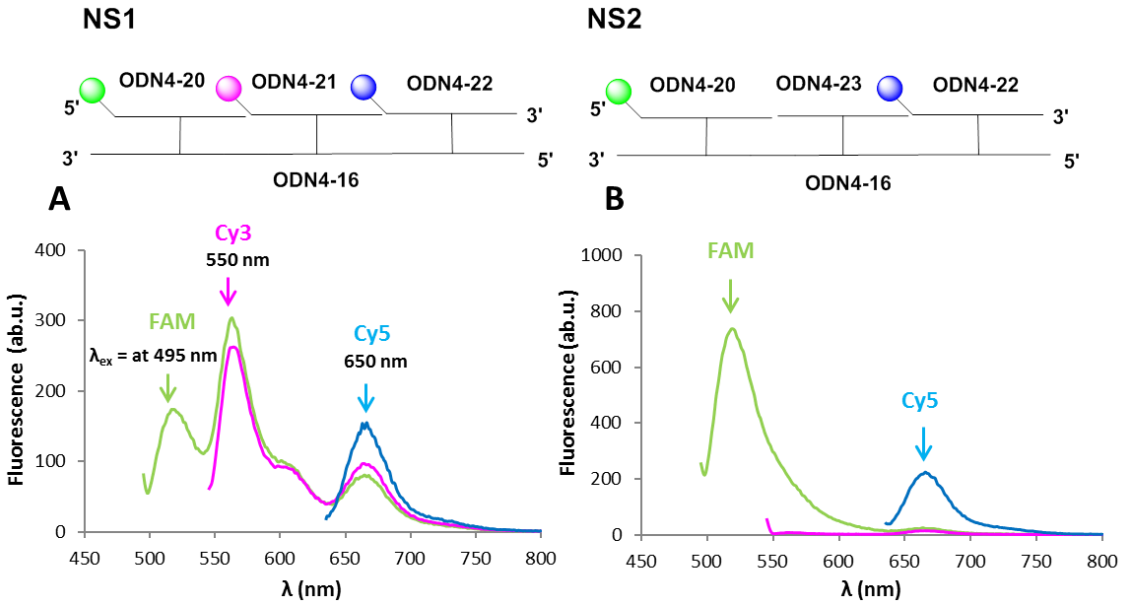

Figure 4.16. Fluorescence emission spectra of the FRET system for the SPAAC multi-crosslinked fluorescent DNA nanoconstructs (A: NS1 and B: NS2). Fluorescein (FAM) is excited at 495 nm (green) and energy is transferred to Cy3 (which emits at 570 nm) and Cy5 (which emits at 670 nm). Cy3 is excited at 550 nm (pink) and energy is transferred to Cy5 (which emits at 670 nm). Cy5 is excited at 650 nm (blue) and emits at 670 nm. NS1 and NS2 were dissolved in 200 µL phosphate buffer (NaH_2PO_4, 10 mM) with a total of 200 mM NaCl at pH 7.4, ab.u .= arbitrary unit.

The fluorescent nanoconstruct NS3 was also studied as a comparison (Figure 4.17 A). NS3 differs from NS1 in that the Cy5 dye is attached directly to the long template DNA strand rather than one of the short 10-mer strands. Comparison with NS1 suggested that having the Cy5 moiety on the template strand somehow led to a decrease in the FRET efficiency from FAM to Cy3, but also to an increase in the efficiency from Cy3 to Cy5, perhaps

because of a difference in the orientations of the dye moieties between NS1 and NS3. Control nanoconstruct NS4, which lacks a bridging Cy3 dye, shows weak energy transfer from FAM to Cy5 (Figure 4.17 B), it is likely that FAM and Cy5 are closer in space compared to nanoconstruct NS2. The emission of FAM around 520 nm in NS4 is surprisingly low.

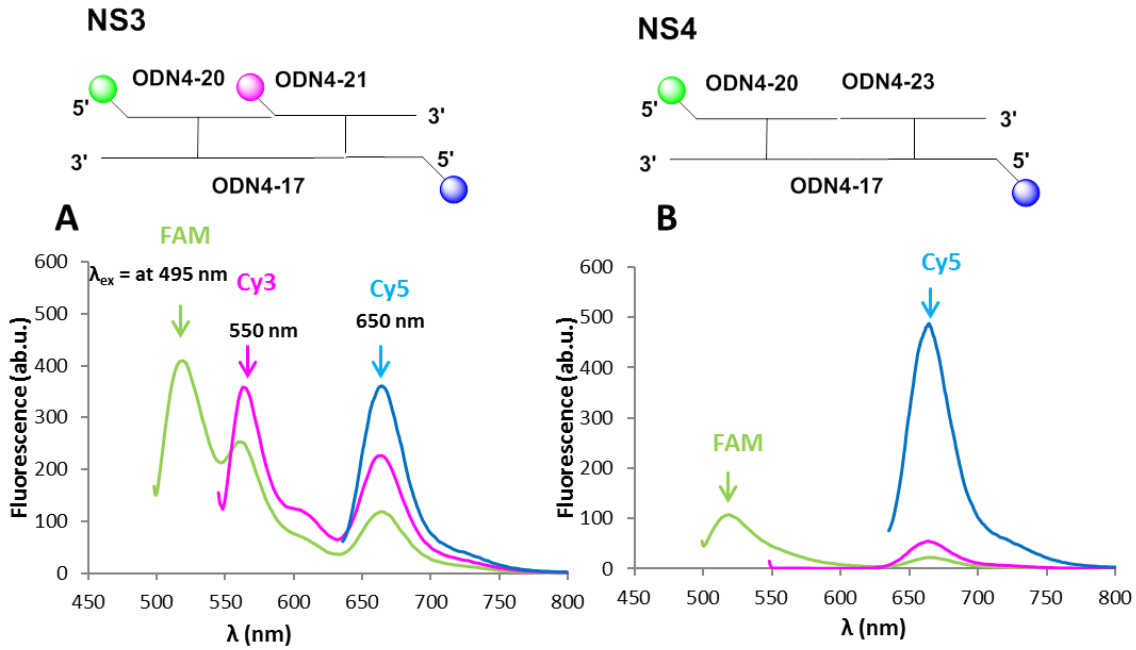

Figure 4.17. Fluorescence emission spectra of the FRET system for the SPAAC multi-crosslinked fluorescent DNA nanoconstructs (A: NS3 and B: NS4). Fluorescein (FAM) is excited at 495 nm (green) and energy is transferred to Cy3 (which emits at 570 nm) and Cy5 (which emits at 670 nm). Cy3 is excited at 550 nm (pink) and energy is transferred to Cy5 (which emits at 670 nm). Cy5 is excited at 650 nm (blue) and emits at 670 nm. NS3 and NS4 were dissolved in 200 µL phosphate buffer (NaH_2PO_4, 10 mM) with a total of 200 mM NaCl at pH 7.4, ab.u .= arbitrary unit.

In consideration of the low efficiency of energy transfer from FAM to Cy5 through Cy3 in nanoconstruct NS1, and the improved efficiency of transfer from Cy3 to Cy5 in NS3, new fluorescent nanoconstructs were designed by changing the template DNA. Nanoconstruct

NS5 incorporated two Cy5 dye moieties, one on the template strand, and another on a short 10-mer strand covalently linked to the template strand.

In NS5 (Figure 4.18 A), the efficiency of FRET from FAM to Cy5 *via* Cy3 was better than in nanoconstruct NS1 (Figure 4.16 A), due to the presence of two Cy5 acceptors; however, the overall efficiency was still low. As anticipated, the control nanoconstruct NS6, lacking a bridging Cy3 and with a long distance between FAM and Cy5, did not give a significant fluorescence signal at 670 nm (the emission wavelength of Cy5) when exciting at 495 nm (Figure 4.18 B). However, FAM emission around 520 nm was much stronger than in NS4.

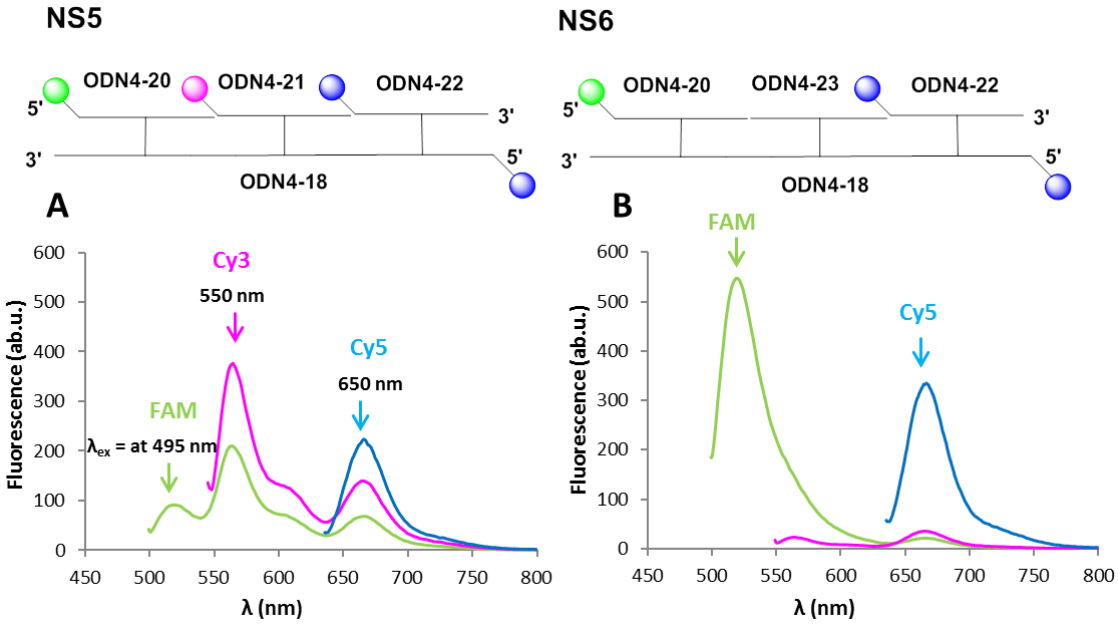

Figure 4.18. Fluorescence emission spectra of the FRET system for the SPAAC multi-crosslinked fluorescent DNA nanoconstructs (A: NS5 and B: NS6). Fluorescein (FAM) is excited at 495 nm (green) and energy is transferred to Cy3 (which emits at 570 nm) and Cy5 (which emits at 670 nm). Cy3 is excited at 550 nm (pink) and energy is transferred to Cy5 (which emits at 670 nm). Cy5 is excited at 650 nm (blue) and emits at 670 nm. NS5 and NS6 were dissolved in 200 µL phosphate buffer (NaH_2PO_4, 10 mM) with a total of 200 mM NaCl at pH 7.4, ab.u .= arbitrary unit.

The triple-azide-labelled 32-mer ODN4-19 was used to make the fluorescent nanoconstruct NS7 by crosslinking with 5′-FAM ODN4-20, 5′-Cy3 ODN4-21 and 5′-Cy5 ODN4-22. This structure incorporated gaps between duplex regions; these were added with the intention of making the nanoconstruct more flexible to allow more efficient energy transfer. The effectiveness of this design was confirmed by the emission spectrum of NS7 in Figure 4.19 A. Nanoconstruct NS7 allowed a much more efficient energy transfer. As expected, its control nanoconstruct NS8 did not give fluorescence energy transfer (Figure 4.19 B). More than 50% energy transfer from FAM to Cy3 was observed in the nanoconstructs NS1, NS5, NS7, but FRET was not efficient from Cy3 to Cy5. The efficiency of FRET is dependent on the sixth power of the distance between the donor and acceptor dyes, making FRET highly sensitive to small changes in distance[91] (details see Section 1.6, Chapter 1). The Förster distance between FAM and Cy3 is *ca.* 56 Å.[181] Cy3 and Cy5 have a Förster distance of *ca.* 50 Å.[92] In our nanoconstructs NS1–NS8, the distances between two dyes (FAM-Cy3, or Cy3-Cy5) are around 35–40 Å (10 or 11 bp), which does not include the intrinsic linkers attaching the dyes to the oligonucleotide strands. Also, the efficiency of FRET in double-stranded nucleic acids is dependent on the orientation factor, a function of the relative orientations of the two dyes.[92] In our nanoconstructs this angle can vary as the dyes are not rigidly attached to the DNA bases. The fluorescence response of FAM is sensitive to pH: below 7, FAM becomes protonated (no longer anionic), and has much lower fluorescence intensity.[182,183] The phosphate buffer (pH 7.4) used is not ideal for FAM fluorescence studies; in future optimization will be carried out using a buffer above pH 8. In addition, other FAM-substitute dyes will be used that do not have a strong pH-dependence of fluorescence, such as ATTO 495 and Alexa Fluor 500.

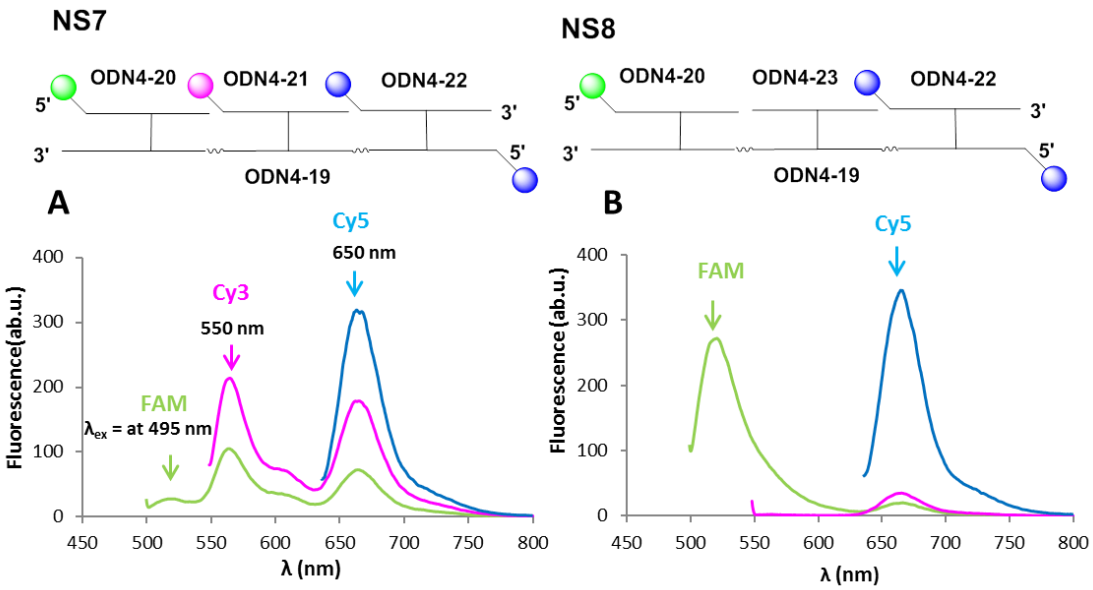

Figure 4.19. Fluorescence emission spectra of the FRET system for the SPAAC multi-crosslinked fluorescent DNA nanoconstructs (A: NS7 and B: NS8). Fluorescein (FAM) is excited at 495 nm (green) and energy is transferred to Cy3 (which emits at 570 nm) and Cy5 (which emits at 670 nm). Cy3 is excited at 550 nm (pink) and energy is transferred to Cy5 (which emits at 670 nm). Cy5 is excited at 650 nm (blue) and emits at 670 nm. NS7 and NS8 were dissolved in 200 µL phosphate buffer (NaH_2PO_4, 10 mM) with a total of 200 mM NaCl at pH 7.4, ab.u .= arbitrary unit.

The above experiments were carried out to help us to understand factors influencing the efficiency of FRET in crosslinked DNA nanoconstructs and to devise methods to improve (and predict) FRET in systems which involve three different dyes (in our test case FAM-Cy3-Cy5). Decreasing the length of dye-labelled oligonucleotides, altering the position of the dyes in the oligonucleotides, or varying the length of the linkers on the dyes, are factors that can be manipulated to make FRET more or less efficient in order to generate nanoconstructs with unique fluorescence spectra.

Comparing nanoconstructs NS1 and NS3, the main difference is the position of Cy5 dye; in NS1, Cy5 is attached to the shorter (10-mer) complementary DNA, however, for NS3, Cy5 is located in the long templating DNA (21-mer). The latter displayed more efficient FRET from Cy3 to Cy5. As a result, NS5 was designed with two Cy5, one in the template and the other in the complementary strand, the rationale being the use of two Cy5 acceptors for the FRET relay. Yet this did not improve the FRET, possibly due to the limited flexibility of the dyes. Consequently, NS7 containing gaps between duplex regions, was developed. The FRET from FAM to Cy3, or Cy3 to Cy5, was improved. These results suggest that Cy5 dye flexibility is important to energy transfer. Hence, varying the length of the Cy5 linker may improve FRET. Previously in the Brown group very short rigid linkers have been used to minimise dye mobility, and these could be evaluated in the present context.[76] Another important factor to consider is the ability of cyanine dyes to stack on the end of the DNA helix and to bind to the minor groove of DNA.[184] This will obviously affect the precise location and orientation of the dyes.

This is a preliminary study (a proof of principle) and in this regard it was encouraging, although some of the results were not predicted. Consequently much more work is now needed to study the fluorescence properties of these fluorescent DNA nanoconstructs. Other fluorescent dyes/combinations can be evaluated, and improved purification protocols for the nanoconstructs will be developed to ensure that small amounts of impurities (incorrectly assembled nanoconstructs) have been removed. The inherent sensitivity of fluorescent dyes means that these minor impurities can have a major effect on fluorescence. Actually this point emphasises the value of our covalent crosslinking strategy. It makes it ultimately possible to obtain pure fluorescent nanoconstructs as they are inherently stable entities and can be rigorously purified under denaturing conditions. This would be impossible for physically assembled DNA nanoconstructs. After a

systematic study which should yield a set of rules to predict FRET in covalently linked DNA nanoconstructs, a more detailed quantitative analysis of the fluorescent properties of the nanoconstructs will be carried out. However, at the current juncture this was deemed to be unjustified.

4.6 Conclusions

BCN-modified oligonucleotides were crosslinked to the complementary azide-labelled strands across the major and minor grooves of the DNA duplexes. In comparison with the DIBO-azide crosslinking click reaction, the BCN/azide SPAAC crosslinking reaction was faster and cleaner.

Instability of the BCN moiety to treatment with 3% TCA in DCM, used to remove 5′-DMT protecting groups during solid phase oligonucleotide synthesis was observed. 10% DCA in toluene can be used as an alternative, and this mild deblocking reagent helps to reduce the percentage of inactivated BCN.

In a pilot study, the synthesis of several crosslinked fluorescent nanoconstructs was carried out by utilising the SPAAC reactions in a convenient, simple and efficient process at room temperature. Various other dyes or quantum dots could also be used in such fluorescent nanoconstructs by crosslinking to the short complementary strands. The advantages of our crosslinked double-stranded nanoconstructs over normal duplexes are: i) their double stranded structure is extremely stable, it is not able to cross-hybridise with other strands; ii) their formation is based on Watson-Crick base pairing, therefore only giving the desired products in a controlled and predictable manner; iii) the products can be purified using denaturing polyacrylamide gel-electrophoresis; iv) the rigid duplex avoids the risk of collisional quenching.

The accurate measurement of FRET efficiency is not justified at this stage. Factors such as potential collisional fluorescence quenching from the BCN crosslinks, pH optima of the dyes, fluorescence lifetimes, binding of the dyes to the DNA duplex and nature of the linkers between the dyes and the DNA strands all need to be investigated. Single molecule

fluorescence studies are also possible on these systems. To this end, further work is currently being undertaken in the Brown group.

CHAPTER 5

Thiazole orange (TO) propargyl dT and its applications

Chapter 5 – Thiazole orange (TO) propargyl dT and its applications

5.1 Introduction

Fluorescent nucleic acid probes are playing increasingly important roles in clinical diagnostics and gene expression,[137] as well as in enabling the detection of biomolecules and monitoring their activities in living cells.[185] However, fluorophore-labelled nucleic acid probes can give a strong fluorescent background, in part due to design flaws, failed hybridization or excess probes binding to non-target biological species. The excess fluorescence also can produce false-positive signals. It is very difficult to remove background fluorescence, especially with *in vivo* assays such as live cell imaging. Therefore, it is necessary to design new nucleic acid probes which give a strong fluorescence signal when binding to the correct target nucleic acid and are efficiently quenched when present in a single-stranded form.

In this context, probes containing an intercalator dye such as thiazole orange (TO) are promising candidates. TO has been reported to be a useful photophysical probe for nucleic acid binding, as the fluorescence quantum yield increases up to 18,900 times upon binding to DNA,[105] as it is essentially non-fluorescent when unbound in aqueous solution. TO is made up of benzothiazole and quinoline moieties connected by a methine bridge. This structure allows TO to intercalate between the base pairs of a DNA duplex *via* rotation of the methine bridge, and is probably responsible for the strong fluorescence increase of TO on binding with DNA or RNA duplexes.[103,104] The intercalation of TO with nucleic acids has been characterized by Nygren *et al.*[106] The highest affinity of TO was seen to occur with double-stranded DNA duplexes; there was 5–10 fold weaker binding to single-stranded polypurines and a further 10–1000 fold weaker binding to single-stranded polypyrimidines.

TO dye has been widely utilised in nucleic acid probes, as described in Section 1.8 (Chapter 1). For instance, TO has been incorporated as a base surrogate into peptide nucleic acid (PNA) to detect base-mismatched hybridization,[186] or has replaced a canonical nucleobase to allow discrimination of a single base mutation.[114] Triplex-forming oligonucleotides (TFOs) containing TO have been shown to dramatically enhance fluorescence upon hybridization to DNA, with fluorescence quantum yields (φ) of 0.9% – 1.5% in the single strand versus 23.5% – 34.9% after the formation of DNA triplexes.[187] Doubly TO-labelled probes were designed by Okamoto, and these showed strong fluorescence after hybridization with complementary target nucleic acid sequences and a low background fluorescence in the single-stranded state.[121,125] This makes them promising candidates for use in live cell RNA imaging.[126]

The present work describes a simple and efficient nucleic acid probe system that has high fluorescence when hybridised to the target DNA or RNA strand and is effectively non-fluorescent in the single-stranded state. To achieve this objective, two alternative thymidine phosphoramidite monomers, both functionalised with TO (Figure 5.1), were synthesised.

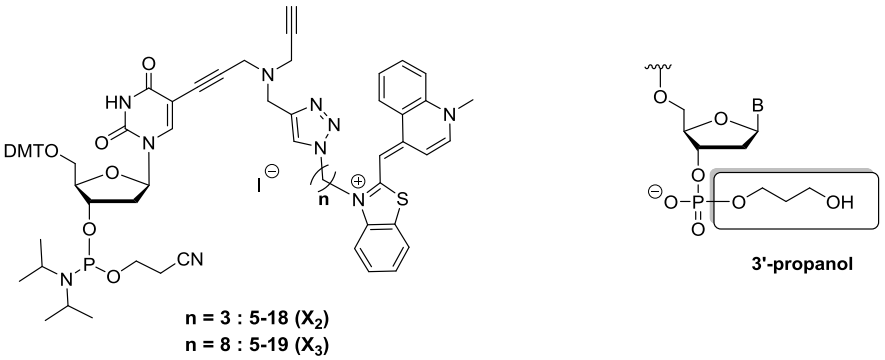

Figure 5.1. Two related phosphoramidite monomers for the insertion of TO into oligonucleotides, and 3′-propanol used to block probes in PCR applications.

TO was introduced into 5-tripropargylamine-2′-deoxyuridine *via* the Cu(I)-catalysed [3+2] azide-alkyne cycloaddition (CuAAC) reaction. The corresponding phosphoramidites were employed in solid phase oligonucleotide synthesis. The resulting nucleic acid probes were suitable for labelling with other fluorescent dye azides by post-synthetic click chemistry (CuAAC) on solid phase (oligonucleotide synthesis support).[157,188] In addition, the PCR blocker 3′-propanol was incorporated into the nucleic acid probes so that the probes were not able to act as PCR primers in reactions.[76,77]

5.2 Synthesis of thiazole orange derivatives (5-10/11)

Thiazole orange (TO) is an asymmetric cyanine dye, composed of a benzothiazole derivative and a quinolinium ring linked *via* a monomethine bridge. Two types of TO can be synthesised according to the positions of the linker-functionalised endocyclic nitrogen: one featuring a linker with the functional group at the quinoline nitrogen (TO_Q); another with functionalization at the benzothiazole nitrogen (TO_B). Most of the TO_Q-peptide conjugates in the literature have demonstrated higher quantum yields than those using TO_B.[108] According to analysis of the NMR structure of homodimeric thiazole orange with DNA, the two nitrogens point toward different grooves of the DNA helix. TO_Q prefers to point into the minor groove, while TO_B is directed towards the base in the major groove.[108,189]

The aim of this work was to join TO to the 5-position of uracil *via* a tripropargylamine linker and to direct the dye into the major groove of the DNA duplex. Functionalizing at the benzothiazole nitrogen (TO_B) seemed to be an appropriate means of achieving this goal. However, the azide-modified TO dyes that are required for click conjugation to DNA or

RNA, are not commercially available. The synthesis of TO dyes functionalised with terminal azides has previously been reported by Wagenknecht *et al*.[118] In their method, TO azide was attached to a 2′-*O*-propargyl uridine post-synthetically by Cu(I)-catalysed azide alkyne cycloaddition chemistry (CuAAC). The precursor **5-5** was synthesised, then converted to compound **5-10** *via* a mesyl intermediate (Scheme 5.1). The TO azide was produced in a one pot conversion with a very low yield (5%).[118] Unfortunately this reaction was unsuccessful and optimization of the TO azide synthesis was necessary.

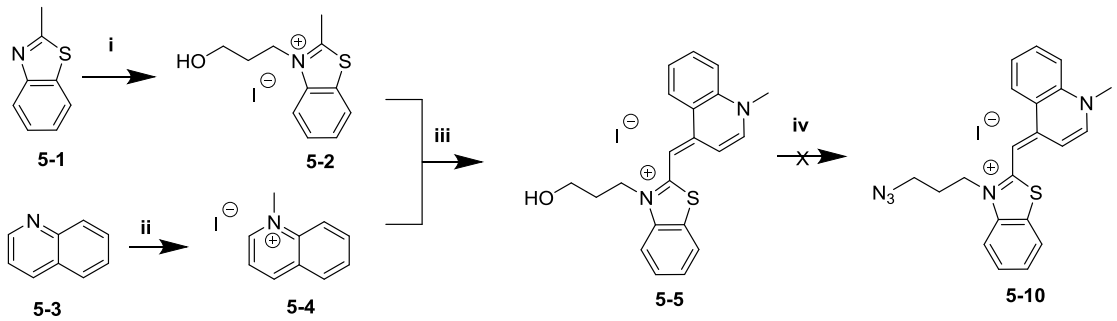

Scheme 5.1. Synthesis of *N*-(3-azidopropyl)-2-[(1,4-dihydro-1-methylquinolin-4-ylidene)methyl] benzothiazolium iodide **5-10** by Wagenknecht.[118] Reagents and conditions: (i) 3-iodo-1-propanol, MeCN, 110 °C, 44 h, 86%; (ii) iodomethane, MeCN, 38 °C, 21 h, 98%; (iii) DCM/MeOH (1:1), anhydrous Et_3N, RT, 16 h, cold Et_2O, 12%; (iv) DMSO, Et_3N, mesyl chloride, RT, 2 h, then NaN_3, 120 °C, 24 h.

In order to improve the synthesis, thiazole orange azides **5-10** and **5-11** were synthesised from azide derivatives of benzothiazole **5-8** and **5-9** by coupling with *N*-methylquinolinium iodide **5-4** respectively (Scheme 5.2). The reaction of alkyl dihalides 1,3-diiodopropane and 1,8-diiodooctane with the commercially available 2-methylbenzothiazole gave iodide salts **5-6** and **5-7**, respectively. After conversion of iodo to azide, *N*-alkyl substituted quinolinium salt **5-4** was coupled to azides, to give

5-10 and **5-11** in yields of 29% and 25% respectively.

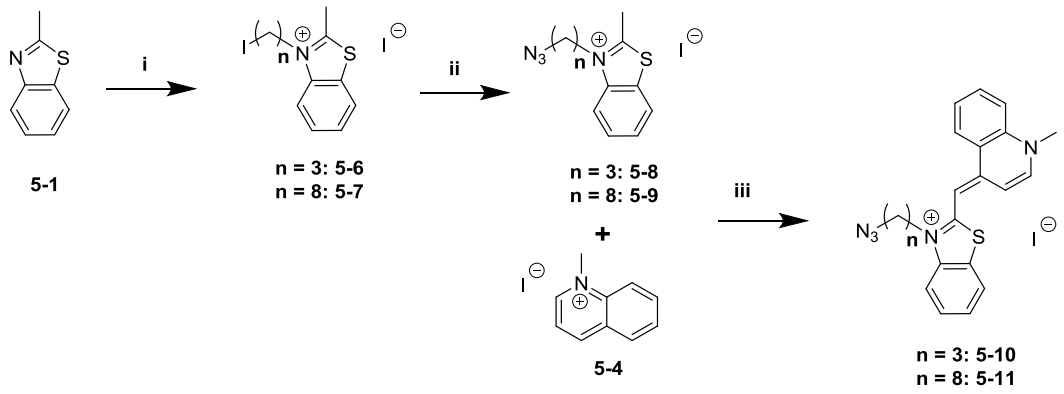

Scheme 5.2. Synthesis of *N*-(3-azidopropyl)-2-[(1,4-dihydro-1-methylquinolin-4-ylidene)methyl] benzothiazolium iodide **5-10** and *N*-(8-azidooctyl)-2-[(1,4-dihydro-1-methylquinolin-4-ylidene)methyl] benzothiazolium iodide **5-11**. Reagents and conditions: (i) n = 3: 1,3-diiodopropane, MeCN, 105 °C, 48 h, 64%; n = 8: 1,8-diiodooctane, MeCN, 150 °C, 27 h, 67%; (ii) n = 3: MeCN, NaN_3 in H_2O, RT, 19 h, 55%; n = 8: MeCN, NaN_3 in H_2O, RT, 19 h, 54%. (iii) DCM/MeOH (1:1), anhydrous Et_3N, RT, 16 h, n = 3: 29%; n = 8: 25%.

5.3 Synthesis of TO-dT phosphoramidite monomers (5-18/19)

The 5-tripropargylamine-modified dT phosphoramidite monomer **5-15** was synthesised from intermediate nucleoside **5-14**, then used for solid phase oligonucleotide synthesis. The 5-tripropargylamine-modified 5′-*O*-(4,4′-dimethoxytrityl)-2′-deoxyuridine **5-14** was subjected to conventional phosphitylation conditions[72] of 2-cyanoethyl *N*,*N*-diisopropylchlorophosphoramidite in a mixture of *N*,*N*-diisopropylethylamine (DIPEA), DCM to afford compound **5-15** in 77% yield.

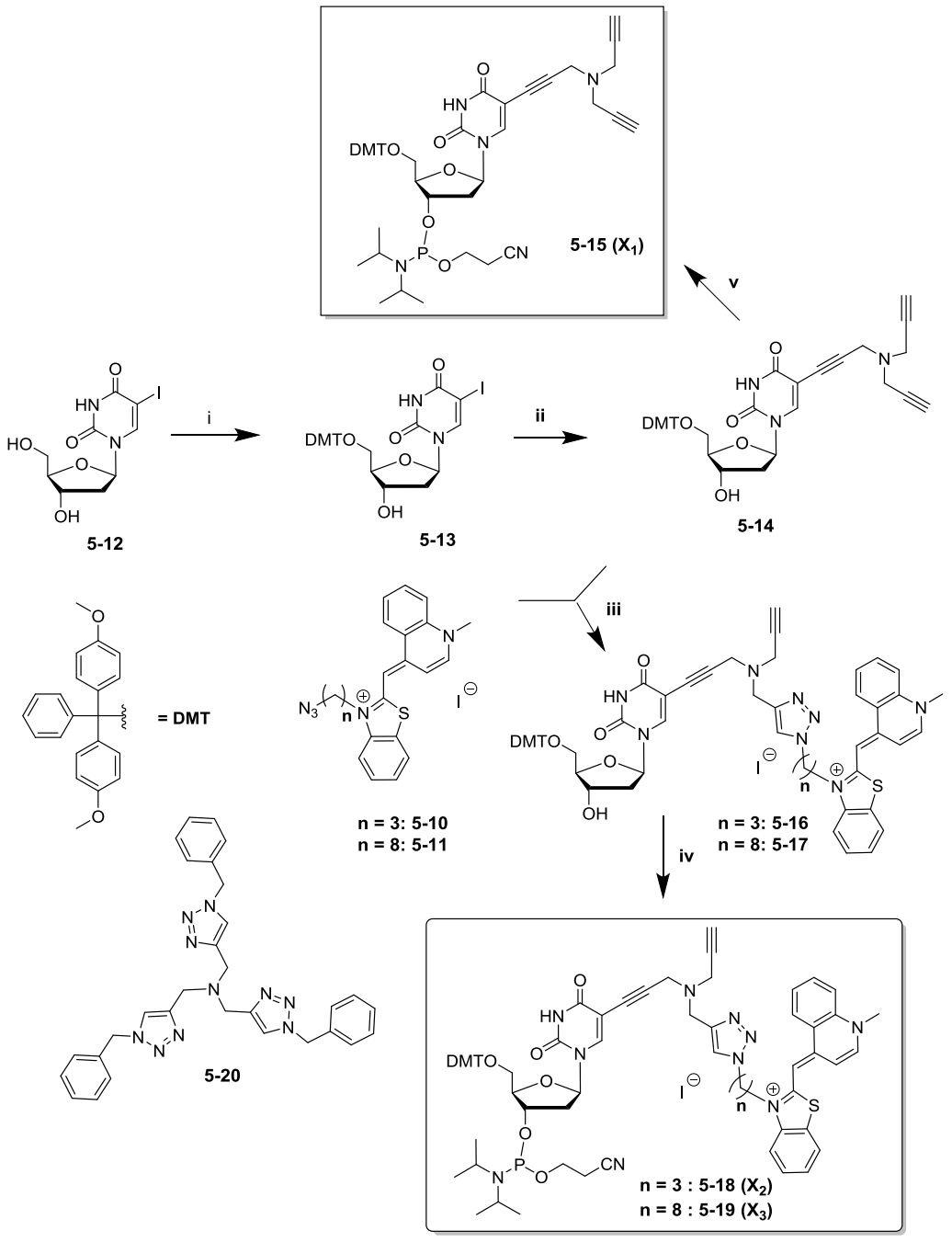

Scheme 5.3. Synthesis of tripropargylamine-modified dT phosphoramidite monomers **5-15** and TO-dT phosphoramidite monomers **5-18** and **5-19**. Reagents and conditions: (i) DMTrCl, pyridine, RT, 1 h, 82%; (ii) DMF, Et_3N, tripropargylamine, CuI, $Pd(PPh_3)_4$, RT, 14 h, 63%; (iii) TBTA (**5-20**), DMF, $CuSO_4 \cdot 5H_2O$, sodium ascorbate in H_2O, RT, 2 h, n = 3: 38%; n = 8: 29%; (iv) anhydrous DCM, anhydrous DMF, DIPEA, 2-cyanoethyl *N*,*N*-diisopropylchlorophosphoramidite, RT, 2 h, n = 3: 70%, n = 8: 66%; (v) anhydrous DCM, DIPEA, 2-cyanoethyl *N*,*N*-diisopropylchlorophosphoramidite, RT, 1.5 h, 77%.

5-Iodo-[5′-*O*-(4,4′-dimethoxytrityl)]-2′-deoxyuridine **5-13** was synthesised by reaction of a slight excess of 4,4′-dimethoxytrityl chloride (DMTrCl) with the commercially available 5-iodo-2′-deoxyuridine **5-12** in 82% yield. A Sonogashira reaction[190] was then carried out using tripropargylamine. The reaction was carried out at room temperature to give the product **5-14** in 63% yield. CuAAC click reactions were carried out between terminal bis-alkyne nucleoside **5-14** and organic azide **5-10** or **5-11** to give the desired products **5-16** and **5-17** with yields of 38% and 29%, respectively after purification. Compounds **5-16** and **5-17** were subjected to conventional phosphitylation conditions to afford phosphoramidite monomers **5-18** and **5-19** in 70% and 66% yield respectively.

5.4 Synthesis of TO-modified oligonucleotides

The three separate monomers; tripropargylamine-modified dT (X_1), TO3-dT (X_2) and TO8-dT (X_3) (Scheme 5.3), were successfully incorporated into four oligonucleotide sequences: 13-mer oligonucleotides (type-S) and 22-mer oligonucleotides (type-L1, L2 and L3) (Table 5.1). Fast deprotecting monomers (UltraMILD monomers Pac-dA, Ac-dC and iPr-Pac-dG, Figure 1.6, Section 1.2, Chapter 1), including above modified monomers (X_1–X_3) were used in the oligonucleotide syntheses. Cleavage of oligonucleotides from solid support and deprotection was achieved by exposure to concentrated aqueous ammonia solution for 4 h at room temperature. Subsequently sequences were purified by HPLC, and characterised by mass spectrometry. The control oligonucleotides (S-control, L-control) and their corresponding complementary strands (S-Acomp, L-Acomp) were also synthesised (Table 5.1).

Codes	Sequences	Mass found (calc.)
S-control	TCATCCTATTCTC	3836 (3836)
S-alkyne	TCATCCTAX_1TCTC	3951 (3951)
S-TO3	TCATCCTAX_2TCTC	4323 (4325)
S-TO8	TCATCCTAX_3TCTC	4394 (4395)
S-Acomp	GAGAATAGGATGA	4072 (4072)
L-control	CGCTTCTGTATCTATATTCATCP	6764 (6764)
L1-(alkyne)2	CGCTTCX_1GTATCTAX_1ATTCATCP	6994 (6994)
L1-(TO3)2	CGCTTCX_2GTATCTAX_2ATTCATCP	7741 (7742)
L2-alkyne	CGCTTCX_1GTATCTATATTCATCP	6879 (6878)
L2-TO3	CGCTTCX_2GTATCTATATTCATCP	7251 (7252)
L2-TO8	CGCTTCX_3GTATCTATATTCATCP	7322 (7322)
L3-alkyne	CGCTTCTGTATCTAX_1ATTCATCP	6879 (6878)
L3-TO3	CGCTTCTGTATCTAX_2ATTCATCP	7251 (7252)
L3-TO8	CGCTTCTGTATCTAX_3ATTCATCP	7322 (7322)
L-Acomp	CTATGATGAATATAGATACAGAAGCGTCAT	9262 (9262)

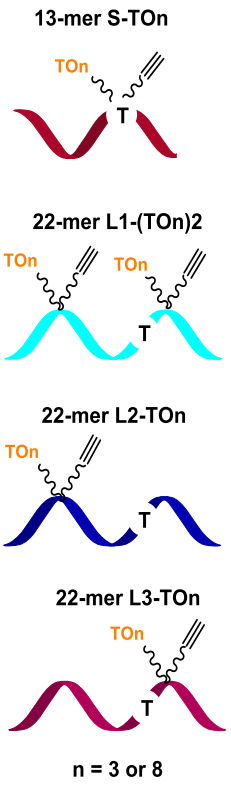

Table 5.1. Oligonucleotide sequences (mass spectra data in Appendix, Figure 9.1.4). X_1 = tripropargylamine-modified dT; X_2 = TO3-dT; X_3 = TO8-dT; P = 3′-propanol PCR blocker (Figure 5.1); the position of mutation to be detected is underlined. The T in the schematic diagram highlights the position of this mutation to be detected relative to the positions of the fluorophores.

5.5 UV melting studies of TO-modified oligonucleotides

For biological applications it is vitally important to understand the properties of the modified DNA duplexes. UV melting studies were carried out to investigate the dissociation temperatures of the TO-modified probes from their complementary DNA and RNA targets and thereby the effect of the TO dye on duplex stability. It was also necessary to study the thermal stability of more complicated nucleic acid probes incorporating up to four TO dyes. The studies were conducted on four types of oligonucleotides (type-S, L1, L2 and L3) with sequences listed in Table 5.1.

5.5.1 Single TO on a T-nucleobase

Biophysical studies were carried out on the 13-mer ODNs (type-S) and the 22-mer ODNs (type-L1–L3). The results of melting studies on the duplexes are shown in Table 5.2. The melting temperature (T_m) of the natural duplexes and tripropargylamine (alkyne)-modified duplexes were found to be similar. Attachment of the tripropargylamine functional group caused a T_m change between +0.4 °C and –0.1 °C.

After attachment of the TO dyes, the melting temperatures of the 13-mer (S) duplexes were 55.4 °C and 53.0 °C respectively for the two TO linkers (TO3, TO8). Compared to the natural control S-ds (43.8 °C) and the tripropargylamine-modified control S-alkyne-ds (44.1 °C), the introduction of TO resulted in a significant improvement in DNA duplex stability, 11.6 °C when using TO3, and 9.2 °C for TO8. TO is an intercalating dye that can stabilize the duplex by π-stacking interactions.[191] The melting studies suggest that the TO-DNA duplex with the longer spacer (TO8) provides TO with a higher degree of flexibility than the shorter spacer (TO3); this unwanted conformational flexibility results in additional conformational flexibility and a decrease in duplex stability.

For the 22-mer oligonucleotides (L1–L3), the T_m values of TO3-probe DNA duplexes were 4–9 °C higher compared with those of the corresponding DNA duplexes with unmodified DNA and tripropargylamine-modified DNA. Incorporation of two TO3-dT monomers (X_2) into L1-(TO3)2 resulted in a *ca.* 3 °C higher T_m value compared to L2-TO3 and L3-TO3 (one TO3-dT addition). This result indicates that multiple additions of a duplex-stabilizing monomer produce an enhanced effect as two independent TO3-dT monomers give a greater increase in duplex stability than a single modification. Comparing L2-TO3 and L3-TO3, which have the same sequence but different positioning of TO, only a 0.7 °C difference in T_m is observed (L2-TO3-ds (66.7 °C) *vs.* L3-TO3-ds

(66.0 °C)). The intercalation of TO3 is known to be dependent on the oligonucleotide sequence and the neighbouring bases.[125] However, in the sequence we used the effect of different neighbouring bases was negligible.

Structures	Duplexes	T_m (°C)	ΔT_m (°C)
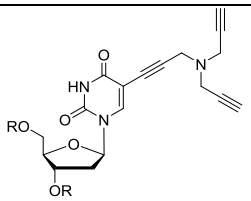	S-alkyne-ds	44.1	+ 0.3
	L1-(alkyne)2-ds	61.1	+ 0.4
	L2-alkyne-ds	61.1	+ 0.4
	L3-alkyne-ds	60.6	– 0.1
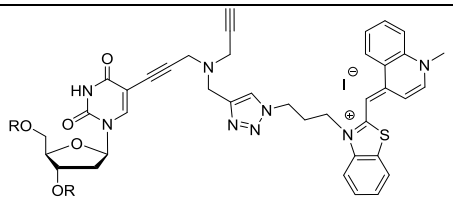	S-TO3-ds	55.4	+ 11.6
	L1-(TO3)2-ds	69.4	+ 8.7
	L2-TO3-ds	66.7	+ 6.0
	L3-TO3-ds	66.0	+ 5.3
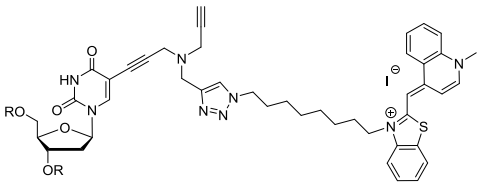	S-TO8-ds	53.0	+ 9.2
	L2-TO8-ds	65.2	+ 4.5
	L3-TO8-ds	64.7	+ 4.0
Natural controls (unmodified duplexes)	S-ds	43.8	
	L-ds	60.7	

Table 5.2. UV melting studies of 13-mer (S) and 22-mer (L1–L3) ODNs with single TO (TO3 or TO8) on a T-nucleobase. T_m: melting temperature; ΔT_m: difference in melting temperature of modified duplexes compared to the corresponding unmodified duplexs (S-ds and L-ds). T_m values are the average of 3 separate melting and annealing curves. Melting temperatures are accurate to ± 0.1 °C. R: DNA.

There was a clear difference between TO3 and TO8 in 22-mer oligonucleotides. The longer linker (TO8) gave rise to less stable DNA duplexes than the shorter linker (TO3). The T_m values were lower by up to 1.5 °C (L2-TO3-ds (66.7 °C) *vs.* L2-TO8-ds (65.2 °C), L3-TO3-ds (66.0 °C) *vs.* L3-TO8-ds (64.7 °C)). These results confirm that TO with a shorter spacer (TO3) is more efficient in stabilizing a TO-DNA duplex.

5.5.2 The effect of mismatches and bulges on the stability of TO-DNA duplexes

To detect the sensitivity of the TO probes to sequence differences, the hybridization selectivity of TO3-modified probes (S-TO3, 13-mer) and (L1-(TO3)2, L2-TO3 and L3-TO3, 22-mer) was investigated by studying fully matched and mismatched duplexes. 13-mer S-TO3 was also used to understand the influence of bulges (an "extra" unpaired nucleobase with no counterpart in DNA duplex) adjacent to the T(TO3)-A base pair. The mismatched and bulged sequences are shown in Table 5.3.

Codes	Sequences	Mass found (calc.)
S-Bulged-T1	GAGAA<u>T</u>TAGGATGA	4376 (4376)
S-Bulged-T2	GAGA<u>T</u>ATAGGATGA	4376 (4376)
S-Bulged-C1	GAGAA<u>C</u>TAGGATGA	4361 (4361)
S-Bulged-C2	GAGA<u>C</u>ATAGGATGA	4361 (4361)
S-C-mismatch	GAGA<u>C</u>TAGGATGA	4048 (4048)
S-T-mismatch	GAGA<u>T</u>TAGGATGA	4063 (4063)
S-G-mismatch	GAGA<u>G</u>TAGGATGA	4088 (4088)
L-G-mismatch	CTATGATGAATAT<u>G</u>GATACAGAAGCGTCAT	9278 (9278)

Table 5.3. Oligonucleotides used for the study of TO-modified DNA duplex stability. S-bulged sequences: the complementary strand of S-TO3 has an "extra" unpaired nucleobase (T or C); S-(C-, T- and G-) mismatch sequences of S-TO3; L-G-mismatch sequence of L1-(TO3)2, L2-TO3 and L3-TO3; position of mismatch to be detected is underlined.

The results of melting studies are shown in Table 5.4. The mismatches cause a major decrease in DNA duplex stability. Compared with the fully matched duplex (S-TO3-ds, 55.4 °C), the T_m of the CT-mismatched duplex (S-TO3-CT-mis, 41.9 °C) was significantly decreased by 13.5 °C. The GT-mismatched duplex melting temperature was reduced by 9.1 °C. In addition, TO3-dT monomer gave a greater increase (around 10 °C, $\Delta T_m^{\ b}$ in

Table 5.4) in mismatched duplex stability compared to the related unmodified mismatched duplexes. This indicates that the mismatched base pair strongly destabilizes the modified DNA duplex, and that the S-TO3 exhibits potent mismatch discrimination, a highly desirable property.

Duplexes	T_m (°C)	ΔT_m[a] (°C)	ΔT_m[b] (°C)
S-TO3-ds (A<u>T</u>)	55.4		
S-TO3-C<u>T</u>-mis	41.9	– 13.5	+ 10.5
S-TO3-T<u>T</u>-mis	43.7	– 11.7	+ 10.0
S-TO3-G<u>T</u>-mis	46.3	– 9.1	+ 10.6
S-ds (A<u>T</u>)	43.8		
S-C<u>T</u>-mis	31.4	– 12.4	
S-T<u>T</u>-mis	33.7	– 10.1	
S-G<u>T</u>-mis	35.7	– 8.1	

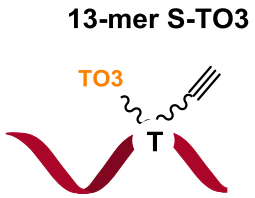

Table 5.4. UV melting studies of 13-mer S-control and S-TO3 forming mismatched duplexes. T_m: melting temperature; ΔT_m[a]: difference in melting temperature of mismatched duplexes compared to the fully complementary duplex; ΔT_m[b]: difference in melting temperature of the 13-mer S-TO3 mismatched duplex and its S-control mismatched duplex. T_m values are the average of 3 separate melting and annealing curves. Melting temperatures are accurate to ± 0. 1 °C. The T in the schematic diagram highlights the position of this mutation to be detected relative to the positions of the fluorophores.

The bulged template DNA strands (S-Bulged-T1/T2, C1/C2, Table 5.3) were designed to contain unpaired pyrimidine bases (C, T). Upon hybridization, depending on the location of the bulge, there is the possibility of 3′-intercalation (Table 5.5, A) or 5′-intercalation of TO into the gap (Table 5.5, B). Melting studies with bulged duplexes (S-3′-C-ds, S-5′-C-ds, S-3′-T-ds and S-5′-T-ds) were carried out to establish the effects of different unpaired nucleobases as bulges. A single TO unit led to greatly enhanced duplex stability in the fully complementary control duplex (S-TO3-ds). In contrast, when

S-TO3 was hybridised to the bulged DNA strands, a great decrease of melting temperature compared to the fully matched duplex (S-TO3-ds) was observed (ΔT_m = –7.6 to –11.3 °C, Table 5.5), but the T_m values were still slightly higher than natural duplexes (S-ds, T_m = 43.8 °C, Table 5.2). In addition, 5′-intercalation was shown to be more stabilising than 3′-intercalation according to the T_m values (Table 5.5). It appears that the bulge weakens the TO3 intercalation in the duplex, particularly on the 3′-intercalation of TO3. Mismatch discrimination studies were also carried out on the 22-mer ODNs L-control, L1-(TO3)2, L2-TO3 and L3-TO3. The fully matched (TA) and TG-mismatched duplexes are discussed here as a simple comparison. The TG-mismatched duplex has a decreased melting temperature of 3–4 °C when compared to the fully matched duplex (Table 5.6).

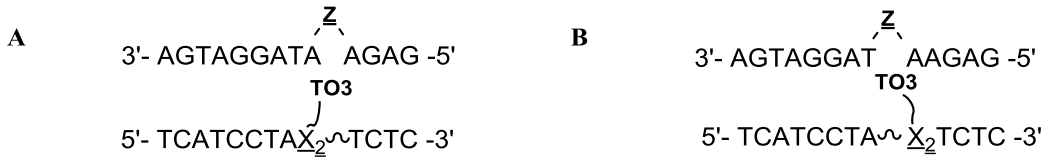

	A (3′-intercalation)		**B** (5′-intercalation)		**Control**
Duplexes	S-3′-T-ds	S-3′-C-ds	S-5′-T-ds	S-5′-C-ds	S-TO3-ds
Z	**T**	**C**	**T**	**C**	
T_m (°C)	45.9	44.1	47.8	47.5	55.4
ΔT_m (°C)	– 9.5	– 11.3	– 7.6	– 7.9	

Table 5.5. UV melting studies of the 13-mer S-TO3 bulged duplexes. T_m: melting temperature; ΔT_m: difference in melting temperature of the bulged duplexes compared to the fully complementary duplex; Z = T or C nucleobase, X_2 = TO3-dT. T_m values are the average of 3 separate melting and annealing curves. Melting temperatures are accurate to ± 0.1 °C.

Duplexes	T_m (°C)	ΔT_m (°C)
L-ds (TA)	60.7	
L-TG-mis	57.4	– 3.3
L1-(TO3)2-ds (TA)	69.4	
L1-(TO3)2-TG-mis	65.9	– 3.5
L2-TO3-ds (TA)	66.7	
L2-TO3-TG-mis	63.2	– 3.5
L3-TO3-ds (TA)	66.0	
L3-TO3-TG-mis	62.3	– 3.7

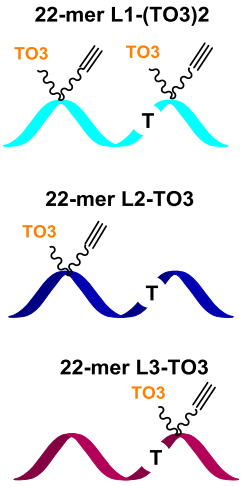

Table 5.6. UV melting studies of the 22-mer L1-(TO3)2, L2-TO3 and L3-TO3. T_m: melting temperature; ΔT_m: difference in melting temperature of L-control, L1-(TO3)2, L2-TO3 and L3-TO3 with the L-G-mismatch strand (TG-mis) compared to the complementary strand (TA). T_m values are the average of 3 separate melting and annealing curves. Melting temperatures are accurate to ± 0.1 °C. The T in the schematic diagram highlights the position of this mutation to be detected relative to the positions of the fluorophores.

5.6 Labelling TO-modified ODNs with fluorescent dyes by the CuAAC reaction

Polytriazoles are Cu(I)-stabilizing ligands in the catalysed Huisgen 1,3-dipolar cycloaddition of azides to terminal alkynes (CuAAC). The ligands tightly bind to Cu(I), stabilising the +1 oxidation state and minimising degradation of oligonucleotides. The copper complex with tris(benzyltriazolylmethyl)amine (TBTA) allows formation of the copper(I)-acetylide/ligand complex quickly, which is the starting point for the catalytic cycle of the Cu(I)-catalysed ligation (Figure 1.9, Section 1.3, Chapter 1).[36] The modified Monomers X_2 and X_3 (Figure 5.1) were synthesised using TBTA ligand **5-20** (Scheme 5.3). Of the various ligands that have been investigated, TBTA is widely used for Cu(I)

catalysed reactions in organic solvents, while tris(3-hydroxypropyltriazolylmethyl)amine (THPTA) ligand is more commonly used for reactions in aqueous solution.[192]

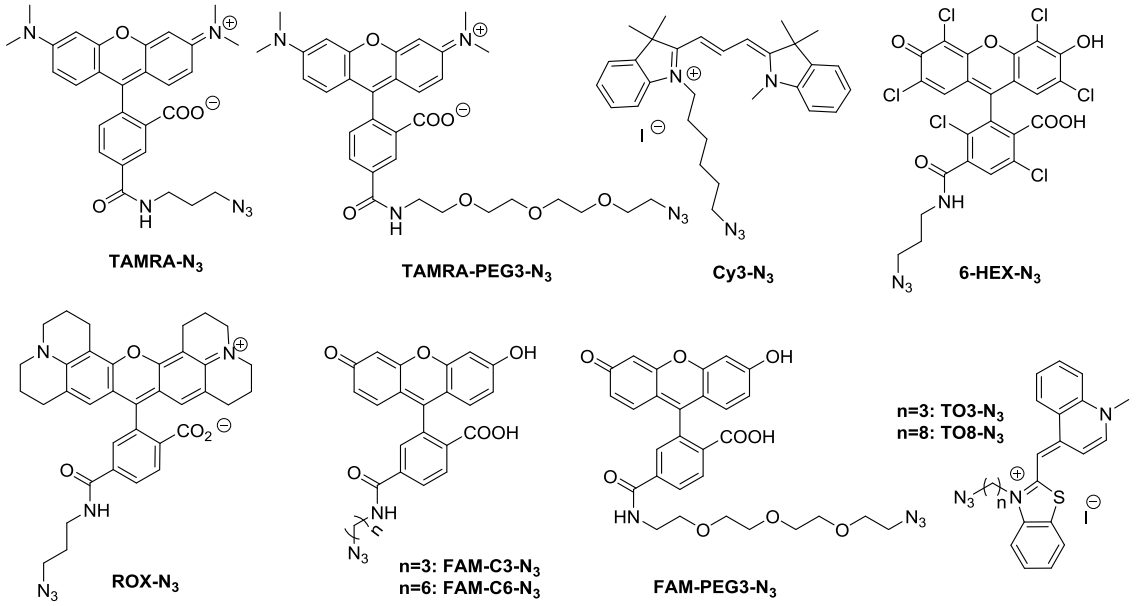

Figure 5.2. Structures of azide dyes for the labelling of TO probes.

The labelling of oligonucleotides with fluorescent dyes (Figure 5.2) was carried out post-synthetically (after oligonucleotide assembly) on the solid support using the CuAAC reaction in the presence of THPTA (Scheme 5.4). Sodium ascorbate and copper(II) sulfate were used to prepare the catalyst Cu(I), and the fluorescent dyes were dissolved in DMSO. All steps were carried out under an atmosphere of argon. After reaction, the solid support was washed several times with H_2O and acetonitrile to remove excess dyes and catalysts, and dried under a stream of argon. Oligonucleotide deprotection and cleavage from solid support was achieved by treating with concentrated aqueous ammonia for 4 h at room temperature. The resulting ODNs were purified by reversed-phase HPLC and characterised by mass spectrometry. The efficiency of dye labelling depends on the click reaction (CuAAC), which may be affected by the dye structures and the number of the added dyes

(steric effects). The HPLC chromatograms (Figure 5.3, Figure 5.4) of the crude labelled oligonucleotides showed that labelling with one or two additions of smaller dyes gives high labelling efficiency, almost 100% if the failed starting oligonucleotides (lacking the alkyne) are taken into account.

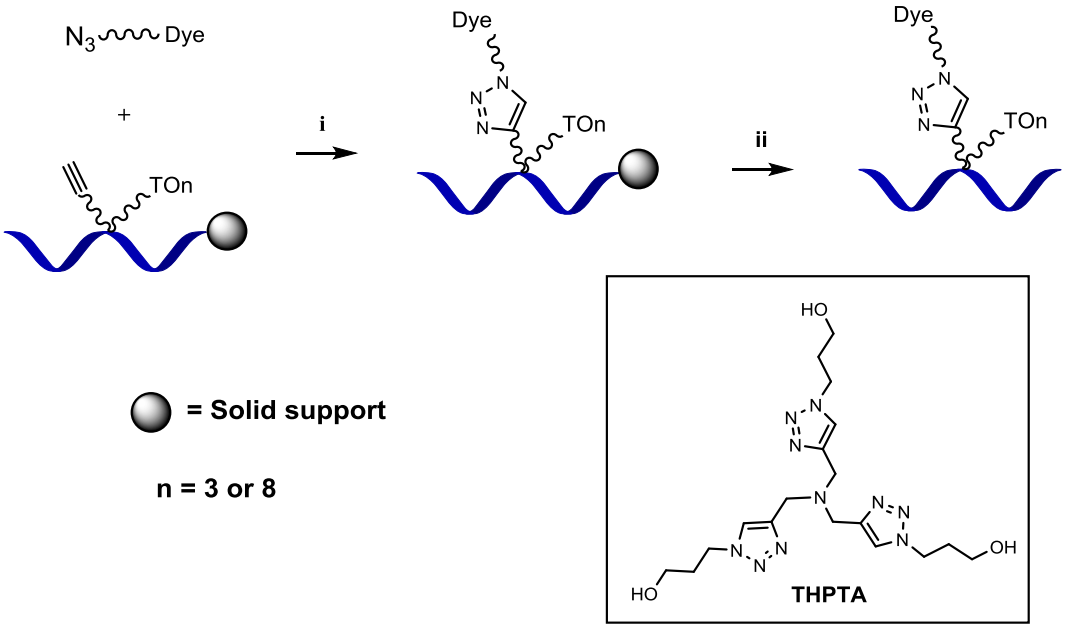

Scheme 5.4. An example of click chemistry post-synthetic labelling with fluorescent dyes on resin-bound oligonucleotides. Conditions: (i) azide dyes (10 eq. for one addition, 15 eq. for two additions), DMSO (20 µL), $CuSO_4 \cdot 5H_2O$ (5 eq. for one addition, 10 eq. for two additions), THPTA (35 eq. for one addition, 70 eq. for two additions), sodium ascorbate (50 eq. for one addition, 100 eq. for two additions), 55 °C, 4 h; (ii) concentrated aqueous ammonia solution (33%), RT, 4 h.

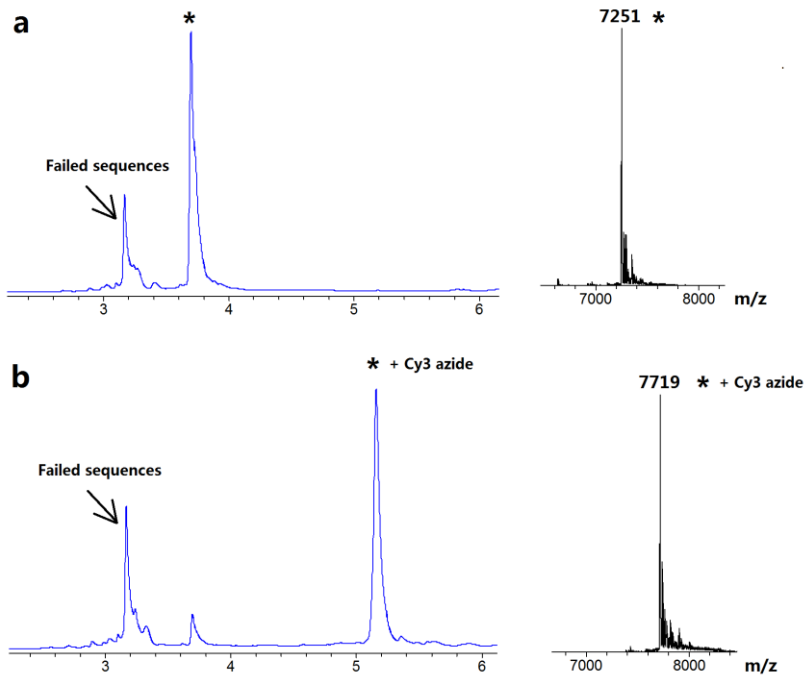

Figure 5.3. HPLC and MS characterisation of crude oligonucleotide L2-TO3 (Table 5.1) (a: starting material) and L2-TO3/Cy3 (b: L2-TO3, labelled with one addition of Cy3 azide). The arrows indicate failed sequences during oligonucleotide assembly. The starred peaks correspond to the associated mass spectra (ESI^-), a: starting material L2-TO3 (calc.: 7252, found: 7251), and b: clicked product L2-TO3/Cy3 (calc.: 7719, found: 7719).

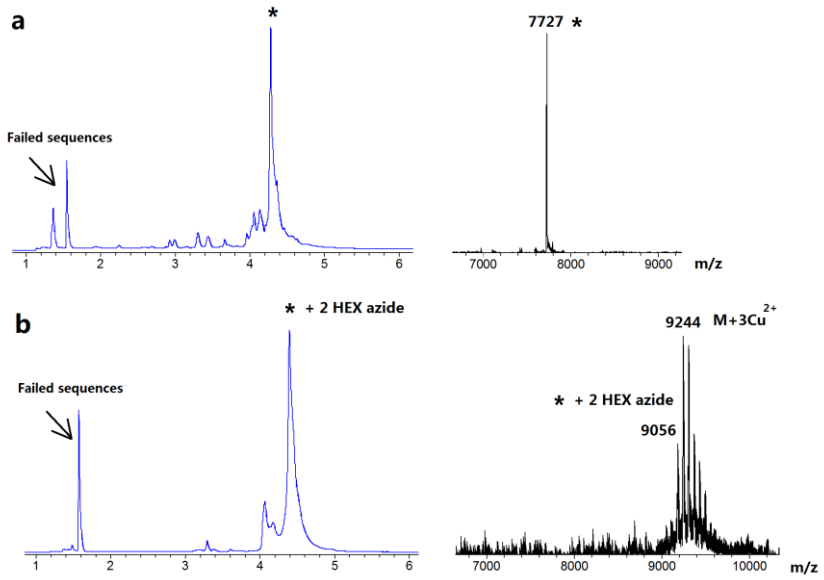

Figure 5.4. HPLC and MS characterisation of crude oligonucleotide L7-(TO3)2 (Table 5.11) (a: starting material) and L7-(TO3/HEX)2 (b: labelled with two additions of HEX azide). The arrows indicate failed sequences during oligonucleotide assembly. The starred peaks correspond to the associated mass spectra (ESI^-), a: starting material L7-(TO3)2 (calc.: 7727, found: 7727), and b: clicked product (calc.: 9057, found: 9056). In the mass spectrum b, the peaks after the molecular weight peak are copper adducts.

5.7 UV melting studies of ODNs containing double TO on the same T-nucleobase

The 13-mer ODNs S-TO3, S-TO8 and the 22-mer ODNs L1-(TO3)2, L2-TO3, L3-TO3, L2-TO8 and L3-TO8 (Table 5.1) each have free terminal alkyne functional groups. This group is able to react with TO azide (TO3, TO8) in the CuAAC reaction (Section 5.6) to obtain oligonucleotides containing two TO dyes (TO3/3, TO3/8 and TO8/8) on the same modified thymidine base. The oligonucleotides are listed in Table 5.7. UV melting studies were carried out to determine the melting temperatures of the doubly TO-modified ODNs and the effect of two TO dyes on DNA duplex stability.

Codes	Sequences	Mass found (calc.)
S-TO3/3	TCATCCTAX_7TCTC	4697 (4699)
S-TO3/8	TCATCCTAX_8TCTC	4767 (4769)
S-TO8/8	TCATCCTAX_9TCTC	4837 (4839)
L1-(TO3/3)2	CGCTTCX_7GTATCTAX_7ATTCATCP	8488 (8490)
L2-TO3/3	CGCTTCX_7GTATCTATATTCATCP	7625 (7627)
L2-TO3/8	CGCTTCX_8GTATCTATATTCATCP	7696 (7697)
L2-TO8/8	CGCTTCX_9GTATCTATATTCATCP	7765 (7766)
L3-TO3/3	CGCTTCTGTATCTAX_7ATTCATCP	7625 (7627)
L3-TO3/8	CGCTTCTGTATCTAX_8ATTCATCP	7696 (7697)
L3-TO8/8	CGCTTCTGTATCTAX_9ATTCATCP	7765 (7766)

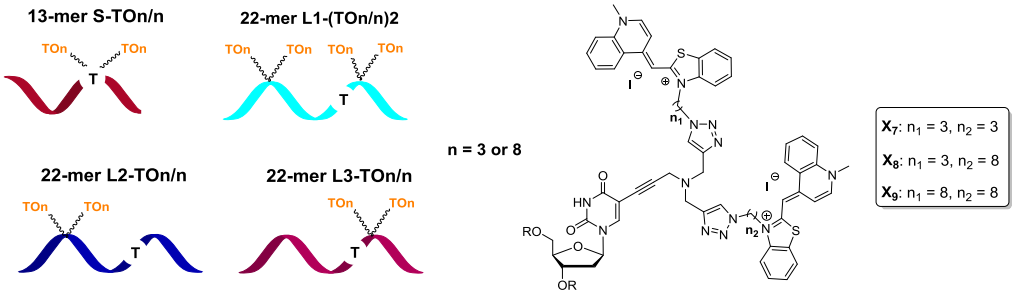

Table 5.7. Oligonucleotides with double TO in each modified T-nucleobase (mass spectra data in Appendix, Figure 9.1.4). Structure of modified T-nucleobase with two TO groups attached with linkers of different lengths (X_7, X_8 and X_9); R = DNA; the position of mutation to be detected is underlined. The T in the schematic diagram highlights the position of this mutation to be detected relative to the positions of the fluorophores.

Melting studies with duplexes (S-TO3/3-ds, S-TO3/8-ds and S-TO8/8-ds) were performed in order to investigate the effect of two TO units in the same position on 13-mer ODNs. The data (Table 5.8, Entries 1–3) showed that doubly labelling with the TO azide resulted in a slightly decreased T_m (TO3/3, ΔT_m = –1.8 °C, and TO3/8, ΔT_m = –1.0 °C) compared to single TO3-labelled S-TO3-ds (T_m = 55.4 °C). In the cases of mixed-length linkers TO3/8 (ΔT_m = +1.4 °C) and two long linkers TO8/8 (ΔT_m = +1.3 °C), slightly higher DNA affinity and hybridization selectivity over S-TO8-ds (53.0 °C) were observed.

UV melting studies were also carried out on L2-TO3/3-ds, L2-TO3/8-ds and L2-TO8/8-ds (Table 5.8, Entries 5–7). The stabilities of L2-TO3/3-ds (ΔT_m = –1.2 °C) and L2-TO3/8-ds (ΔT_m = –0.5 °C) were decreased compared to L2-TO3-ds (66.7 °C). It is worth mentioning that L2-TO8/8-ds destabilized the DNA duplex significantly (around a 3 °C decrease in T_m compared to L2-TO8-ds: 65.2 °C). UV melting studies were also carried out on L3-TO3/3-ds, L3-TO3/8-ds and L3-TO8/8-ds (Table 5.8, Entries 8–10). L2 and L3 have the same sequences, but with TO incorporation in different positions; however their duplexes stabilities were similar. This result indicates that different positions of TO in the same sequence do not give big effect in the DNA duplex thermal stability. In addition, two TO units attached to the same T-nucleobase always appear to decrease duplex stability relative to one TO.

L1-(TO3)2 was labelled with another two TO3 residues to obtain L1-(TO3/3)2. The resulting probe significantly destabilized the duplex (by 4 °C) (Table 5.8, Entry 4). Singly TO-labelled nucleic acid probes confirmed that TO dye intercalates into the duplex *via* π-stacking to increase the stability of duplexes. However, multiple TO monomers located in close proximity to one another, as in L1-(TO3/3)2, prevent effective intercalation due to steric hindrance, consequently reducing stability. In addition, two TO dyes attached to the same T-nucleobase (L2-TO3/3, L3-TO3/3) and separated by 7 bases (L1-(TO3)2) were compared. Inserting 7 nucleobases between TO3-bearing bases as for L1-(TO3)2-ds (T_m = 69.4 °C) resulted in more stable duplexes than those with the dyes located on the same base (L2-TO3/3-ds, T_m = 65.5 °C, L3-TO3/3-ds, T_m = 63.8 °C). The results suggest that two separated additions of TO3-dT monomer (X_2) can give a greater increase in DNA duplex stability.

Entry	Duplexes	T_m (°C)	ΔT_m (°C)
1	S-TO3/3-ds	53.6	– 1.8[c]
2	S-TO3/8-ds	54.4	– 1.0[a] + 1.4[b]
3	S-TO8/8-ds	54.3	+ 1.3[d]
4	L1-(TO3/3)2-ds	65.4	– 4.0[c]
5	L2-TO3/3-ds	65.5	– 1.2[c]
6	L2-TO3/8-ds	66.2	– 0.5[a] + 1.0[b]
7	L2-TO8/8-ds	62.4	– 2.8[d]
8	L3-TO3/3-ds	63.8	– 2.2[c]
9	L3-TO3/8-ds	64.8	– 1.3[a] + 0.1[b]
10	L3-TO8/8-ds	63.7	– 1.0[d]

Table 5.8. UV melting studies of 13-mer S and 22-mer L1–L3 ODNs with double TO incoporation on the same T-nucleobase. T_m: melting temperature; ΔT_m: difference in melting temperature of double TO compared to single TO on the same T-nucleobase (Table 5.2) (a: the difference between TO3 and TO3/8; b: the difference between TO8 and TO3/8; c: the difference between TO3 and TO3/3; d: the difference between TO8 and TO8/8). T_m values are the average of 3 separate melting and annealing curves. Melting temperatures are accurate to ± 0. 1 °C.

5.8 Fluorescence studies of TO-modified ODNs

TO-modified derivatives of 13-mer ODNs S-TO3, S-TO8, S-TO3/3, S-TO3/8 and S-TO8/8 were used for fluorescence studies. The emission spectra were measured prior to and after hybridization with fully complementary DNA at room temperature. When S-TO3 or S-TO8 (i.e. singly TO-labelled ODNs), were in the single-stranded state, the emission spectra contained a single, broad band with the maximum emission at 530 nm when exciting at 510 nm. Hybridization with the complementary strand enhanced the emission intensity, with 11–12 times greater emission than in the single-stranded state (Figure 5.5 A). Fluorescence intensity was not significantly dependent on the spacer length of TO for singly TO-labelled ODNs (S-TO3 *vs.* S-TO8): both linker types gave similar results in the free strand and duplex states. The mismatched hybrid duplexes

(S-CT-mis, S-TT-mis, S-GT-mis) gave similar fluorescence emission (Figure 5.5 B) to the fully matched duplex (S-TO3-ds). Mismatched base-pairs were found to significantly lower the stability of DNA duplexes, described in Section 5.5 (Table 5.4), but there was very little difference of fluorescence emission for the S-TO3 probe hybridised with mismatched sequences.

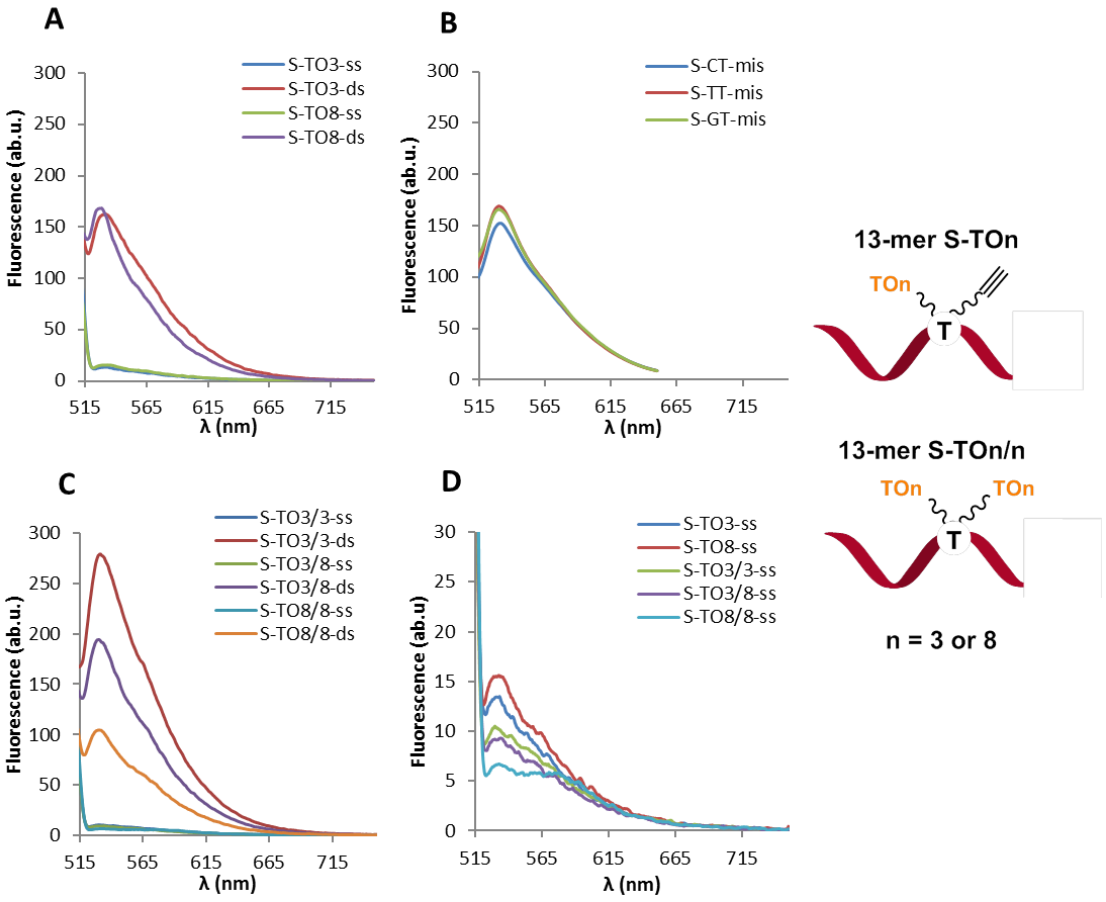

Figure 5.5. Comparison of room temperature steady state emission of the 13-mer (S) TO-modified ODNs. All the results were obtained using λ_{ex} = 510 nm. A: single strand (ss) and double strand (ds) of S-TO3, S-TO8; B: double strand (ds): S-TO3 with CT-mismatch, TT-mismatch and GT-mismatch in DNA duplexes; C: single strand (ss) and double strand (ds): S-TO3/3, S-TO3/8 and S-TO8/8. D: single strand (ss): S-TO3, S-TO8, S-TO3/3, S-TO3/8 and S-TO8/8. The T in the schematic diagram highlights the position of this mutation to be detected relative to the positions of the fluorophores; ab.u .= arbitrary unit.

Figure 5.5 C shows fluorescence spectra of doubly TO-labelled 13-mer ODNs S-TO3/3, S-TO3/8, and S-TO8/8 measured before and after hybridisation to the complementary ODN. The emission maximum is around 530 nm for single-stranded and double-stranded TO-modified DNA. The doubly TO-labelled ODNs S-TO3/3, S-TO3/8 and S-TO8/8 in single strand gave slightly weaker fluorescence intensity compared to the singly TO-labelled ODNs S-TO3 and S-TO8 (Figure 5.5 D). Upon hybridization, however the emission intensity improved significantly, which made the duplex clearly distinguishable from the single-stranded state (ds/ss = 26.4:1 for S-TO3/3). S-TO3/3-ds gave the strongest fluorescence, *ca.* 2-fold stronger than S-TO3-ds. This result suggests that both the TO3 dyes are able to intercalate. However, the emission maximum of the S-TO8/8-ds duplex incorporating two TO8 dyes was lower in intensity than the S-TO8-ds duplex with only one TO8 unit (Figure 5.5 A, C). The fluorescence was found to be dependent on the spacer length in the case of two TO on the same T-nucleobase,

Fluorescence studies were also carried out using 22-mer ODNs. A *ca.* 3-fold difference of fluorescence intensity was found between the double-stranded and single-stranded states for L2-TO3 and L2-TO8 (Figure 5.6 A), but L2-TO3 gave stronger fluorescence than L2-TO8 whether in the single-stranded or double-stranded state. Particularly interesting results were obtained when two TO moieties were attached to a single T-nucleobase on L2 (L2-TO3/3, L2-TO3/8 and L2-TO8/8). The fluorescence of L2-TO3/3 and L2-TO3/8 was reduced efficiently in absence of template DNA, and increased in the double-stranded state (ds/ss = 6.1:1 for L2-TO3/3, ds/ss = 8.8:1 for L2-TO3/8, Figure 5.6 B). In contrast, although L2-TO8/8 showed a clear fluorescence enhancement in the double-stranded state over the single-stranded state (ds/ss = 7.7:1), the fluorescence was much lower than for L2-TO3/3 and L2-TO3/8. This result indicates that the fluorescence of two TO on the same T-nucleobase is dependent on the linker length.

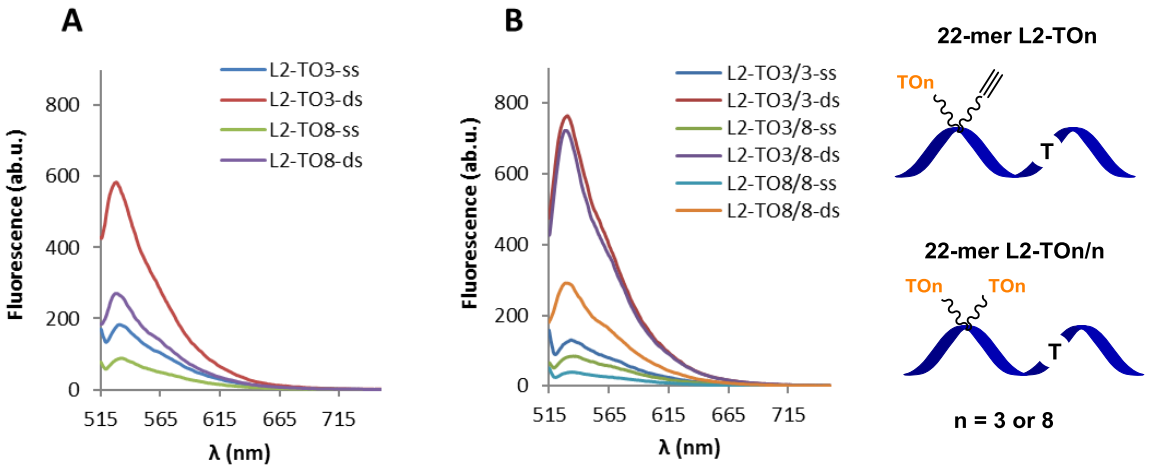

Figure 5.6. Comparison of room temperature steady state emission of the 22-mer L2 TO-modified ODNs. All the results were obtained using λ_{ex} = 510 nm. A: single strand (ss) and double strand (ds) of L2-TO3 and L2-TO8; B: single strand (ss) and double strand (ds) of L2-TO3/3, L2-TO3/8 and L2-TO8/8. The T in the schematic diagram highlights the position of this mutation to be detected relative to the positions of the fluorophores; ab.u .= arbitrary unit.

The same fluorescence studies were carried out on all L3-TO probes for comparison. L3-TO3 and L3-TO8 gave slightly weaker fluorescence whether in the single-stranded or double-stranded state (Figure 5.7 A) compared to the L2-TO probes bearing TO in a different position in the same sequence (Figure 5.6 A). Okamoto *et al.* confirmed that the fluorescence intensity of TO is dependent on the oligonucleotide sequences.[125] In L2 ODNs, TO is incorporated between a C and a G base, a pyrimidine and a purine. However, TO is located between two A (purine) bases in L3. The difference in neighbouring bases may explain the difference in fluorescence properties between L2-TO and L3-TO probes; for example it has been observed that TO confers greater fluorescence when intercalated between pyrimidines.[106] Compared to L2-TO probes (ds/ss = 3.1:1 for L2-TO3 and ds/ss = 3.1:1 for L2-TO8), L3-TO probes also showed smaller changes in emission

intensity before and after hybridization (ds/ss = 3.0:1 for L3-TO3 and ds/ss = 1.6:1 for L3-TO8).

Doubly TO-labelled bases were also studied in the L3 oligonucleotides. The results were similar to those obtained with L2-TO/TO probes, discussed above. The fluorescence quenching of L3-TO/TO probes was very effective in the single strand. Upon hybridization, fluorescence was released and gave strong emission (Figure 5.7 B). The L3-TO3/8 probe afforded the greatest fluorescence change between the single-stranded and double-stranded states (ds/ss = 8.0:1). However, the emission intensity of L3-TO3/8-ds in the duplex state was much lower than L3-TO3/3-ds, and L3-TO8/8-ds showed the weakest fluorescence (Figure 5.7 B).

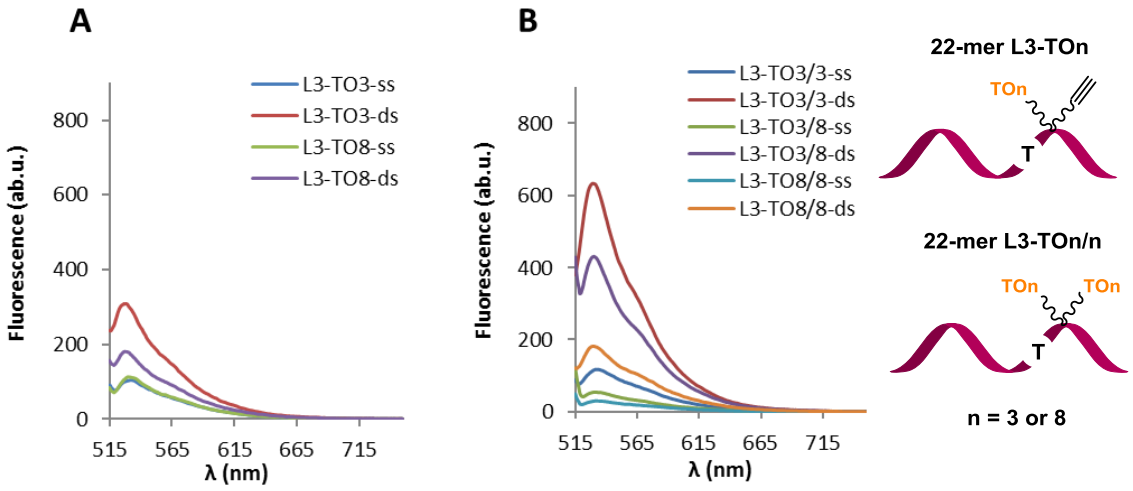

Figure 5.7. Comparison of room temperature steady state emission of the 22-mer L3 TO-modified ODNs. All the results were obtained using λ_{ex} = 510 nm. A: single strand (ss) and double strand (ds) of L3-TO3 and L3-TO8; B: single strand (ss) and double strand (ds) of L3-TO3/3, L3-TO3/8 and L3-TO8/8. The T in the schematic diagram highlights the position of this mutation to be detected relative to the positions of the fluorophores; ab.u .= arbitrary unit.

In addition, fluorescence studies were performed on the L1-(TO3)2 probe with two separated TO3 units (X_2) in the single-stranded and double-stranded states. The fluorescence intensity of L1-(TO3)2 probe was slightly higher in single strand than when the two TO3 units were on the same T-nucleobase (L2-(TO3/3) and L3-(TO3/3)), and lower after hybridization (Figure 5.8 A). However, the use of the L1-(TO3)2 probe resulted in higher thermal stability. Taking these factors into consideration, the L1-(TO3/3)2 probe was designed, containing two modified bases, each bearing two TO3 dyes. As shown in Figure 5.8 B, the fluorescence intensity of the L1-(TO3/3)2 probe containing four TO3 dyes increased significantly on hybridizing with the target strand, and a very weak fluorescence was observed for the non-hybridized state due to strong fluorescence quenching. This increase in fluorescence intensity makes the scaffold suitable for probe design, potentially affording excellent sensitivity for the detection of target DNA by duplex formation.

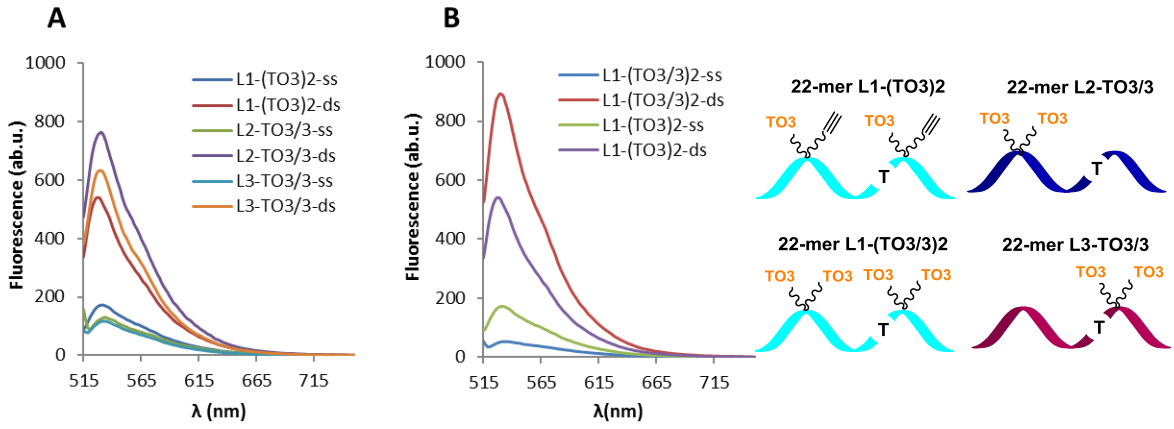

Figure 5.8. Comparison of room temperature steady state emission of the 22-mer L1–L3 TO-modified ODNs. All the results were obtained using λ_{ex} = 510 nm. A: single strand (ss) and double strand (ds) of L1-(TO3)2, L2-TO3/3 and L3-TO3/3; B: single strand (ss) and double strand (ds) of L1-(TO3)2 and L1-(TO3/3)2. The T in the schematic diagram highlights the position of this mutation to be detected relative to the positions of the fluorophores; ab.u .= arbitrary unit.

In summary, two TO3 units incorporated into L1-(TO3)2 gave a greater increase in duplex stability (*ca.* 3 °C higher T_m value) compared to L2-TO3 and L3-TO3 (one TO3 addition). In addition, a significant change in fluorescence emission was observed before and after hybridization (ds/ss = 17.1:1) using the L1-(TO3/3)2 probe containing four TO3 dyes. These excellent results encouraged us to develop a new TO-modified probe system, which is discussed below.

5.9 Development of a novel TO-modified probe system

In general, non-intercalating fluorescent dyes in nucleic acid probes tend to form duplexes of lower thermal stability than the corresponding unmodified duplexes, and the effect of dyes on DNA duplex stability depends on the nature and location of the dye. For example, it has been demonstrated that oligonucleotide sequences with dyes at the 3′ or 5′-ends of DNA do not produce significant destabilization of the duplex.[193] However, fluorophores covalently attached to G-quadruplex and i-motif DNA structures have been reported to cause decreases in thermal stability by 1–11 °C.[194] Incorporation of fluorescent dyes into internal positions in double stranded oligonucleotides resulted in destabilisation in comparison to the natural double stranded oligonucleotides.[195]

Following the observation of significant thermal stabilisation of TO-modified DNA duplexes and the fluorescent "on-off" properties presented above, we decided to develop a novel TO-modified probe system, with each modified nucleobase bearing one TO and one of various different dyes, e.g. fluorescein (FAM), carboxytetramethylrhodamine (TAMRA), cyanine3 (Cy3), 6-hexachloro-fluorescein (HEX), 6-carboxy-X-rhodamine (ROX), and ATTO647N. These dyes were chosen for their bright fluorescence and compatibility with PCR applications, as well as covering a wide wavelength range. It was

anticipated that placing an intercalative quencher (thiazole orange) on the same nucleobase as a strong fluorophore would give rise to efficient collisional quenching of the fluorophore in the single strand but much weaker quenching when the probe is hybridised to its DNA target. This is because in the duplex the thiazole orange will be buried in the core of the duplex and rigidly held in place by base stacking, whereas in the single stranded probe both dyes will be free to interact. This novel approach was devised because thiazole orange alone does not provide a range of different colours, and importantly does not have strong and stable fluorescence over a wide temperature range.

UV melting and fluorescence studies were undertaken with a 13-mer S-TO oligonucleotide bearing TO and Cy3 (i.e. S-TO3/Cy3). Major duplex destabilisation (up to 6.9 °C) was observed compared to the S-TO3 DNA duplex. As expected, the mismatched and bulged duplexes displayed significantly greater destabilisation. However, they have similar stability to the corresponding natural complementary duplex (Appendix, Table 9.3.1). The S-TO3/Cy3 probe did not display a large difference in fluorescence after hybridization to its complementary target DNA (ds/ss = 2.1:1). In addition, the fluorescence of the S-TO3/Cy3 probe was found to be dependent on temperature. This is attributable to the fact that the quantum yield of Cy3 strongly depends on temperature as confirmed by Spiriti *et al*.[196] This dependency limits the use of Cy3 in fluorescence melting applications such as real-time PCR. In view of this limitation, Cy3 was replaced by TAMRA, which was attached to the thymine base by two different linkers (Figure 5.2). However, S-TO3/TAMRA and S-TO3/TAMRA-PEG3 conferred *ca*. –4.0 °C lower duplex stability than S-TO3/Cy3. The fluorescence of both probes in the duplex form was around 3.3-fold greater than in the single-stranded form. These results indicate that probes bearing TO3/Cy3 or TO3/TAMRA were not suitable for use as fluorescent "on-off" probes, and optimization was required. The ROX dye was seen as a good alternative to Cy3 and

TAMRA, as the fluorescence is known to have low temperature-dependence and lower spectral overlap between the emission of TO and the excitation of ROX. This was expected to lead to efficient collisional quenching in the singe-stranded state and restoration of strong fluorescence upon hybridization.

5.9.1 Biophysical studies of ODNs bearing TO/ROX pairs

The DNA 22-mers L2-TO and L3-TO (having the same sequences with TO incorporated on a different T-nucleobase), and the 13-mer S-TO, were labelled with ROX dye azides by the CuAAC reaction (Scheme 5.4), to afford the corresponding TO/ROX probes (Table 5.9). The TO-free ROX-only control probes S-ROX, S-ROX/ROX, L2-ROX, L2-ROX/ROX, L3-ROX and L3-ROX/ROX were also synthesised (Table 5.9). The TO/ROX control probes (L4-TO/ROX and L5-TO/ROX) were synthesised by incorporating 5-octadiynyl-dU (X_4) and amino-modified C6-dT monomers (X_5) into the oligonucleotides during solid phase synthesis, followed by labelling with TO azides, and then reacted with 5(6) ROX activated ester. All oligonucleotides were purified by reversed-phase HPLC and analysed by mass spectrometry.

A

Codes	Sequences	Mass found (calc.)
S-ROX	TCATCCTAX_{10}TCTC	4567 (4568)
S-ROX/ROX	TCATCCTAX_{11}TCTC	5183 (5184)
S-TO3/ROX	TCATCCTAX_{12}TCTC	4940 (4942)
S-TO8/ROX	TCATCCTAX_{13}TCTC	5011 (5012)
L2-ROX	CGCTTCX_{10}GTATCTATATTCATCP	7496 (7495)
L2-ROX/ROX	CGCTTCX_{11}GTATCTATATTCATCP	8113 (8112)
L2-TO3/ROX	CGCTTCX_{12}GTATCTATATTCATCP	7870 (7869)
L2-TO8/ROX	CGCTTCX_{13}GTATCTATATTCATCP	7940 (7939)
L3-ROX	CGCTTCTGTATCTAX_{10}ATTCATCP	7497 (7495)
L3-ROX/ROX	CGCTTCTGTATCTAX_{11}ATTCATCP	8112 (8112)
L3-TO3/ROX	CGCTTCTGTATCTAX_{12}ATTCATCP	7870 (7869)
L3-TO8/ROX	CGCTTCTGTATCTAX_{13}ATTCATCP	7939 (7939)
L4-TO3/ROX	CGCTTCX_{14}GTATCTAX_{16}ATTCATCP	7898 (7900)
L4-TO8/ROX	CGCTTCX_{15}GTATCTAX_{16}ATTCATCP	7968 (7970)
L5-TO3/ROX	CGCTTCX_{16}GTATCTAX_{14}ATTCATCP	7898 (7900)
L5-TO8/ROX	CGCTTCX_{16}GTATCTAX_{15}ATTCATCP	7969 (7970)

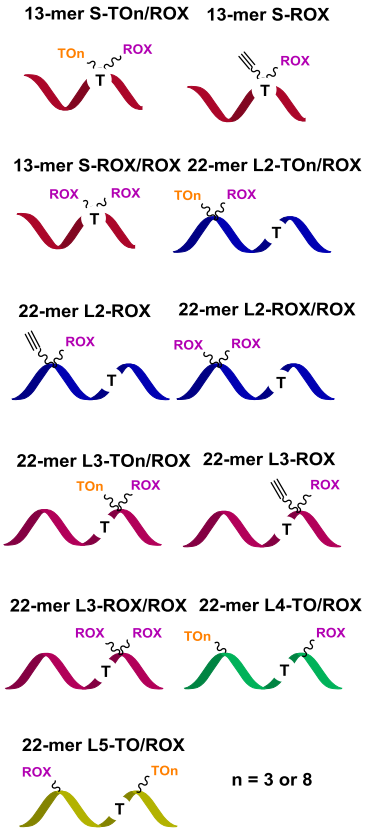

B

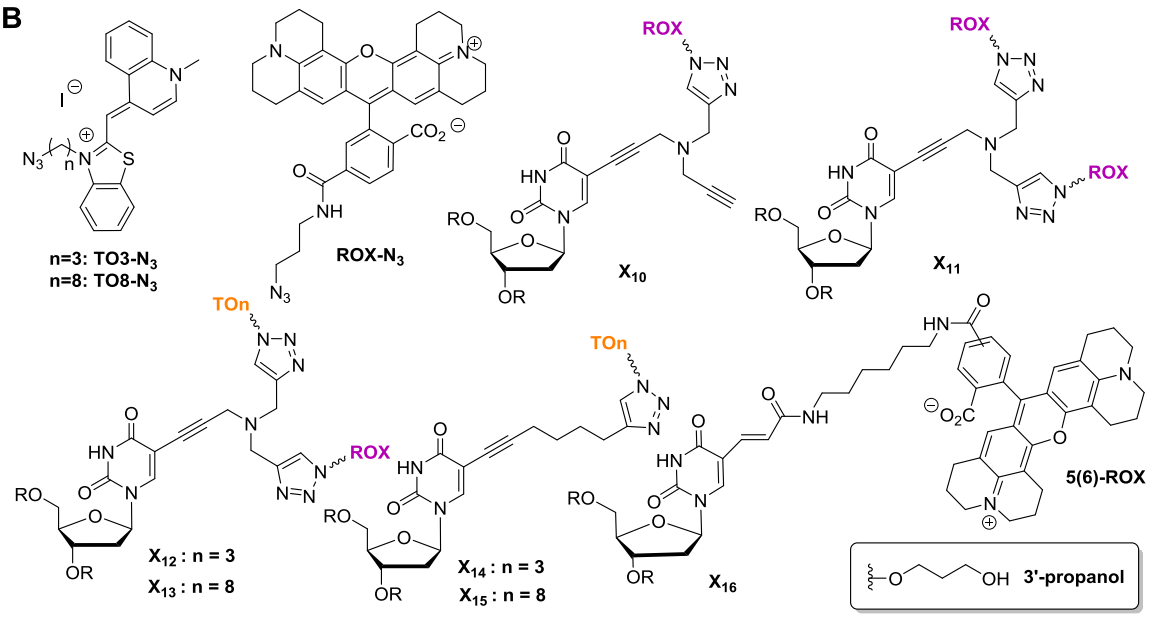

Table 5.9. A: Oligonucleotide sequences (mass spectra data in Appendix, Figure 9.1.4) and schematic representation of the key features; the T highlights the position of this mutation to be detected (underlined in the sequence table) relative to the fluorophores. B: Structures of TO3, TO8, ROX azide dyes and the monomers (X_{10}–X_{16}) used for the modified oligonucleotides. P = 3′-propanol; R = DNA.

The thermal stability of the 13-mer S-TO3 probe after labelling with ROX (Table 5.10, Entries 1–2) decreased to 47.0 °C (ΔT_m = –8.4 °C), but importantly it was still high (even higher than unmodified duplex (T_m = 43.8 °C), Table 5.2). The addition of ROX also reduced the stabilities of the 22-mer L2-TO and L3-TO probes; T_m values were decreased by *ca.* 2–4 °C compared to L2-TO and L3-TO probes (Table 5.10, Entries 5–12). This is not surprising as ROX, unlike TO, probably does not interact with the DNA duplex. In addition, the L2-TO/ROX probes produced more stable duplexes (*ca.* 1.5 °C) than the L3-TO/ROX probes. No significant difference in stability of the L-TO/ROX probe systems was observed regarding the length of the linker attaching TO (TO3 *vs.* TO8). However, TO3 slightly stabilised the DNA duplex relative to TO8 (Table 5.10, Entries 1–4).

Entry	Duplexes	T_m (°C)	ΔT_m (°C)
1	S-TO3-ds	55.4	
2	S-TO3/ROX-ds	47.0	– 8.4
3	S-TO8-ds	53.0	
4	S-TO8/ROX-ds	46.3	– 6.7
5	L2-TO3-ds	66.7	
6	L2-TO3/ROX-ds	63.1	– 3.6
7	L2-TO8-ds	65.2	
8	L2-TO8/ROX-ds	62.6	– 2.6
9	L3-TO3-ds	66.0	
10	L3-TO3/ROX-ds	61.7	– 4.3
11	L3-TO8-ds	64.7	
12	L3-TO8/ROX-ds	61.1	– 3.6

Table 5.10. UV melting studies of TO and ROX on the same T-nucleobase of the 13-mer (S) and 22-mer (L2 and L3) ODNs. T_m: melting temperature; ΔT_m: difference in melting temperature after labelling with ROX dye. T_m values are the average of 3 separate melting and annealing curves. Melting temperatures are accurate to ± 0. 1 °C.

Fluorescence emission scans at room temperature were carried out to compare the TO/ROX probes and the ROX/ROX control probes by exciting at two different wavelengths (λ_{ex} = 510 nm, the excitation maximum of TO, and λ_{ex} = 585 nm, the excitation maximum of ROX). Emission spectra prior to and after hybridization with fully complementary DNA were also taken. Single-stranded S-TO/ROX probes were efficiently quenched when excited at 510 nm, giving low emission (Figure 5.9). Upon hybridization, the TO and ROX units were separated from one to another due to the intercalation of TO into the DNA duplex, giving strong ROX fluorescence with a maximum emission intensity at around 607 nm. In the S-TO/ROX probes, the fluorescence was independent of the length of the TO linker (comparing TO3 and TO8). A great difference in fluorescence intensity at 607 nm was observed before and after hybridization to the fully complementary DNA strand when exciting at 510 nm (S-TO3/ROX: ds/ss = 13.8:1; S-TO8/ROX: ds/ss = 12.1:1, Figure 5.9 A). A slightly weaker emission intensity at 607 nm was obtained by exciting at 585 nm (S-TO3/ROX: ds/ss = 8.3:1; S-TO8/ROX: ds/ss = 10.1:1, Figure 5.9 B). Interestingly, the emission intensity of the S-TO/ROX duplexes on excitation at 510 nm was 1.3-fold stronger than was obtained when exciting 585 nm. These results indicate that efficient FRET occurs from TO to ROX.

The same fluorescence experiments were performed on the ROX-only control probes (TO-free), i.e. the S-ROX and S-ROX/ROX probes. Weak fluorescence intensity at 607 nm was obtained when exciting at 510 nm before and after hybridization (Figure 5.9 C). As expected, the strongest fluorescence at 607 nm was obtained by excitation at 585 nm (Figure 5.9 D), which is the absorption maximum of ROX dye. In addition, the emission intensity of the S-ROX/ROX probe was significantly reduced compared to the S-ROX probe before and after hybridization. This may be attributed to fluorescence quenching caused by the interaction of the two adjacent ROX dyes. The

S-ROX probe gave strong fluorescence when excited at 585 nm in the single-stranded and double-stranded states, with a only 2-fold increase upon hybridization.

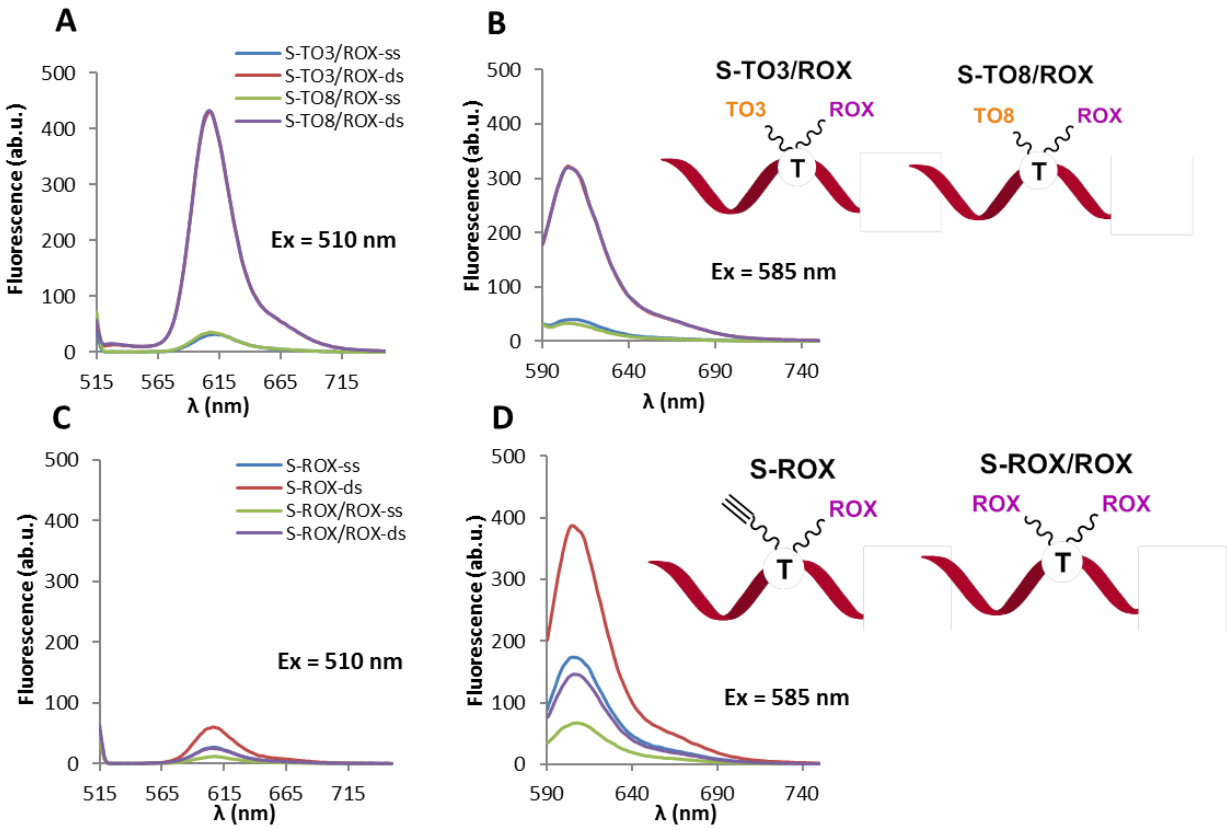

Figure 5.9. Comparison of room temperature steady state emission of the 13-mer ODNs S-TO3/ROX, S-TO8/ROX, S-ROX and S-ROX/ROX. A: λ_{ex} = 510 nm, single strand (ss) and double strand (ds) of S-TO3/ROX, S-TO8/ROX; B: λ_{ex} = 585 nm, single strand (ss) and double strand (ds) of S-TO3/ROX, S-TO8/ROX; C: λ_{ex} = 510 nm, single strand (ss) and double strand (ds) of S-ROX, S-ROX/ROX; D: λ_{ex} = 585 nm, single strand (ss) and double strand (ds) of S-ROX, S-ROX/ROX. The T in the schematic diagram highlights the position of this mutation to be detected relative to the positions of the fluorophores; ab.u.= arbitrary unit.

Further studies were performed on the 22-mer L-TO/ROX probes (L2–L5, Table 5.9). In the L2-TO/ROX probe system, TO3 and TO8 gave similar fluorescence intensities in the double-stranded state. Less fluorescence quenching was obtained with TO3 than with TO8 in single strand when exciting at 510 nm (Figure 5.10 A). The L2-TO/ROX probes and the L3-TO/ROX probes differ in the position of the T-nucleobase bearing the TO/ROX modification. In the L3-TO/ROX probes, similar fluorescence intensities were observed before hybridization for TO3 and TO8, and slightly stronger fluorescence was observed for L3-TO3/ROX than L3-TO8/ROX after hybridizing with the target nucleic acid sequences (Figure 5.10 B). As controls, L4-TO/ROX and L5-TO/ROX (Figure 5.10 C, D) were designed to have a 7 base separation between TO and ROX dyes rather than being located on the same T-nucleobase. A comparison of the L4-TO/ROX and L5-TO/ROX probes showed that both display slightly stronger (*ca.* 1.1–1.3-fold) fluorescence than the L2-TO/ROX and L3-TO/ROX probes in the single-stranded and double-stranded states, especially before hybridization. TO3/ROX probes consistently gave stronger fluorescence than TO8/ROX both before and after hybridization in the L4-TO/ROX and L5-TO/ROX probes. These results indicate that the fluorescence properties were somewhat dependent on the sequence of the probe and the positions of modification.

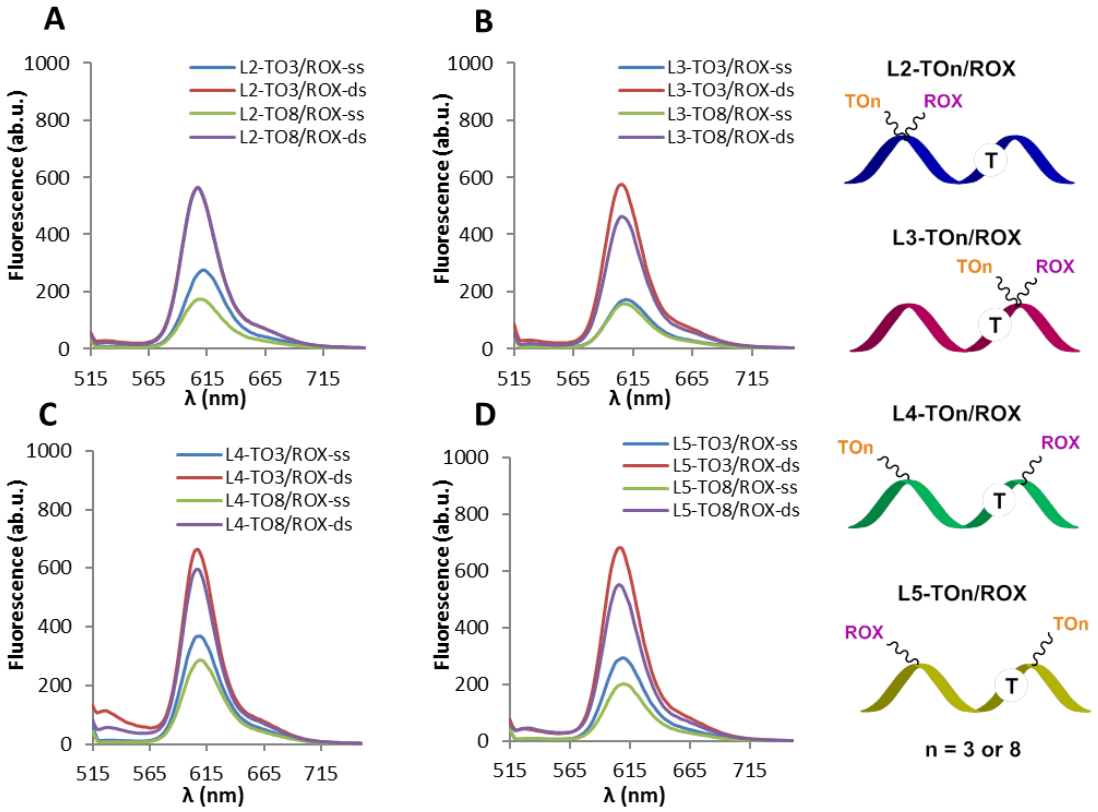

Figure 5.10. Comparison of room temperature steady state emission of the 22-mer TO/ROX modified ODNs. All the results were obtained using λ_{ex} = 510 nm. A: single strand (ss) and double strand (ds) of L2-TO3/ROX, L2-TO8/ROX; B: single strand (ss) and double strand (ds) of L3-TO3/ROX, L3-TO8/ROX; C: single strand (ss) and double strand (ds) of L4-TO3/ROX, L4-TO8/ROX; D: single strand (ss) and double strand (ds) of L5-TO3/ROX, L5-TO8/ROX. The T in the schematic diagram highlights the position of this mutation to be detected relative to the positions of the fluorophores; ab.u .= arbitrary unit.

Although the results obtained for L2-TO/ROX and L3-TO/ROX were disappointing, it has been shown previously that multiple additions of TO dye-bearing moities can have a stabilising effect on duplex formation and fluorescence intensity. The incorporation of a second TO/ROX pair into the probes was investigated to determine if it would give greater duplex stability and a superior fluorescent response.

5.9.2 Fluorescence studies of the L1-(TO3/ROX)2 and L7-(TO3/ATTO647N)2

The cystic fibrosis transmembrane conductance regulator (CFTR) is a 1480 amino acid membrane-bound glycoprotein.[197] The 22-mer wild-type probe L1-(TO3)2 was designed to act as a fluorescent "on-off" probe for the AT-rich CFTR R516G locus. The mutant probe L7-(TO3)2 was designed to be complementary to the mutant template (L-G-mismatch, Table 5.3). Two TO3-dT monomers (X_2) were incorporated into oligonucleotides L1-(TO3)2 and L7-(TO3)2, and their corresponding TO-free controls were prepared using 5-octadiynyl-dU monomer (X_4) during oligonucleotide synthesis, then labelled with ROX, FAM-C6, HEX and ATTO647N azides. The oligonucleotides for this study are listed in Table 5.11.

A

Codes	Sequences	Mass found (calc.)
L6-(alkyne)2	CGCTTCX$_4$GTATCTAX$_4$ATTCATCP	6944 (6944)
L6-(ROX)2	CGCTTCX$_{17}$GTATCTAX$_{17}$ATTCATCP	8178 (8177)
L1-(TO3/ROX)2	CGCTTCX$_{12}$GTATCTAX$_{12}$ATTCATCP	8975 (8975)
L8-(alkyne)2	CGCTTCX$_4$GTATCCAX$_4$ATTCATCP	6929 (6929)
L7-(TO3)2	CGCTTCX$_2$GTATCCAX$_2$ATTCATCP	7727 (7727)
L8-(FAM-C6)2	CGCTTCX$_{18}$GTATCCAX$_{18}$ATTCATCP	7930 (7930)
L7-(TO3/FAM-C6)2	CGCTTCX$_{21}$GTATCCAX$_{21}$ATTCATCP	8728 (8728)
L8-(HEX)2	CGCTTCX$_{19}$GTATCCAX$_{19}$ATTCATCP	8260 (8259)
L7-(TO3/HEX)2	CGCTTCX$_{22}$GTATCCAX$_{22}$ATTCATCP	9056 (9057)
L8-(ATTO647N)2	CGCTTCX$_{20}$GTATCCAX$_{20}$ATTCATCP	8622 (8621)
L7-(TO3/ATTO647N)2	CGCTTCX$_{23}$GTATCCAX$_{23}$ATTCATCP	9419 (9419)

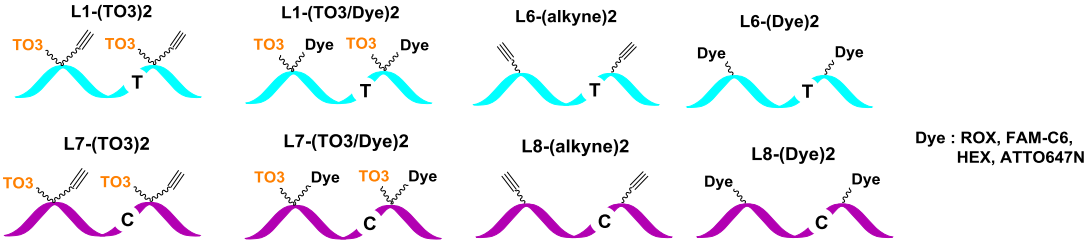

B

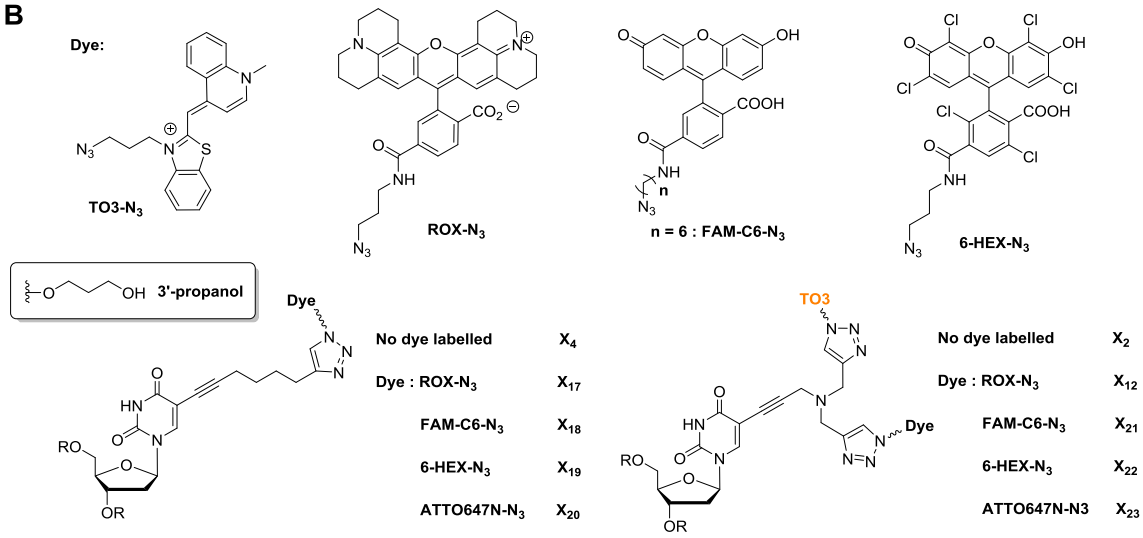

Table 5.11. A: Oligonucleotide sequences (mass spectra data in Appendix, Figure 9.1.4) and schematic representation of the key features; the T or C highlights the position of this mutation to be detected (underlined in the sequence table) relative to the fluorophores. B: Structures of TO3, ROX, FAM-C6, 6-HEX azide dyes and the monomers (X_2, X_4, X_{12} and X_{17}–X_{23}) used for the modified oligonucleotides. P = 3′-propanol; R = DNA.

Fluorescence emission scans at room temperature were carried out to compare the L1-(TO3/ROX)2 probe with its corresponding TO-free control HyBeacon L6-(ROX)2 probe by exciting at two different wavelengths (λ_{ex} = 510 nm, the excitation maximum of TO, and λ_{ex} = 585 nm, the excitation maximum of ROX). Measurements of emission spectra before and after hybridization to fully complementary DNA were performed to study the change in fluorescence signal upon binding to target DNA.

As expected, efficient fluorescence quenching was observed for the single-stranded probe L1-(TO3/ROX)2 on excitation at 510 nm and 585 nm, yielding low emission (Figure 5.11). Strong fluorescence intensity was observed for the double-stranded probe L1-(TO3/ROX)2 when excited at 510 nm and 585 nm, and the double-stranded (ds) fluorescence was greater at 510 nm ($ds_{510\ nm}/ds_{585\ nm}$ = 1.3:1). This indicates efficient FRET from TO to ROX. Probe L1-(TO3/ROX)2 displayed a great difference in fluorescence intensity at 607 nm before and after hybridization to its fully complementary strand (ds/ss = 6.3:1, λ_{ex} = 510 nm; ds/ss = 6.8:1, λ_{ex} = 585 nm). Corresponding fluorescence experiments were performed on the control HyBeacon probe L6-(ROX)2. A weak fluorescence signal at 607 nm was obtained when exciting at 510 nm before and after hybridization (Figure 5.11 A). The strongest fluorescence at 607 nm was obtained by excitation at 585 nm (Figure 5.11 B), which is the absorption maximum of ROX dye. However, the fluorescence emission only increased by approximately 2–3 fold upon hybridization. These results led us to conclude that L1-(TO3/ROX)2 was a potential probe to discriminate between the target sequence and variants, with fluorescence properties similar to the traditional HyBeacon probe L6-(ROX)2. Furthermore, the L1-(TO3/ROX)2 probe has the additional advantage that it can also be detected at lower wavelength (TO absorption), giving a stronger fluorescence signal compared to when exciting at the absorption maximum of ROX.

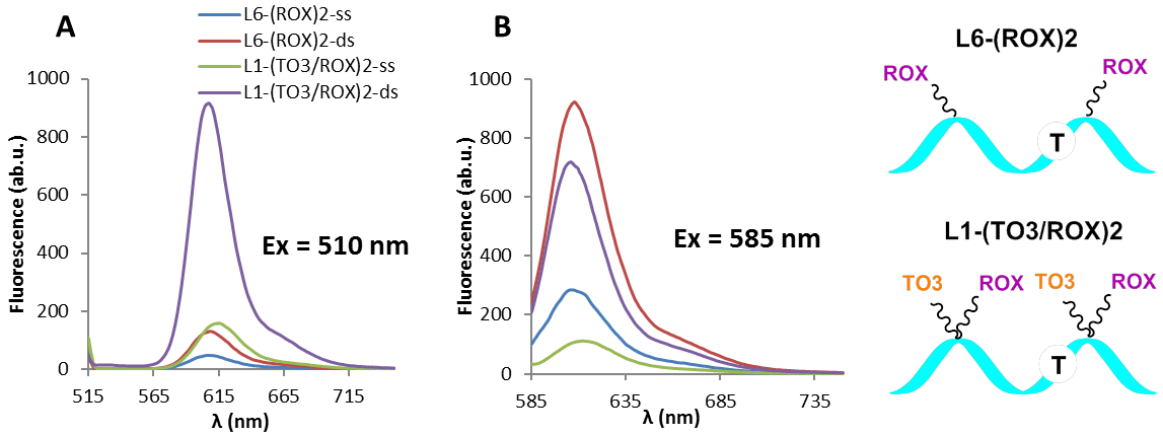

Figure 5.11. Comparison of room temperature steady state emission of the 22-mer probe L1-(TO3/ROX)2 and its control HyBeacon probe L6-(ROX)2. A: λ_{ex} = 510 nm (the excitation maximum of TO3); B: λ_{ex} = 585 nm (the excitation maximum of ROX). The T in the schematic diagram highlights the position of this mutation to be detected relative to the positions of the fluorophores; ab.u .= arbitrary unit.

Additional fluorescence experiments were carried out on the mutant probe L7-(TO3/ATTO647N)2 and its TO-free control HyBeacon probe L8-(ATTO647N)2. Notably, the probe L7-(TO3/ATTO647N)2 gave strong fluorescence on excitation at 510 nm after hybridising with its complementary strand (Figure 5.12 A). There was a significant difference in the fluorescence intensity before and after hybridization (ds/ss = 19.5:1). For control HyBeacon probe L8-(ATTO647N)2, almost no fluorescence was observed in either the single-stranded or double-stranded states on excitation at 510 nm. The probe L7-(TO3/ATTO647N)2 in the double-stranded state gave a slightly stronger fluorescence than the control HyBeacon probe L8-(ATTO647N)2 on excitation at 647 nm, and a much lower fluorescence intensity was observed for non-hybridized L7-(TO3/ATTO647N)2 (λ_{ex} = 647 nm, L7-(TO3/ATTO647N)2: ds/ss = 12.4:1; L8-(ATTO647N)2: ds/ss = 3.6:1; Figure 5.12 B). This mutant probe has two additions of TO3/ATTO647N that can be monitored at a lower wavelength (510 nm). It gave a stronger fluorescence on excitation at 647 nm than the control HyBeacon probe L8-(ATTO647N)2.

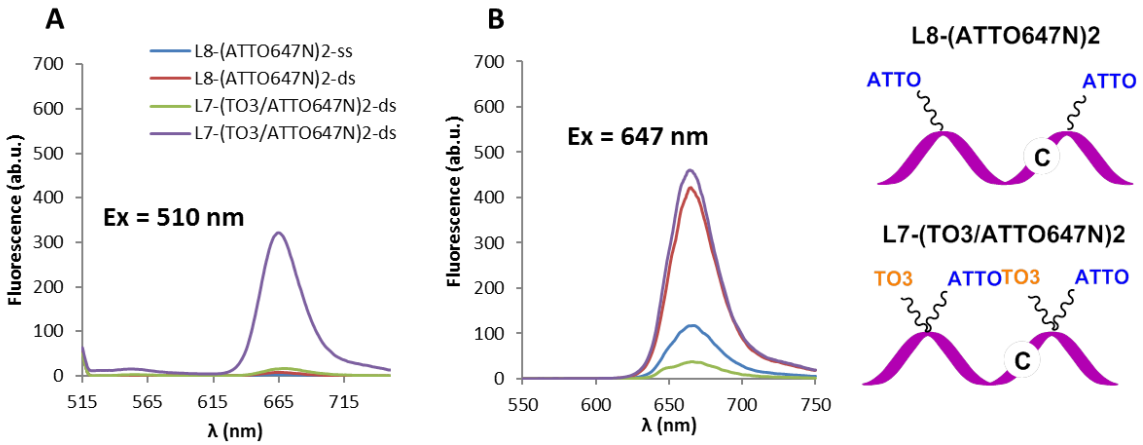

Figure 5.12. Comparison of room temperature steady state emission of the 22-mer probe L7-(TO3/ATTO647N)2 and its control HyBeacon probe L8-(ATTO647N)2. A: λ_{ex} = 510 nm (the excitation maximum of TO3); B: λ_{ex} = 647 nm (the excitation maximum of ATTO647N). The C in the schematic diagram highlights the position of this mutation to be detected relative to the positions of the fluorophores; ab.u .= arbitrary unit.

Fluorescence studies were also performed on the mutant probes L7-(TO3/HEX)2 and L7-(TO3/FAM-C6)2 and their TO-free control HyBeacon probes L8-(HEX)2 and L8-(FAM-C6)2 (Appendix, Figure 9.4.1 and Figure 9.4.2). A large increase in fluorescence intensity was observed for the two probes upon hybridization compared to their control HyBeacon probes L8-(HEX)2 and L8-(FAM-C6)2. However, the fluorescence was not found to be as strong as was obtained with the TO-free control HyBeacon probes, especially for the L7-(TO3/FAM-C6)2 probe. Based on the fluorescence studies, the higher the excitation wavelength of the dye, the greater the fluorescence intensity was obtained. This result suggests that an intercalator dye with a lower excitation wavelength than TO might improve the whole probe system by giving improved fluorescence for lower wavelength emitting dyes. The optimization of the new probe system is discussed in Chapter 6.

5.10 Fluorescence melting studies of L-TO/ROX probes using a Roche LightCycler®

Darby *et al.*[198] have used molecular beacons to determine the melting properties of intramolecular DNA duplexes, triplexes and quadruplexes using a Roche LightCycler®, which has one excitation source (488 nm) and three channels for recording fluorescence emission at 530 nm (F1), 640 nm (F2) and 705 nm (F3). The applications of the Roche LightCycler® are restricted by the limited (single) excitation source (488 nm). However, the technique remains of interest because it is simple to use, requires only small amounts of material, and can process 32 samples in parallel. The TO-modified probes discussed herein should be compatible with the Roche LightCycler® due to TO's broad excitation wavelength range, with its excitation maximum at 510 nm.

A Roche LightCycler® was used to perform fluorescence melting studies on the probes L1-(TO3/ROX)2, L2-TO3/ROX and L3-TO3/ROX, hybridised to their corresponding complementary strands. The double-stranded ROX-free control probe L1-(TO3)2 showed a dramatic decrease in fluorescence as the temperature increased. It was also found that the fluorescence of TO (λ_{ex} = 510 nm, λ_{em} = 530 nm) strongly related to (inversely dependent on) temperature, an observation that is consistent with studies by Nygren *et al.*[106] This is an undesirable property for hybridisation probes. However, encouragingly the probes bearing TO/ROX did not display any temperature dependence. On excitation at 488 nm, the emission for these probes was in the red region due to FRET from TO to ROX (ROX: λ_{ex} = 585 nm, λ_{em} = 607 nm). The probe L1-(TO3/ROX)2, which incorporates two TO3/ROX into the T-modified nucleotides, was used for comparison with the singly TO3/ROX probes (L2-TO3/ROX and L3-TO3/ROX). These probes could be monitored using the 530 nm (F1) and 640 nm (F2) recording channels. In the fluorescence melting

curve (Figure 5.13 A), the fluorescence intensity of the L1-(TO3/ROX)2 probe-target DNA duplex was higher than for the L2-TO3/ROX and L3-TO3/ROX probes, and in the melting derivatives (Figure 5.13 B), all three probes can be seen to form highly stable duplexes with the target ODNs. T_m values ranged from 61.1 °C to 62.2 °C. The probe L2-TO3/ROX formed a more stable duplex than the probes L1-(TO3/ROX)2 and L3-TO3/ROX, which gave similar duplex stability. Fluorescence melting experiments were also carried out using the control HyBeacon probe L6-(ROX)2 which bear no TO; however, the narrow excitation wavelength range of a Roche LightCycler® limited their applicability in this system.

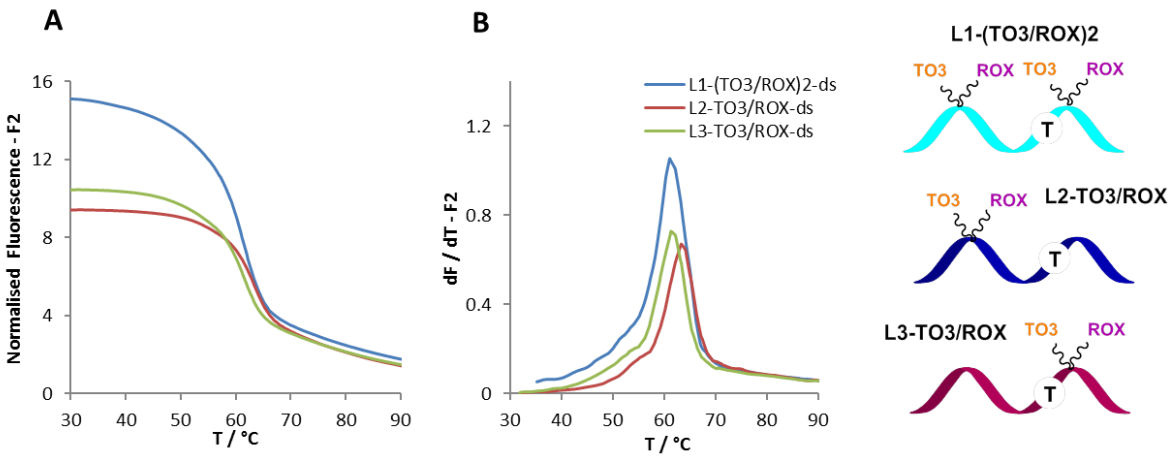

Figure 5.13. A: melting curves and B: melting derivatives of 22-mer probes L1-(TO3/ROX)2, L2-TO3/ROX and L3-TO3/ROX, based on fluorescence emission at 640 nm (F2) of the Roche LightCycler®. The T in the schematic diagram highlights the position of this mutation to be detected relative to the positions of the fluorophores.

In summary, two additions of TO/ROX-bearing nucleotides gave a stronger fluorescence signal than was obtained for just one addition of TO/ROX. This demonstrates that the L1-(TO3/ROX)2 probe is more compatible with the Roche LightCycler® than the probe

L2-TO3/ROX and L3-TO3/ROX. It should be noted that the L-TO3/ROX probes can directly be used in a Roche LightCycler® and detected in the F1 or F2 channels without the usual addition of an excess of intercalator dyes.

In addition, a Roche LightCycler® was used to measure the fluorescence melting of the mutant probe L7-(TO3/ATTO647N)2 and its TO3-free control HyBeacon probe L8-(ATTO647N)2 upon hybridization, exciting at 488 nm and monitoring at 705 nm (F3). No signal was obtained for the control HyBeacon probe L8-(ATTO647N)2 due to the limitation of the excitation source. The mutant probe L7-(TO3/ATTO647N)2 could be used to detect the target by measuring the difference in thermal stability of fully matched and mismatched duplexes (for data see Appendix, Figure 9.5.1). The same experiments were also carried out using the mutant probe L7-(TO3/HEX)2 and its control HyBeacon probe L8-(HEX)2. The L7-(TO3/HEX)2 probe resulted in a significant improvement in DNA duplex stability, and gave a stronger fluorescence signal when detecting the target sequence and variants compared to the control HyBeacon probe L8-(HEX)2 when monitoring in both F1 (530 nm) and 640 nm (F2) recording channels (for data see Appendix, Figure 9.5.2).

5.11 The application of L-(TO3/dye)2 probes in real-time PCR

HyBeacon probes have been widely used for allele discrimination and DNA quantification, and have been especially useful in real-time polymerase chain reaction (PCR) to detect specific DNA sequences rapidly and reliably.[76,77,97,98] For this reason, derivatives of 22-mer wild-type L1-(TO3)2 and mutant L7-(TO3)2 with different dyes were designed for the AT-rich CFTR R516G locus (as a test case for the detection of a single nucleotide

polymorphism (SNP)[199]) to ensure that the probes can anneal to the template at the PCR extension temperature.

Codes	Sequences	Mass found (calc.)
P1	CCTGGCACCATTAAAGAAAATATCATC	8220 (8220)
P2	ACATAGTTTCTTACCTCTTCTAGTTGG	8206 (8206)
WT	CCTGGCACCATTAAAGAAAATATCATCTTTGGTGTTTCCTAT GATGAATATAGATACAGAAGCGTCATCAAAGCATGCCAACT AGAAGAGGTAAGAAACTATGT	32156 (32159)
MT	CCTGGCACCATTAAAGAAAATATCATCTTTGGTGTTTCCTAT GATGAATATGGATACAGAAGCGTCATCAAAGCATGCCAACT AGAAGAGGTAAGAAACTATGT	32172 (32175)

Table 5.12. PCR templates (WT: wild-type tempalte; MT: mutant template) and primers (P1: forward primer; P2: reverse primer); position of mismatch to be detected is underlined.

To demonstrate the applications of TO/Dye pairs in oligonucleotides as "on-off" switch probes, wild-type and mutant probes were designed to be complementary to the wild-type template (WT) and mutant template (MT) at the R516G locus of the CFTR gene. For these experiments synthetic template DNA (wild-type and mutant) and primer sequences for the CFTR R516G mutation locus were prepared (Table 5.12). Asymmetric real-time PCR was undertaken in order to determine the threshold cycle (C_T) values at different concentration of template DNA using GoTaq® DNA polymerase. PCR reactions were monitored with the wild-type probe L1-(TO3/ROX)2, which can hybridise to the PCR product (template DNA), giving a fluorescence signal. Figure 5.14 shows the real-time PCR fluorescence accumulation graph using different concentrations of wild-type template varying from 10 pg to 100 ng per 20 µL reaction. The C_T value varied from 37 (for 10 pg per 20 µL) to 5 (for 10 ng or more per 20 µL). Based on these results, a concentration of 1 ng of template DNA per 20 µL was used in the PCR reactions described below.

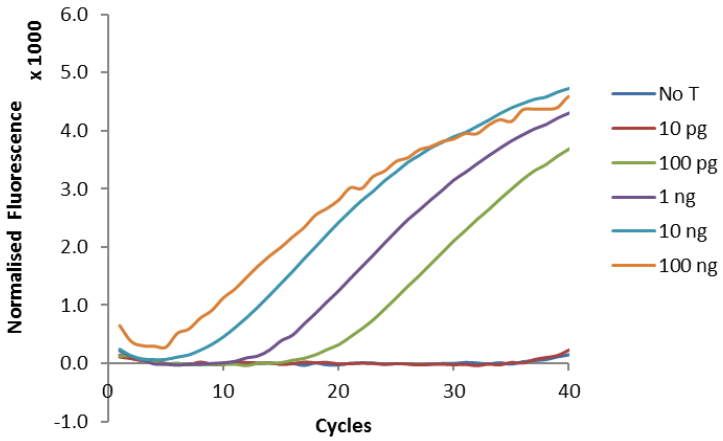

Figure 5.14. Fluorescence accumulation of real-time PCR using the wild-type probe L1-(TO3/ROX)2. Different amounts of wild-type template were used from 10 pg to 100 ng. No T (no template, blue): C_T = 37; 10 pg (red): C_T = 37; 100 pg (green): C_T = 16; 1 ng (purple): C_T = 11; 10 ng (light blue): C_T = 5; 100 ng (orange): C_T = 5.

5.11.1 Evaluation of the L1-(TO3/ROX)2 probe

To test the thermal stability and fluorescence properties of L1-(TO3/ROX)2 in real-time PCR applications, fluorescence melting studies were performed on the wild-type probe L1-(TO3/ROX)2 bearing two additions of TO/ROX and the TO3-free control HyBeacon probe L6-(ROX)2 (Table 5.11), hybridised to the wild-type template (WT) and mutant template (MT). L1-(TO3/ROX)2 hybridized with the wild-type template showed a fluorescence decrease as the temperature increased (Figure 5.15 C). T_m values were calculated from the derivatives of post-amplification fluorescence melting curves. L1-(TO3/ROX)2 hybridized with the wild-type template (WT) to form a fully matched duplex and gave a T_m of 59.0 °C; on hybridisation to the mutant template (MT), the T_m was 3.0 °C lower than for the fully matched duplex (Figure 5.15 D). The base pair mismatch caused by substitution of G for A (i.e. TG-mismatch) is generally the least destabilizing mismatch and therefore the most difficult to identify (GA is also fairly stable).

This has generally well-known, and has been reported by Sagi *et al.* as well as many others.[200]

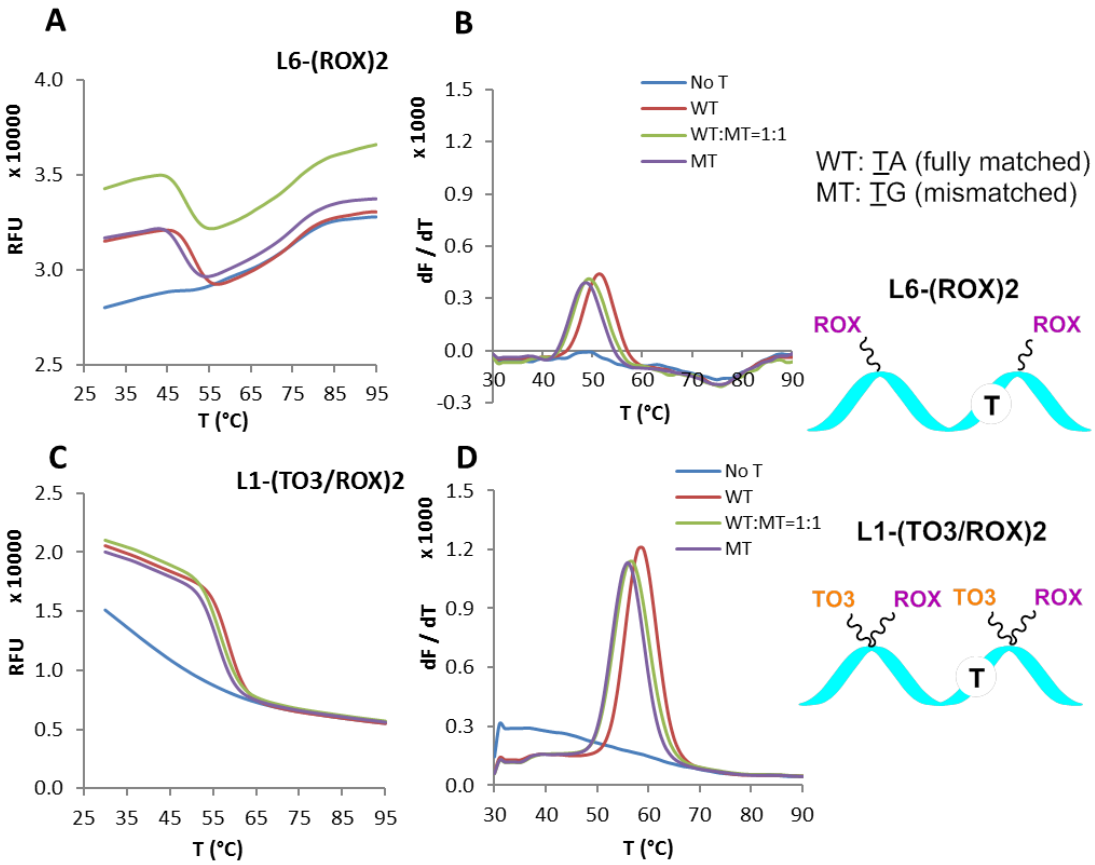

Figure 5.15. Fluorescence melting curves (A, C) and derivatives of post-amplification fluorescence melts (B, D) using the wild-type probe L1-(TO3/ROX)2 (C, D) and the corresponding control HyBeacon probe L6-(ROX)2 (A, B). Blue (No T): no template; red (WT): wild-type template; green (WT:MT = 1:1): wild-type: mutant template, ratio = 1:1; purple (MT): mutant template. All output was monitored in the ROX channel of the CFX96^{TM} real-time PCR instrument (excitation range 560–590 nm, detector range 610–650 nm). KOD XL DNA polymerase, 20 cycles and 1 ng of template ODNs were used. Notes: L1-(TO3/ROX)2 is a wild-type probe that gives a fully matched duplex upon hybridization with wild-type template (WT), and forms a TG-mismatched duplex when pairs with mutant template (MT). The T in the schematic diagram highlights the position of this mutation to be detected relative to the positions of the fluorophores.

When a 1:1 ratio of wild-type target (WT) and mutant target (MT) was used for an asymmetric real-time PCR amplification, a single T_m was observed at 57.0 °C, closer to the T_m of the mismatched duplex (56.0 °C) than the matched one (59.0 °C). The post-amplification fluorescence melt of L6-(ROX)2 HyBeacon probe-template duplexes gave lower T_m values of 51.0 °C (WT) and 49.0 °C (MT) (Figure 5.15 B). This value was 8.0 °C lower compared to that obtained for the L1-(TO3/ROX)2 probe, indicating that L1-(TO3/ROX)2 gave more stable duplexes than the TO-free control HyBeacon probe L6-(ROX)2. This is important as it shows that shorter probes could be used in the new TO/Dye probe system; this is certain to improve mismatch discrimination.

The difference in intensity of fluorescence between the mismatched duplex and the fully complementary duplex was not large, and the fully matched duplex was slightly more fluorescent than the mismatched one (Figure 5.15 C). Although L1-(TO3/ROX)2 is a potential nucleic acid probe, it is not sufficiently sensitive to detect the mutation. In view of this, a two-probe system was designed to optimise the fluorescence properties of the mismatched duplex. This work is described in Section 5.12.

5.11.2 Evaluation of the L1-(TO3/FAM)2 probes

FAM is one of the most commonly used dyes because of its compatibility with most fluorescence detection equipment for DNA labelling and sequence detection. FAM dyes functionalized with two different linkers (FAM-C3, FAM-PEG3) were incorporated into the wild-type probe L1-(TO3)2, giving L1-(TO3/FAM-C3)2 and L1-(TO3/FAM-PEG3)2. Their TO3-free control HyBeacon probes L6-(FAM-C3)2 and L6-(FAM-PEG3)2 were also synthesised (Table 5.13).

A

Codes	Sequences	Mass found (calc.)
L6-(FAM-C3)2	CGCTTCX$_{24}$GTATCTAX$_{24}$ATTCATCP	7861 (7861)
L1-(TO3/FAM-C3)2	CGCTTCX$_{26}$GTATCTAX$_{26}$ATTCATCP	8659 (8659)
L6-(FAM-PEG3)2	CGCTTCX$_{25}$GTATCTAX$_{25}$ATTCATCP	8098 (8097)
L1-(TO3/FAM-PEG3)2	CGCTTCX$_{27}$GTATCTAX$_{27}$ATTCATCP	8896 (8895)

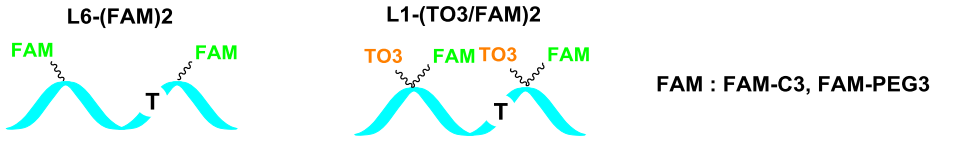

B

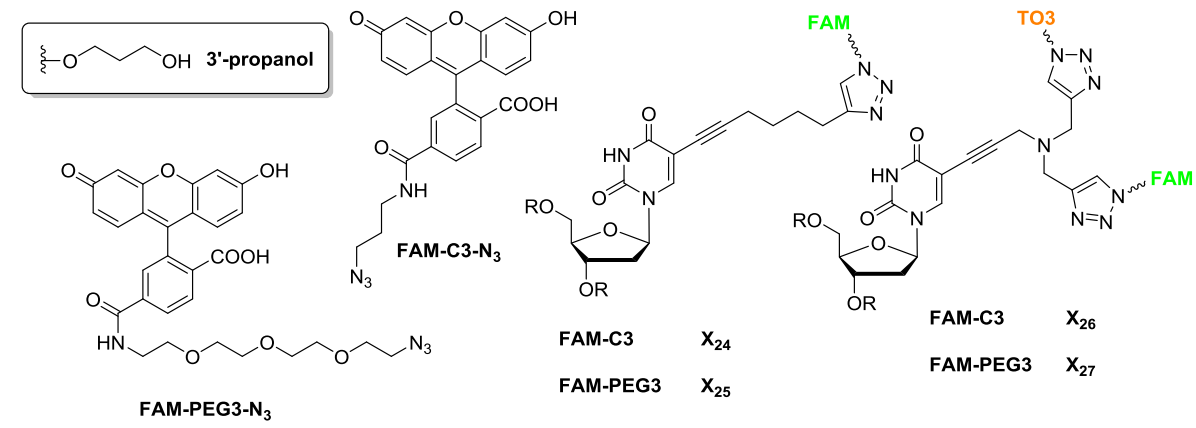

Table 5.13. A: Oligonucleotide sequences (mass spectra data see Appendix, Figure 9.1.4) and schematic representation of the key features; the T highlights the position of this mutation to be detected (underlined in the sequence table) relative to the positions of the fluorophores. B: Structures of FAM-C3 and FAM-PEG3 azide dyes and the monomers (X_{24}–X_{27}) used for the modified oligonucleotides; P = 3′-propanol; R = DNA.

The fluorescence response of FAM is sensitive to pH: below 7, FAM becomes protonated (no longer anionic), and has much lower fluorescence intensity.[182,183] GoTaq® polymerase was chosen for all asymmetric real-time PCR reactions, because of the GoTaq® polymerase buffer's higher pH value (pH 8.5) relative to KOD XL DNA polymerase

buffer (pH 7.45). This increased pH was expected to improve the fluorescence of FAM-labelled probes.

Fluorescence melting studies of probes with wild-type or mutant templates were performed in order to explore potential applications of the FAM/TO3 combination. The wild-type probes L1-(TO3/FAM-C3)2 and L1-(TO3/FAM-PEG3)2 were compared to test the effect of flexible linkers (for probe L1-(TO3/FAM-PEG3)2 data see Appendix, Figure 9.6.1). However, the use of different lengths of linkers produced no observable differences. The fully matched duplex with the probe L1-(TO3/FAM-C3)2 was found to have an average T_m value of 54.0 °C (Figure 5.16, D). The stability of the mismatched duplex was reduced by 3.0 °C. The results obtained were similar to those obtained for ROX dye. In the absence of TO, the stability of control duplexes was decreased by around 10.0 °C: the T_m was 45.0 °C for fully matched duplexes (Figure 5.16, B), and the TG-mismatched duplexes were less stable (T_m = 42.0 °C).

The fluorescence properties of all tested duplexes and single-strands are shown in Figure 5.16 (A, C). For the TO-free control HyBeacon probe L6-(FAM-C3)2, double incorporation of FAM dyes gave a high fluorescence signal and a small difference in fluorescence upon hybridization; this is believed to be due to the two FAM dye moieties being held apart in the double-stranded form, decreasing collisional quenching, and not being strongly quenched in the single stranded form. The melting curve and derivative are complex, but a clear melting temperature can be discerned. In the L1-(TO3/FAM-C3)2 probe, double incorporation of FAM and TO dyes quenched the fluorescence more efficiently in single strand and gave a weaker background signal as expected. A significant difference in intensity before and after hybridization was obtained for L1-(TO3/FAM-C3)2, but the fluorescence intensities of L1-(TO3/FAM-C3)2 were much weaker than those of its

corresponding control HyBeacon probe. This may be attributed to fluorescence resonance energy transfer (FRET); FAM (λ_{ex} = 495 nm, λ_{em} = 520 nm) acts as an energy donor, transferring energy to TO (λ_{ex} = 510 nm, λ_{em} = 530 nm) *via* through-space resonant dipolar coupling.

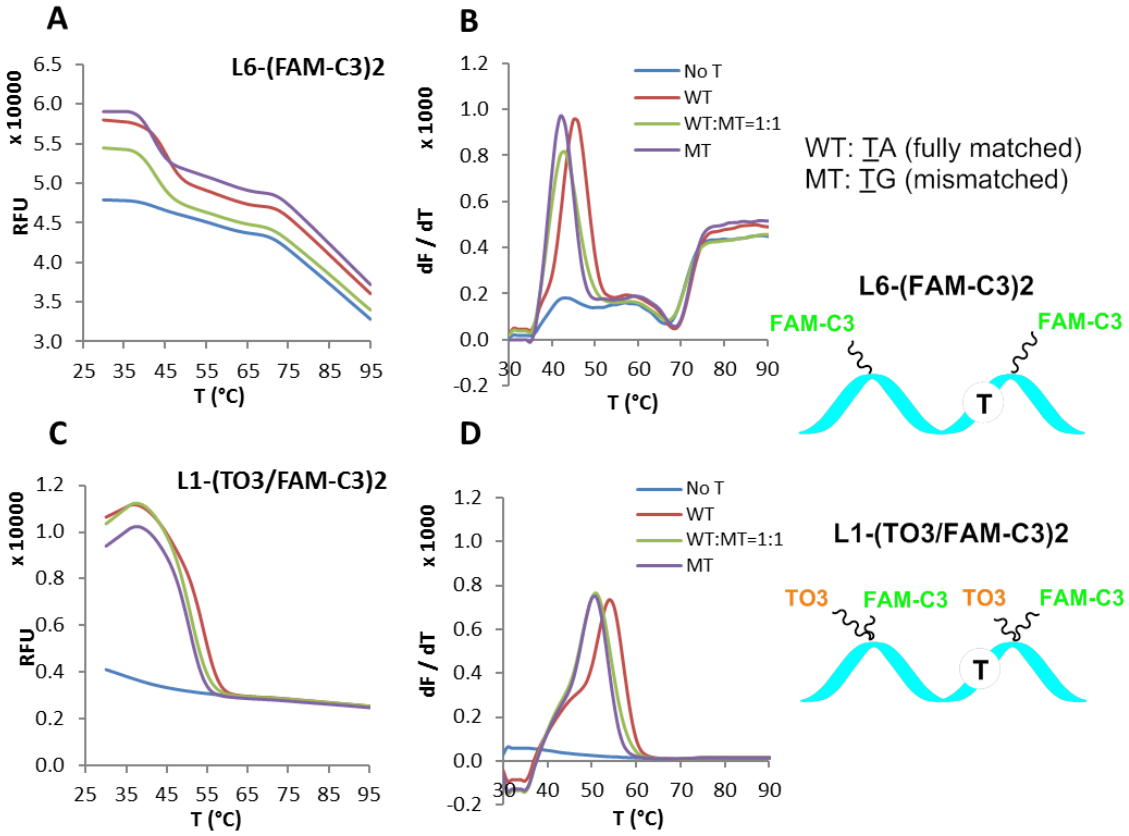

Figure 5.16. Fluorescence melting curves (A, C) and derivatives of post-amplification fluorescence melts (B, D) using the wild-type probe L1-(TO3/FAM-C3)2 (C, D) and the corresponding control HyBeacon probe L6-(FAM-C3)2 (A, B). Blue (No T): no template; red (WT): wild-type template; green (WT:MT = 1:1): wild-type: mutant template, ratio = 1:1; purple (MT): mutant template. All output was monitored in the FAM channel of the CFX96™ real-time PCR instrument (excitation range 450–490 nm, detector range 510–530 nm). GoTaq® DNA polymerase, 30 cycles and 1 ng of template ODNs were used. Notes: L1-(TO3/FAM-C3)2 is a wild-type probe that gives a fully matched duplex upon hybridization with wild-type template (WT), and forms a TG-mismatched duplex when pairs with mutant template (MT). The T in the schematic diagram highlights the position of this mutation to be detected relative to the positions of the fluorophores.

5.11.3 Evaluation of the L7-(TO3/ATTO647N)2 probe

The fluorescence melting properties of the mutant probe L7-(TO3/ATTO647N)2 and its TO3-free control HyBeacon probe L8-(ATTO647N)2 (Table 5.11) were studied in order to confirm that the probe L7-(TO3/ATTO647N)2 is compatible with the Cy5 channel of CFX96™ in real-time PCR. Asymmetric real-time PCR was carried out using KOD XL DNA polymerase (Figure 5.17) or GoTaq® DNA polymerase (Appendix, Figure 9.6.2), in order to confirm that the probe can be used with different polymerases.

Fluorescence melting analysis of the L7-(TO3/ATTO647N)2 and L8-(ATTO647N)2 probes was carried out. The results show a significant difference in T_m values between the wild-type (51.0 °C) and mutant (59.0 °C) template-probe duplexes using the mutant probe L7-(TO3/ATTO647N)2, based on the derivative of the post-amplification fluorescence melting curve (Figure 5.17 D). The TO-free control HyBeacon probe L8-(ATTO647N)2 has lower stability than L7-(TO3/ATTO647N)2 when binding to the wild-type (46.0 °C) and mutant (52.0 °C) template (Figure 5.17 B). The fluorescence intensities of L8-(ATTO647N)2 and L7-(TO3/ATTO647N)2 on hybridizing to their complementary strands were similar; however, fluorescence quenching was extremely efficient in single strand for the L7-(TO3/ATTO647N)2 probe, which was not the case for L8-(ATTO647N)2 (Figure 5.17 A and C). The same experiments were also carried out on the probe L7-(TO3/HEX)2 and its control HyBeacon probe L8-(HEX)2 (for data see Appendix, Figure 9.6.3 and Figure 9.6.4). Similar results were obtained, which indicate that the mutant probe L7-(TO3/HEX)2 is compatible with the HEX channel of CFX96™ in real-time PCR.

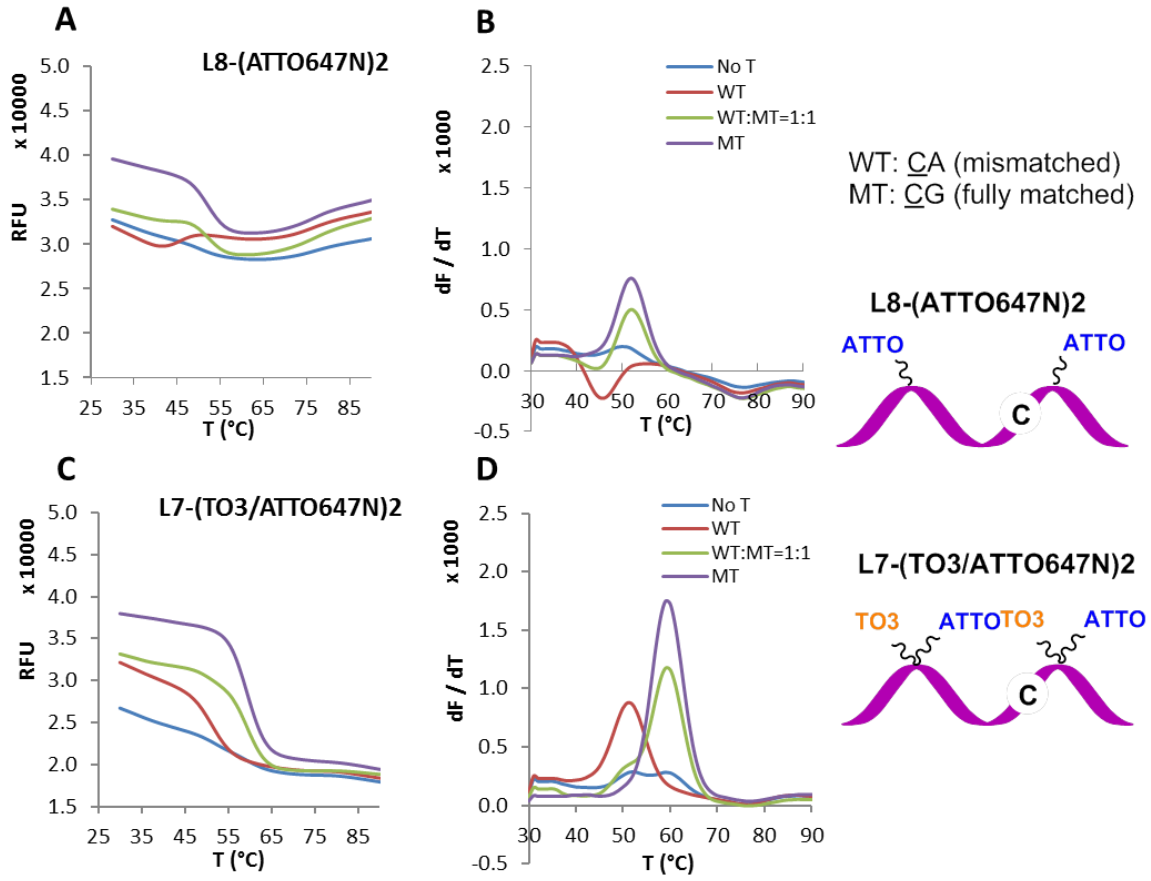

Figure 5.17. Fluorescence melting curves (A, C) and derivatives of post-amplification fluorescence melts (B, D) using the mutant probe L7-(TO3/ATTO647N)2 (C, D) and the corresponding control HyBeacon probe L8-(ATTO647N)2 (A, B). Blue (No T): no template; red (WT): wild-type template; green (WT:MT = 1:1): wild-type: mutant template, ratio = 1:1; purple (MT): mutant template. All output was monitored in the Cy5 channel of the CFX96™ real-time PCR instrument (excitation range 620–650 nm, detector range 675–690 nm). KOD XL DNA polymerase, 20 cycles and 1 ng of template were used. Notes: L7-(TO3/ATTO647N)2 is a mutant probe that gives a CA-mismatched duplex upon hybridization with wild-type template (WT), and forms a fully matched duplex when pairs with mutant template (MT). The C in the schematic diagram highlights the position of this mutation to be detected relative to the positions of the fluorophores.

5.12 Evaluation of wild-type and mutant probes in real-time PCR applications

As mentioned above, the wild-type probes are not sufficiently sensitive to detect a G substitution (i.e. TG-mismatch), which is the least destabilizing (and most demanding) compared to other mutations. The T_m on hybridization to the mutant template (G-mutation) was only 3.0 °C lower than the fully matched duplexes (Section 5.11). In addition, in both cases similar fluorescence intensity was observed, which is desirable, as it means that both wild-type and mutant can be identified. In view of this, a two-probe system was developed containing wild-type and mutant probes, which was evaluated in an asymmetric real-time PCR reaction to detect the CFTR R516G mutation. In this two-probe system, the wild-type probe showed preference for pairing to the wild-type template, and the mutant probe paired preferentially to the mutant template.

A series of real-time PCR experiments were set up varying the ratio of wild-type and mutant templates. The wild-type probe L1-(TO3/ROX)2 and mutant probes L7-(TO3/ATTO647N)2 or L7-(TO3/HEX)2 were used. The real-time PCR reactions were monitored in different channels depending on the dye used: the wild-type template was monitored in the ROX channel of the CFX96^{TM} real-time PCR instrument (excitation range 560–590 nm, detector range 610–650 nm), and the mutant template was detected in the HEX channel (excitation range 515–535 nm, detector range 560–580 nm) when the mutant probe L7-(TO3/HEX)2 was added, or in the Cy5 channel (excitation range 620–650 nm, detector range 675–690 nm) when the mutant probe L7-(TO3/ATTO647N)2 was used. When the real-time PCR reactions were monitored using the ROX channel, the wild-type template was found to bind preferentially to the wild-type probe L1-(TO3/ROX)2 over the mutant probe L7-(TO3/ATTO647N)2, as shown in Figure 5.18 A. As the amount of mutant template increased, the peak signal decreased

significantly, accompanied by a reduction in the T_m value from 59.0 °C to 56.0 °C. The reactions were monitored in the Cy5 channel when L7-(TO3/ATTO647N)2 was used (Figure 5.18 B). The mutant probe L7-(TO3/ATTO647N)2 bound to the mutant template (MT) (Figure 5.18 B, orange), showing a T_m value of 60.0 °C, higher than when pairing with the wild-type template (WT). However, the L7-(TO3/ATTO647N)2 probe was still able to detect the wild-type template (WT), giving a weaker signal, with a T_m value of 48.0 °C (Figure 5.18 B, red). The mutant probe L7-(TO3/HEX)2 was studied in the HEX channel, giving similar results to L7-(TO3/ATTO647N)2 (Appendix, Figure 9.7.1). These results suggest that the two-probe system is compatible with the different channels of the CFX96^{TM} real-time PCR instrument, and is able to detect and quantify the mutation (TG-mismatch).

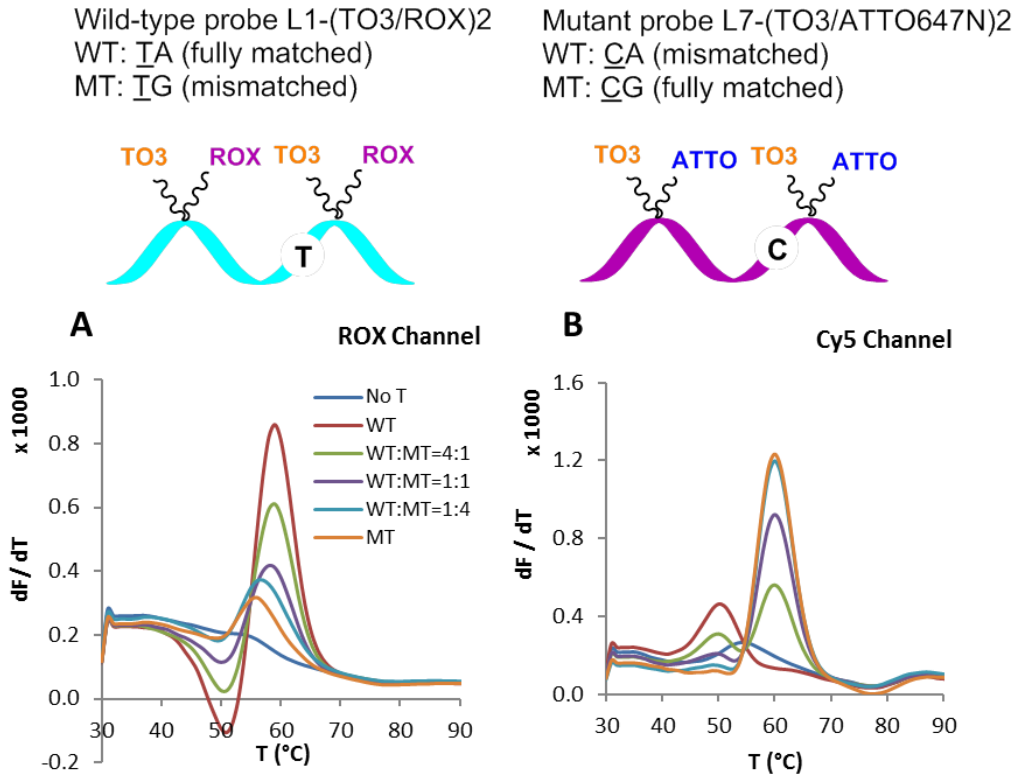

Figure 5.18. Fluorescence melting derivatives of mixture of the wild-type probe L1-(TO3/ROX)2 and mutant probe L7-(TO3/ATTO647N)2. Blue (No T): no template; red (WT): wild-type template; green (WT:MT = 4:1): (wild-type: mutant template, ratio = 4:1); purple (WT:MT = 1:1): (wild-type: mutant template, ratio = 1:1); light blue (WT:MT = 1:4): (wild-type: mutant template, ratio = 1:4); orange (MT): mutant template. A was monitored in the ROX channel of the CFX96™ real-time PCR instrument (excitation range 560–590 nm, detector range 610–650 nm); B was monitored in the Cy5 channel of the CFX96™ real-time PCR instrument (excitation range 620–650 nm, detector range 675–690 nm). KOD XL DNA polymerase, 20 cycles and 1 ng of template ODNs were used. The position of mutation to be detected is underlined. The T or C in the schematic diagram highlights the position of this mutation to be detected relative to the positions of the fluorophores.

5.13 Conclusions

Thiazole orange (TO) was successfully utilised in fluorescent DNA probes. Because of its strong fluorescence on intercalation in the DNA duplex and its weak fluorescence when unbound, TO was found to be an efficient fluorescent "on-off" DNA probe for detecting duplex formation.

This study focused on the preparation of doubly dye-labelled DNA probes. The probes were designed to display strong fluorescence enhancements on hybridization, with only weak fluorescence in the unhybridized state due to collisional quenching. To prepare these probes, TO azide with a 3- or 8-carbon linker (TO3, TO8) was reacted with a DNA strand bearing a terminal alkyne (tripropargylamine-modified dT, X_1) to give monomers X_2 and X_3 (Scheme 5.3) by the CuAAC reaction. The tripropargylamine functional group was introduced to the 5-position of thymidine (major groove) *via* Sonogashira coupling. The corresponding phosphoramidites of these TO/alkyne monomers were efficiently incorporated into oligonucleotides during solid phase synthesis.

A significant difference in emission intensity was observed before and after hybridization for the 13-mer probe S-TO3 (ds/ss = 12.1:1). Incorporation of TO3 caused a large increase in the thermal stability of the probe/target duplex ($\Delta T_{m\,(S\text{-}TO3\text{-}ds)}$ = + 11.6 °C) compared to the unmodified control duplex. Two X_2 moieties were incorporated into the probe L1-(TO3)2. It was demonstrated that two additions were more stabilizing than one in the probes L2-TO3 and L3-TO3 ($\Delta T_{m\,(L1\text{-}(TO3)2\text{-}ds)}$ = + 8.7 °C, $\Delta T_{m\,(L2\text{-}TO3\text{-}ds)}$ = + 6.0 °C, $\Delta T_{m\,(L3\text{-}TO3\text{-}ds)}$ = + 5.3 °C). Doubly TO-labelled probes (TO/TO-probes) with two TO units incorporated into the same T-nucleobase showed slightly increased emission compared with singly TO-labelled probes in the double-stranded state, and the fluorescence was efficiently quenched in single strand. However, incorporation of two TO units on the same

T-nucleobase led to a decrease of thermal stability, presumably due to the steric hindrance preventing efficient duplex intercalation of both TO units simultaneously. TO3 and TO8 were compared, showing that TO3 gave greater duplex stability and fluorescence than TO8. The shorter linker TO3 was therefore used in further studies.

The wild-type probes L1-(TO3/ROX)2 and L1-(TO3/FAM-C3)2 and the mutant probes L7-(TO3/HEX)2 and L7-(TO3/ATTO647N)2 were designed for the detection of the CFTR R516G mutation. All probes displayed a significant increase of fluorescence intensity after hybridization to their target sequences. The wild-type probe L1-(TO3/ROX)2 and mutant probe L7-(TO3/ATTO647N)2 gave fluorescence intensities that were as strong as their TO3-free control HyBeacon probes. Our analysis suggests that a great fluorescence in the double-stranded state is achieved from the TO3/ATTO647N, or TO3/ROX combinations. The TO3/FAM combination gives the worst result; possibly because the TO3 dye acts as a fluorescence (FRET) acceptor. However, FAM is one of the most commonly used dyes, compatible with most fluorescence detection instrumentation. We speculate that if the spectral overlap between the emission of the donor dye and the excitation of the acceptor dye is minimised, the result will be a greater fluorescence in the double-stranded state and effective fluorescence quenching in single strand (collisional quenching is not strongly wavelength-dependent). This could be achieved by using an alternative intercalator dye to TO, such as benzothiazole orange (BO), with λ_{em} (max) = 485 nm. This approach is discussed in Chapter 6.

Further optimization was carried out on a two-probe (wild-type and mutant) system. The signals could then be detected in two different channels, one channel for wild-type template (WT), another for mutant template (MT). To demonstrate this principle, the wild-type probe L1-(TO3/ROX)2 and the mutant probe L7-(TO3/ATTO647N)2 were used

in a real-time PCR reaction. The reaction was monitored in the ROX and Cy5 channels of the CFX96^{TM} real-time PCR instrument, and was used to successfully confirm of the nature of the mutation.

CHAPTER 6

Benzothiazole orange (BO) propargyl dT and its applications

Chapter 6 – Benzothiazole orange (BO) propargyl dT and its applications

6.1 Introduction

In the clinic diagnostics field, multi-functional and sensitive fluorescent probes are essential.[93,201] To this end, nucleic acid probes modified with thiazole orange (TO) and a second different fluorophore were used to detect the R516G mutation in the CFTR gene, as described in Chapter 5. This simple probe system retains the benefits of HyBeacon probes but also gives higher duplex thermal stability upon hybridization to the target DNA. It was noted that this probe system can be used for detection at different wavelengths, and was found to be compatible with applications in the CFX96™ real-time PCR and Roche LightCycler® instruments. However, despite these advantages, the TO/dye-modified probes were found to have a number of limitations (i.e. the TO/FAM combination did not perform better in terms of fluorescence changes on melting than the equivalent HyBeacon probes). This chapter aims to address these problems by optimizing the fluorescent "on-off" design by replacing TO with an intercalator dye that has lower excitation and emission wavelengths. This addition would be important for applications which involve independent excitation of dyes at different wavelengths for multiplex detection.

Benzothiazole orange (BO), a fluorescent intercalating dye that is structurally related to TO, was chosen because of its photophysical properties that include an absorbance maximum at 444 nm,[107] and a 400-fold enhancement in fluorescence intensity upon DNA binding.[102] Yarmoluk *et al.* have reported that the free TO dye forms H-aggregates while BO forms less stable J-aggregates. This results in BO and TO dyes having different hydrophobic surfaces, a fact that affects their DNA intercalation properties. BO intercalates into DNA more weakly than TO.[107] Nevertheless, BO has been used as a

fluorescent ligand that can bind to a specific site in DNA duplexes and DNA-RNA hybrids.[132] BO has attracted much interest due to its excellent nucleic acid staining properties.[119] However, there have been fewer reports of BO as a component of fluorescent "on-off" nucleic acid probes than for its analogue TO. Therefore, we decided to explore BO in this context. An alternative thymidine phosphoramidite monomer **6-7** (X_6) (Figure 6.1), functionalized with BO instead of TO was synthesised, and its photophysical properties studied in the context of the probe design described in Chapter 5.

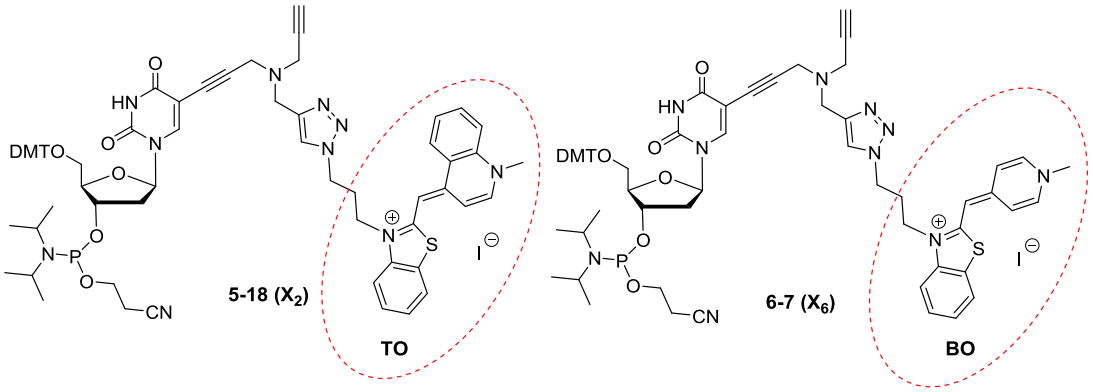

Figure 6.1. Phosphoramidite monomers for the insertion of TO (**5-18**, X_2) and BO (**6-7**, X_6) into oligonucleotides.

6.2 Synthesis of BO derivatives (6-3)

Benzothiazole orange (BO) is an asymmetric cyanine dye, consisting of a benzothiazole derivative and a pyridine ring linked *via* a methine bridge. In order to compare the properties of BO probes to those of TO probes, attachment to the oligonucleotide was made at the benzothiazole nitrogen of BO *via* the introduction of a propargyl azide linker. Reaction of alkyl dihalide 1,3-diiodopropane with the commercially available 2-methylbenzothiazole yielded iodide salt **5-6** with a yield of 64% (Chapter 5, Scheme 5.2). Addition of methyl iodide to 4-chloropyridine at 0 °C afforded 4-chloro-1-methylpyridium iodide **6-1** (61%).[202] Coupling of benzothiazole derivative **5-6** with 4-chloro-1-methylpyridium iodide **6-1**, and subsequent displacement of the iodine in **6-2** by lithium azide gave azido benzothiazolium salt **6-3** (Scheme 6.1). The reaction proceeded with formation of many by-products, resulting in a disappointingly low yield of 10%. The by-products were not isolated or formally characterised, but the mass spectrum of the crude reaction was consistent with the formation of **6-4** and **6-5** through inter- and intramolecular S_N2 reactions with the loss of iodide. An alternative pathway, analogous to that used for the synthesis of TO, was used whereby the azide **5-8** was first synthesised, followed by the coupling reaction to **6-1**. However, poorer yields were obtained *via* this route, possibly due to the low stability of **5-8**.

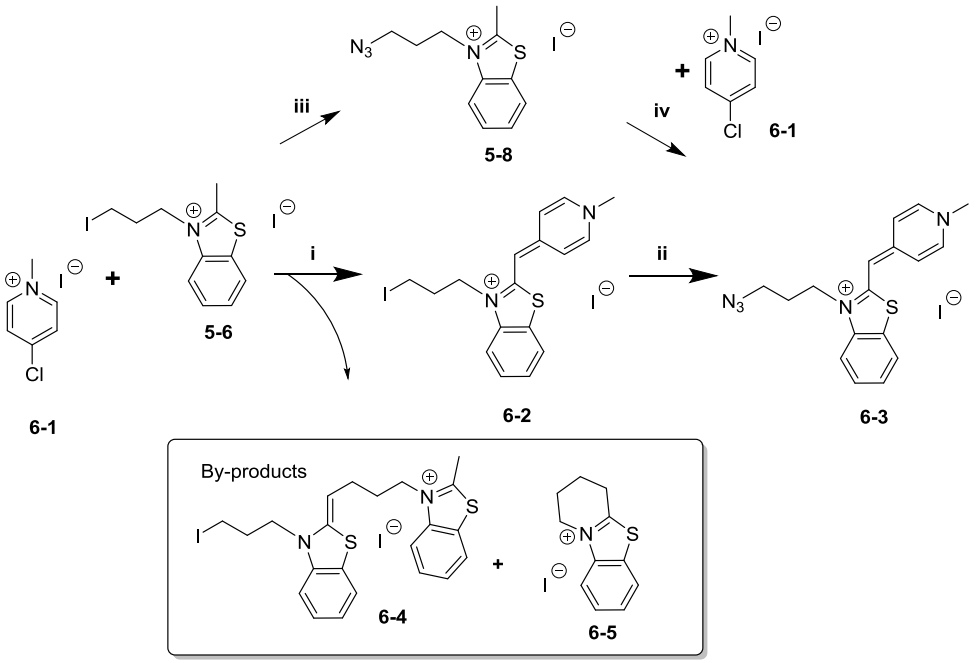

Scheme 6.1. Synthesis of *N*-(3-azidopropyl)-2-[(1,4-dihydro-1-methylpyridin-4-ylidene)methyl] benzothiazolium iodide **6-3**. Reagents and conditions: (i) DCM/MeCN (1:1), anhydrous Et_3N, RT, 10 min, 10%; (ii) 20 wt.% aq. lithium azide solution, DMF, RT, 10 min, 76%; (iii) MeCN, NaN_3 in H_2O, RT, 19 h, 55%. (iv) DCM/MeCN (1:1), anhydrous Et_3N, RT, 10 min, 12%.

6.3 Synthesis of BO3-dT phosphoramidite monomer (6-7)

CuAAC was then used to couple terminal alkyne **5-14** and azido benzothiazolium salt **6-3** to give the desired product **6-6** in a moderate yield (26%). Phosphitylation[72] of alcohol **6-6** using 2-cyanoethyl *N*,*N*-diisopropylchlorophosphoramidite in a mixture of *N*,*N*-diisopropylethylamine (DIPEA), DCM and DMF gave BO3-dT phosphoramidite monomer **6-7** (X_6) in 63% yield.

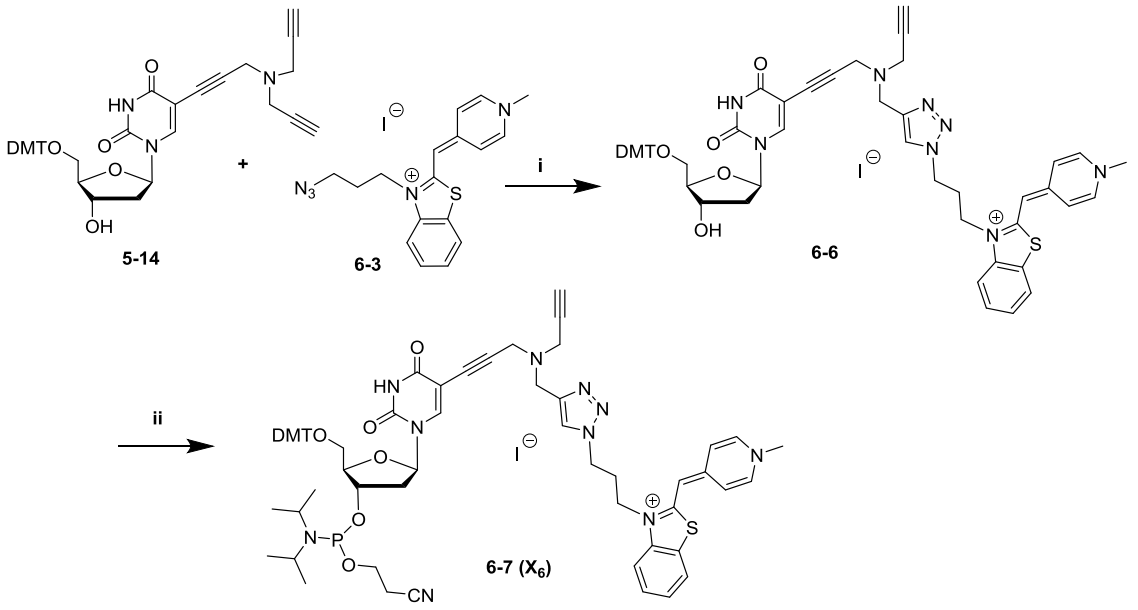

Scheme 6.2. Synthesis of phosphoramidite **6-7** (X_6). Reagents and conditions: (i) TBTA (**5-20**), DMF, $CuSO_4 \cdot 5H_2O$, sodium ascorbate in H_2O, RT, 2 h, 26%; (ii) anhydrous DCM, anhydrous DMF, DIPEA, 2-cyanoethyl *N*,*N*-diisopropylchlorophosphoramidite, RT, 2 h, 63%.

6.4 Synthesis of BO-modified oligonucleotides

BO3-dT phosphoramidite monomer (**6-7**) X_6 (Scheme 6.2) was successfully incorporated into two oligonucleotides: L1-(BO3)2 (wild-type) and L7-(BO3)2 (mutant) (Table 6.1). Both are 22-mer oligonucleotides, the key difference being that the former is complementary to the wild-type sequence of L-Acomp while the later has a single base substitution that detects L-Gcomp. Fast deprotecting monomers (UltraMILD monomers, Pac-dA, Ac-dC and iPr-Pac-dG, Seaction 1.2, Chapter 1) were used in the synthesis of these oligonucleotides. Cleavage of oligonucleotides from solid support and deprotection was achieved by exposure to concentrated aqueous ammonia solution for 4 h at room temperature. The deprotected oligonucleotides were purified using reversed-phase HPLC, and characterised by mass spectrometry (Figure 6.2).

Codes	Sequences	Mass found (calc.)
L1-(BO3)2	CGCTTCX_6GTATCTAX_6ATTCATCP	7641 (7642)
L7-(BO3)2	CGCTTCX_6GTATCCAX_6ATTCATCP	7626 (7626)
L-control	CGCTTCTGTATCTATATTCATCP	6764 (6764)
L-Acomp	CTATGATGAATATAGATACAGAAGCGTCAT	9262 (9262)
L-Gcomp	CTATGATGAATATGGATACAGAAGCGTCAT	9278 (9278)

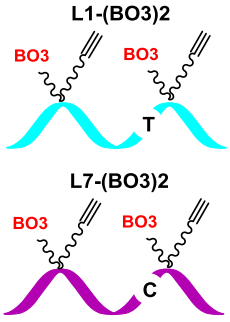

Table 6.1. Oligonucleotide sequences (mass spectra data in Appendix, Figure 9.1.5) and schematic representation of the key features. The position of mutation to be detected is underlined, the T or C in the schematic diagram highlights the position of this mutation to be detected relative to the positions of the fluorophores. X_6 = BO3-dT; P = 3′-propanol PCR blocker.

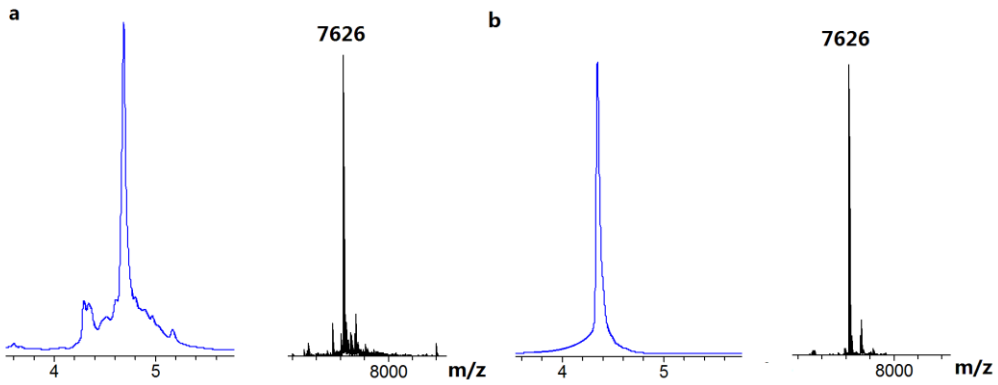

Figure 6.2. a: HPLC chromatogram and mass spectrum (ESI^-) of crude oligonucleotide L7-(BO3)2 and b: HPLC chromatogram and mass spectrum (ESI^-) of purified oligonucleotide L7-(BO3)2 (calc.: 7626, found: 7626).

6.5 UV melting studies of L-(BO3)2

Before using these novel probes in biological applications, it is important to determine the effect of these modifications on duplex stability. To this end, the ultraviolet absorption of oligonucleotides at 260 nm was monitored as the temperature was raised

to identify the melting temperature of DNA hybridized with the BO-modified probes, and also to quantify the effect of the BO dye intercalation on duplex stability. The studies were conducted on L1-(BO3)2 and L7-(BO3)2 oligonucleotides with sequences listed in Table 6.1.

The results of the melting studies are shown in Table 6.2 and Figure 6.3. The melting temperature (T_m) of the natural duplex (L-C-TA-ds) and tripropargylamine-modified duplex were found to be similar, in accordance with results shown in Chapter 5.5. After introducing the BO dye, the T_m of fully matched wild-type L1-(BO3)2 duplex increased by 3.9 °C compared to the natural control L-C-TA-ds (60.7 °C). The mutant L7-(BO3)2 duplex gave a high T_m value (67.2 °C) when pairing to its complementary strand. However, when it was paired to the wild-type sequence (i.e. generating a CA-mismatch, L7-(BO3)2-CA-ds), the T_m was lowered by 9.2 °C to 58.0 °C. The TG-mismatched duplex (L1-(BO3)2-TG-ds) had a melting temperature of 61.2 °C with a reduction of 3.4 °C compared to the fully matched L1-(BO3)2 duplex. These results suggest that two additions of BO3 lead to a greater increase in duplex stability, and that mismatched base pairs destabilize the DNA duplex significantly. In comparison with L1-(TO3)2-ds (69.4 °C, Chapter 5), L1-(BO3)-ds, as expected, gave a lower T_m value (64.6 °C) due to the less efficient intercalation of BO. Overall, the introduction of BO into oligonucleotide probes resulted in a good improvement of DNA duplex stability in comparison to the unmodified duplex; however, its duplex stabilisation by intercalation is weaker than that of TO.

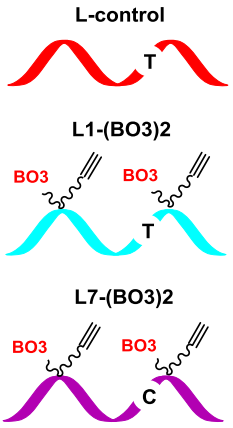

Duplex	Oligonucleotides (Base pairing at site of interest)	T_m (°C)	ΔT_m (°C)
1	L-control + L-Acomp (L-C-TA-ds)	60.7	
2	L-C-TA-ds + 40 eq. TO3-azide	66.7	+ 6.0 (*vs.* duplex 1)
3	L-C-TA-ds + 40 eq. BO3-azide	62.1	+ 1.4 (*vs.* duplex 1)
4	L1-(BO3)2 + L-Acomp (TA-ds)	64.6	+ 3.9 (*vs.* duplex 1)
5	L1-(BO3)2 + L-Gcomp (TG-ds)	61.2	– 3.4 (*vs.* duplex 4)
6	L7-(BO3)2 + L-Gcomp (CG-ds)	67.2	
7	L7-(BO3)2 + L-Acomp (CA-ds)	58.0	– 9.2 (*vs.* duplex 6)

Table 6.2. UV melting studies of the 22-mer BO-modified ODNs, and the effect of free dye (TO3-N_3 or BO3-N_3) on the natural control duplex. T_m: melting temperature; ΔT_m: difference in melting temperature compared to the relevant control; T_m values are the average of 3 separate melting and annealing curves. Melting temperatures are accurate to ± 0.1 °C. The T or C in the schematic diagram highlights the position of this mutation to be detected relative to the positions of the fluorophores.

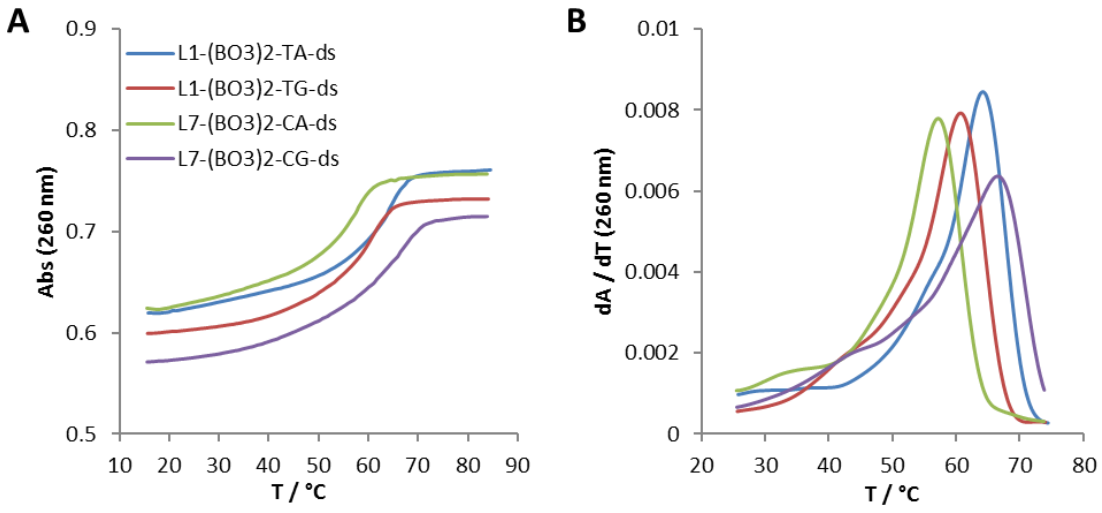

Figure 6.3. Representative UV melting curves (A) and their derivatives (B) for ODNs with two BO3 units (wild-type probe L1-(BO3)2 and mutant probe L7-(BO3)2). Blue: L1-(BO3)2-TA-ds (TA-match); red: L1-(BO3)2-TG-ds (TG-mismatch); green: L7-(BO3)2-CA-ds (CA-mismatch); purple: L7-(BO3)2-CG-ds (CG-match).

To further investigate the effects of both intercalating dyes on duplex stability, UV melting studies were also carried out using the free (unattached) TO and BO azide dyes (Table 6.2). TO3-azide or BO3-azide dye (40 eq.) was added to the natural control (L-C-TA-ds). For TO3-azide, the thermal stability increased by 6.0 °C compared to the control duplex (L-C-TA-ds) while it increased by just 1.4 °C in case of BO3-azide. This result confirms that the TO intercalation is more stabilising than that of BO. More importantly the L1-(BO)2 probe, which contains two thymine bases with BO3 attached, increases duplex stability (ΔT_m = + 2.5 °C) more effectively than the free BO3 dye intercalating into an unmodified duplex (L-C-TA-ds), thus proving that direct covalent attachment is benefical in this context.

6.6 Fluorescence studies of L-(BO3/dye)2 probes

The R516G mutation in the CFTR gene and its wild-type control were chosen as the target sequences to evaluate the fluorescent "on-off" properties of the wild-type probe L1-(BO3)2 and mutant probe L7-(BO3)2. To this end, fluorescence studies were carried out on L1-(BO3)2 and L7-(BO3)2 prior to and after hybridization with their fully complementary DNA strands at room temperature to determine the differences in emission intensities in the single-stranded (ss) and double-stranded (ds) states (Figure 6.4). In both cases, a 2.5-fold increase upon matched hybridization was observed.

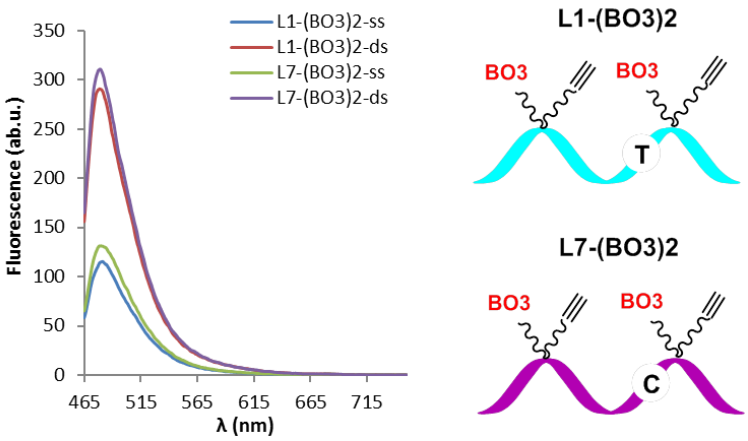

Figure 6.4. Comparison of room temperature steady state emission of the 22-mer L1-(BO3)2 and L7-(BO3)2 in the single-stranded (ss) and double-stranded (ds) states. All the results were obtained using λ_{ex} = 453 nm. The T or C in the schematic diagram highlights the position of this mutation to be detected relative to the positions of the fluorophores; ab.u .= arbitrary unit.

The BO3-only control probes (L1-(BO3)2 and L7-(BO3)2) did not give large fluorescence changes upon hybridization, as shown in Figure 6.4. Next, BO3-modified probes were synthesised with two additions of modified thymidine (X_{28}–X_{31}, Table 6.3), each bearing a BO3 and an additional fluorophore. Fluorescein (FAM), 6-hexachloro-fluorescein (HEX), 6-carboxy-X-rhodamine (ROX), and ATTO647N were chosen to label these BO-modified probes. These combinations span a range of mutually compatible excitation and emission wavelengths. It was also expected that if the intercalative quencher used in Chapter 5: thiazole orange (TO), was replaced by benzothiazole orange (BO) that similar fluorescence "on-off" properties would be retained. BO should intercalate between base pairs in duplex DNA in a comparable way to TO, but with a lower excitation wavelength.

To allow direct comparison to the results obtained using the equivalent TO3-modified probes, similar experiments were conducted using the BO3/dye modified probes. The oligonucleotides used for this study are listed in Table 6.3.

A

Codes	Sequences	Mass found (calc.)
L1-(BO3/FAM-C3)2	CGCTTCX_{28}GTATC<u>T</u>AX_{28}ATTCATCP	8556 (8559)
L1-(BO3/ROX)2	CGCTTCX_{29}GTATC<u>T</u>AX_{29}ATTCATCP	8876 (8875)
L7-(BO3/HEX)2	CGCTTCX_{30}GTATC<u>C</u>AX_{30}ATTCATCP	8956 (8957)
L7-(BO3/ATTO647N)2	CGCTTCX_{31}GTATC<u>C</u>AX_{31}ATTCATCP	9318 (9319)
L6-(FAM-C3)2	CGCTTCX_{24}GTATC<u>T</u>AX_{24}ATTCATCP	7846 (7846)
L6-(ROX)2	CGCTTCX_{17}GTATC<u>T</u>AX_{17}ATTCATCP	8177 (8177)
L8-(HEX)2	CGCTTCX_{19}GTATC<u>C</u>AX_{19}ATTCATCP	8259 (8259)
L8-(ATTO647N)2	CGCTTCX_{20}GTATC<u>C</u>AX_{20}ATTCATCP	8621 (8621)

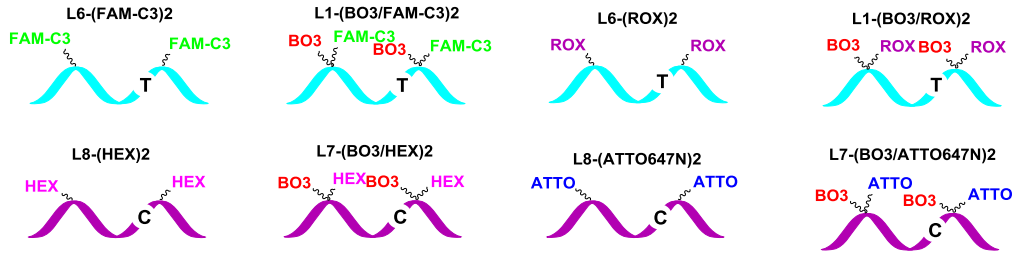

B

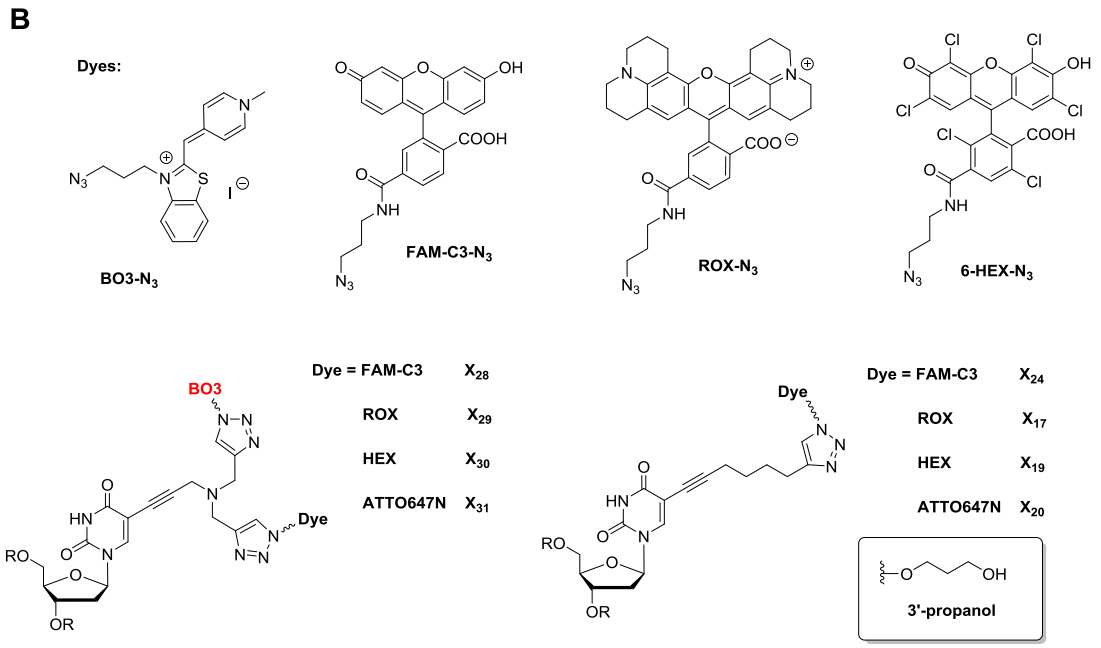

Table 6.3. A: Oligonucleotide sequences (mass spectra data in Appendix, Figure 9.1.5) and schematic representation of the key features; the T or C highlights the position of this mutation to be detected (underlined in the sequence table) relative to the positions of the fluorophores. B: Structures of BO3, FAM-C3, ROX, HEX azide dyes and the monomers (X_{17}, X_{19}, X_{20}, X_{24} and X_{28}–X_{31}) used for the modified oligonucleotides. P = 3′-propanol; R = DNA.

Initially, probe L1-(BO3/FAM-C3)2 and its control HyBeacon probe L6-(FAM-C3)2 were excited at two different wavelengths (λ_{ex} = 454 nm, the excitation maximum of BO, and λ_{ex} = 492 nm, the excitation maximum of FAM). Measurements of emission spectra before and after hybridization with fully complementary DNA were also performed to study the responsiveness of the two BO units. As expected, the single-stranded L1-(BO3/FAM-C3)2 probe showed efficient fluorescence quenching on excitation at 454 nm and 492 nm, and gave low emission (Figure 6.5 A, B, blue). A significant difference in fluorescence intensity was observed at 518 nm before and after hybridization with a fully complementary strand (L1-(BO3/FAM-C3)2: ds/ss = 11.5:1, λ_{ex} = 454 nm; ds/ss = 10.0:1, λ_{ex} = 492 nm). On duplex formation, L1-(BO3/FAM-C3)2 displayed a fluorescence intensity that was very slightly stronger (*ca.* 1.1-fold) on excitation at 454 nm compared to 492 nm (Figure 6.5 A, B, red). This strong fluorescence on excitation at 454 nm is attributed to the efficient FRET from BO3 to FAM-C3. The same fluorescence experiments were also performed on the BO3-free control HyBeacon probe L6-(FAM-C3)2. As expected, weak fluorescence intensity at 518 nm was observed on excitation at 454 nm before and after hybridization (Figure 6.5 A). This was 2.5-fold lower than the L1-(BO3/FAM-C3)2 probe. The strongest fluorescence at 518 nm was obtained by excitation at 492 nm (Figure 6.5 B), which is the absorption maximum of FAM. However, its fluorescence emission only increased by *ca.* 1.5-fold upon hybridization. The DNA probe bearing two additions of BO3/FAM-C3 pair, displays more sensitivity upon hybridization compared to the HyBeacon probe L6-(FAM-C3)2. In addition, the single-stranded L1-(BO3/FAM-C3)2 probe gave *ca.* 7-fold lower fluorescence background compared to the L6-(FAM-C3)2 HyBeacon probe when exciting at 492 nm. These results indicate that L1-(BO3/FAM-C3)2 can be excited at the BO and FAM channels to give brightly fluorescence signals compared to its control HyBeacon probe L6-(FAM-C3)2.

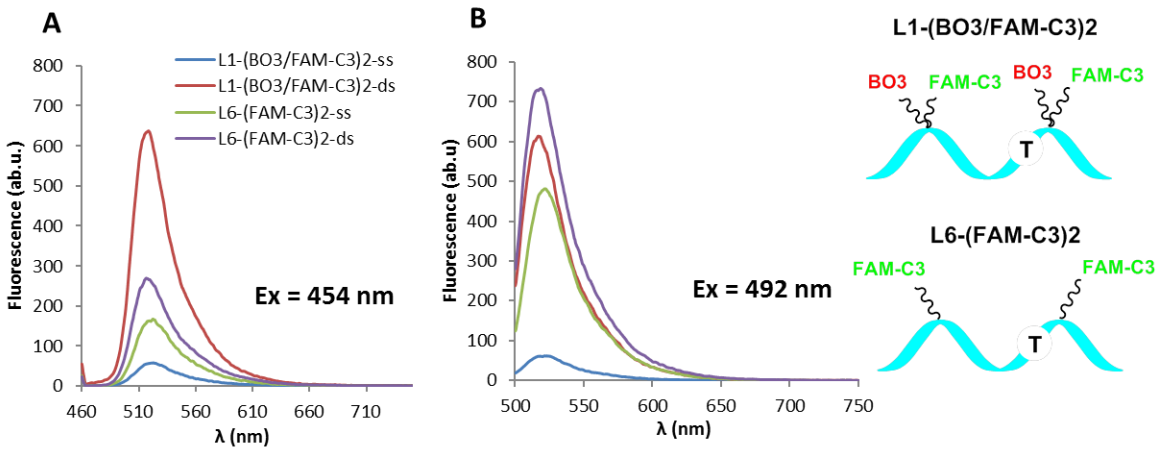

Figure 6.5. Comparison of room temperature steady state emission of the 22-mer probe L1-(BO3/FAM-C3)2 and its control HyBeacon probe L6-(FAM-C3)2 in the single-stranded (ss) and double-stranded (ds) states. A: λ_{ex} = 454 nm (the excitation maximum of BO3); B: λ_{ex} = 492 nm (the excitation maximum of FAM-C3). The T in the schematic diagram highlights the position of this mutation to be detected relative to the positions of the fluorophores; ab.u .= arbitrary unit.

The very promising results for L1-(BO3/FAM-C3)2 probe encouraged us to apply the same method using different dyes to develop a probe system to cover a wider wavelength range. The wild-type probe L1-(BO3)2 and its control L6 were labelled with FAM-C3 and ROX dyes, while the mutant probe L7-(BO3)2 and its control L8 were labelled with HEX and ATTO647N dyes. For these dyes, the emission wavelength becomes progressively red shifted (FAM – 518 nm, HEX – 556 nm, ROX – 607 nm, ATTO647N – 665 nm).

For mutant probe L7-(BO3/HEX)2 (Appendix, Figure 9.4.3), it is worth noting that there was a significant difference of fluorescence intensities before and after hybridization (ds/ss = 18.5:1) compared to the control HyBeacon probe L8-(HEX)2 (Appendix, Figure 9.4.4) on excitation at 455 nm. However, fluorescence energy transfer of the L7-(BO3/HEX)2 probe was not efficient in the duplex, the fluorescence emission was *ca.*-1.3-fold weaker upon excitation at 455 nm than at 540 nm, and also *ca.* 2-fold weaker

than the control HyBeacon probe L8-(HEX)2 when exciting at 540 nm. This is possibly due to the purity of the L7-(BO3/HEX)2 probe that can bind to with metal atom (i.e. iron or copper) during oligonucleotide purification, which was confirmed by mass spectrometry (Appendix, Figure 9.1.5).

For L1-(BO3/ROX)2, similar results to that of L1-(BO3/FAM-C3)2 were obtained and are shown in Appendix (Figure 9.4.5). Probe L1-(BO3/ROX)2 displayed low emission in the single-stranded state on excitation at 453 or 586 nm. On hybridization of probe L1-(BO3/ROX)2 to its complementary strand, stronger ROX emission was observed at 607 nm with the signal being 1.1-fold stronger upon excitation at 453 nm than at 586 nm (λ_{ex} = 453 nm: ds/ss = 7.8:1; λ_{ex} = 586 nm: ds/ss = 8.1:1). This result indicates that efficient FRET from BO3 to ROX was observed in the BO3/ROX combination.

For L7-(BO3/ATTO647N)2, there was a significant difference in the fluorescence intensity before and after hybridization (ds/ss = 9.7:1 and ds/ss = 8.9:1 for excitation at 452 and 647 nm, Figure 6.6), with the similar intensity after hybridization being comparable to the control HyBeacon probe L8-(ATTO647N)2 when excited at 647 nm. However, fluorescence emission around 480 nm was also apparent indicating that the overlap between the emission of BO and the excitation of ATTO647N does not allow efficient FRET (Figure 6.6 A). Finally, as expected, no fluorescence signal was observed on excitation at 452 nm for the BO3-free control HyBeacon probe L8-(ATTO647N)2.

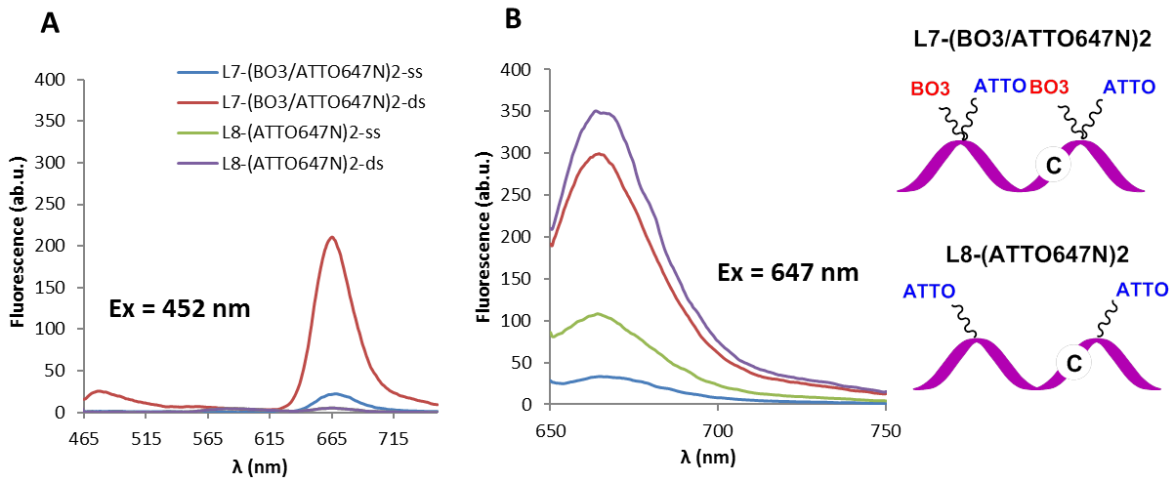

Figure 6.6. Comparison of room temperature steady state emission of the 22-mer probe L7-(BO3/ATTO647N)2 and its control HyBeacon probe L8-(ATTO647N)2 in the single-stranded (ss) and double-stranded (ds) states. A: λ_{ex} = 452 nm (the excitation maximum of BO3); B: λ_{ex} = 647 nm (the excitation maximum of ATTO647N). The C in the schematic diagram highlights the position of this mutation to be detected relative to the positions of the fluorophores; ab.u .= arbitrary unit.

In summary, modified probes (wild-type and mutant detecting) were designed to contain two additions of a T-nucleobase that bears a BO and an additonal fluorophore. This allows the hybridised probes to be detected in two different channels (excitation at BO or the additonal fluorophore). These modified probes had similar fluorescence intensities to their BO3-free control fluorescent HyBeacon probes, but improtantly displayed 8–18-fold stronger fluorescence changes upon hybridization. It is worth mentioning that the BO/FAM combination gives efficient FRET, which is a great improvement on the TO/FAM combination in Chapter 5.

6.7 The application of L-(BO3/dye)2 probes in real-time PCR

BO3-modified probes, like HyBeacon probes, should be suitable for use in real-time PCR. In order to evaluate this, wild-type probes (L1-(BO3/FAM-C3)2, L1-(BO3/ROX)2) were synthesised to be complementary to the wild-type target at the R516G locus in the CFTR gene, and mutant probes (L7-(BO3/HEX)2, L7-(BO3/ATTO647N)2) which are complementary to the R516G mutation were also synthesised. As mentioned above, four reporter dyes (FAM, HEX, ROX and ATTO647N) were chosen as they suitable for use in the CFX96^{TM} real-time PCR instrument, and cover all four available channels. The BO dye can be detected in the FAM channel while the others (FAM, HEX, ROX, ATTO647N) were detected in their respective channels (ATTO647N in the Cy5 channel).

Therefore, these four BO3-modified probes were evaluated to detect the CFTR R516G mutation in the CFTR gene in a real-time PCR scenario. Real-time PCR reactions were previously employed for L-(TO3/dye)2 probes as described in Chapter 5. The same experiments were repeated here, but with new BO3-bearing probes instead. Synthetic DNA templates (wild-type and mutant) and the required primer sequences for the CFTR R516G locus were prepared as described in Chapter 5, Table 5.12. GoTaq® DNA polymerase was used for all asymmetric real-time PCR reactions. KOD XL DNA polymerase was also used for all asymmetric real-time PCR reactions (data see Appendix, Figure 9.6.5 – Figure 9.6.8).

Fluorescence melting curves were obtained for the wild-type probes L1-(BO3/FAM-C3)2 and L1-(BO3/ROX)2 hybridized to the wild-type (WT) and mutant (MT) templates after the PCR reactions. The probe L1-(BO3/ROX)2 was monitored in the ROX channel, and gave reasonable fluorescence curves, with a decrease in fluorescence as the temperature

increased (Figure 6.7 A). T_m values were obtained by taking the derivatives of post-amplification fluorescence melting curves (Figure 6.7 B). Probe L1-(BO3/ROX)2 was hybridized to the wild-type template (WT), giving a T_m of 50.0 °C, while with a mutant template (i.e. TG-mismatch), displayed a T_m of 47.0 °C. This result is consistent with the TO/dye-probe studies described in Chapter 5. It is noteworthy that Sagi *et al.*[200] as well as many others have reported that the base pair mismatch caused by mutation of G for A (i.e. TG-mismatch) generally has a lower duplex destabilizing effect and is therefore the most difficult mismatched base pair to identify. The control HyBeacon probe L6-(ROX)2 gave a T_m of 46.0 °C upon hybridization to the wild-type template (WT) when using GoTaq® DNA polymerase. Similar results were obtained for L1-(BO3/FAM-C3)2 when monitoring in the FAM channel (Appendix, Figure 9.6.5).

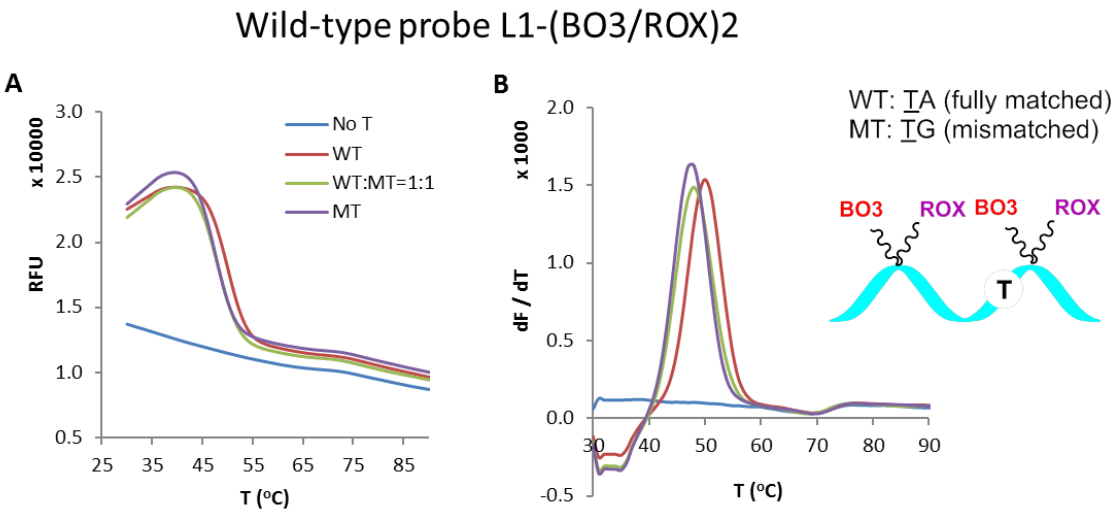

Figure 6.7. Fluorescence melting curves (A) and derivatives of post-amplification fluorescence melts (B) using the wild-type probe L1-(BO3/ROX)2. Blue (No T): no template; red (WT): wild-type template; green (WT: MT = 1:1): wild-type template: mutant template, ratio = 1:1; purple (MT): mutant template. All output was monitored in the ROX channel of the CFX96™ real-time PCR instrument (excitation range 560–590 nm, detector range 610–650 nm). GoTaq® DNA polymerase, 30 cycles and 1 ng of template ODNs were used. Note: L1-(BO3/ROX)2 is a wild-type probe that gives a fully matched duplex upon hybridization with wild-type template (WT), and forms a TG-mismatched duplex when pairs with mutant template (MT). The T in the schematic diagram highlights the position of this mutation to be detected relative to the positions of the fluorophores.

The fluorescence melting properties of the mutant probes L7-(BO3/HEX)2 and L7-(BO3/ATTO647N)2 were also studied. Asymmetric real-time PCR was carried out as before using the wild-type (WT) and mutant (MT) templates. Probe L7-(BO3/ATTO647N)2 was hybridized with the mutant template (MT), resulting in a duplex with a T_m of 49.0 °C, and with wild-type template (WT), showing a significantly lower T_m of 8.0 °C than for the fully matched duplex (Figure 6.8 B). The same results were also obtained for probe L7-(BO3/HEX)2, showed in Appendix (Figure 9.6.6).

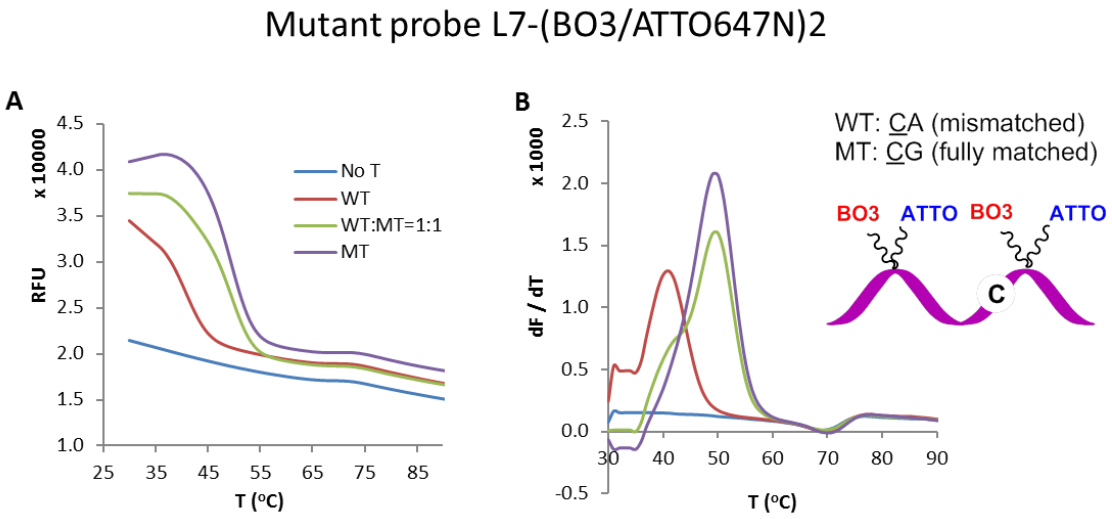

Figure 6.8. Fluorescence melting curves (A) and derivatives of post-amplification fluorescence melts (B) using the mutant probe L7-(BO3/ATTO647N)2. Blue (No T): no template; red (WT): wild-type template; green (WT: MT = 1:1): wild-type template: mutant template, ratio = 1:1; purple (MT): mutant template. All output was monitored in the Cy5 channel of the CFX96™ real-time PCR instrument (excitation range 620–650 nm, detector range 675–690 nm). GoTaq® DNA polymerase, 30 cycles and 1 ng of template ODNs were used. Note: L7-(BO3/ATTO647N)2 is a mutant probe that gives a CA-mismatched duplex upon hybridization with wild-type template (WT), and forms a fully matched duplex when pairs with mutant template (MT). The C in the schematic diagram highlights the position of this mutation to be detected relative to the positions of the fluorophores.

6.8 Evaluation of wild-type and mutant probes in real-time PCR applications

L-(BO3/dye)2 probes were designed to detect and quantify the CFTR R516G mutation site. However, the wild-type probes L1-(BO3/FAM-C3)2 and L1-(BO3/ROX)2 are not sufficiently sensitive for a G-mutation detection, which is the least destabilizing (and most demanding) compared to other mutations. The T_m of the duplex formed with the mutant template (G-mutation, i.e. TG-mismatch) was only 3 °C lower than for the fully matched duplex (TA-match). Fluorescence intensity was similar in both cases. In order to improve

the probe/target duplex stability and fluorescence response, a two-probe system was designed, as described in Chapter 5. In this section, a wild-type L1-(BO3/ROX)2 probe and a mutant L7-(BO3/ATTO647N)2 probe were utilised in the same asymmetric real-time PCR.

When monitored in the ROX channel (Figure 6.9 A), as the ratio of mutant template (MT) to wild-type template (WT) increased, the peak fluorescence signal for the wild-type duplex decreased significantly, and the decrease of this signal was accompanied with a reduction in T_m value from 49 °C to 46 °C. The difference in T_m values between the fully matched (TA) and mismatched (TG) duplexes was not sufficient for the mutation to be detected using this channel. However, a highly destabilizing CA-mismatch led to a great difference in T_m between the matched (CG) and mismatched (CA) duplexes when the mutant probe L7-(BO3/ATTO647N)2 was used, resulting in two clearly discernible peaks when monitored using the Cy5 channel (Figure 6.9 B). The melting curve derivatives show a peak at 41 °C for the mismatched duplex of mutant probe to wild-type target (WT), and another peak at 49 °C for the fully-matched duplex of mutant probe to mutant target (MT). As the ratio of mutant template (MT) to wild-type template (WT) decreased, this signal was progressively and clearly lowered. This result indicates that the wild-type probe favours base pairing to the wild-type template (WT), and the mutant probe preferentially binds to the mutant template (MT). It was worth noted that the mutant probe successfully bound to the wild-type sequence when only wild-type template was present, however, *ca.* 2-fold weaker signal was observed. Finally, it should be noted that similar results were also obtained by mutant probe L7-(BO3/HEX)2, L7-(BO3/ATTO647N)2 and wild-type probe L1-(BO3/FAM-C3)2, L1-(BO3/ROX)2 when using GoTaq® or KOD XL DNA polymerase (Appendix, Figure 9.7.2 – Figure 9.7.6).

Overall, the two-probe system can be potentially used to detect and quantify mutations, such as the G-mutation (i.e. TG-mismatch) in DNA. Monitoring fluorescence signals in two channels simultaneously in the CFX96™ real-time PCR instrument gives useful information on the ratio of wild-type target (WT) to mutant target (MT) in the analytical sample.

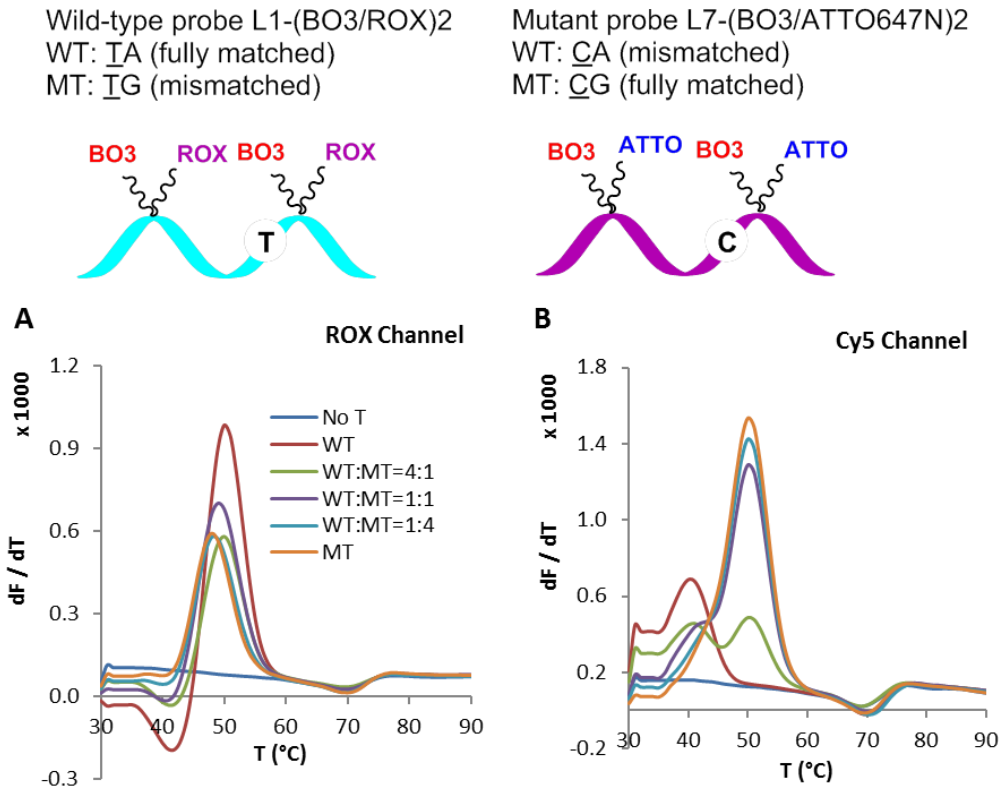

Figure 6.9. Fluorescence melting derivatives of mixture of the wild-type probe L1-(BO3/ROX)2 and mutant probe L7-(BO3/ATTO647N)2. Blue (No T): no template; red (WT): wild-type template; green (WT:MT = 4:1): (wild-type: mutant template, ratio = 4:1); purple (WT:MT = 1:1): (wild-type: mutant template, ratio = 1:1); light blue (WT:MT = 1:4): (wild-type: mutant template, ratio = 1:4); orange (MT): mutant template. A was monitored in the ROX channel (excitation range 560–590 nm, detector range 610–650 nm); B was monitored in the Cy5 channel (excitation range 620–650 nm, detector range 675–690 nm). Gotaq® DNA polymerase, 30 cycles and 1 ng of template ODNs were used. The position of mutation to be detected is underlined. The T or C in the schematic diagram highlights the position of this mutation to be detected relative to the positions of the fluorophores.

6.9 Conclusions

Benzothiazole orange (BO), which has a similar chemical structure to TO dye, was used as a fluorescent label in DNA probes. BO was selected because of its similarities to TO and its lower excitation and emission wavelengths. BO-modified oligonucleotides were expected to produce bright "on-off" fluorescent probes, especially in the case of the BO/FAM combination.

A CuAAC reaction between a BO azide and an alkyne bearing dT (tripropargylamine-modified dT, X_1) afforded monomers X_6 (Figure 6.1). The corresponding phosphoramidites were multiply incorporated into oligonucleotides during solid-phase synthesis. Two additions of BO led to an increase in thermal stability of duplexes (for L1-(BO3)2-ds, ΔT_m = + 3.9 °C) that was 2.5 °C higher than the stability enhancement when using a large excess of free BO azide dye (ΔT_m = + 1.4 °C). The wild-type probes L1-(BO3/FAM-C3)2 and L1-(BO3/ROX)2, and mutant probes L7-(BO3/HEX)2 and L7-(BO3/ATTO647N)2, displayed significant differences in fluorescence intensity before and after hybridization (ds/ss = *ca.* 8–18:1). While the FRET from FAM to TO was limited (Chapter 5), it was found that the FRET from BO to FAM was efficient, constituting an improvement on the TO/FAM combination. The BO/dye probe system retains the bright fluorescence characteristic of HyBeacon probes, and has additional benefits, e.g. greater duplex stability and the possibility of multi-channel detection**.**

The BO/dye probes were suitable for use on the CFX96^{TM} real-time PCR instrument, and their fluorescence response was easily monitored using different channels according to the dye used. A two-probe system was used in further optimization.

CHAPTER 7

Conclusions and future work

Chapter 7 – Conclusions and future work

The aim of this work was to explore the use of 'click' chemistry in the synthesis of modified oligonucleotides. Click chemistry is a method that has been widely exploited in the nucleic acid field due to its high selectivity and remarkable efficiency. The most popular click reactions are the copper-catalysed and strain-promoted alkyne-azide cycloadditions (CuAAC and SPAAC respectively), both of which were investigated in detail.

The synthesis of long DNA structures *in vitro* is required for gene synthesis and nanoconstruct formation. The solid phase phosphoramidite method is a highly efficient process, but oligonucleotide synthesis is limited to *ca.* 150 bases in length. Therefore, a chemical method to make longer DNA was developed. Initially, oligonucleotide ligation was carried out on the solid phase by the CuAAC or SPAAC reaction. The alkyne and azide functional groups were incorporated into the 5′- and 3′-end of ODNs during solid phase oligonucleotide synthesis or post-synthetically.

In the CuAAC reaction, 3′-alkyne ODNs in solution were reacted with resin-bound 5′-azide ODNs in the presence of Cu(I) without template DNA to form the biocompatible triazole analogue **tz1** (Chapter 2). No significant difference was observed between the reactions using different resin pore sizes. 77-mer ODNs were obtained, however, partial degradation of the oligonucleotides was found to occur due to the solid-phase CuAAC conditions (copper salts, high temperatures, long reaction times).

To avoid some of these problems, a copper-free SPAAC methodology was used to assemble long oligonucleotides on the solid phase (Chapter 3). Using a masked azide approach, multiple sequential ligations allow the efficient assembly of oligonucleotides up

to 186 bases in length and importantly did not require additional template oligonucleotides. In addition, the solid phase SPAAC reaction was successfully used to synthesise 121 base oligonucleotides with unnatural 5′-5′ linkages that could potentially be used in artificial DNA nanoconstructs.

The SPAAC reaction was also used to form stable covalent crosslinks in fluorescently labelled double-stranded DNA for FRET studies. The BCN/azide SPAAC reaction across the minor and major grooves of the DNA duplexes was faster and cleaner than the DIBO/azide reaction (Chapter 4). However, optimization of the design, synthesis and purification of the resultant fluorescent nanoconstructs is still required. During the course of these studies, the BCN moiety usually used for SPAAC was found to be unstable in the presence of 3% TCA in DCM, the conditions required for DMT removal during oligonucleotide synthesis. Optimisation of synthesis showed that 10% DCA in toluene was a milder alternative, generating a lower percentage of inactivated BCN.

Thiazole orange (TO) and benzothiazole orange (BO) modified nucleic acid probes were designed. They were shown to have strong fluorescence upon intercalation into the DNA duplex and weak fluorescence when unbound. The TO azide dye with a 3- or 8-carbon linker (TO3, TO8) was synthesised, and attached at the 5-position of thymidine (major groove). Their corresponding phosphoramidites (X_2, X_3) were singly or doubly incorporated into oligonucleotides during solid phase oligonucleotide synthesis (Chapter 5). Comparison of oligonucleotides containing two units of TO3 or TO8 on the same nucleobase showed that TO3 gave better duplex stability and higher fluorescence than TO8. A wild-type probe L1-(TO3)2 and mutant probe L7-(TO3)2 were designed for the detection of the CFTR R516G mutation; those probes could be labelled with various dyes (e.g. FAM, HEX, ROX and ATTO647N) by CuAAC, to give two-colour

probe systems, which form more stable duplexes upon hybridization compared to the TO-free control HyBeacon probes, and can be used for two-channel fluorescence detection. However, sensitivity was reduced when the probe-target duplex contained a TG-mismatch. Therefore, a two-probe system was designed containing a wild-type probe and a mutant probe, which allowed the mutation to be clearly identified. Further studies showed that the scope of the TO-modified probe system can be increased by using the BO dye which extends the available range to lower wavelengths. This is discussed in Chapter 6.

In order to compare the properties of BO probes to those of TO probes, the same method was used to incorporate BO into oligonucleotides, i.e. by attaching the dye at the 5-position of thymidine (X_6). Thermal stability and fluorescence studies were carried out on BO-modified DNA probes. BO gave slightly weaker intercalation compared to the TO-modified DNA probes. However, fluorescence energy transfer from FAM to BO was found to be efficient in the FAM/BO-modified probes, while it was less efficient in FAM/TO-modified probes.

CHAPTER 8

Experimental

Chapter 8 – Experimental

8.1 General methods

All reagents were purchased from Aldrich, Fluka, Avocado, or Proligo and used without purification with the exception of the following solvents, which were purified by distillation: THF (over sodium wire and benzophenone), DCM, DIPEA, Et_3N and pyridine (over calcium hydride). Chemical transformations were carried out under an atmosphere of argon using oven-dried glassware. Column chromatography was carried out under pressure using Fisher scientific DAVISIL 60Å (35–70 micron) silica. The thin layer chromatography (TLC) was performed using Merck Kieselgel 60 F24 silica gel plates (0.22 mm thickness, aluminium backed) and the compounds were visualized by 254/365 nm UV irradiation and additionally stained with the following solutions:

Anisaldehyde (for alcohols, sugars, amines): *p*-anisaldehyde (11.5 mL), glacial acetic acid (4.75 mL), conc. sulfuric acid (15.65 mL) and 95% ethanol (422.5 mL).

Phosphomolybdic acid (for alcohols): phosphomolybdic/molybdophosphoric acid (10 g), 95% ethanol (200 mL).

Cerium sulfate (for oxidisable groups): ceric (II) sulfate hydrate (8 g), 15% sulphuric acid (100 mL).

Marys' Reagent (for carboxylic acids): 4,4′-bis-dimethylamino benzhydrol (0.4 g), acetone (100 mL).

^{1}H NMR spectra were measured at 300 MHz on a Bruker AC300 spectrometer or at 400 MHz on a Bruker DPX400 (AVIIIHD 400) spectrometer, or at 500 MHz on a Bruker AVIIIHD 500 spectrometer. The ^{13}C NMR spectra were measured at 101 MHz on a Bruker AC300 spectrometer or at 101 MHz on a Bruker DPX400 spectrometer. The ^{31}P

NMR spectra were recorded on a Bruker AC300 spectrometer at 300 MHz or at 162, 202 MHz on a Bruker AVIIIHD 400 spectrometer. All ^{1}H spectra were internally referenced to the appropriate residual undeuterated solvent signal.[203] ^{1}H and ^{13}C assignments were also aided by DEPT, COSY (^{1}H-^{1}H) and HMQC/HMBC (^{1}H-^{13}C) experiments.

Low-resolution mass spectra (LRMS) were recorded using electrospray ionisation (ESI^{+} or ESI^{-}) on a Fisons VG platform instrument or a Waters ZMD quadrupole mass spectrometer in HPLC grade acetonitrile or methanol. High-resolution mass spectra (HRMS) were recorded in HPLC grade acetonitrile or methanol using electrospray ionisation (EI) on a Bruker APEX III FT-ICR mass spectrometer.

8.2 Synthesis

8.2.1 Purification of tris(3-hydroxypropyltriazolylmethyl)amine (THPTA)[204] (2-1)

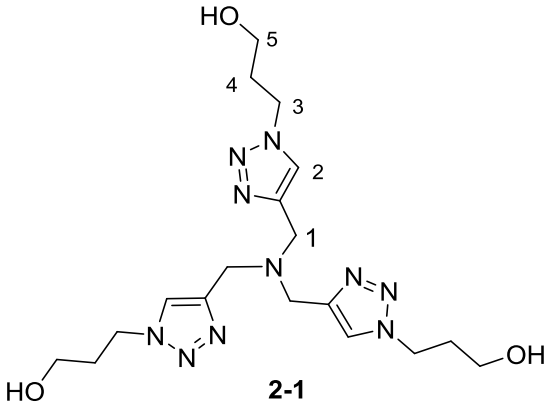

2-1

R_f: 0.30 (10% MeOH/DCM)

^{1}H NMR (300 MHz; DMSO-d_6): δ 8.03 (3 H, s, **H2**), 4.65 (3 H, t, J = 5.1 Hz, O**H**), 4.41 (6 H, t, J = 7.1 Hz, **H3**), 3.62 (6 H, br. s, **H1**), 3.40 (6 H, app. q, J = 5.9 Hz, **H5**), 1.96 (6 H, app. quin, J = 6.6 Hz, **H4**).

LRMS [ESI$^+$, MeOH] *m/z* (%): 457.2 ([M+Na]$^+$, 100%).

8.2.2 Synthesis of 5′-*O*-(4,4′-dimethoxytrityl)-3′-*O*-propargyl-5-methyl-deoxycytidine

8.2.2.1 Synthesis of 5′-*O*-(4,4′-dimethoxytrityl)-thymidine[154] (2-3)

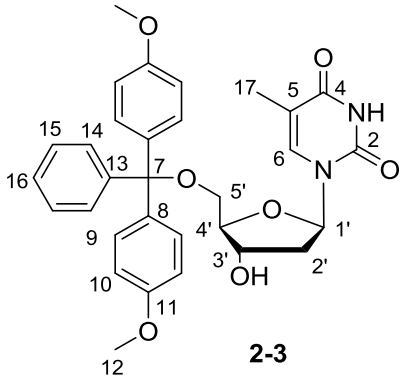

2-3

Thymidine **2-2** (1.74 g, 7.20 mmol, 1.0 eq.) was co-evaporated with anhydrous pyridine (10 mL) under high vacuum, and placed under vacuum for 30 min. It was then dissolved in anhydrous pyridine (10 mL) and added dropwise to a solution of DMTrCl (3.00 g, 8.85 mmol, 1.3 eq.) dissolved in anhydrous pyridine (8 mL). Molecular sieves (pore size 3 Å, 300 mg) were added to act as a desiccant. The reaction was stirred at room temperature for 16 h under an atmosphere of argon. The reaction mixture was diluted with DCM (20 mL). The organic layer was washed with H_2O (30 mL × 2) and saturated brine (30 mL × 2), dried over Na_2SO_4, filtered and concentrated under vacuum. The mixture was co-evaporated with toluene for removal of pyridine. The crude product was purified by

column chromatography (0–3% MeOH/DCM, 0.5% pyridine) to give the pure product **2-4** as yellow gum (1.84 g, 3.38 mmol, 47%).

R_f: 0.53 (5% MeOH/DCM, 0.5% pyridine)

^{1}H NMR (300 MHz, DMSO-d_6): δ 11.31 (1 H, s, **NH**), 7.50 (1 H, s, **H6**), 7.43–7.36 (2 H, m, **H14**), 7.34–7.20 (7 H, m, **H9**, **H15, H16**), 6.89 (4 H, d, *J* = 8.1 Hz, **H10**), 6.20 (1 H, app. t, *J* = 6.8 Hz, **H1′**), 5.31 (1 H, d, *J* = 4.8 Hz, **OH**), 4.35–4.27 (1 H, m, **H3′**), 3.88 (1 H, app. q, *J* = 3.3 Hz, **H4′**), 3.74 (6 H, s, **H12**), 3.26–3.13 (2 H, m, **H5′**), 2.25 (1 H, app. dt, *J* = 13.6, 6.8 Hz, **H2′a**), 2.19–2.09 (1 H, m, **H2′b**), 1.45 (3 H, s, **H17**).

LRMS [ESI$^+$, MeOH] *m/z* (%): 567.2 ([M+Na]$^+$, 100%).

8.2.2.2 Synthesis of 5′-*O*-(4,4′-dimethoxytrityl)-3′-*O*-propargyl-thymidine[154] (2-4)

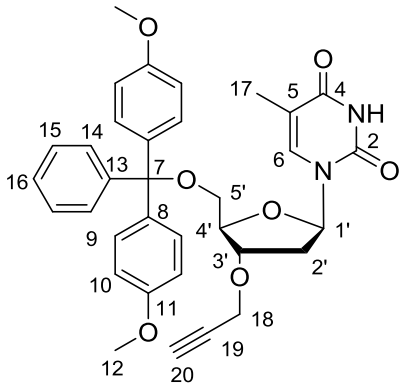

2-4

5′-*O*-(4,4′-Dimethoxytrityl)-thymidine **2-3** (11.6 g, 20.2 mmol, 1.0 eq.) was co-evaporated with anhydrous pyridine (10 mL × 3), and then THF (10 mL × 3) under high vacuum before drying overnight under vacuum. The compound was dissolved in THF (80 mL) and sodium hydride (60% dispersion in mineral oil, 2.02 g, 50.6 mmol, 2.5 eq.) was added at

0 °C. The reaction mixture was left to stir at room temperature for 1 h. Propargyl bromide (80% in toluene, 4.84 mL, 56.1 mmol, 2.8 eq.) was added at 0 °C and the reaction was left to stir at room temperature for 12 h. H_2O was added to quench the reaction and the solvent was removed under vacuum. The residue was dissolved in DCM (10 mL), washed with H_2O (20 mL × 2) and saturated aqueous KCl (20 mL × 2). The organic layer was separated, dried over Na_2SO_4, filtered, and the solvent was removed under vacuum. Upon purification by column chromatography (0–5% MeOH/DCM, 0.5% pyridine), the pure compound was isolated as a white foam (5.40 g, 9.28 mmol, 46%), an impure fraction was also isolated as yellow foam (5.32g, 9.14 mmol, 45%), which could be purified by another silica-gel column.

R_f: 0.43 (10% MeOH/DCM, 0.5% pyridine)

^{1}H NMR (300 MHz, DMSO-d_6): δ 11.34 (1 H, s, **NH**), 7.50 (1 H, s, **H6**), 7.43–7.20 (9 H, m, **H9, H14, H15, H16**), 6.91 (4 H, d, *J* = 8.8 Hz, **H10**), 6.13 (1 H, app. t, *J* = 7.0 Hz, **H1′**), 4.50–4.43 (1 H, m, **H3′**), 4.22 (2 H, d, *J* = 2.1 Hz, **H18**), 4.04 (1 H, app. q, *J* = 2.9 Hz, **H4′**), 3.74 (6 H, s, **H12**), 3.51 (1 H, t, *J* = 2.1 Hz, **H20**), 3.26 (2 H, dd, *J* = 10.5, 3.9 Hz, **H5′a**), 3.17 (2 H, dd, *J* = 10.5, 3.7 Hz, **H5′b**), 2.42–2.24 (2 H, m, **H2′**), 1.45 (3 H, s, **H17**).

LRMS [ESI$^+$, MeOH] *m/z* (%): 605.2 ([M+Na]$^+$, 58%).

8.2.2.3 Synthesis of 5′-*O*-(4,4′-dimethoxytrityl)-3′-*O*-propargyl-5-methyl-deoxycytidine[154] (2-5)

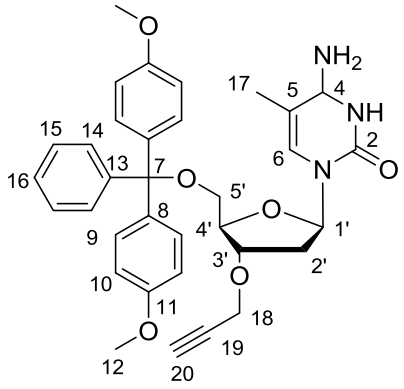

2-5

5′-*O*-(4,4′-Dimethoxytrityl)-3′-*O*-propargyl-thymidine **2-4** (5.40 g, 9.29 mmol, 1.0 eq.) was co-evaporated with anhydrous pyridine (10 mL × 3) then dissolved in pyridine (60 mL). *N*-Methylimidazole (9.61 mL, 120 mmol, 12.9 eq.) was added and the mixture was stirred for 15 min at 0 °C. Phosphorus oxychloride (3.24 mL, 35.3 mmol, 3.8 eq.) was then added dropwise (over 60 min) and the reaction mixture was left to stir at 0 °C for 30 min and at room temperature for a further 30 min. Phosphorus oxychloride (1.20 mL, 13.1 mmol, 1.4 eq.) was then added dropwise (over 20 min) and the reaction mixture was left to stir at 0 °C for 15 min and at room temperature for a further 15 min. Concentrated aqueous ammonia solution (60 mL) was added at 0 °C and the reaction was left to stir at room temperature for 19 h. The solvent was removed under vacuum and the residue was dissolved in DCM, washed with H_2O (20 mL × 2) and then washed with saturated aqueous KCl (20 mL × 2). The organic layer was separated, dried over Na_2SO_4, filtered, and the solvent was removed under vacuum. Purification was carried out by column chromatography (0–8% MeOH/DCM, 0.5% pyridine). The pure product **2-5** was isolated as yellow foam (2.65 g, 4.55 mmol, 49%).

R_f: 0.43 (10% MeOH/DCM, 0.5% pyridine)

^{1}H NMR (300 MHz, DMSO-d_6): δ 7.47 (1 H, s **H6**), 7.43–7.23 (9H, m, **H9, H14, H15, H16**), 6.91 (4 H, d, *J* = 8.8 Hz, **H10**), 6.16 (1 H, dd, *J* = 7.9, 5.9 Hz, **H1′**), 4.52–4.32 (1 H, m, **H3′**), 4.22 (2 H, br. s, **H18**), 4.03 (1 H, app. q, *J* = 3.0 Hz, **H4′**), 3.74 (6 H, s, **H12**), 3.51 (1 H, t, *J* = 2.2 Hz, **H20**), 3.25 (1 H, dd, *J* = 10.6, 3.7 Hz, **H5′a**), 3.17 (1 H, dd, *J* = 10.6, 3.3 Hz, **H5′b**), 2.32 (1 H, ddd, *J* = 13.6, 5.9, 2.3 Hz, **H2′a**), 2.16 (1 H, ddd, *J* = 13.6, 7.9, 6.2 Hz, **H2′b**), 1.49 (3 H, s, **H17**). Compound contains about 1 eq. residual pyridine.

LRMS [ESI$^+$, MeOH] *m/z* (%): 604.2 ([M+Na]$^+$, 100%).

8.2.2.4 Preparation of 5′-*O*-(4,4′-dimethoxytrityl)-3′-*O*-propargyl-5-methyl-deoxycytidine on the solid support[154] (2-6)

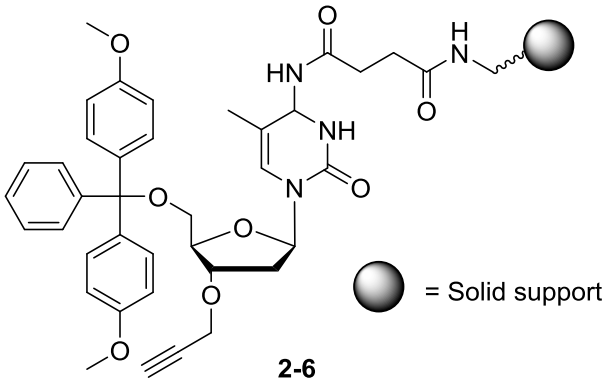

2-6

The solid support for oligonucleotide synthesis (GE Healthcare custom primer support™ amino, 1.50 g, 50.0 µmol of amine) was activated in 3% trichloroacetic acid (TCA) in DCM (15 mL) for 4 h in a stoppered glass vessel fitted with a sinter and tap. The solvents were removed by filtration and the support was washed with Et_3N:DIPEA (9:1), DCM and

Et_2O (5 mL × 3 of each), then dried under vacuum for 30 min. The support was soaked in anhydrous pyridine (5 mL) for 10 min. Succinic anhydride (600 mg, 6.00 mmol) and DMAP (120 mg, 0.96 mmol) were dissolved in anhydrous pyridine (10 mL) and added to the vessel, which was rotated for 20 h at room temperature. The solvent was removed by filtration and the support was washed with pyridine, DCM and Et_2O (5 mL × 3), dried and soaked in pyridine for 10 min. A mixture of diisopropylcarbodiimide (DIC, 368 μL, 2.36 mmol), hydroxybenzotriazole (HOBt, 368 mg, 2.73 mmol) and 5′-*O*-(4,4′-dimethoxytrityl)-3′-*O*-propargyl-5-methyl-deoxycytidine (130 mg, 0.22 mmol) were dissolved in pyridine (5 mL) and added to the solid support in the vessel, which was rotated for 20 h. Pentachlorophenol (180 mg, 0.69 mmol) was added and the reaction vessel was left to rotate for 1 h. The solvents were removed by filtration and the support was washed with pyridine, DCM and Et_2O. 10% Piperidine in DMF (5 mL) was added and rotated for 1 min and the solid support was then washed with DMF, DCM and Et_2O. Capping reagent (oligonucleotide synthesis grade, acetic anhydride/pyridine/THF and *N*-methyl imidazole in THF, 1:1, 15 mL) was added and the vessel was rotated for 1 h after which the support was washed with pyridine, DCM and Et_2O (5 mL × 3) then left to dry under vacuum overnight.

8.2.2.5 Calculation of the loading of 5′-*O*-(4,4′-dimethoxytrityl)-3′-*O*-propargyl-5-methyl-deoxycytidine on the solid support

The loading of 5′-*O*-(4,4′-dimethoxytrityl)-3′-*O*-propargyl-5-methyl-deoxycytidine on the support was determined by measuring DMT absorption at 504 nm, the DMT protecting group was cleaved by 3% TCA in DCM. 1.0 mg of support was soaked in 3% TCA in DCM (1 mL). Two same experiments were carried out to prepare 5′-*O*-(4,4′-

dimethoxytrityl)-3′-*O*-propargyl-5-methyl-deoxycytidine on solid support, the loading of the two different batches of resin were calculated. The absorbance of the solution at 504 nm (Abs) was 0.37 and 0.35 for pure solvent (0.2 mL) respectively. Loading was 22.4 µmol g^{-1} and 23.7 µmol g^{-1}.

8.2.3 Synthesis of 5′-*O*-(4,4′-dimethoxytrityl)-*N(4)*-(9-fluorenylmethoxycarbonyl)-2′-deoxycytidine-3′-*O*-(2-cyanoethyl-*N*,*N*-diisopropyl)phosphoramidite[205] (2-8)

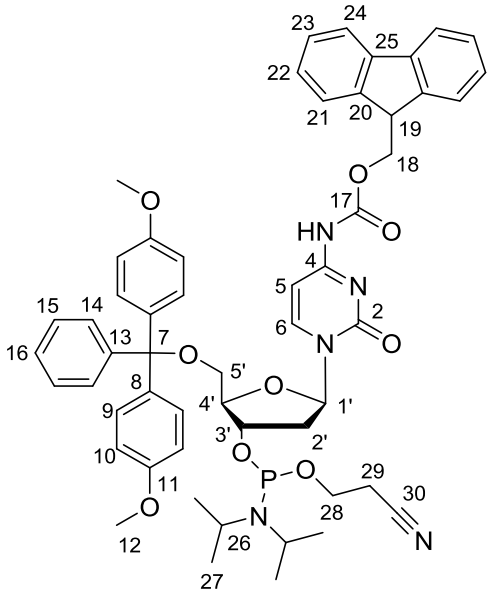

2-8

5′-*O*-(4,4′-Dimethoxytrityl)-*N*(4)-Fmoc-2′-deoxycytidine **2-7** (1.00 g, 1.33 mmol, 1.0 eq.) was co-evaporated with anhydrous DCM (5 mL × 3) under high vacuum, and then dissolved in anhydrous DCM (10 mL) under an atmosphere of argon. Anhydrous DIPEA (580 µL, 3.33 mmol, 2.5 eq.) was added, followed by the dropwise addition of 2-cyanoethyl *N*,*N*-diisopropylchlorophosphoramidite (360 µL, 1.60 mmol, 1.2 eq.). The reaction mixture was stirred at room temperature for 1.5 h and transferred under argon into

a separating funnel containing degassed DCM (15 mL). The mixture was washed with degassed saturated aqueous KCl (20 mL) and the organic layer was separated, dried over anhydrous Na_2SO_4, filtered, and concentrated under vacuum. The crude product was purified by column chromatography under argon pressure (40% hexane/EtOAc, 0.5% pyridine). The product **2-8** was isolated as a white solid (1.00 g, 1.05 mmol, 79%).

R_f: 0.42 (10% MeOH/DCM, 0.5% pyridine)

^{1}H NMR (400 MHz, CD_3CN-d_3): δ 8.81 (1 H, s, N**H**), 8.19 (0.5 H, d, *J* = 7.5 Hz, **H6**), 8.14 (0.5 H, d, *J* = 7.5 Hz, **H6**), 7.85 (2 H, d, *J* = 7.3 Hz, **H24**), 7.75 (2 H, dd, *J* = 7.5, 2.0 Hz, **H21**), 7.50–7.38 (4 H, m, **H23, H14**), 7.37–7.22 (9 H, m, **H22**, **H9**, **H15**, **H16**), 6.91–6.83 (5 H, m, **H5**, **H10**), 6.24–6.05 (1 H, m, **H1′**), 4.66–4.52 (1 H, m, **H3′**), 4.48 (2 H, d, *J* = 7.0 Hz, **H18**), 4.29 (1 H, t, *J* = 7.0 Hz, **H19**), 4.20–4.08 (1 H, m, **H4′**), 3.76 (6H, s, **H12**), 3.73–3.51 (4 H, m, **H26, H28**), 3.45–3.32 (2H, m, **H5′**), 2.63 (1 H, t, *J* = 5.9 Hz, **H29a**), 2.60–2.50 (2 H, m, containing t, *J* = 5.9 Hz, **H29b**, **H2′a**), 2.37–2.25 (1 H, m, **H2′b**), 1.21–1.12 (9 H, m, **H27**), 1.07 (3 H, d, *J* = 6.6 Hz, **H27**).

^{31}P NMR (300 MHz, CD_3CN-d_3): δ 149.45, 149.40.

LRMS [ESI^+, MeOH] *m/z* (%): 952.5 ($[M+H]^+$, 100%).

8.2.4 Synthesis of 6-azidohexanoic acid NHS ester

8.2.4.1 Synthesis of 6-azidohexanoic acid[206] (3-1)

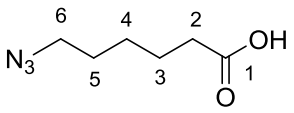

3-1

6-Bromohexanoic acid (1.00 g, 5.10 mmol, 1.0 eq.) was dissolved in DMF (3 mL) and then sodium azide (670 mg, 12.2 mmol, 2.4 eq.) was added. The mixture was stirred at 85 °C for 3 h. The crude reaction mixture was cooled to room temperature, diluted with DCM (20 mL), and washed with H_2O (20 mL × 2) and brine (20 mL × 2). The organic layer was separated, dried over anhydrous Na_2SO_4, filtered, and the solvent was removed under vacuum to give **3-1** (511 mg, 3.25 mmol, 64%) as an oil, which was used without further purification.

R_f : 0.36 (15% EtOAc/DCM)

^{1}H NMR (400 MHz, $CDCl_3$-*d*): δ 3.29 (2 H, t, *J* = 6.9 Hz, **H6**), 2.39 (2 H, t, *J* = 7.5 Hz, **H2**), 1.84–1.54 (4 H, m, **H3, H5**), 1.51–1.36 (2 H, m, **H4**).

^{13}C NMR (101 MHz, $CDCl_3$-*d*): δ 179.6 (**C1**), 51.2 (**C6**), 33.8 (**C2**), 28.6 (**C5**), 26.2 (**C4**), 24.2 (**C3**).

LRMS [ESI$^-$, MeOH] *m/z* (%): 156.1 ([M-H]$^-$, 100%).

8.2.4.2 Synthesis of 6-azidohexanoic acid NHS ester[206] (3-2)

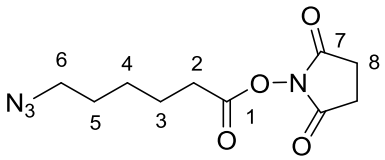

3-2

6-Azidohexanoic acid (511 mg, 3.25 mmol, 1.0 eq.) and N-hydroxysuccinimide (374 mg, 3.25 mmol, 1.0 eq.) were dissolved in $CHCl_3$/DMF 9:1 (1 mL), and then *N*-(3-dimethylaminopropyl)-*N′*-ethylcarbodiimide hydrochloride (EDC, 623 mg, 3.25 mmol, 1.0 eq.) was added, and the mixture stirred at room temperature overnight. Solvents were removed under vacuum. The residue was purified by column chromatography (0–10% EtOAc/DCM) to give the product **3-2** (308 mg, 1.21 mmol, 37%).

R_f: 0.74 (30% EtOAc/DCM)

^{1}H NMR (400 MHz, $CDCl_3$-*d*): δ 3.31 (2 H, t, *J* = 6.8 Hz, **H6**), 2.85 (4 H, s, **H8**), 2.64 (2 H, t, *J* = 7.4 Hz, **H2**), 1.80 (2 H, app. quin, *J* = 7.6 Hz, **H5**), 1.58 (2 H, app. quin, *J* = 7.2 Hz, **H3**), 1.56–1.46 (2 H, m, **H4**).

^{13}C NMR (101 MHz, $CDCl_3$-*d*): δ 169.2 (**C7**), 169.2 (**C1**), 51.1 (**C6**), 30.8 (**C2**), 28.4 (**C5**), 25.6 (**C4**), 25.6 (**C8**), 24.2 (**C3**).

LRMS [ESI$^+$, MeOH] *m/z* (%): 277.1 ([M+Na]$^+$, 100%).

8.2.5 Synthesis of thiazole orange (TO) dyes

8.2.5.1 Synthesis of *N*-(3-hydroxypropyl)-2-methylbenzothiazolium iodide[115,207] (5-2)

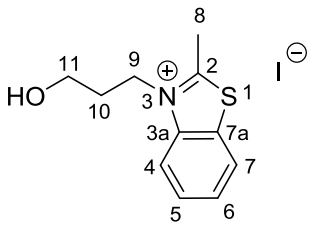

5-2

2-Methylbenzothiazole **5-1** (9.63 g, 65.5 mmol, 2.0 eq.) and 3-iodo-1-propanol (6.00 g, 32.3 mmol, 1.0 eq.) were dissolved in acetonitrile (18 mL) under an atmosphere of argon. The reaction mixture was stirred at 110 °C under reflux for 44 h, then cooled to room temperature. The solvent was removed under vacuum. The precipitate was collected and washed with cold Et_2O (30 mL × 3), dried under vacuum to give the crude product **5-2** as a yellow solid (9.34 g, 27.9 mmol, 86%).

R_f: 0.29 (10% MeOH/DCM)

^{1}H NMR (400 MHz, DMSO-d_6): δ 8.47 (1 H, dd, *J* = 8.1, 1.0 Hz, **H7**), 8.31 (1 H, d, *J* = 8.4 Hz, **H4**), 7.89 (1 H, ddd, *J* = 8.4, 7.1, 1.0 Hz, **H5**), 7.80 (1 H, ddd, *J* = 8.1, 7.1, 1.0 Hz **H6**), 4.78 (2 H, t, *J* = 7.3 Hz, **H9**), 4.70 (1 H, br. s., **OH**), 3.52 (2 H, t, *J* = 5.7 Hz, **H11**), 3.23 (3 H, s, **H8**), 2.03 (2 H, app. quin, *J* = 6.4 Hz, **H10**).

^{13}C NMR (101 MHz, DMSO-d_6): δ 177.8 (**C2**), 141.4 (**C3a**), 129.8 (**C5**), 129.5 (**C7a**), 128.5 (**C6**), 125.2 (**C7**), 117.3 (**C4**), 57.9 (**C11**), 47.4 (**C9**), 31.0 (**C10**), 17.5 (**C8**).

LRMS [ESI$^+$, MeOH] *m/z* (%): 208.1 ([M-I]$^+$, 100%).

8.2.5.2 Synthesis of *N*-methylquinolinium iodide[207] (5-4)

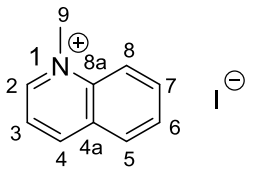

5-4

Quinoline **5-3** (4.57 mL, 38.7 mmol, 1.0 eq.) and iodomethane (2.65 mL, 42.6 mmol, 1.1 eq.) were dissolved in acetonitrile (15 mL) under an atmosphere of an atmosphere of argon. The reaction mixture was stirred at 38 °C for 21 h, then cooled to room temperature. The solvent was removed under vacuum. The precipitate was collected and washed with cold Et_2O (20 mL × 3), and dried under vacuum to give the crude product **5-4** as a yellow solid (10.3 g, 38.0 mmol, 98%).

R_f: 0.20 (10% MeOH/DCM)

^{1}H NMR (400 MHz, DMSO-d_6): δ 9.53 (1 H, d, *J* = 5.6 Hz, **H2**), 9.30 (1 H, d, *J* = 8.4 Hz, **H4**), 8.52 (1 H, d, *J* = 8.9 Hz, **H8**), 8.49 (1 H, dd, *J* = 8.3, 1.2 Hz, **H5**), 8.30 (1 H, ddd, *J* = 8.9, 7.2, 1.2 Hz, **H7**), 8.19 (1 H, dd, *J* = 8.4, 5.6 Hz, **H3**), 8.07 (1 H, ddd, *J* = 8.3, 7.2, 1.2 Hz, **H6**), 4.65 (3 H, s, **H9**).

^{13}C NMR (101 MHz, DMSO-d_6): δ 150.7 (**C2**), 147.5 (**C4**), 138.8 (**C8a**), 136.0 (**C7**), 130.8 (**C5**), 130.4 (**C6**), 129.7 (**C4a**), 123.5 (**C3**), 120.2 (**C8**), 45.9 (**C9**).

LRMS [ESI$^+$, MeOH] *m/z* (%): 144.1 ([M-I]$^+$, 100%).

8.2.5.3 Synthesis of *N*-(3-hydroxypropyl)-2-[(1,4-dihydro-1-methylquinolin-4-ylidene)methyl]benzothiazolium iodide[115,208] (5-5)

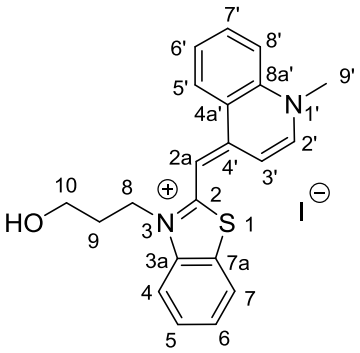

5-5

N-(3-Hydroxypropyl)-2-methylbenzothiazolium iodide **5-2** (1.69 g, 5.00 mmol, 1.0 eq.) and *N*-methylquinolinium iodide **5-4** (1.50 g, 5.50 mmol, 1.1 eq) were dissolved in DCM/MeOH (1:1, 20 mL) under an atmosphere of argon. Anhydrous Et_3N (1.70 mL, 12.5 mmol, 2.5 eq.) was added, giving in an immediate deep red colour. The reaction mixture was stirred at room temperature for 16 h. The solvent was removed under vacuum and the product was collected on a sintered funnel and washed with cold Et_2O (25 mL × 3) and dried under vacuum to give the product **5-5** as a red solid which was used without further purification (293 mg, 0.62 mmol, 12%).

R_f: 0.49 (10% MeOH/DCM)

^{1}H NMR (400 MHz, DMSO-d_6): δ 8.72 (1 H, d, *J* = 8.4 Hz, **H5′**), 8.62 (1 H, d, *J* = 7.2 Hz, **H2′**), 8.10–7.93 (3 H, m, **H8′, H7, H7′**), 7.80–7.70 (2 H, m, **H6′, H4**), 7.59 (1 H, ddd, *J* = 8.2, 7.6, 1.0 Hz, **H5**), 7.40 (1 H, app. t, *J* = 7.6 Hz, **H6**), 7.34 (1 H, d, *J* = 7.2 Hz, **H3′**), 7.02 (1 H, s, **H2a**), 5.06 (1 H, br. s., **OH**), 4.61 (2 H, t, *J* = 6.9 Hz, **H8**), 4.16 (3 H, s, **H9′**), 3.58 (2 H, t, *J* = 5.6 Hz, **H10**), 1.99 (2 H, app. quin, *J* = 6.2 Hz, **H9**). Compound contains about 0.2 eq. starting material *N*-methylquinolinium iodide **(5-4).**

^{13}C NMR (101 MHz, DMSO-d_6): δ 159.8 (**C2**), 149.1 (**C4′**), 145.5 (**C2′**), 140.5 (**C3a**), 138.5 (**C8a′**), 133.5 (**C7′**), 128.8 (**C5**), 127.5 (**C6′**), 125.8 (**C5′**), 124.9 (**C6**), 124.5 (**C4a′**), 124.4 (**C7a**), 123.3 (**C7**), 119.0 (**C8′**), 113.0 (**C4**), 108.3 (**C3′**), 88.2 (**C2a**), 57.8 (**C10**), 43.5 (**C8**), 42.9 (**C9′**), 30.6 (**C9**).

LRMS [ESI$^+$, MeOH] *m/z* (%): 349.1 ([M-I]$^+$, 100%).

8.2.5.4 Synthesis of *N*-(3-iodopropyl)-2-methylbenzothiazolium iodide[209] (5-6)

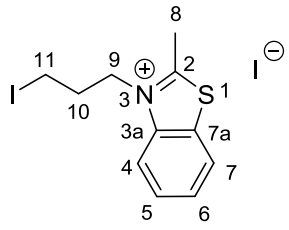

5-6

2-Methylbenzothiazole **5-1** (8.31 mL, 65.3 mmol, 1.0 eq.) and 1,3-diiodopropane (15.0 mL, 131 mmol, 2.0 eq.) were dissolved in acetonitrile (40 mL) under an atmosphere of argon. The reaction mixture was stirred at 105 °C under reflux for 48 h, then cooled to room temperature. The solvent was removed under vacuum. The precipitate was collected and washed with cold Et_2O (30 mL × 3), dried under vacuum to give the crude product **5-6** as a yellow solid (18.6 g, 41.9 mmol, 64%).

R_f: 0.29 (10% MeOH/DCM)

^{1}H NMR (400 MHz, DMSO-d_6): δ 8.47 (1 H, d, *J* = 8.1 Hz, **H7**), 8.35 (1 H, d, *J* = 8.5 Hz, **H4**), 7.95–7.86 (1 H, m, **H5**), 7.85–7.76 (1 H, m, **H6**), 4.75 (2 H, t, *J* = 7.3 Hz, **H9**), 3.43 (2 H, t, *J* = 5.6 Hz, **H11**), 3.23 (3 H, s, **H8**), 2.45–2.30 (2 H, m, **H10**).

^{13}C NMR (101 MHz, DMSO-d_6): δ 178.2 (**C2**), 141.4 (**C3a**), 129.9 (**C5**), 129.6 (**C7a**), 128.4 (**C6**), 125.2 (**C7**), 117.1 (**C4**), 50.3 (**C9**), 32.0 (**C10**), 17.1 (**C8**), 2.7 (**C11**).

LRMS [ESI$^+$, MeOH] *m/z* (%): 318.0 ([M-I]$^+$, 100%).

8.2.5.5 Synthesis of *N*-(8-iodooctyl)-2-methylbenzothiazolium iodide[103] (5-7)

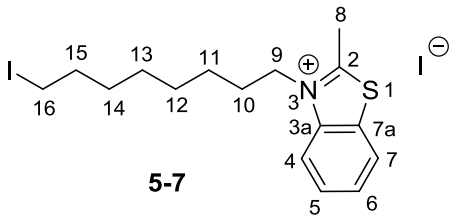

5-7

2-Methylbenzothiazole **5-1** (5.22 mL, 41.0 mmol, 1.0 eq.) and 1,8-diiodooctane (8.15 mL, 41.0 mmol, 1.0 eq.) were dissolved in acetonitrile (15 mL) under an atmosphere of argon. The reaction mixture was stirred at 150 °C under reflux for 27 h, then cooled to room temperature. The solvent was removed under vacuum. The precipitate was collected and washed with cold Et_2O (30 mL × 3), dried under vacuum to give the crude product **5-7** as a yellow solid (14.2 g, 27.5 mmol, 67%).

^{1}H NMR (400 MHz, DMSO-d_6): δ 8.48–8.44 (1 H, m, **H7**), 8.34 (1 H, d, *J* = 8.5 Hz, **H4**), 7.92–7.86 (1 H, m, **H5**), 7.80 (1 H, t, *J* = 7.6 Hz, **H6**), 4.71 (2 H, t, *J* = 7.8 Hz, **H9**), 3.26 (2 H, t, *J* = 6.9 Hz, **H16**), 3.22 (3 H, s, **H8**), 1.84 (2 H, app. quin, *J* = 7.5 Hz, **H10**), 1.73 (2 H, app. quin, *J* = 6.9 Hz, **H15**), 1.44 (2 H, app. quin, *J* = 7.3 Hz, **H11**), 1.38–1.23 (6 H, m, **H12, H13, H14**).

^{13}C NMR (101 MHz, DMSO-d_6): δ 177.5 (**C2**), 141.3 (**C3a**), 129.9 (**C5**), 129.6 (**C7a**), 128.6 (**C6**), 125.2 (**C7**), 117.4 (**C4**), 49.6 (**C9**), 33.2 (**C15**), 30.2, 28.9, 28.3, 28.1 (**C14**, **C13**, **C12, C10**), 26.3 (**C11**), 17.4 (**C8**), 9.7 (**C16**).

R_f: 0.35 (10% MeOH/DCM)

LRMS [ESI$^+$, MeOH] *m/z* (%): 388.0 ([M-I]$^+$, 100%).

8.2.5.6 Synthesis of *N*-(3-azidopropyl)-2-methylbenzothiazolium iodide (5-8)

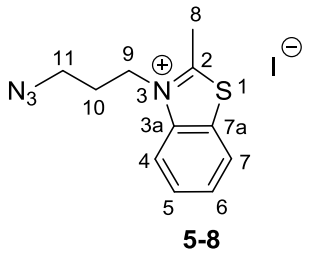

5-8

N-(3-Iodopropyl)-2-methylbenzothiazole iodide **5-6** (3.18 g, 7.15 mmol, 1.0 eq.) was suspended in acetonitrile (120 mL), a solution of sodium azide (580 mg, 8.92 mmol, 1.25 eq.) dissolved in H_2O (8 mL) was added dropwise. The reaction mixture was stirred at room temperature for 19 h. The solvent was removed under vacuum. The crude mixture was purified by column chromatography (1–10% MeOH/DCM) to give the compound **5-8** as a yellow-green foam (2.18 g, 6.06 mmol, 55%).

^{1}H NMR (400 MHz, DMSO-d_6): δ 8.49 (1 H, d, *J* = 8.5 Hz, **H7**), 8.36 (1 H, d, *J* = 8.4 Hz, **H4**), 7.93–7.87 (1 H, m, **H5**), 7.84–7.78 (1 H, m, **H6**), 4.78 (2 H, t, *J* = 7.6 Hz, **H9**), 3.60 (2 H, t, *J* = 6.7 Hz, **H11**), 3.24(3 H, s, **H8**), 2.14 (2 H, app. quin, *J* = 7.1 Hz, **H10**).

^{13}C NMR (101 MHz, DMSO-d_6): δ 178.1 (**C2**), 141.3 (**C3a**), 130.0 (**C5**), 129.6 (**C7a**), 128.5 (**C6**), 125.2 (**C7**), 117.2 (**C4**), 48.2 (**C11**), 47.3 (**C9**), 27.4 (**C10**), 17.6 (**C8**).

LRMS [ESI$^+$, MeOH] *m/z* (%): 233.1 ([M-I]$^+$, 100%).

8.2.5.7 Synthesis of *N*-(8-azidooctyl)-2-methylbenzothiazolium iodide (5-9)

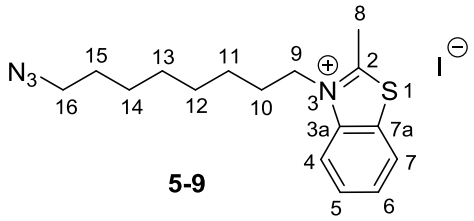

5-9

N-(8-Iodooctyl)-2-methylbenzothiazolium iodide **5-7** (7.00 g, 13.6 mmol, 1.0 eq.) was suspended in acetonitrile (300 mL), a solution of sodium azide (1.33 g, 20.4 mmol, 1.5 eq.) dissolved in H_2O (12 mL) was added dropwise. The reaction mixture was stirred at room temperature for 19 h. The solvent was removed under vacuum. The crude mixture was purified by column chromatography (1–10% MeOH/DCM) to give the compound **5-9** as a yellow-green foam (3.17 g, 7.37 mmol, 54%).

^{1}H NMR (400 MHz, DMSO-d_6): δ 8.45 (1 H, d, *J* = 8.1 Hz, **H7**), 8.34 (1 H, d, *J* = 8.4 Hz, **H4**), 7.89 (1 H, t, *J* = 7.5 Hz, **H5**), 7.80 (1 H, t, *J* = 7.6 Hz, **H6**), 4.71 (2 H, t, *J* = 7.8 Hz, **H9**), 3.31 (2 H, t, *J* = 6.9 Hz, **H16**), 3.22 (3 H, s, **H8**), 1.84 (2 H, app. quin, *J* = 7.4 Hz, **H10**), 1.52 (2 H, app. quin, *J* = 6.9 Hz, **H15**), 1.47–1.38 (2 H, m, **H11**), 1.37–1.28 (6 H, m, **H12, H13, H14**).

^{13}C NMR (101 MHz, DMSO-d_6): δ 177.5 (**C2**), 141.3 (**C3a**), 129.9 (**C5**), 129.6 (**C7a**), 128.8 (**C6**), 125.2 (**C7**), 117.3 (**C4**), 51.1 (**C16**), 49.7 (**C9**), 28.9, 28.6 (**C13, C14**), 28.6 (**C15**), 28.2 (**C10**), 26.5 (**C12**), 26.3 (**C11**), 16.8 (**C8**).

LRMS [ESI$^+$, MeOH] *m/z* (%): 303.2 ([M-I]$^+$, 100%).

8.2.5.8 Synthesis of *N*-(3-azidopropyl)-2-[(1,4-dihydro-1-methylquinolin-4-ylidene) methyl]benzothiazolium iodide[118] (5-10)

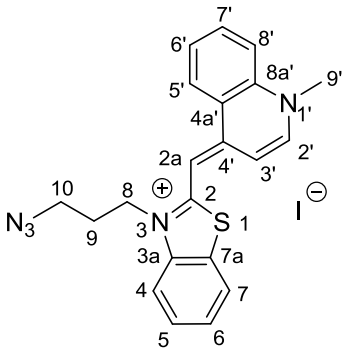

5-10

N-(3-Azidopropyl)-2-methylbenzothiazolium iodide **5-8** (3.03 g, 8.40 mmol, 1.0 eq.) and *N*-methylquinolinium iodide **5-4** (2.74 g, 10.1 mmol, 1.2 eq.) were dissolved in DCM/MeOH (1:1, 50 mL) under an atmosphere of argon. Anhydrous Et_3N (2.93 mL, 21.1 mmol, 2.5 eq.) was added, giving in an immediate deep red colour. The reaction mixture was stirred at room temperature for 16 h. The solvent was removed under vacuum and the product **5-10** was collected and washed with cold Et_2O (50 mL × 3) and dried under vacuum. The crude mixture was purified by column chromatography (1–10% MeOH/DCM) to give the compound **5-10** as a red solid (1.20 g, 2.39 mmol, 29%).

R_f: 0.29 (EtOAc/MeOH/conc. aq. NH_3 5:1:1)

^{1}H NMR (400 MHz, DMSO-d_6): δ 8.77 (1 H, d, *J* = 8.4 Hz, **H5′**), 8.65 (1 H, d, *J* = 7.2 Hz, **H2′**), 8.20–7.91 (3 H, m, **H8′, H7, H7′**), 7.81–7.77 (2 H, m, **H6′**, **H4**), 7.65–7.59 (1 H, m, **H5**), 7.42 (1 H, t, *J* = 7.6 Hz, **H6**), 7.41 (1 H, d, *J* = 7.2 Hz, **H3′**), 6.95 (1 H, s, **H2a**), 4.66 (2 H, t, *J* = 7.2 Hz, **H8**), 4.19 (3 H, s, **H9′**), 3.60 (2 H, t, *J* = 6.4 Hz, **H10**), 2.07 (2 H, app. quin, *J* = 6.8 Hz, **H9**).

^{13}C NMR (101 MHz, DMSO-d_6): δ 159.8 (**C2**), 149.3 (**C4′**), 145.7 (**C2′**), 140.4 (**C3a**), 138.5 (**C8a′**), 133.7 (**C7′**), 128.7 (**C5**), 127.6 (**C6′**), 125.8 (**C5′**), 125.0 (**C6**), 124.6 (**C4a′**), 124.4 (**C7a**), 123.4 (**C7**), 118.9 (**C8′**), 113.2 (**C4**), 108.7 (**C3′**), 87.5 (**C2a**), 48.5 (**C10**), 43.6 (**C8**), 42.9 (**C9′**), 26.6 (**C9**).

LRMS [ESI^{+}, MeOH] *m/z* (%): 374.1 ([M-I]$^{+}$, 100%).

8.2.5.9 Synthesis of *N*-(8-azidooctyl)-2-[(1,4-dihydro-1-methylquinolin-4-ylidene) methyl]benzothiazolium iodide (5-11)

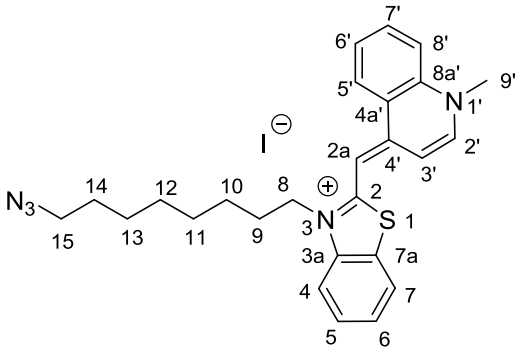

5-11

N-(8-Azidooctyl)-2-methylbenzothiazolium iodide **5-9** (3.17 g, 7.37 mmol, 1.0 eq.) and *N*-methylquinolinium iodide **5-4** (2.60 g, 9.58 mmol, 1.3 eq.) were dissolved in DCM/MeOH (1:1, 40 mL) under an atmosphere of argon. Anhydrous Et_3N (2.57 mL,

18.4 mmol, 2.5 eq.) was added, giving in an immediate deep red colour. The reaction mixture was stirred at room temperature for 16 h. The solvent was removed under vacuum and the product **5-11** was collected and washed with cold Et_2O (50 mL × 3) and dried under vacuum. The crude mixture was purified by column chromatography (1–10% MeOH/DCM) to give the compound **5-11** as a red solid (1.06 mg, 1.86 mmol, 25%).

R_f: 0.20 (10% MeOH/DCM)

^{1}H NMR (400 MHz, DMSO-d_6): δ 8.74 (1 H, d, *J* = 8.4 Hz, **H5′**), 8.62 (1 H, d, *J* = 7.2 Hz, **H2′**), 8.09–7.99 (3 H, m, **H8′, H7, H7′**), 7.82–7.75 (2 H, m, **H6′, H4**), 7.64–7.57 (1 H, m, **H5**), 7.44–7.38 (2 H, m, **H6, H3′**), 6.94 (1 H, s, **H2a**), 4.63 (2 H, t, *J* = 7.1 Hz, **H8**), 4.17 (3 H, s, **H9′**), 3.25 (2 H, t, *J* = 6.7 Hz, **H15**), 1.79 (2 H, app. quin., *J* = 7.4 Hz, **H9**), 1.53–1.40 (4 H, m, **H10, H14**), 1.39–1.31 (2 H, m, **H13**), 1.29–1.21 (4 H, m, **H11, H12**).

^{13}C NMR (101 MHz, DMSO-d_6): δ 159.1 (**C2**), 149.2 (**C4′**), 145.6 (**C2′**), 140.4 (**C3a**), 138.4 (**C8a′**), 133.8 (**C7′**), 128.8 (**C5**), 127.8 (**C6′**), 125.7 (**C5′**), 124.8 (**C6**), 124.5 (**C4a′**), 124.4 (**C7a**), 123.5 (**C7**), 119.0 (**C8′**), 113.5 (**C4**), 108.8 (**C3′**), 88.5 (**C2a**), 51.0 (**C15**), 46.1 (**C8**), 42.5 (**C9′**), 29.1, 28.9 , 28.6 (**C12**, **C13**, **C14**), 27.4 (**C9**), 26.5, 26.4 (**C11**, **C10**).

LRMS [ESI$^+$, MeOH] *m/z* (%): 444.2 ([M-I]$^+$, 100%).

HRMS [ESI$^+$, MeOH] calc. for $C_{26}H_{30}N_5S$, [M-I]$^+$, 444.2216, found 444.2209.

8.2.6 Synthesis of TO-modified nucleosides and phosphoramidites

8.2.6.1 Synthesis of 5-iodo-5′-*O*-(4,4′-dimethoxytrityl)-2′-deoxyuridine[210] (5-13)

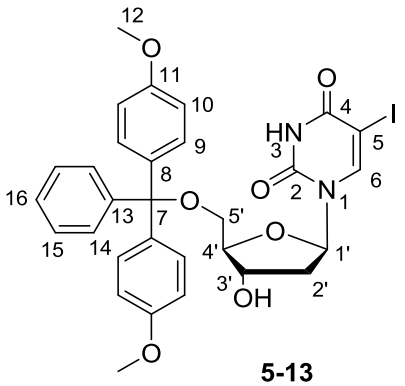

5-13

5-Iodo-2′-deoxyuridine **5-12** (6.05 g, 17.1 mmol, 1.0 eq.) was co-evaporated with anhydrous pyridine (10 mL × 3) and dissolved in anhydrous pyridine (20 mL). To this was added dropwise a solution of DMTrCl (6.93 g, 20.5 mmol, 1.2 eq.) in anhydrous pyridine (10 mL) over a period of 5 min and the reaction was stirred at room temperature for 1 h. The reaction was quenched by the addition of MeOH (30 mL) and then stirred for 5 min. The reaction volume was reduced under vacuum, diluted with DCM (30 mL) and washed with distilled H_2O (30 mL × 2) and saturated $NaHCO_3$ solution (30 mL × 2). The organic layers were combined, dried over anhydrous Na_2SO_4, filtered, and the solvent was removed under vacuum. Following purification by column chromatography (0–4% MeOH/DCM, 5% pyridine) the title compound **5-13** was afforded as a white foam (8.35 g, 12.7 mmol, 82%).

R_f: 0.44 (10% MeOH/DCM, 0.5% pyridine)

^{1}H NMR (400 MHz, DMSO-d_6): δ 8.03 (1 H, s, **H6**), 7.41 (2 H, d, *J* = 4.3 Hz, **H14**), 7.36–7.20 (6 H, m, **H9, H15**), 7.23 (1 H, t, *J* = 7.2 Hz, **H16**), 6.91 (4 H, d, *J* = 8.9 Hz, **H10**),

6.12 (1 H, t, *J* = 6.9 Hz, **H1′**), 4.22 (1 H, dt, *J* = 6.4, 3.2 Hz, **H3′**), 3.94–3.89 (1 H, m, **H4′**), 3.75 (6 H, s, **H12**), 3.21 (1 H, dd, *J* = 10.7, 4.9 Hz, **H5′a**), 3.17 (1 H, dd, *J* = 10.7, 3.1 Hz, **H5′b**), 2.24 (1 H, ddd, *J* = 13.7, 6.9, 6.4 Hz, **H2′a**), 2.22–2.15 (1 H, m, **H2′b**).

^{13}C NMR (101 MHz, DMSO-d_6): δ 161.1 (**C2**), 158.6 (**C4**), 150.6 (**C^{Ar}**), 145.3 (**C^{Ar}**), 144.7 (**C6**), 135.9 (**C^{Ar}**), 130.2 (**C9**), 128.5 (**CH^{Ar}**), 128.1 (**CH^{Ar}**), 127.2 (**C16**), 113.8 (**C10**), 86.3 (**C7**), 86.3 (**C4′**), 85.3 (**C1′**), 71.1 (**C3′**), 70.4 (**C5**), 64.20 (**C5′**), 55.0 (**C12**), 40.4 (**C2′**).

LRMS [ESI$^+$, MeOH] *m/z* (%): 678.8 ([M+Na]$^+$, 100%).

8.2.6.2 Synthesis of 5′-*O*-(4,4′-dimethoxytrityl)-5-[(*N*,*N*-dipropyn-2-yl)-3-aminopropyn-1-yl)]-2′-deoxyuridine[211] (5-14)

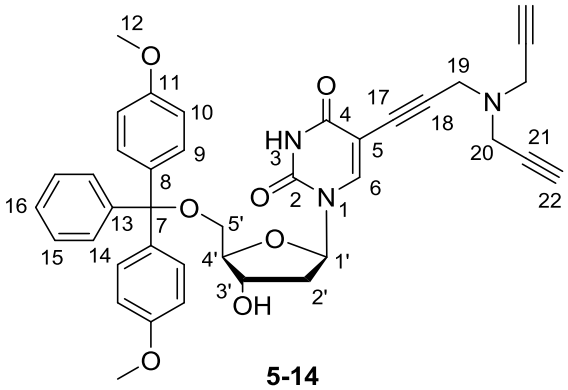

5-14

5-Iodo-5′-*O*-(4,4′-dimethoxytrityl)-2′-deoxyuridine **5-13** (5.25 g, 8.14 mmol, 1.0 eq.) was co-evaporated with anhydrous DMF (4 mL × 3) and dried for 2 h under vacuum. The compound **5-13** and copper(I) iodide (0.31 g, 1.63 mmol, 0.2 eq.) were dissolved in anhydrous DMF/Et_3N (1:1, 40 mL), followed by the addition of tripropargylamine (4.61 mL, 32.6 mmol, 4.0 eq.). The reaction was stirred under an atmosphere of argon for

10 min at room temperature, then tetrakis(triphenylphosphine)palladium(0) (0.94 g, 0.81 mmol, 0.1 eq.) was added. The reaction mixture was stirred at room temperature for 14 h. After the solvent was removed under vacuum, DCM was added and washed with distilled H_2O (50 mL × 2) and brine (50 mL × 2). The organic layers were combined, dried over anhydrous Na_2SO_4, filtered, and the solvent was concentrated under vacuum. Following purification by column chromatography (20–60% EtOAc/toluene, 0.5% pyridine) the title compound **5-14** was afforded as a colourless foam (3.40 g, 5.15 mmol, 63%).

R_f: 0.18 (50% EtOAc/toluene, 0.5% pyridine)

^{1}H NMR (400 MHz, DMSO-d_6): δ 11.70 (1 H, s, **NH**), 7.93 (1 H, s, **H6**), 7.41 (2 H, d, *J* = 7.6 Hz, **H14**), 7.34–7.20 (7 H, m, **H9**, **H15**, **H16**), 6.88 (4 H, d, *J* = 8.2 Hz, **H10**), 6.12 (1 H, t, *J* = 6.6 Hz, **H1′**), 5.35 (1 H, d, *J* = 4.3 Hz, **OH**), 4.32–4.25 (1 H, m, **H3′**), 3.95–3.91 (1 H, m, **H4′**), 3.73 (6 H, s, **H12**), 3.36 (2 H, s, **H19**), 3.32 (4 H, d, *J* = 2.1 Hz, **H20**), 3.28–3.24 (1 H, m, **H5a′**), 3.22 (2 H, t, *J* = 2.1 Hz, **H22**), 3.10 (1 H, dd, *J* = 10.1, 2.2 Hz, **H5b′**), 2.33–2.24 (1 H, m, **H2a′**), 2.23–2.16 (1 H, m, **H2b′**).

^{13}C NMR (101 MHz, DMSO-d_6): δ 162.1 (**C2**), 158.5 (**C4**), 150.0 (**C^{Ar}**), 145.7 (**C^{Ar}**), 143.5 (**C6**), 136.8 (**C^{Ar}**), 130.2 (**C9**), 128.4 (**CH^{Ar}**), 128.0 (**CH^{Ar}**), 127.2 (**C16**), 113.7 (**C10**), 98.8 (**C5**), 88.1 (**C7**), 86.3 (**C4′**), 86.2 (**C17**), 85.5 (**C1′**), 79.4, 77.4 (**C18**, **C21**), 76.5 (**C22**), 70.9 (**C3′**), 64.2 (**C5′**), 55.5 (**C12**), 42.5 (**C19**), 41.5 (**C20**), 40.2 (**C2′**).

LRMS [ESI$^+$, MeOH] *m/z* (%): 666.0 ([M+H]$^+$, 100%).

8.2.6.3 Synthesis of 5′-*O*-(4,4′-dimethoxytrityl)-5-[(*N*,*N*-dipropyn-2-yl)-3-aminopropyn-1-yl)]-2′-deoxyuridine-3′-*O*-(2-cyanoethyl-*N*,*N*-diisopropyl) phosphoramidite[211] (5-15)

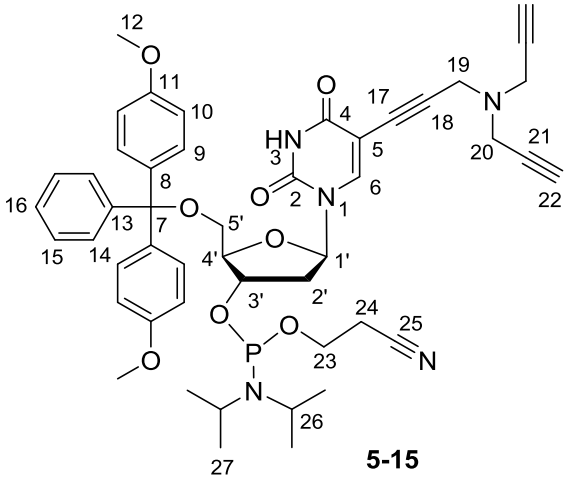

5-15

5′-*O*-(4,4′-Dimethoxytrityl)-5-[(*N*,*N*-dipropyn-2-yl)-3-aminopropyn-1-yl)]-2′-deoxyuridine **5-14** (300 mg, 0.46 mmol, 1.0 eq.) was dissolved in anhydrous DCM (3 mL) under an atmosphere of argon. Anhydrous DIPEA (200 µL, 1.15 mmol, 2.5 eq.) was added, followed by the dropwise addition of 2-cyanoethyl *N*,*N*-diisopropylchlorophosphoramidite (120 µL, 0.55 mmol, 1.2 eq.). The reaction mixture was stirred at room temperature for 1.5 h and transferred under argon into a separating funnel containing degassed DCM (15 mL). The mixture was washed with degassed saturated aqueous KCl (20 mL) and the organic layer was separated, dried over anhydrous Na_2SO_4, filtered, and concentrated under vacuum. The crude phosphoramidite product was precipitated using anhydrous DCM (1 mL) and anhydrous hexane (20 mL). After 5 times of precipitation, the product **5-15** was isolated as a colourless foam (303 mg, 0.35 mmol, 77%).

R_f: 0.65 (5% MeOH/DCM, 0.5% pyridine)

^{1}H NMR (400 MHz, CD_2Cl_2-d_2): δ 8.00 (0.5 H, s, **H6**), 7.96 (0.5 H, s, **H6**), 7.45 (2 H, d, *J* = 7.6 Hz, **H14**), 7.38–7.29 (6 H, m, **H9, H15**), 7.27–7.21 (1 H, m, **H16**), 6.87 (2 H, d, *J* = 8.7 Hz, **H10**), 6.85 (2 H, d, *J* = 8.7 Hz, **H10**), 6.29–6.22 (1 H, m, **H1′**), 4.66–4.58 (1 H, m, **H3′**), 4.24–4.15 (1 H, m, **H4′**), 3.89–3.76 (8 H, m, **H26** overlaps with s, **H12** at 3.79), 3.76–3.51 (4 H, m, **H23**, **H5′**), 3.43–3.31 (8 H, m, **H19**, **H20**, **H22**), 2.63 (1 H, t, *J* = 6.2 Hz, **H24a**), 2.60–2.51 (1 H, m, **H2′a**), 2.47 (1 H, t, *J* = 6.2 Hz, **H24b**), 2.35–2.29 (1 H, m, **H2′b**), 1.20–1.15 (9 H, m, **H27**), 1.10 (3 H, d, *J* = 6.7 Hz, **H27**).

^{31}P NMR (162 MHz, CD_2Cl_2-d_2): δ 149.81, 148.74.

8.2.6.4 Synthesis of 5′-*O*-(4,4′-dimethoxytrityl)-5-[(*N*-(1-(3-(2-((1,4-dihydro-1-methylquinolin-4-ylidene)methyl)benzothiazolium)propyl)triazol-4-yl-methyl))-*N*-(propyn-2-yl)-3-aminopropyn-1-yl)]-2′-deoxyuridine iodide (5-16)

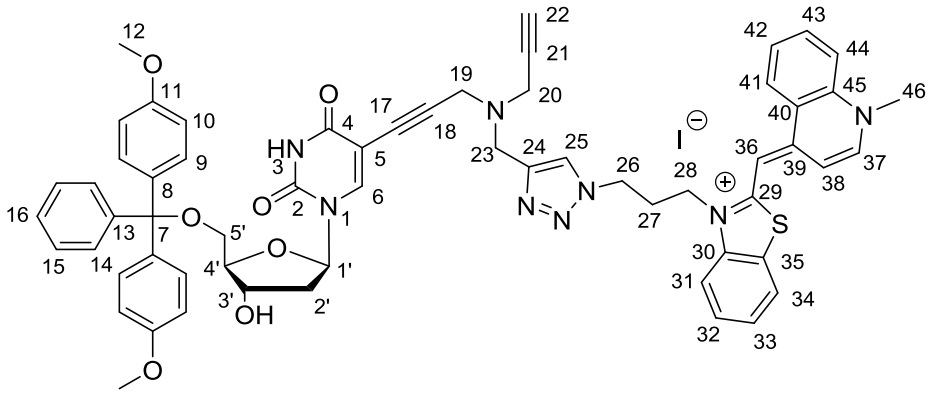

5-16

N-(3-Azidopropyl)-2-[(1,4-dihydro-1-methylquinolin-4-ylidene)methyl]benzothiazolium iodide **5-10** (400 mg, 0.80 mmol, 1.0 eq.) and 5′-*O*-(4,4′-dimethoxytrityl)-5-[(*N*,*N*-dipropyn-2-yl)-3-aminopropyn-1-yl)]-2′-deoxyuridine **5-14** (633 mg, 0.96 mmol, 1.2 eq.) were dissolved in DMF (8 mL), and added the TBTA ligand **5-20** (212 mg, 0.40 mmol,

0.5 eq.), a H_2O solution (1 mL) of sodium ascorbate (317 mg, 1.60 mmol, 2 eq.) was added, followed to add a H_2O solution (1 mL) of copper sulphate (100 mg, 0.40 mmol, 0.5 eq.). The reaction mixture was stirred at room temperature for 2 h. The solvent was removed under vacuum, and the residue was dissolved in 10% MeOH in DCM (25 mL). The mixture was washed with a 5% Na_2EDTA solution (25 mL × 3), then with distilled H_2O (30 mL × 2) and brine (30 mL × 2). The organic layers were combined, dried over anhydrous Na_2SO_4, filtered, and the solvent was concentrated under vacuum. Following purification by column chromatography (1–10% MeOH/DCM, 0.5% pyridine) the title compound **5-16** was afforded as an orange foam (350 mg, 0.30 mmol, 38%).

R_f: 0.17 (EtOAc/MeOH/conc. aq. NH_3 5:1:1)

^{1}H NMR (400 MHz, DMSO-d_6): δ 11.68 (1 H, s, **NH**), 8.74 (1 H, d, *J* = 8.5 Hz, **H41**), 8.64 (1 H, d, *J* = 7.2 Hz, **H37**), 8.09–7.97 (4 H, m, **H25, H43, H44, H34**), 7.91 (1 H, s, **H6**), 7.86–7.82 (1 H, m, **H42**), 7.70 (1 H, d, *J* = 8.5 Hz, **H31**), 7.63–7.57 (1 H, m, **H32**), 7.44–7.33 (4 H, m, **H14, H33, H38**), 7.29–7.20 (6 H, m, **H9, H15**), 7.19–7.13 (1 H, m, **H16**), 6.89 (1 H, s, **H36**), 6.85–6.81 (4 H, m, **H10**), 6.10 (1 H, t, *J* = 6.6 Hz, **H1′**), 5.33 (1 H, d, *J* = 4.4 Hz, **O**H), 4.69–4.59 (4 H, m, **H26, H28**), 4.29–4.22 (1 H, m, **H3′**), 4.18 (3 H, s, **H46**), 3.93–3.88 (1 H, m, **H4′**), 3.68 (6 H, s, **H12**), 3.66 (2 H, s, **H23**), 3.35 (2 H, s, **H19**), 3.28 (2 H, d, *J* = 2.1 Hz, **H20**), 3.22 (1H, t, *J* = 2.1 Hz, **H22**), 3.21–3.18 (1 H, m, **H5′a**), 3.07 (1 H, dd, *J* = 10.4, 2.4 Hz, **H5′b**), 2.43 (2 H, app. quin, *J* = 7.4 Hz, **H27**), 2.31–2.22 (1 H, m, **H2′a**), 2.22–2.13 (1 H, m, **H2′b**).

^{13}C NMR (126 MHz, DMSO-d_6): δ 162.1 (**C2**), 159.7 (**C29**), 158.5 (**C4**), 149.8 (**C^{Ar}**), 149.3 (**C39**), 145.7 (**C37**), 145.1 (**C^{Ar}**), 143.9 (**C^{Ar}**), 143.3 (**C6**), 140.3 (**C30**), 138.4 (**C45**), 136.1 (**C^{Ar}**), 135.7 (**C24**), 133.8 (**C43**), 130.2 (**C9**), 128.7 (**C32**), 128.4 (**C15**), 128.0 (**C14**), 127.7 (**C42**), 127.1 (**C16**), 126.0 (**C41**), 125.0 (**C33**), 124.8 (**C25**), 124.5 (**C40**), 124.4

(**C35**), 123.5 (**C34**), 118.8 (**C44**), 113.7 (**C10**), 113.0 (**C31**), 108.7 (**C38**), 98.9 (**C5**), 88.6 (**C7**), 87.7 (**C36**), 86.3 (**C4′**), 86.2 (**C17**), 85.5(**C1′**), 79.5, 77.3 (**C18**, **C21**), 76.5 (**C22**), 70.9 (**C3′**), 64.1 (**C5′**), 55.5 (**C12**), 47.7 (**C23**), 47.2 (**C26**), 43.9 (**C28**), 43.0 (**C46**), 42.7 (**C19**), 41.7 (**C20**), 40.1 (**C2′**), 27.2 (**C27**).

LRMS [ESI$^+$, MeOH] *m/z* (%): 1033.4 ([M-I]$^+$, 100%).

HRMS [ESI$^+$, MeOH] calc. for $C_{60}H_{57}O_7N_8S$, [M-I]$^+$, 1033.4065, found 1033.4028.

8.2.6.5 Synthesis of 5′-*O*-(4,4′-dimethoxytrityl)-5-[(*N*-(1-(8-(2-((1,4-dihydro-1-methylquinolin-4-ylidene)methyl)benzothiazolium)octyl)triazol-4-yl-methyl))-*N*-(propyn-2-yl)-3-aminopropyn-1-yl)]-2′-deoxyuridine iodide (5-17)

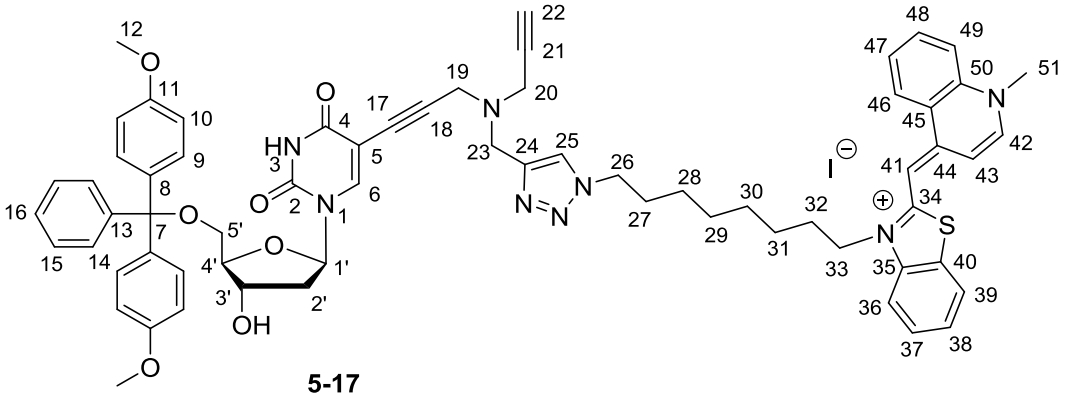

5-17

N-(8-Azidooctyl)-2-[(1,4-dihydro-1-methylquinolin-4-ylidene)methyl]benzothiazolium iodide **5-11** (550 mg, 0.96 mmol, 1.0 eq.) and 5′-*O*-(4,4′-dimethoxytrityl)-5-[(*N*,*N*-dipropyn-2-yl)-3-aminopropyn-1-yl)]-2′-deoxyuridine **5-14** (763 mg, 1.15 mmol, 1.2 eq.) were dissolved in DMF (10 mL), and added the TBTA ligand **5-20** (256 mg, 0.48 mmol, 0.5 eq.), a H_2O solution (1 mL) of sodium ascorbate (382 mg, 1.93 mmol, 2.0 eq.) was added, followed to add a H_2O solution (1 mL) of copper sulphate (120 mg, 0.48 mmol,

0.5 eq.). The reaction mixture was stirred at room temperature for 2 h. The solvent was removed under vacuum, and the residue was dissolved in 10% MeOH in DCM (25 mL). The mixture was washed with a 5% Na_2EDTA solution (25 mL × 3), then with distilled H_2O (30 mL × 2) and brine (30 mL × 2). The organic layers were combined, dried over anhydrous Na_2SO_4, filtered, and the solvent was concentrated under vacuum. Following purification by column chromatography (1–10% MeOH/DCM, 0.5% pyridine) the title compound **5-17** was afforded as an orange foam (405 mg, 0.28 mmol, 29%).

R_f: 0.18 (EtOAc/MeOH/conc. aq. NH_3 5:1:1)

^{1}H NMR (400 MHz, DMSO-d_6): δ 11.69 (1 H, s, **NH**), 8.73 (1 H, d, *J* = 8.6 Hz, **H46**), 8.63–8.60 (1 H, m, **H42**), 8.08–7.97 (3 H, m, **H48, H49, H39**), 7.91 (1 H, s, **H25**), 7.90 (1 H, s, **H6**), 7.81–7.73 (2 H, m, **H47, H36**), 7.62–7.56 (1 H, m, **H37**), 7.41–7.34 (3 H, m, **H43, H14**), 7.28–7.22 (7 H, m, **H38, H9, H15**), 7.19–7.13 (1 H, m, **H16**), 6.93 (1 H, s, **H41**), 6.87–6.81 (4 H, m, **H10**), 6.13–6.07 (1H, m, **H1′**), 5.34 (1 H, d, *J* = 4.6 Hz, **OH**), 4.61 (2 H, t, *J* = 7.1 Hz, **H33**), 4.30–4.21 (3 H, m, **H3′, H26**), 4.17 (3 H, s, **H51**), 3.92–3.87 (1 H, m, **H4′**), 3.69 (6 H, s, **H12**), 3.61 (2 H, s, **H23**), 3.32 (2 H, s, **H19**), 3.26 (2 H, br. s, **H20**), 3.24–3.18 (2 H, m, **H22**, **H5′a**), 3.09–3.03 (1H, m, **H5′b**), 2.34–2.12 (2 H, m, **H2′**), 1.83–1.66 (4 H, m, **H32, H27**), 1.56–1.20 (8 H, m, **H28, H29, H30, H31**).

^{13}C NMR (101 MHz, DMSO-d_6): δ 162.2 (**C2**), 159.7 (**C34**), 158.5 (**C4**), 149.6, 149.2 (**C44**, $\mathbf{C^{Ar}}$), 145.6 (**C42**), 145.2 ($\mathbf{C^{Ar}}$), 143.7 ($\mathbf{C^{Ar}}$), 144.1 (**C6**), 140.5 (**C35**), 138.4 (**C50**), 136.6 ($\mathbf{C^{Ar}}$), 135.6 (**C24**), 133.8 (**C48**), 130.1 (**C9**), 128.7 (**C37**), 128.3 ($\mathbf{CH^{Ar}}$), 128.0 ($\mathbf{CH^{Ar}}$), 127.7 (**C47**), 127.1 (**C16**), 125.8 (**C46**), 124.9 (**C38**), 124.6 (**C25**), 124.4 (**C40**), 124.4 (**C45**), 123.4 (**C39**), 118.9 (**C49**), 113.7 (**C10**), 113.5 (**C36**), 108.5 (**C43**), 99.5 (**C5**), 88.7 (**C7**), 88.4 (**C41**), 86.3 (**C4′**), 86.3 (**C17**), 85.5 (**C1′**), 79.0, 77.3 (**C21**, **C18**), 76.3 (**C22**), 70.9 (**C3′**), 64.0 (**C5′**), 55.7 (**C12**), 50.1 (**C26**), 47.8 (**C23**), 46.0 (**C33**), 42.6 (**C51**),

42.1, 41.8 (**C19**, **C20**), 40.5 (**C2′**), 29.0, 28.9, 28.7 (**C27**, **C28**, **C29**), 26.7 (**C32**), 26.4 (**C30**), 26.1 (**C31**).

LRMS [ESI$^+$, MeOH] *m/z* (%): 1103.4 ([M-I]$^+$, 100%).

HRMS [ESI$^+$, MeOH] calc. for $C_{65}H_{67}O_7N_8S$, [M-I]$^+$, 1103.4848, found 1103.4812.

8.2.6.6 Synthesis of 5′-*O*-(4,4′-dimethoxytrityl)-5-[(*N*-(1-(3-(2-((1,4-dihydro-1-methylquinolin-4-ylidene)methyl)benzothiazolium)propyl)triazol-4-yl-methyl))-*N*-(propyn-2-yl)-3-aminopropyn-1-yl)]-2′-deoxyuridine-3′-*O*-(2-cyanoethyl-*N*,*N*-diisopropyl)phosphoramidite iodide (5-18)

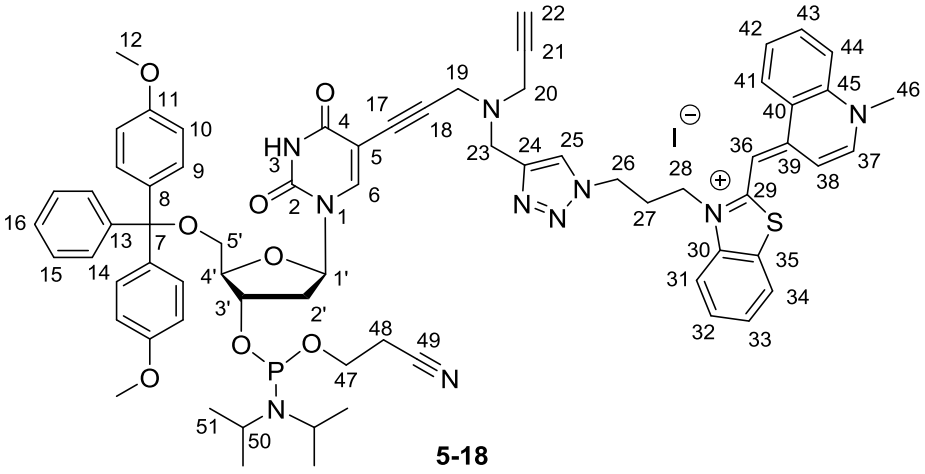

5′-*O*-(4,4′-Dimethoxytrityl)-5-[(*N*-(1-(3-(2-((1,4-dihydro-1-methylquinolin-4-ylidene) methyl)benzothiazolium)propyl)triazol-4-yl-methyl))-*N*-(propyn-2-yl)-3-aminopropyn-1-yl)]-2′-deoxyuridine iodide **5-16** (240 mg, 207 µmol, 1.0 eq.) was co-evaporated 3 times with anhydrous pyridine and dried overnight under vacuum, then it was co-evaporated with anhydrous DCM (5 mL × 3) and dried again under vacuum. After 1 h the compound **5-16** was dissolved in anhydrous DCM (3 mL) under an atmosphere of argon with a few

drops of anhydrous DMF to improve the solubility, then anhydrous DIPEA (108 µL, 621 µmol, 3.0 eq.) was added, followed by the dropwise addition of 2-cyanoethyl *N*,*N*-diisopropylchlorophosphoramidite (116 µL, 518 µmol, 2.5 eq.). The reaction mixture was stirred at room temperature for 2 h and transferred under argon into a separating funnel containing degassed DCM (15 mL). The mixture was washed with degassed saturated aqueous KCl (20 mL) and the organic layer was separated, dried over anhydrous Na_2SO_4, filtered, and concentrated under vacuum. The crude phosphoramidite product was precipitated using anhydrous DCM (1 mL) and anhydrous hexane (20 mL). After 5 times of precipitation, the product **5-18** was isolated as a dark orange foam (195 mg, 143 µmol, 70%).

R_f: 0.29 (10% MeOH/DCM, 0.5% pyridine)

^{1}H NMR (500 MHz, CD_2Cl_2-d_2): δ 8.70–8.63 (1 H, m, **H41**), 8.51 (1 H, d, *J* = 7.3 Hz, **H37**), 8.02 (1 H, s, **H25**), 7.98 (1 H, s, **H6**), 7.80–7.74 (2 H, m, **H44, H34**), 7.62 (1 H, d, *J* = 7.9 Hz, **H43**), 7.60–7.56 (1 H, m, **H42**), 7.47–7.41 (4 H, m, **H31, H32, H33, H38**), 7.37–7.27 (8 H, m, **H14**, **H15**, **H9**), 7.24–7.18 (1 H, m, **H16**), 6.87–6.82 (4 H, m, **H10**), 6.71 (1 H, s, **H36**), 6.25 (1 H, dd, *J* = 12.7, 6.3 Hz, **H1′**), 4.78–4.70 (2 H, m, **H28**), 4.67–4.52 (3 H, m, **H26, H3′**), 4.22–4.13 (1 H, m, **H4′**), 4.09 (3 H, s, **H46**), 3.86–3.78 (2 H, m, **H47**), 3.76 (6 H, s, **H12**), 3.73–3.64 (2 H, m, **H50**), 3.63–3.52 (3 H, m, **H5′**, **H22**), 3.40–3.31 (4 H, m, **H23, H19**), 3.30–3.25 (2 H, m. **H20**), 2.63 (1 H, t, *J* = 6.2 Hz, **H48a**), 2.61–2.50 (3 H, m, **H2′a**, **H27**), 2.48 (1 H, t, *J* = 6.2 Hz, **H48b**), 2.37–2.27 (1 H, m, **H2′b**), 1.20–1.15 (9 H, m, **H51**), 1.09 (3 H, d, *J* = 6.6 Hz, **H51**).

^{31}P NMR (202 MHz, CD_2Cl_2-d_2): δ 148.92.

8.2.6.7 Synthesis of 5′-*O*-(4,4′-dimethoxytrityl)-5-[(*N*-(1-(8-(2-((1,4-dihydro-1-methylquinolin-4-ylidene)methyl)benzothiazolium)octyl)triazol-4-yl-methyl))-*N*-(propyn-2-yl)-3-aminopropyn-1-yl)]-2′-deoxyuridine-3′-*O*-(2-cyanoethyl-*N*,*N*-diisopropyl)phosphoramidite iodide (5-19)

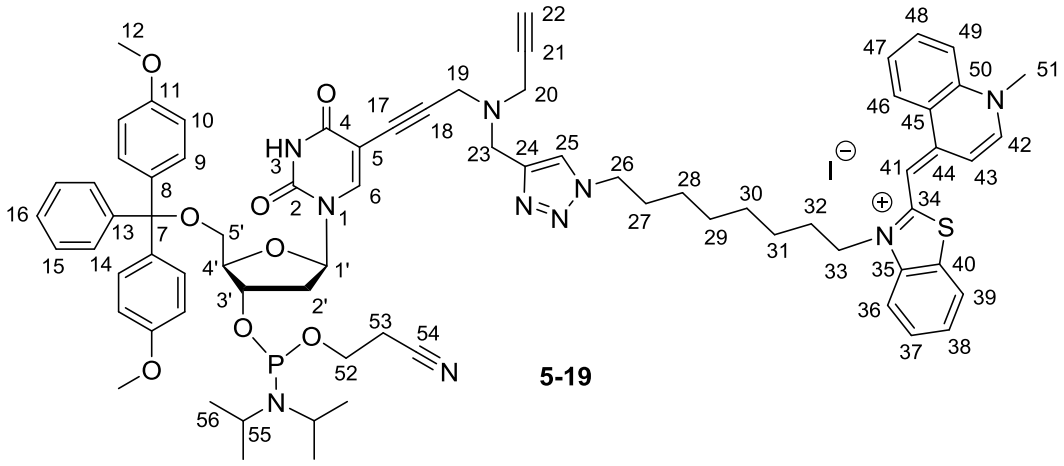

5′-*O*-(4,4′-Dimethoxytrityl)-5-[(*N*-(1-(8-(2-((1,4-dihydro-1-methylquinolin-4-ylidene) methyl)benzothiazolium)octyl)triazol-4-yl-methyl))-*N*-(propyn-2-yl)-3-aminopropyn-1-yl)]-2′-deoxyuridine iodide **5-17** (202 mg, 164 µmol, 1.0 eq.) was co-evaporated with anhydrous pyridine (5 mL × 3) and dried overnight under vacuum, then it was co-evaporated with anhydrous DCM (5 mL × 3) and dried again under vacuum. After 1 h the compound **5-17** was dissolved in anhydrous DCM (3 mL) under an atmosphere of argon with a few drops of anhydrous DMF to improve the solubility, then anhydrous DIPEA (70 µL, 400 µmol, 2.5 eq.) was added, followed by the dropwise addition of 2 cyanoethyl *N*,*N*-diisopropylchlorophosphoramidite (73 µL, 328 µmol, 2.0 eq.). The reaction mixture was stirred at room temperature for 2.0 h and transferred under argon into a separating funnel containing degassed DCM (15 mL). The mixture was washed with degassed saturated aqueous KCl (20 mL) and the organic layer was separated, dried over anhydrous Na_2SO_4, filtered, and concentrated under vacuum. The crude phosphoramidite

product was precipitated using anhydrous DCM (1 mL) and anhydrous hexane (20 mL). After 5 times of precipitation, the product **5-19** was isolated as a dark orange foam (155 mg, 108 μmol, 66%).

R_f: 0.52 (10% MeOH/DCM, 0.5% pyridine)

^{1}H NMR (400 MHz, CD_2Cl_2-d_2): δ 8.81 (1 H, d, *J* = 6.9 Hz, **H42**), 8.42 (1 H, d, *J* = 8.3 Hz, **H46**), 7.97 (1 H, s, **H25**), 7.93 (1 H, s, **H6**), 7.93–7.88 (1 H, m, **H48**), 7.86–7.76 (2 H, m, **H49, H39**), 7.74–7.68 (1 H, m, **H47**), 7.53 (1 H, d, *J* = 6.3 Hz, **H36**), 7.47–7.38 (4 H, m, **H37, H43, H14**), 7.35–7.25 (7 H, m, **H38, H9, H15**), 7.22–7.16 (1 H, m, **H16**), 6.86–6.80 (4 H, m, **H10**), 6.72 (1 H, s, **H41**), 6.30–6.18 (1 H, m, **H1′**), 4.63–4.56 (1 H, m, **H3′**), 4.40 (2 H, t, *J* = 7.2 Hz, **H33**), 4.29–4.25 (2 H, m, **H26**), 4.24 (3 H, s, **H51**), 4.21–4.17 (1 H, m, **H4′**), 3.75 (6 H, s, **H12**), 3.73–3.66 (4 H, m, **H52**, **H55**), 3.65–3.51 (3 H, m, **H22**, **H5′**), 3.36–3.27 (4 H, m, **H23, H19**), 3.25–3.21 (2 H, m, **H20**), 2.64–2.49 (2 H, m, containing t, *J* = 6.2 Hz, **H53a**, **H2′a**), 2.46 (1 H, t, *J* = 6.2 Hz, **H53b**), 2.33–2.26 (1 H, m, **H2′b**), 1.92 (2 H, app. quin, *J* = 7.6 Hz, **H32**), 1.83 (2 H, app. quin, *J* = 7.0 Hz, **H27**), 1.67–1.36 (8 H, m, **H28, H29, H30, H31**), 1.18–1.11 (9 H, m, **H56**), 1.08 (3 H, d, *J* = 6.9 Hz, **H56**).

^{31}P NMR (162 MHz, CD_2Cl_2-d_2): δ 148.73.

8.2.7 Synthesis of the tris(benzyltriazolylmethyl)amine (TBTA) ligand[192] (5-20)

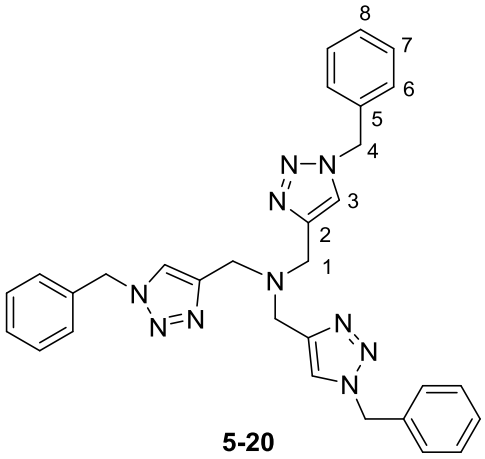

5-20

A solution of tripropargylamine (1.80 mL, 12.5 mmol, 1.0 eq.) was mixed with acetonitrile (25 mL) and then slowly added to benzyl azide (9.40 mL, 75.1 mmol, 6.0 eq.), 2,6-lutidine (1.50 mL, 12.5 mmol, 1.0 eq.), and tetrakis(acetonitrile) copper(I) hexafluorophosphate (122 mg, 323 μmol, 0.020 eq.). The reaction mixture was stirred at room temperature for 3 days under an atmosphere of argon, and a white solid precipitated out from the reaction mixture. The solid was filtered off and washed with cold acetonitrile (30 mL × 3), then dried under high vacuum overnight. The product **5-20** was obtained as a white solid (2.44 g, 4.60 mmol, 37%).

R_f: 0.41 (5% MeOH/DCM)

^{1}H NMR (300 MHz, DMSO-d_6): δ 8.08 (3 H, s, **H3**), 7.53–7.08 (15 H, m, **ArH**), 5.59 (6 H, s, **H4**), 3.63 (6 H, s, **H1**).

LRMS [ESI$^+$, MeOH] *m/z* (%): 531.3 ([M+H]$^+$, 100%); 553.2 ([M+Na]$^+$, 93%).

8.2.8 Synthesis of benzothiazole orange (BO) dyes

8.2.8.1 Synthesis of 4-chloro-1-methylpyridium iodide[212] (6-1)

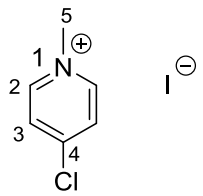

6-1

4-Chloropyridine hydrochloride (10.0 g, 66.7 mmol, 1 eq.) was dissolved in H_2O (10 mL). Excess saturated $NaHCO_3$ solution was added until pH 7 was reached. DCM (100 mL) was added to extract 4-chloropyridine. The orangic layer was collected, and then concentrated under vacuum. Iodomethane (10.0 mL, 240 mmol, 3.6 eq.) was added to the reaction in a 100 mL flask covered by foil. The reaction mixture was left at 4 °C for 3 days. The precipitate was collected and washed with cold Et_2O (30 mL × 3), then dissolved in acetonitrile (100 mL), the solvent was collected and removed under vacuum to give product **6-1** as a brown solid (10.3 g, 40.4 mmol, 61%).

R_f: 0.25 (10% MeOH/DCM)

^{1}H NMR (400 MHz, DMSO-d_6): δ 9.00 (2 H, d, J = 6.9 Hz, **H2**) 8.35 (2 H, d, J = 6.9 Hz, **H3**) 4.29 (3 H, s, **H5**).

^{13}C NMR (101 MHz, DMSO-d_6): δ 152.1 (**C4**), 147.2 (**C2**), 128.4 (**C3**), 47.5 (**C5**).

LRMS [ESI$^+$, MeOH] *m/z* (%): 128.1 ([M-I]$^+$, 100%).

8.2.8.2 Synthesis of *N*-(3-iodopropyl)-2-[(1,4-dihydro-1-methylpyridin-4-ylidene)methyl]benzothiazolium iodide (6-2)

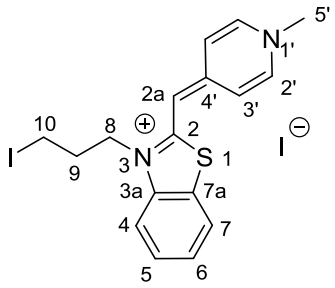

6-2

N-(3-Iodopropyl)-2-methylbenzothiazolium iodide **5-6** (3.18 g, 7.15 mmol, 1.0 eq.) and 4-chloro-1-methylpyridium iodide **6-1** (3.64 g, 14.3 mmol, 2.0 eq.) were dissolved in DCM/MeCN (1:1, 50 mL) under an atmosphere of argon. Anhydrous Et_3N (2.50 mL, 17.9 mmol, 2.5 eq.) was added, giving in an immediate deep red colour. The reaction mixture was stirred for 10 min at room temperature. The solvent was removed under vacuum and the product **6-2** was collected and washed with cold Et_2O (50 mL × 3) and dried under vacuum. The crude mixture was purified by column chromatography (1–10% MeOH/DCM) to give the compound **6-2** as a yellow solid (0.40 g, 0.87 mmol, 10%).

R_f: 0.30 (EtOAc/MeOH/conc. aq. NH_3 5:1:1)

^{1}H NMR (400 MHz, DMSO-d_6): δ 8.33 (2 H, d, *J* = 7.1 Hz, **H2′**), 7.92 (1 H, d, *J* = 7.5 Hz, **H7**), 7.61 (1 H, d, *J* = 8.4 Hz, **H4**), 7.53 (1 H, t, *J* = 7.5 Hz, **H5**), 7.42 (2 H, d, *J* = 7.1 Hz, **H3′**), 7.31 (1 H, t, *J* = 7.5 Hz, **H6**), 6.31 (1 H, s, **H2a**), 4.29 (2 H, t, *J* = 7.2 Hz, **H8**), 4.00 (3 H, s, **H5′**), 3.39 (2 H, t, *J* = 7.2 Hz, **H10**), 2.25 (2 H, app. quin, *J* = 7.2 Hz, **H9**).

^{13}C NMR (126 MHz, DMSO-d_6): δ 153.3 (**C2**), 150.8 (**C4′**), 142.9 (**C2′**), 140.9 (**C3a**), 127.7 (**C5**), 124.2 (**C6**), 123.1 (**C7a**), 122.6 (**C7**), 117.4 (**C3′**), 111.5 (**C4**), 97.2 (**C2a**), 45.3 (**C5′**), 44.7 (**C8**), 25.2 (**C10**), 20.7 (**C9**).

LRMS [ESI$^+$, MeOH] *m/z* (%): 409.0 ([M-I]$^+$, 100%).

HRMS [ESI$^+$, MeOH] calc. for $C_{17}H_{18}N_2IS$, [M-I]$^+$, 409.0230, found 409.0230.

8.2.8.3 Synthesis of *N*-(3-azidopropyl)-2-[(1,4-dihydro-1-methylpyridin-4-ylidene) methyl]benzothiazolium iodide (6-3)

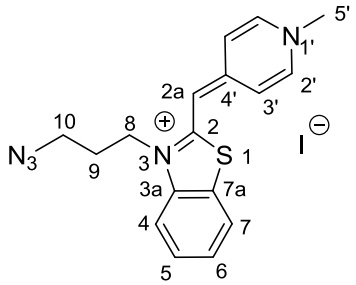

6-3

N-(3-Iodopropyl)-2-[(1,4-dihydro-1-methylpyridin-4-ylidene)methyl]benzothiazolium iodide **6-2** (0.20 g, 0.37 mmol, 1 eq.) was dissolved in DMF (10 mL). Lithium azide solution (20% in water, 0.22 mL, 0.93 mmol, 2.5 eq.) was added dropwise. Reaction mixture was stirred at room temperature for 10 min. The solvent was removed under vacuum. The crude mixture was purified by column chromatography (1–10% MeOH/DCM) to give the compound **6-3** as a yellow solid (125 mg, 0.28 mmol, 76%).

R_f: 0.29 (EtOAc/MeOH/conc. aq. NH_3 5:1:1)

^{1}H NMR (400 MHz, DMSO-d_6): δ 8.32 (2 H, d, *J* = 7.2 Hz, **H2′**), 7.92 (1 H, dd, *J* = 7.8, 1.0 Hz, **H7**), 7.59 (1 H, d, *J* = 8.1 Hz, **H4**), 7.57–7.51 (1 H, m, **H5**), 7.44 (2 H, d, *J* = 7.2 Hz, **H3′**), 7.35–7.29 (1 H, m, **H6**), 6.30 (1 H, s, **H2a**), 4.32 (2 H, t, *J* = 7.2 Hz, **H8**), 4.00 (3 H, s, **H5′**), 3.54 (2 H, t, *J* = 6.6 Hz, **H10**), 1.99 (2 H, app. quin, *J* = 7.1 Hz, **H9**).

^{13}C NMR (101 MHz, DMSO-d_6): δ 156.7 (**C2**), 150.7 (**C4′**), 142.8 (**C2′**), 140.4 (**C3a**), 128.2 (**C5**), 124.1 (**C6**), 123.8 (**C7a**), 123.1 (**C7**), 119.0 (**C3′**), 112.2 (**C4**), 89.6 (**C2a**), 48.2 (**C10**), 45.5 (**C5′**), 43.1 (**C8**), 26.2 (**C9**).

LRMS [ESI$^+$, MeOH] m/z (%): 324.1 ([M-I]$^+$, 100%).

HRMS [ESI$^+$, MeOH] calc. for $C_{17}H_{18}N_5S$, [M-I]$^+$, 324.1277, found 324.1275.

8.2.9 Synthesis of BO-modified nucleosides and phosphoramidites

8.2.9.1 Synthesis of 5′-*O*-(4,4′-dimethoxytrityl)-5-[(*N*-(1-(3-(2-((1,4-dihydro-1-methylpyridin-4-ylidene)methyl)benzothiazolium)propyl)triazol-4-yl-methyl))-*N*-(propyn-2-yl)-3-aminopropyn-1-yl)]-2′-deoxyuridine iodide (6-6)

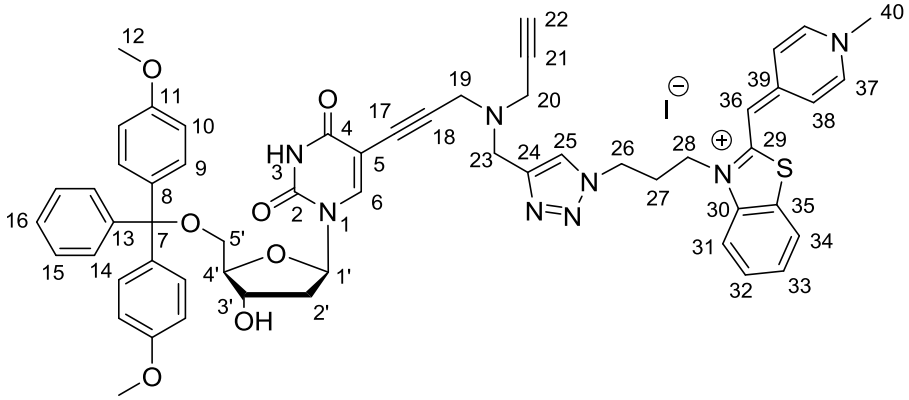

6-6

N-(3-Azidopropyl)-2-[(1,4-dihydro-1-methylpyridin-4-ylidene)methyl]benzothiazolium iodide **6-3** (340 mg, 0.75 mmol, 1.0 eq.) and 5′-*O*-(4,4′-dimethoxytrityl)-5-[(*N*,*N*-dipropyn-2-yl)-3-aminopropyn-1-yl)]-2′-deoxyuridine **5-14** (646 mg, 0.98 mmol, 1.3 eq.) were dissolved in DMF (8 mL), and added the TBTA ligand **5-20** (200 mg, 0.37 mmol, 0.5 eq.), a H_2O solution (1 mL) of sodium ascorbate (299 mg, 1.5 mmol, 2.0 eq) was added, followed to add a H_2O solution (1 mL) of copper sulphate (94.1 mg, 0.37 mmol, 0.5 eq.). The reaction mixture was stirred at room temperature for 2 h. The solvent was removed under vacuum, and the residue was dissolved in 10% MeOH in DCM (25 mL). The mixture was washed with a 5% Na_2EDTA solution (25 mL × 3), then with distilled H_2O (30 mL × 2) and brine (30 mL × 2). The organic layers were combined, dried over anhydrous Na_2SO_4, filtered, and the solvent was concentrated under vacuum. Following

purification by column chromatography (1–10% MeOH/DCM, 0.5% pyridine) the title compound **6-6** was afforded as a yellow foam (250 mg, 0.25 mmol, 26%).

R_f: 0.25 (10% MeOH/DCM, 0.5% pyridine)

^{1}H NMR (400 MHz, DMSO-d_6): δ 11.69 (1 H, s, **NH**), 8.32 (2 H, d, *J* = 7.0 Hz, **H37**), 7.95 (1 H, s, **H25**), 7.92 (1 H, s, **H6**), 7.90 (1 H, d, *J* = 7.8 Hz, **H34**), 7.51–7.47 (2 H, m, **H31, H32**), 7.42–7.33 (4 H, m, **H38, H14**), 7.32–7.22 (7 H, m, **H33, H9, H15**), 7.18 (1 H, t, *J* = 7.2 Hz, **H16**), 6.87–6.82 (4 H, m, **H10**), 6.17 (1 H, s, **H36**), 6.10 (1 H, t, *J* = 6.6 Hz, **H1′**), 5.33 (1 H, d, *J* = 4.3 Hz, **OH**), 4.54 (2 H, t, *J* = 6.8 Hz, **H26**), 4.33–4.22 (3 H, m, **H28, H3′**), 3.98 (3 H, s, **H40**), 3.93–3.88 (1 H, m, **H4′**), 3.69 (6 H, s, **H12**), 3.64 (2 H, s, **H23**), 3.35 (2H, s, **H19**), 3.28 (2 H, br. s, **H20**), 3.25–3.18 (2 H, m, **H5′a, H22**), 3.12–3.04 (1 H, m, **H5′b**), 2.36–2.13 (4 H, m, **H27, H2′**).

^{13}C NMR (126 MHz, DMSO-d_6): δ 162.0 (**C2**), 158.6 (**C4**), 156.6 (**C29**), 150.8 (**C39**), 149.8 (**C^{Ar}**), 145.2 (**C^{Ar}**), 143.9 (**C^{Ar}**), 143.3 (**C6**), 142.7 (**C37**), 140.2 (**C30**), 136.0 (**C^{Ar}**), 135.7 (**C24**), 130.1 (**C9**), 128.4, 128.3 (**C32**, **C15**), 128.0 (**C14**), 127.1 (**C16**), 124.6 (**C25**), 124.1 (C**33**), 123.8 (**C35**), 123.1 (**C34**), 119.0 (**C38**), 113.7 (**C10**), 112.1 (**C31**), 98.9 (**C5**), 89.5 (**C36**), 88.6 (**C7**), 86.4, 86.3 (**C4′**, **C17**), 85.5 (**C1′**), 79.4, 77.3 (**C18**, **C22**), 76.5 (**C21**), 70.9 (**C3′**), 64.1 (**C5′**), 55.5 (**C12**), 47.6 (**C23**), 47.2 (**C26**), 45.5 (**C40**), 43.0 (**C28**), 42.6 (**C19**), 41.7 (**C20**), 40.2 (**C2′**), 27.1 (**C27**).

LRMS [ESI$^+$, MeOH] *m/z* (%): 681.3 ([M-I-DMT+H]$^+$, 100%); 303.1 ([DMT]$^+$, 100%).

HRMS [ESI$^+$, MeOH] calc. for $C_{56}H_{55}O_7N_8S$, [M-I]$^+$, 983.3909, found 983.3866.

8.2.9.2 Synthesis of 5′-*O*-(4,4′-dimethoxytrityl)-5-[(*N*-(1-(3-(2-((1,4-dihydro-1-methylpyridin-4-ylidene)methyl)benzothiazolium)propyl)triazol-4-yl-methyl))-*N*-(propyn-2-yl)-3-aminopropyn-1-yl)]-2′-deoxyuridine-3′-*O*-(2-cyanoethyl-*N*,*N*-diisopropyl)phosphoramidite iodide (6-7)

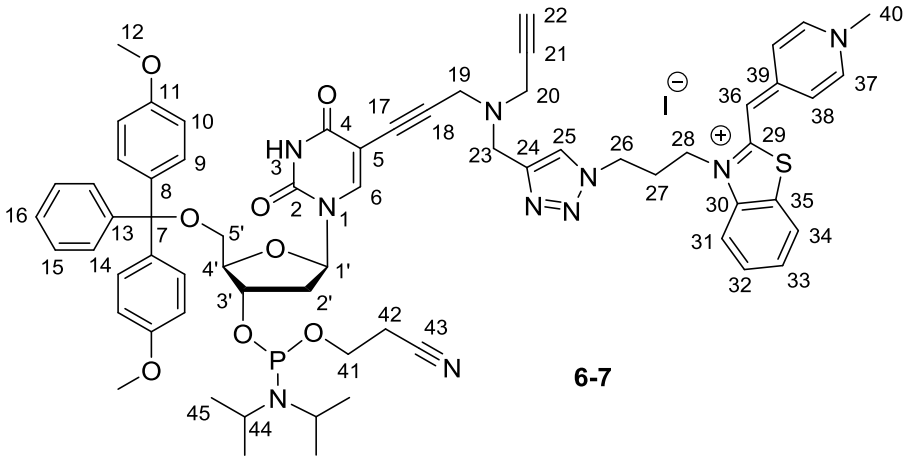

6-7

5′-*O*-(4,4′-Dimethoxytrityl)-5-[(*N*-(1-(3-(2-((1,4-dihydro-1-methylpyridin-4-ylidene) methyl)benzothiazolium)propyl)triazol-4-yl-methyl))-*N*-(propyn-2-yl)-3-aminopropyn-1-yl)]-2′-deoxyuridine iodide **6-6** (250 mg, 225 µmol, 1.0 eq.) was co-evaporated with anhydrous pyridine (5 mL × 3) and dried overnight under vacuum, then it was co-evaporated with anhydrous DCM (5 mL × 3) and dried again under vacuum. After 1 h the compound **6-6** was dissolved in anhydrous DCM (3 mL) under an atmosphere of argon with a few drops of anhydrous DMF to improve the solubility, then anhydrous DIPEA (98 µL, 562 µmol, 2.5 eq.) was added, followed by the dropwise addition of 2-cyanoethyl *N*,*N*-diisopropylchlorophosphoramidite (100 µL, 450 µmol, 2.0 eq.). The reaction mixture was stirred at room temperature for 2 h and transferred under argon into a separating funnel containing degassed DCM (15 mL). The mixture was washed with degassed saturated aqueous KCl (20 mL) and the organic layer was separated, dried over anhydrous Na_2SO_4, filtered, and concentrated under vacuum. The crude phosphoramidite product was

precipitated using anhydrous DCM (1 mL) and anhydrous hexane (20 mL). After 5 times of precipitation, the product **6-7** was isolated as a yellow foam (190 mg, 145 µmol, 64%).

R_f: 0.42 (10% MeOH/DCM, 0.5% pyridine)

^{1}H NMR (400 MHz, DMSO-d_6): δ 11.67 (1 H, br. s., **NH**), 8.32 (2 H, d, *J* = 6.4 Hz, **H37**), 7.96 (1 H, s, **H25**), 7.93 (1 H, s, **H6**), 7.89 (1 H, d, *J* = 7.7 Hz, **H34**), 7.53–7.45 (2 H, m, **H31, H32**), 7.41–7.33 (4 H, m, **H38**, **H14**), 7.31–7.21 (7 H, m, **H33, H9, H15**), 7.20–7.14 (1 H, m, **H16**), 6.88–6.80 (4 H, m, **H10**), 6.19 (1 H, s, **H36**), 6.14–6.05 (1 H, m, **H1′**), 4.55 (2 H, t, *J* = 6.6 Hz, **H26**), 4.50–4.42 (1 H, m, **H3′**), 4.30 (2 H, t, *J* = 7.3 Hz, **H28**), 4.10–4.01 (1 H, m, **H4′**), 3.99 (3 H, s, **H40**), 3.70 (6 H, s, **H12**), 3.67–3.64 (2 H, m, **H44**), 3.63–3.56 (2 H, m, **H41**), 3.57–3.43 (2 H, m, **H5′**), 3.41–3.09 (7 H, m, **H19**, **H20**, **H22**, **H23**), 2.98–2.84 (1 H, m, **H2′a**), 2.76 (1 H, t, *J* = 5.8 Hz, **H42a**), 2.64 (1 H, t, *J* = 5.8 Hz, **H42b**), 2.46–2.39 (1 H, m, **H2′b**), 2.37–2.24 (2 H, m, **H27**), 1.17–1.05 (9 H, m, **H45**), 0.98 (3 H, d, *J* = 6.6 Hz, **H45**).

^{31}P NMR (162 MHz, DMSO-d_6): δ 147.58, 147.19.

8.3 Oligonucleotide synthesis and purification

8.3.1 General

Standard DNA phosphoramidites, solid supports (controlled pore glass, CPG and macroporous polystyrene, MPPS), activated alkyne ester (BCN) and additional reagents were purchased from Link Technologies, Glen Research, Jena Bioscience, Berry Associates and Applied Biosystems. NAP Sephadex gel-filtration columns were purchased from GE Healthcare and used according to the manufacturer's instructions. All oligonucleotides were synthesized on an Applied Biosystems 394 automated DNA/RNA synthesizer using a standard 1.0 μmol phosphoramidite cycle of acid-catalysed detritylation, coupling, capping, and iodine oxidation. Stepwise coupling efficiencies and overall yields were determined by automated trityl cation conductivity monitoring and in all cases were >98.0%. All β-cyanoethyl phosphoramidite monomers except for TO3-dT (X_2), TO8-dT (X_3) and BO3-dT (X_6) monomers (anhydrous DCM) were dissolved in anhydrous acetonitrile to a concentration of 0.1 M immediately prior to use. Standard DNA phoshoramidites were used for the majority of oligonucleotide sequences. In the case of oligonucleotides containing TO3-dT, TO8-dT, BO3-dT, 5′-iodo-dT, Cy5, fast deprotecting monomers were used (UltraMILD monomers, Pac-dA, Ac-dC and iPr-Pac-dG, Link Technologies). The coupling time for normal A, G, C, and T monomers was 35 s, and the coupling time for the modified phosphoramidite monomers (TO3-dT, TO8-dT, BO3-dT, 5′-iodo-dT, 5′-BCN and 5′-DMT-*N*4-Fmoc-2′-deoxycytidine) was extended to 360 s. Aminolink C7 DNA and aminolink C6 DNA were used for the introduction of the 3′-amino-moiety and 5′-amino-moiety into oligonucleotides, respectively.

Cleavage of the oligonucleotides from the solid support and subsequent deprotection was achieved by exposure to concentrated aqueous ammonia solution for 1 h at room

temperature, followed by heating in a sealed tube for 5 h at 55 °C. In the case of oligonucleotides containing TO3-dT, TO8-dT, BO3-dT, 5′-iodo-dT and Cy5 deprotection were carried out for 4 h at room temperature or 1 h at 55 °C.

The oligonucleotides were purified by reversed-phase HPLC on a Gilson system using a Luna® 10 μm C8 100 Å pore Phenomenex column (10 × 250 mm) with a gradient of acetonitrile in ammonium acetate, triethylammonium acetate (TEAA) or triethylammonium bicarbonate (TEAB) over 20 min at a flow rate of 4 mL min^{-1}. For unmodified oligonucleotides, the ammonium acetate buffer (buffer A: 0.1 M ammonium acetate, pH 7.0; buffer B: 0.1 M ammonium acetate, pH 7.0, with 50% acetonitrile) was used (0% to 50% buffer B over 20 min). For modified oligonucleotides, the TEAA buffers (buffer A: 0.1 M triethylammonium acetate, pH 7.0; buffer B: 0.1 M triethylammonium acetate, pH 7.0, with 50% acetonitrile) or TEAB buffers (buffer A: 0.1 M triethylammonium bicarbonate, pH 7.5; buffer B: 0.1 M triethylammonium bicarbonate, pH 7.5, with 50% acetonitrile) were used (0% to 80% buffer B over 20 min). Elution was monitored by UV absorption at 260–295 nm. After HPLC purification, oligonucleotides were desalted using NAP-25 then NAP-10 columns (GE Healthcare) according to the manufacturer's instructions when using TEAA buffer, or NAP-10 columns only when using ammonium acetate buffer. The oligonucleotides were then aliquoted into Eppendorf tubes and stored at –20 ºC. All oligonucleotides were characterised by electrospray mass spectrometry. Mass spectrometry of oligonucleotides was recorded in water using a Bruker micrOTOF™ II focus ESI-TOF MS instrument in ES^- mode. Data were processed using MaxEnt.

8.3.2 Synthesis of 5′-azide oligonucleotides

8.3.2.1 Conversion of 5′-OH to 5′-azide on the solid phase

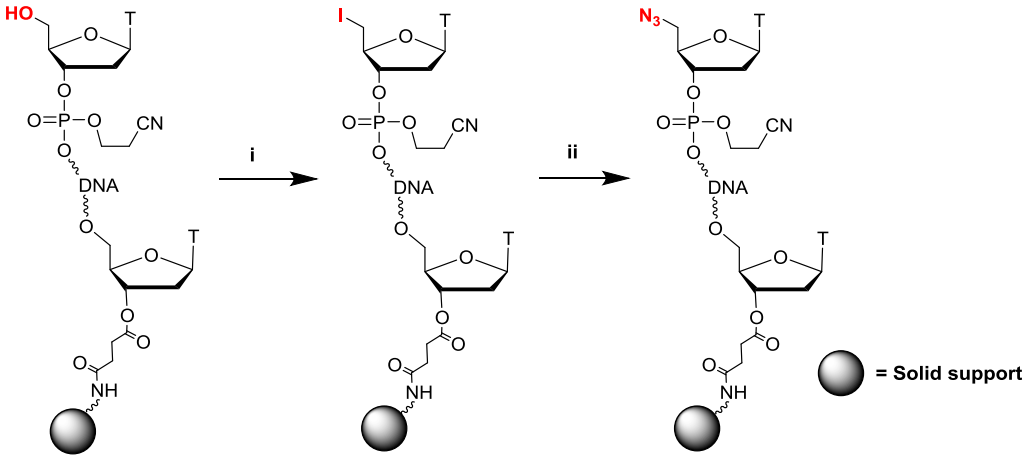

ODN2-5/3-5 (Table 2.1, Chapter 2; Table 3.1, Chapter 3) was assembled on the 1.0 μmol scale (trityl-off) as described in the general method with normal HO-dT at the 5′-end. For conversion of the 5′-hydroxyl group to 5′-iodo (i), the support-bound oligomer in the synthesis column was treated with a 0.5 M solution of methyltriphenoxyphosphonium iodide ($[MeP(OPh)_3]^+I^-$) in anhydrous DMF (1.0 mL), and two 1 mL syringes were used to pass the reagent through the column periodically over 15 min at room temperature. The column was then washed with anhydrous DMF (1 mL × 3). To convert the 5′-iodo-dT to 5′-azido-dT (ii), sodium azide (50 mg) was suspended in anhydrous DMF (1 mL), heated for 15 min at 70 °C then cooled down. The supernatant was taken up into a 1 mL syringe, passed back and forth through the column then left at 55 °C for 4 h. The column was then washed with DMF and acetonitrile (1 mL × 3) separately, and dried by the passage of a stream of argon gas.

8.3.2.2 Conversion of 5′-iodo to 5′-azide and deprotection of Fmoc-dC on the solid phase

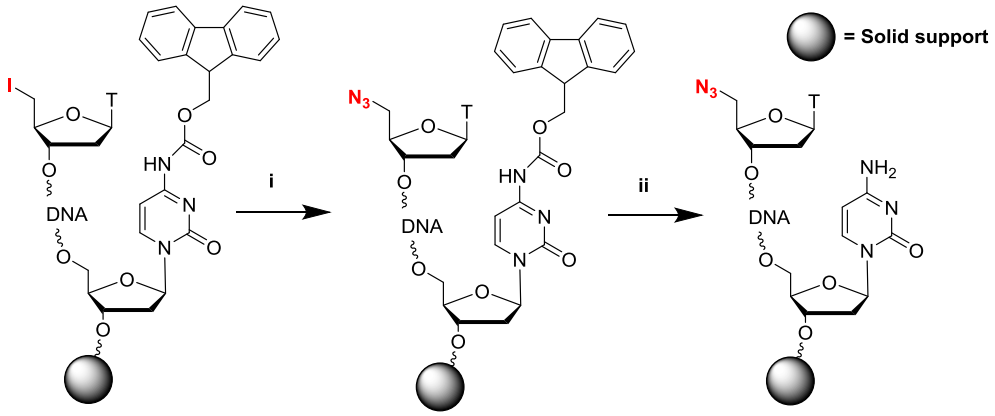

ODN2-6/3-6 (1000 Å, 17-mer) and ODN2-7/3-7 (3000 Å, 17-mer) (Chapter 2, Chapter 3) were also assembled on the 1.0 µmol scale (trityl-off) as described in the general method, and were modified at the 5′-end by addition of 5′-iodo-dT phosphoramidite. To convert the 5′-iodo-dT to 5′-azido-dT (i), as described above (Section 8.3.2.1). The Fmoc protecting groups of ODN2-6/3-6 and ODN2-7/3-7 were cleaved using 20% piperidine in DMF as follows (ii): two 1 mL syringes were attached to the column and the reagent was passed back and forth periodically (every 2 min) for 20 min at room temperature. The column was then thoroughly washed with DMF and acetonitrile (1 mL × 3) separately, and dried by the passage of a stream of argon gas.

8.3.2.3 Synthesis of 5′-iodo-3′-azide oligonucleotides

5′-Iodo-3′-azide oligonucleotides ODN3-17/3-18 (Table 3.3, Chapter 3) were synthesised on the 1.0 µmol scale, as explained in the oligonucleotide synthesis and purification section, using 5′-iodo-dT phosphoramidite monomer and aminolink C7 synthesis column.

As the 5′-iodo group is labile under the normal conditions of oligonucleotide deprotection (5 h at 55 °C in aqueous ammonia solution), fast deprotecting monomers were used (UltraMILD monomers, Pac-dA, Ac-dC and iPr-Pac-dG, Link Technologies). Cleavage of the oligonucleotides from the solid support and deprotection was achieved by exposure to concentrated aqueous ammonia solution for 4 h at room temperature. NAP-10 gel-filtration was used to remove the cleaved protecting groups, after which the deprotected oligonucleotides were freeze-dried and labelled with 6-azidohexanoic acid NHS ester as explained in Section 8.4.1 – labelling oligonucleotides with azide.

8.3.3 Synthesis of 3′-alkyne oligonucleotides

3′-Alkyne oligonucleotides (Tabel 2.1, Chapter 2) were synthesized on the 1.0 μmol scale using 5′-*O*-(4,4′-dimethoxytrityl)-3′-*O*-propargyl-5-methyl-deoxycytidine on the solid support (22.4 or 23.7 μmol g^{-1} loading, AM polystyrene, Section 8.2.2.5) in a twist column (Glen Research). The required sequence was assembled in the 3′ to 5′-direction by the standard phosphoramidite oligonucleotide method. The oligonucleotides were then cleaved and deprotected by exposure to concentrated aqueous ammonia solution for 5 h at 55 °C, then purified by reversed-phase HPLC, and desalted on a NAP-10 sephadex column.

8.4 Oligonucleotide labelling

8.4.1 Labelling oligonucleotides with azide (3′-azide ODNs)

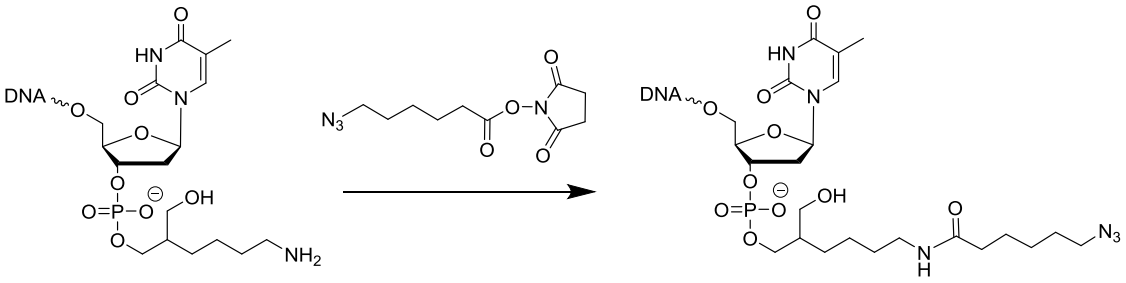

6-Azidohexanoic acid NHS ester (1 mg) was dissolved in DMSO (80 µL), and then be added post-synthetically to the 1.0 µmol freeze dried amino-modified oligonucleotide in 0.5 M Na_2CO_3/$NaHCO_3$ buffer (80 µL) at pH 8.75. After 4 h at room temperature, the labelled oligonucleotide was desalted using a NAP-10 sephadex column, and then purified by reversed-phase HPLC and desalted with a NAP-10 sephadex column as described above.

8.4.2 Labelling of oligonucleotides with DIBO alkyne (3′-DIBO ODNs)

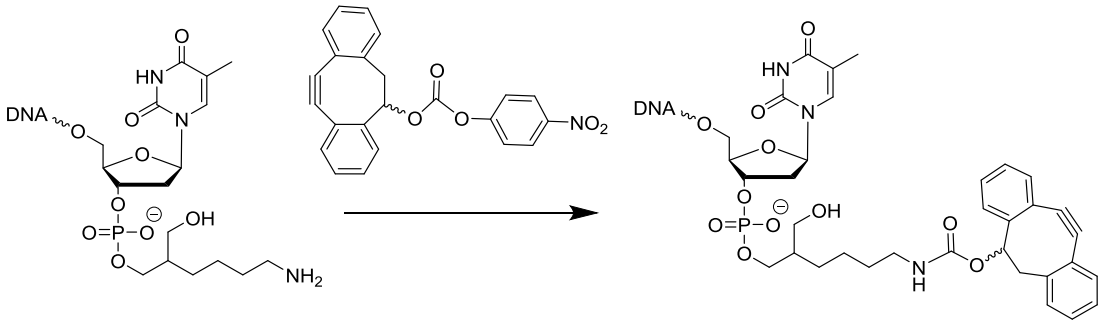

DIBO activated *p*-nitrophenyl carbonate (1 mg, provided by the Brown group) was dissolved in DMF (80 µL), and then be added post-synthetically to the 1.0 µmol freeze dried amino-modified oligonucleotide in 0.5 M Na_2CO_3/$NaHCO_3$ buffer (80 µL) at pH

8.75 and left for 4 h at 55 °C. The labelled oligonucleotide was desalted using a NAP-25 sephadex column, purified by reversed-phase HPLC, then desalted with a NAP-10 sephadex column as described above. In addition, 3-mer oligonucleotide (i.e. ODN3-1, Table 3.1, Chapter 3) was washed with DCM for 3 times.

8.4.3 Labelling oligonucleotides with click-easy BCN (3′-BCN ODNs)

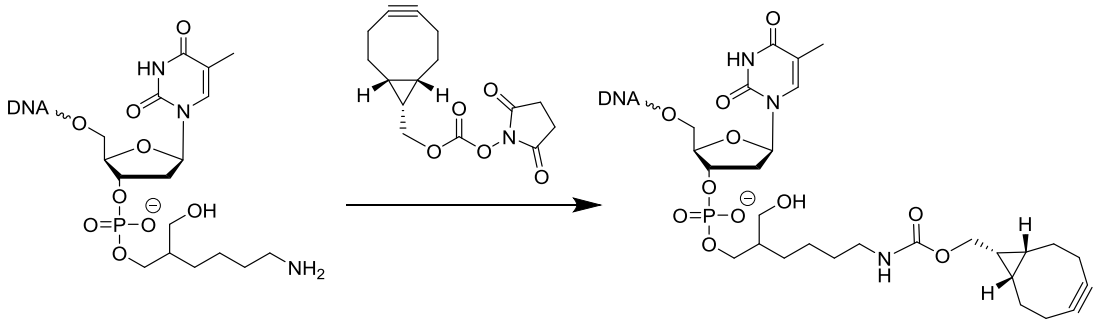

The click-easy BCN *N*-hydroxysuccinimide carbonate (1 mg) was dissolved in DMF (80 μL), and then be added post-synthetically to the freeze dried 1.0 μmol amino-modified oligonucleotide in 0.5 M Na_2CO_3/$NaHCO_3$ buffer (80 μL) at pH 8.75. After 4 h at 55 °C, the fully-labelled oligonucleotide was desalted using a NAP-25 sephadex column, and then purified by reversed-phase HPLC and desalted with a NAP-25 sephadex column as described above.

8.5 Click reaction

8.5.1 Oligonucleotide ligation on the solid phase (ODN2-12/2-13) by CuAAC

A solution of CuI click catalyst was prepared from tris(3-hydroxypropyltriazolylmethyl) amine ligand (THPTA, 1.2 μmol in H_2O, 5.2 μL), sodium ascorbate (1.6 μmol in H_2O,

3.2 μL) and $CuSO_4 \cdot 5H_2O$ (0.16 μmol in H_2O, 1.6 μL). The CuI solution was mixed with the 3′-alkyne oligonucleotide (ODN2-3, 3eq. or ODN2-4, 10eq.) in a mixture of H_2O (10 μL) and DMF (20 μL). The mixture was added to the azide oligonucleotide in the solid support (2 nmol). All CuAAC reactions were carried out in PCR tubes (250 μL, sealed with parafilm) and heated in a heating block at 40 °C for 21 h, 55 °C for 21 h or 70 °C for 7 h. After the click reaction, the solid support was washed with H_2O and acetonitrile (1 mL × 3), then dried by the passage of a stream of argon gas. The resultant ligated oligonucleotide was cleaved from the solid support, deprotected by treating with concentrated aqueous ammonia solution for 5 h at 55 °C in a sealed tube. The cleaved protecting groups were removed using a NAP-10 gel-filtration column (GE Healthcare). All ligated oligonucleotide products were analysed by reversed-phase HPLC and mass spectrometry.

8.5.2 Labelling with fluorescent dyes on the solid phase by CuAAC

A solution of CuI click catalyst was prepared from tris(3-hydroxypropyltriazolylmethyl) amine ligand (THPTA, 2.1 μmol for one addition, 35 eq.; 4.2 μmol for two additions, 70 eq.; both in H_2O, 5.2 μL), sodium ascorbate (3.0 μmol for one addition, 50 eq.; 6.0 μmol for two additions, 100 eq.; both in H_2O, 3.2 μL) and $CuSO_4 \cdot 5H_2O$ (0.3 μmol for one addition, 5 eq.; 0.6 μmol for one addition, 1.2 μmol for two additions, 10 eq., both in H_2O, 1.6 μL). The CuI solution was mixed with the fluorescent dye azide (0.6 μmol, 10 eq. for one addition; 0.9 μmol, 15 eq. for two additions) in 20 μL of DMSO. The mixture was added to the TO- or BO-modified oligonucleotide in the solid support (60 nmol). All CuAAC reactions were carried out in PCR tubes (250 μL, sealed with parafilm) and heated in a heating block at 55 °C for 4 h. After the click reaction, the solid support was washed

with H_2O and acetonitrile (1 mL × 3), then dried by the passage of a stream of argon gas. The resultant ligated oligonucleotide was cleaved from the solid support, deprotected by treating with concentrated aqueous ammonia solution for 4 h at room temperature in a sealed tube. All ligated oligonucleotide products were analysed by reversed-phase HPLC and mass spectrometry.

8.5.3 Oligonucleotide ligation on the solid phase (ODN3-16) by SPAAC

The 3′-azide oligonucleotide (ODN3-15) was dissolved in 20 μL of 10% pyridine/H_2O (pH 9.8) and added to the BCN oligonucleotide (ODN3-14) on the solid support (2 nmol). All SPAAC reactions were carried out in PCR tubes (250 μL, sealed with parafilm) and put in a heating block at 40 °C for 21 h. After the click reaction, the solid support was washed with H_2O and acetonitrile (1 mL × 3), and dried by the passage of a stream of argon gas. The resultant ligated oligonucleotide was cleaved from the solid support, then deprotected by treating with concentrated aqueous ammonia solution for 5 h at 55 °C in a sealed tube. The cleaved protecting groups were removed using a NAP-10 gel-filtration column (GE Healthcare). All the ligated oligonucleotide products were analysed by reversed-phase HPLC and mass spectrometry.

8.5.4 Multiple ligation on the solid phase (ODN3-21/3-22) by SPAAC

5′-BCN oligonucleotide (ODN3-14, Table 3.3, Chapter 3) was ligated to 3′-azide-5′-iodo oligonucleotide (ODN3-17/3-18) in 10% aq. pyridine (20 μL, pH 9.8) for 21 h at 40 °C, as explained above in Section 8.5.3. Next, to convert 5′-iodo to 5′-azido on the solid support, sodium azide (10 mg) was suspended in anhydrous DMF (0.5 mL), heated for 15 min at

70 °C then cooled down and transferred to 1.5 mL Eppendorf tube containing the washed 5′-iodo oligonucleotide on the solid support (ODN19a or ODN20a). The mixture was heated for 5 h at 55 °C then washed with DMF, H_2O and acetonitrile. This was followed by reacting of the 5′-azido oligonucleotides (ODN19b and ODN20b) with 3′-BCN oligonucleotide (ODN3-4) in 10% aq. pyridine (20 μL, pH 9.8) for 21 h at 40 °C, followed by washing and deprotection as explained above in Section 8.5.3.

8.5.5 Crosslink of triple-azide-labelled ODNs and dye-labelled BCN ODNs by SPAAC to form the fluorescent nanoconstructs (NS1–NS8)

To a solution of 2 nmol FAM-modified BCN oligonucleotide ODN4-20 (Table 4.4, Chapter 4) in 0.2 M NaCl (10 μL) was added the triple-azide-labelled oligonucleotide (2 nmol in 0.2 M NaCl, 70 μL). After 5 min, Cy3-modified BCN oligonucleotide ODN4-21 (2 nmol in 0.2 M NaCl, 10 μL) was added and the reaction was left for 5 min before adding Cy5-modified BCN oligonucleotide ODN4-22 (2 nmol in 0.2 M NaCl, 10 μL), the final concentration was 20 μM of each oligonucleotide. The reaction mixture was left at room temperature for a specified period of time (2 h) before adding formamide (100 μL) and loading directly onto a 15% polyacrylamide/7 M urea gel. It was electrophoresed at a constant power of 20 W for 2.5 h in 0.1 M TBE buffer. The gel-purified product was analysed and characterised by mass spectrometry. The same methods were used to synthesise other nanoconstructs. The reaction was repeated on a 5 nmol scale under the same conditions. The reaction mixture was left at room temperature for 2 h before desalting using NAP-10 column and purifying by HPLC as described above.

8.6 Biophysical studies

8.6.1 Extinction coefficient calcuation

Samples (TO3-N_3 and BO-N_3, Chapter 5 and Chapter 6) were prepared in MeOH and absorbance readings were recorded for 6 different concentrations at 20 °C. The starting concentration was prepared to give the absorbance reading below 1 and the other concentrations were prepared by subsequent dilution of the first one. Absorbance values were plotted against concentration and a straight line was drawn through the points intercepting the Y-axis at 0. The extinction coefficient was taken as the gradient of the line. Samples were analysed in 1 mL cuvette (Hellma Precision Cells made of Quartz SUPRASIL, 114B-QS, 1 cm pathlength) using a Cary 50 Bio UV-Vis spectrophotometer with a scan range of 200–800 nm.

The extinction coefficients were calculated according to the Beer-Lambert law:

$$\varepsilon = \frac{A}{c\,l}\ [M^{-1}cm^{-1}]$$

ε – extinction coefficient of the sample, **A** – absorbance of the sample at λ_{max}, **c** – concentration (M), **l** – pathlength (1 cm).

8.6.2 UV melting analysis

All the UV melting measurements were made on a Varian Cary 4000 UV-VIS spectrophotometer with Cary temperature controller. Cary Win UV Thermal software was used with an absorption wavelength of 260 nm. Samples were analysed in 1 mL cuvettes (Hellma synthetic quartz 'precision cell QG'; 1 cm pathlength) and were made to 1.25 μM oligonucleotide concentration (totally volume = 800 μL) in phosphate buffer (NaH_2PO_4,

10 mM) with a total of 200 mM NaCl at pH 7.34. The samples were initially denatured by heating to 85 °C at 10 °C min^{-1} then cooled to 16 °C at 1 °C min^{-1} and then maintaining at 16 °C for 2 min before heating to 85 °C at 1 °C min^{-1}. UV absorption was recorded every 0.5 °C. The melting temperature (T_m) values were derived from the derivatives of melting curves and calculated at 260 nm using Cary Win UV Thermal application software. Three successive melting curves were measured and averaged.

Table 8.1. The thermal protocol used was as follows:

Stage	**Data interval (°C)**	**Rate (°C min^{-1})**	**End Temp (°C)**	**Hold time (min)**
1 (Melt 1)	1.00	10.00	85.00	2.00
2 (Anneal 1)	0.50	1.00	16.00	2.00
3 (Melt 2)	0.50	1.00	85.00	2.00
4 (Anneal 2)	0.50	1.00	16.00	2.00
5 (Melt 3)	0.50	1.00	85.00	2.00
6 (Anneal 3)	0.50	1.00	16.00	2.00
7 (Melt 4)	0.50	1.00	85.00	2.00
8 (Anneal 4)	0.50	10.00	16.00	2.00

8.6.3 Fluorescence scan analysis

Fluorescence studies were performed on a Perkin Elmer LS50B luminescence spectrometer fitted with a Perkin Elmer PTP-1 Peltier temperature controller. FLWinlab TempScan software was used with settings of 600 nm min^{-1} scan speed. Optimum excitation wavelength, scan range wavelengths and excitation/emission slit width were used for each individual sample.

Table 8.2. Conditions for fluorescence scan analysis

	Start (nm)	**End (nm)**	**Excitation (nm)**	**Excitation slit**	**Emission Slit**	**Emission Read (nm)**
For DNA nanoconstructs (Chapter 4)						
FAM	500	800	495	4	5	
Cy3	550	800	550	4	5	
Cy5	650	800	650	4	5	
For Thiazole orange (Chapter 5)						
TO	515	750	510	6	7	530
TO/FAM	515	750	510	4	5	530
	495	750	490	4	5	530
TO/HEX	515	750	510	4	5	560
	540	750	536	4	5	560
TO/ROX	515	750	510	6	7	607
	585	750	585	6	7	607
TO/ATTO647N	515	750	510	6	7	665
	650	750	647	6	7	665
For Benzothiazole orange (Chapter 6)						
BO	460	750	453	6	7	479
BO/FAM	460	750	454	4	5	518
	500	750	492	4	5	518
BO/HEX	460	750	455	4	5	560
	545	750	540	4	5	560
BO/ROX	460	750	453	6	7	607
	590	750	586	6	7	607
BO/ATTO647N	460	750	452	6	7	665
	650	750	647	6	7	665

In cases where several samples were compared the slit width and excitation wavelength settings were kept constant (Table 8.2). Where multiple dyes were compared excitation wavelength was taken as the absorption maxima as specified in the experimental discussion.

The samples were prepared in phosphate buffer (NaH_2PO_4, 10 mM) with a total of 200 mM NaCl at pH 7.4, with labelled oligonucleotide concentration of 0.3 μM (0.36 μM for target strand). The oligonucleotide samples for duplexes were heated to 95 °C to denature for 5 min before being allowed to slowly cool to room temperature to anneal, and analysed in a 200 μL quartz cuvette (Hellma quartz 'SUPRASIL QS'; 200 μL volume, 1 cm pathlength) with a collection angle of 90°. The spectra are an average of three spectra.

8.6.4 Fluorescence melting analysis in a Roche LightCycler®

Fluorescence melting experiments were partly conducted on a Roche LightCycler® 1.5 instrument in LightCycler glass capillaries (20 μL volume) using Roche LightCycler Software Version 3.5. The LightCycler has one excitation source (488 nm) and three channels for recording fluorescence emission at 530 nm (F1), 640 nm (F2) and 705 (F3). The melting profiles for up to 32 samples could be recorded simultaneously. In a quick experiment the samples (0.5 μM, 20 μL) were first denatured by heating to 95 °C at a rate of 10.0 °C min^{-1}. The samples were then maintained at 95 °C for 2 min before annealing by cooling to 30 °C at 10.0 °C min^{-1}. They were held at 30 °C for a further 5 min and then melted by heating to 95 °C at 10.0 °C min^{-1}. The fluorescence melting curve data were converted to the first derivatives giving the melting peaks (-d(F)/dT where F is fluorescence and T is temperature in °C). Recordings were taken during both the melting steps as well as during annealing.

8.6.5 Polyacrylamide gel electrophoresis (PAGE)

For gel electrophoresis methods, 10 × TBE buffer was prepared by adding tris base (108 g), boric acid (55 g) and EDTA acid (9.3 g) to H_2O (1 L total volume) at pH 8.3. The buffer was stored at 4 °C in the dark.

For denaturing polyacrylamide gel electrophoresis (PAGE) oligonucleotide analysis and purification a 20% polyacrylamide gel was prepared. To acrylamide (35 mL of 40% acrylamide in H_2O, Fisher) and 10 × TBE buffer (7 mL) was added urea (29.4 g) and H_2O to a total volume of 70 mL. Immediately before loading the gel was cross-linked with *N,N,N′N′*-tetramethylethylene diamine (TEMED) (49 μL) and 10% ammonium persulfate (APS) (490 μL). The gel was loaded into glass plates in a vertical electrophoresis tank with 10 or 15 well comb and allowed to set. The comb was then removed and the gel pre-run in TBE buffer for 30 min at an applied wattage of 20 W. A reference dye mixture (xylene cyanol and bromophenol blue) was loaded into the first well. Oligonucleotide and reaction samples were prepared at a concentration of 0.2 M per sample in 100 μL (H_2O: formamide, 1:1). The gel was run for 3 h at a constant applied wattage of 20 W. The gel was then removed and imaged using a G:Box imaging system (Syngene) and GeneSnap (v7.08, Syngene) software. Fluorescent bands were imaged with transluminator darkroom lighting and EtBr/UV filter. UV active bands were imaged with Epi shortwave UV darkroom lighting and shortwave bandpass filter.

In cases of oligonucleotide purification, up to 5 OD of oligonucleotide was divided between 10 wells. Following separation required bands were removed from the gel with a surgical blade, crushed and suspended in H_2O (2 mL) then incubated with shaking at 37 °C for 16 h. The supernatant was removed, the volume increased to 2.5 mL (H_2O) and the oligonucleotide desalted with a NAP-25 gel filtration column (GE Healthcare). In an

alternative case a 15% denaturing gel was prepared by decreasing the volume of acrylamide and increasing the volume of H_2O.

8.6.6 Asymmetric polymerase chain reaction (PCR)

All PCR reaction samples were prepared under sterilised conditions in a LabCaire PCR workstation. Reactions were undertaken using a BioRad CFX96 Real-Time PCR Detection System, with CFX Manager software (BioRad) monitoring on FAM channel (excitation range 450–490 nm, detector range 510–530 nm), HEX channel (excitation range 515–535 nm, detector range 560–580 nm), ROX channel (excitation range 560–590 nm, detector range 610–650 nm) and Cy5 channel (excitation range 620–650 nm, detector range 675–690 nm).

A negative control sample with no template was prepared for each PRC reaction. Reactions were run in 0.2 mL low-profile white 8-tube strips with optically clear lids (BioRad). Sample preparation and thermal protocols differed for each PCR probe using different polymerases as detailed below.

Asymmetric PCR - GoTaq® DNA polymerase or KOD XL DNA polymerase

Sample conditions:

Template: 10 ng per sample (WT, MT, Table 5.12, Chapter 5)

Forward primer: 0.05 μM

Reverse primer: 0.5 μM

Probe (wild-type and mutant): 0.5 μM L1-(TO3/ROX)2, L7-(TO3/FAM-C6)2, L7-(TO3/HEX)2, L7-(TO3/ATTO)2, L1-(BO3/FAM-C3)2, L7-(BO3/HEX)2, L1-(BO3/ROX)2, L7-(BO3/ATTO)2.

Buffer and DNA polymerase: 5 × Colorless GoTaq® Reaction buffer: 4 μL, 1 unit of GoTaq® DNA polymerase or 10 × PCR buffer for KOD XL DNA Polymerase: 2 μL, 0.5 unit of KOD XL DNA polymerase

500 μM each dNTP

Total volume: 20 μL

Amplification was performed on a real-time PCR instrument (Bio-Rad CFX96) using the following procedure: an initial denaturing at 95 °C for 2 min, followed by 30 cycles of denaturing at 95 °C for 30 sec, primer annealing at 53 °C for 30 sec, and extension at 72 °C for 30 sec. Further extension was carried out at 72 °C for 5 min. This was followed by melting experiments involving heating the amplification mixture to 95 °C for 30 sec, cooling to 30 °C, then increasing the temperature at 1 °C sec^{-1} to 95 °C and holding at each temperature for 5 sec.

Appendix

Appendix

9.1 Oligonucleotide data

Figure 9.1.1. Oligonucleotide mass spectra data; sequence discussed in Chapter 2

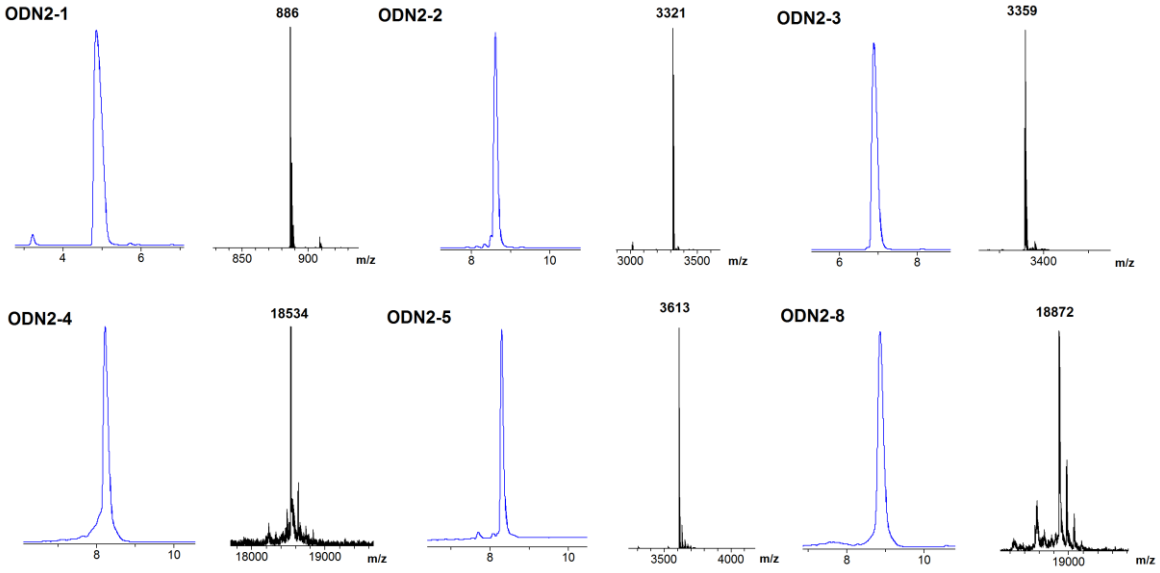

Figure 9.1.2. Oligonucleotide mass spectra data; sequence discussed in Chapter 3

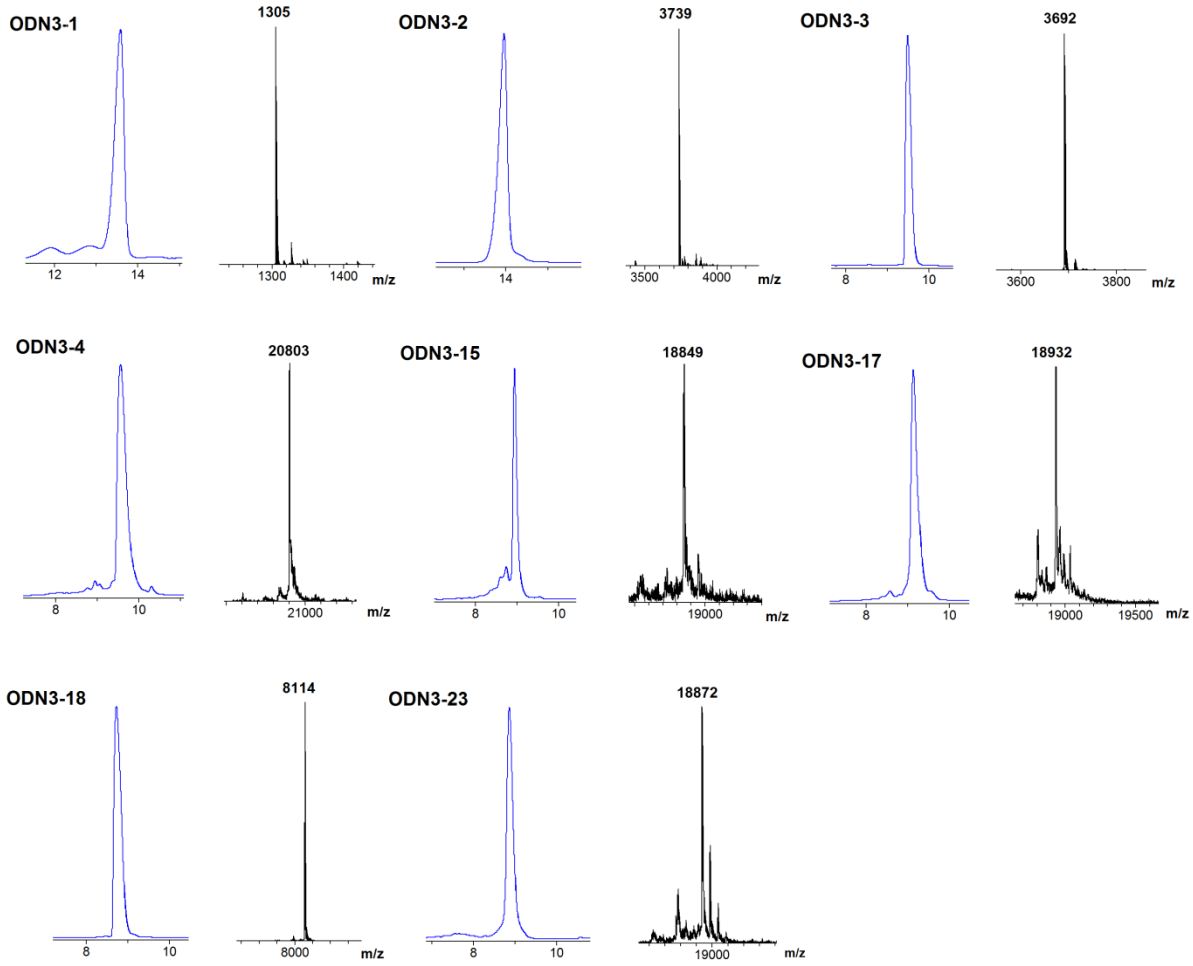

Figure 9.1.3. Oligonucleotide mass spectra data; sequence discussed in Chapter 4

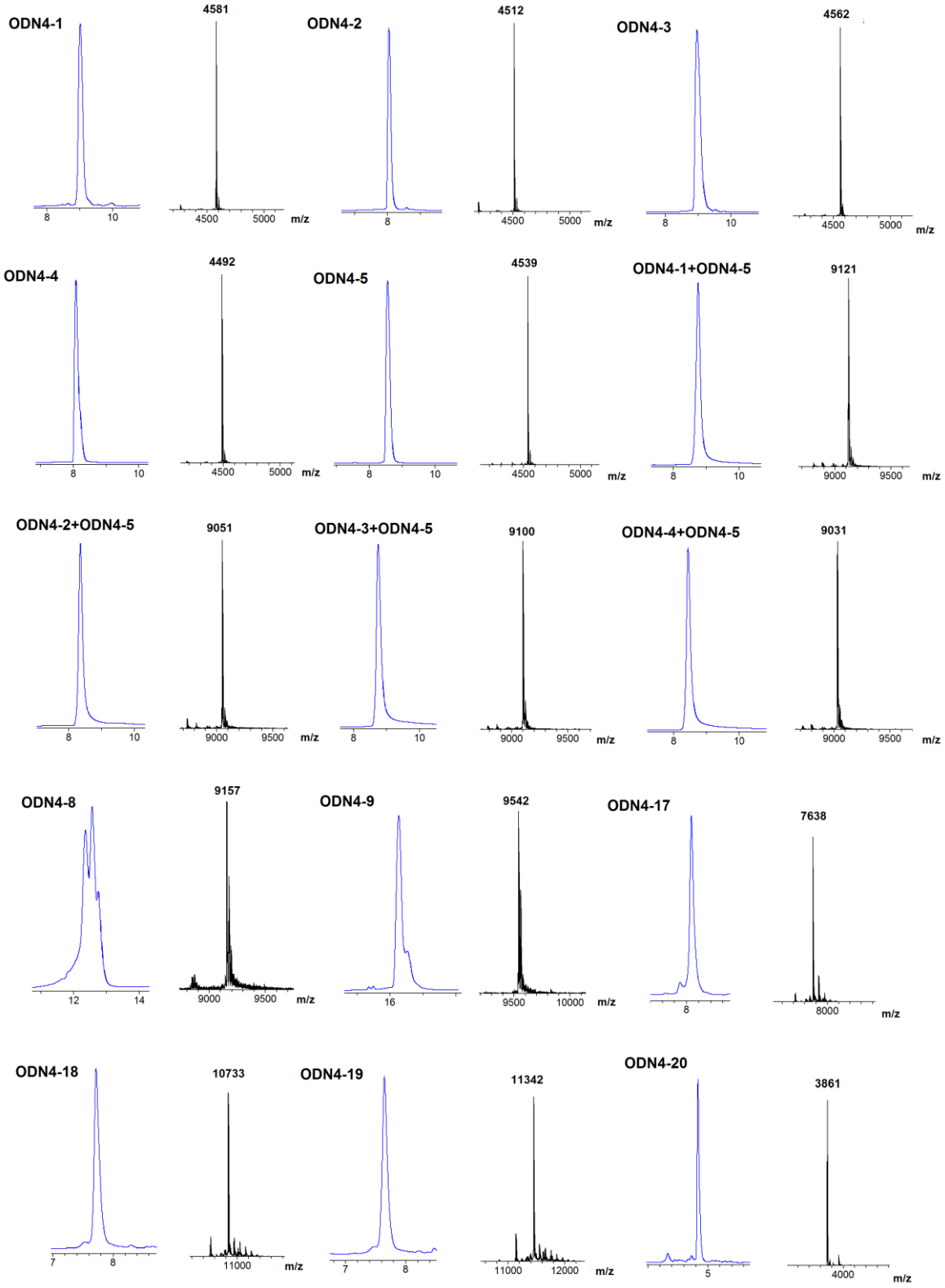

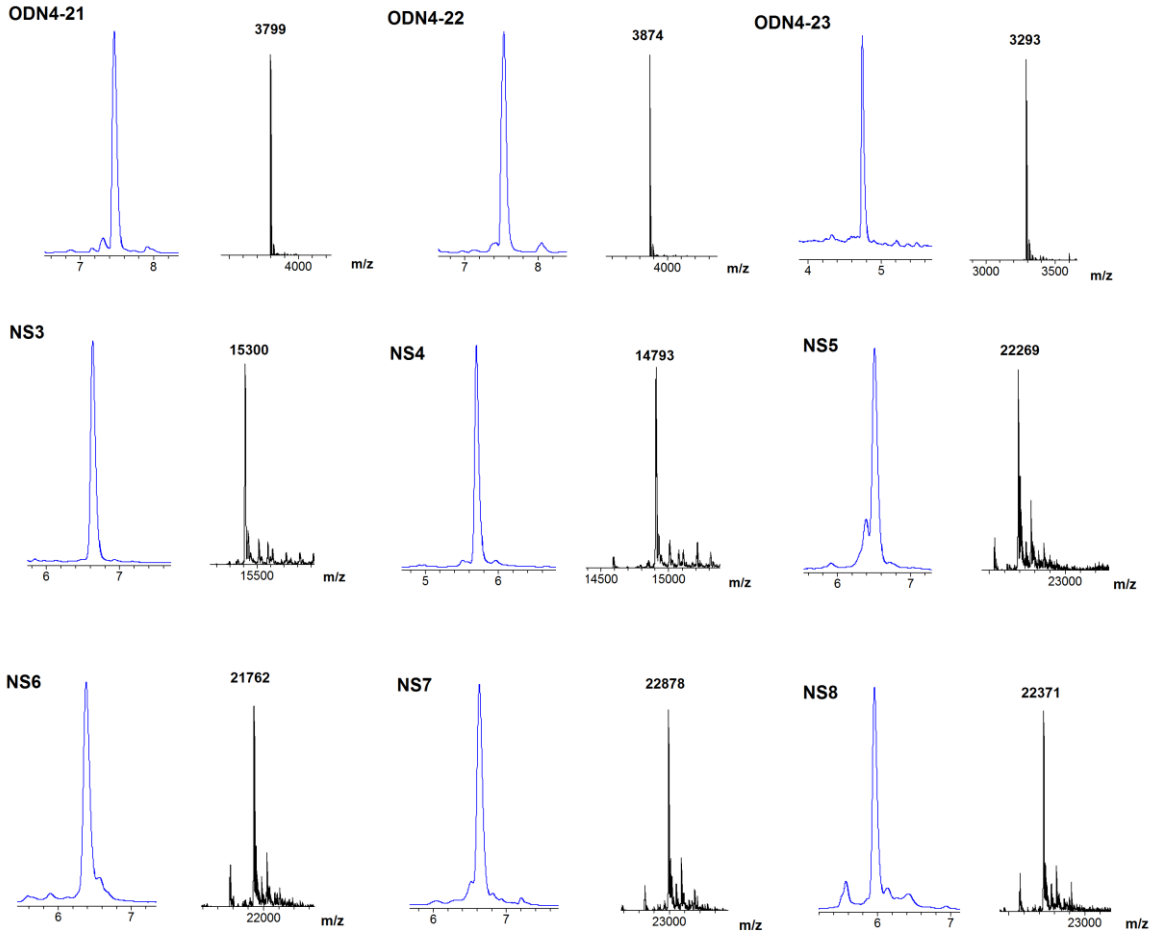
ODN4-21
3799
ODN4-22
3874
ODN4-23
3293
NS3
15300
NS4
14793
NS5
22269
NS6
21762
NS7
22878
NS8
22371
m/z

Figure 9.1.4. Oligonucleotide mass spectra data; sequence discussed in Chapter 5

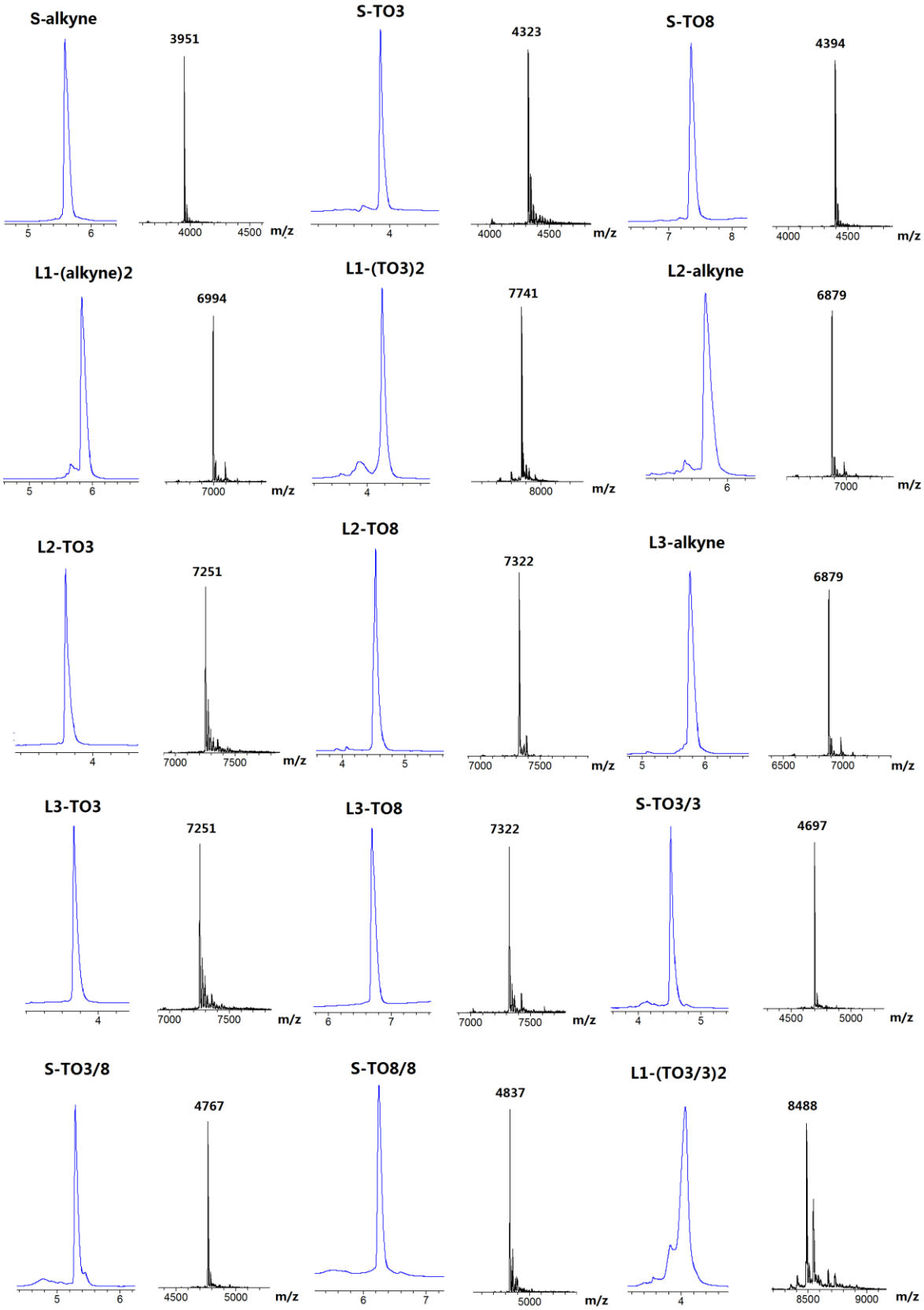

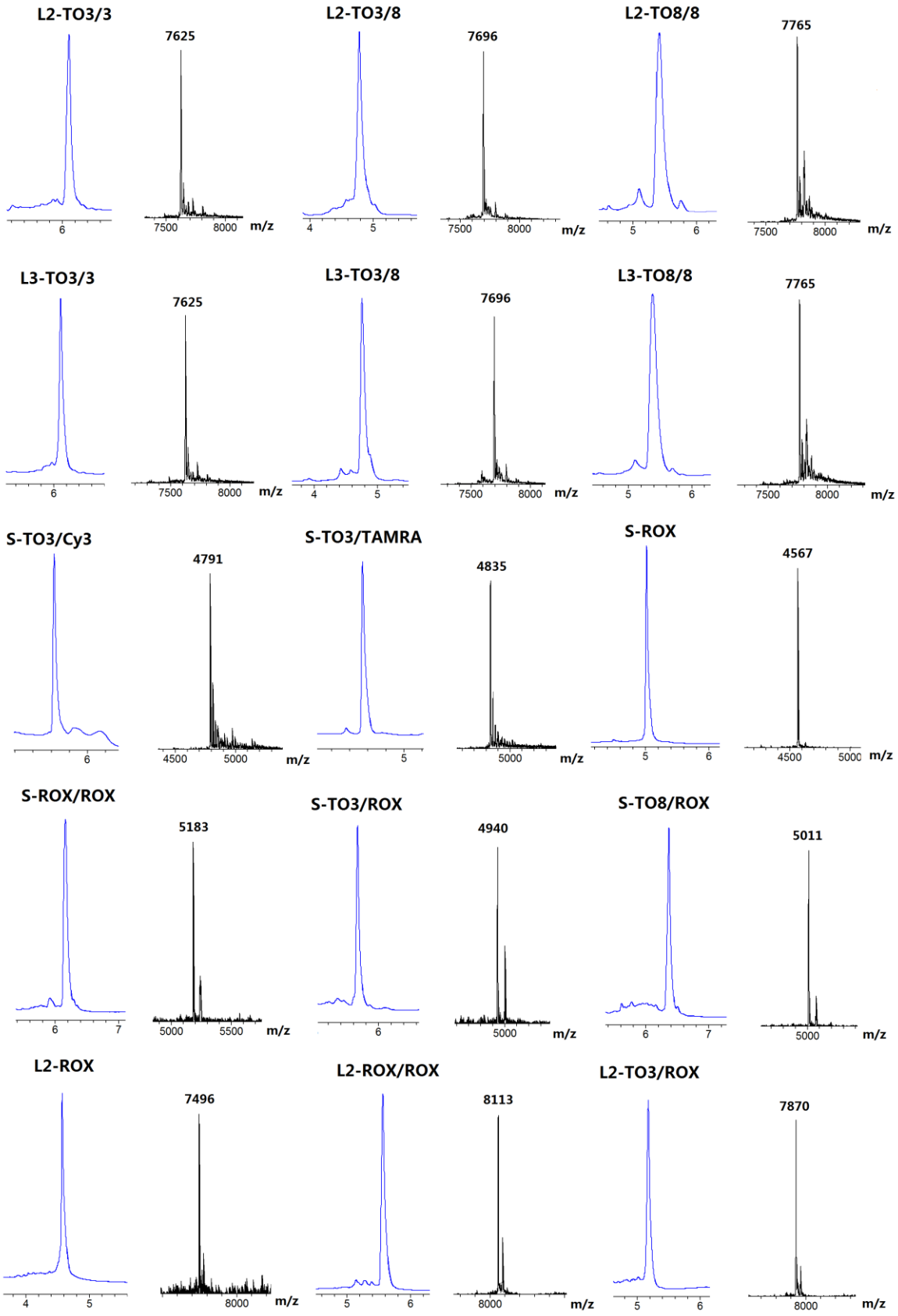
L2-TO3/3
7625
L2-TO3/8
7696
L2-TO8/8
7765
L3-TO3/3
7625
L3-TO3/8
7696
L3-TO8/8
7765
S-TO3/Cy3
4791
S-TO3/TAMRA
4835
S-ROX
4567
S-ROX/ROX
5183
S-TO3/ROX
4940
S-TO8/ROX
5011
L2-ROX
7496
L2-ROX/ROX
8113
L2-TO3/ROX
7870
m/z

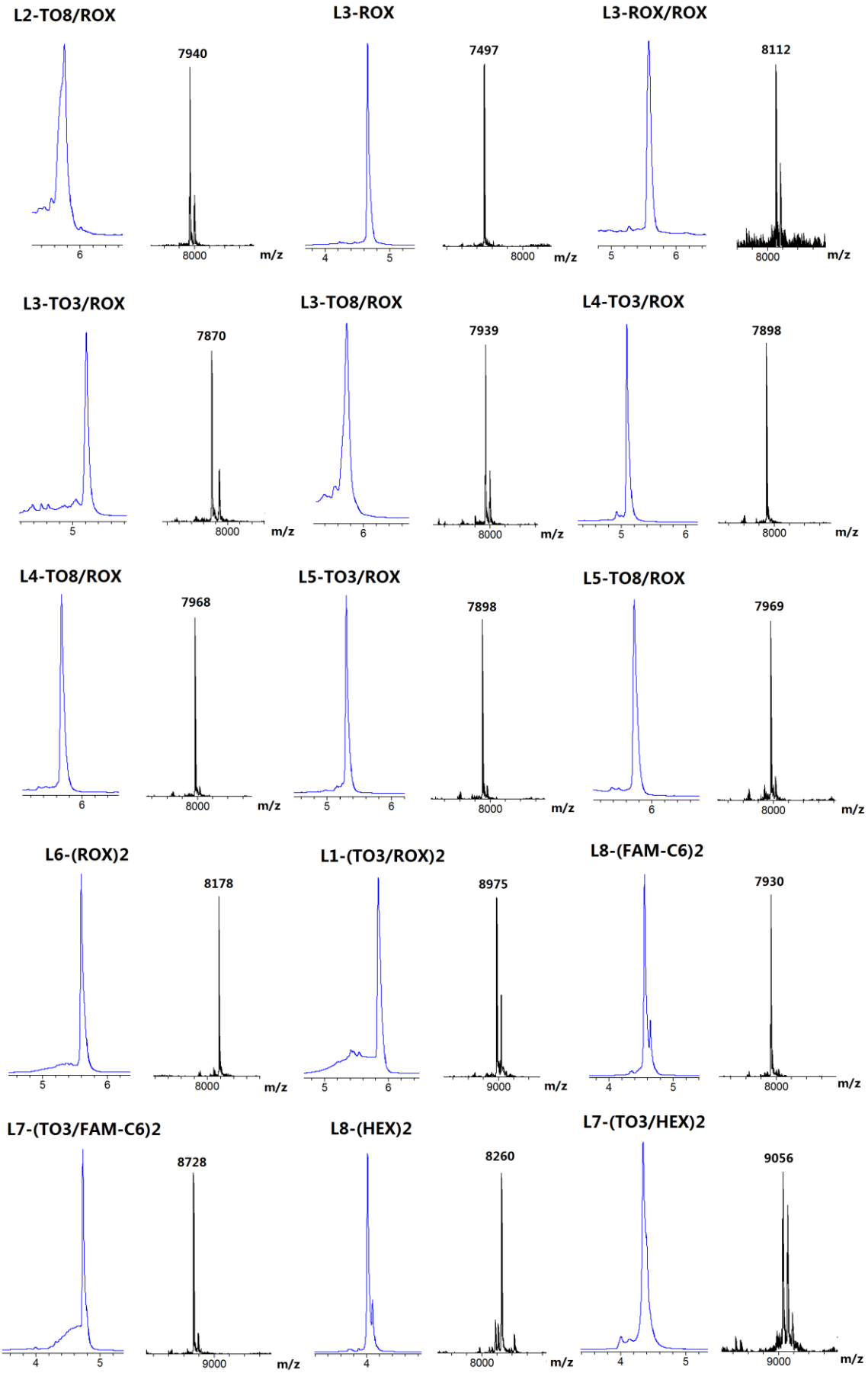
L2-TO8/ROX
7940
L3-ROX
7497
L3-ROX/ROX
8112
L3-TO3/ROX
7870
L3-TO8/ROX
7939
L4-TO3/ROX
7898
L4-TO8/ROX
7968
L5-TO3/ROX
7898
L5-TO8/ROX
7969
L6-(ROX)2
8178
L1-(TO3/ROX)2
8975
L8-(FAM-C6)2
7930
L7-(TO3/FAM-C6)2
8728
L8-(HEX)2
8260
L7-(TO3/HEX)2
9056
m/z

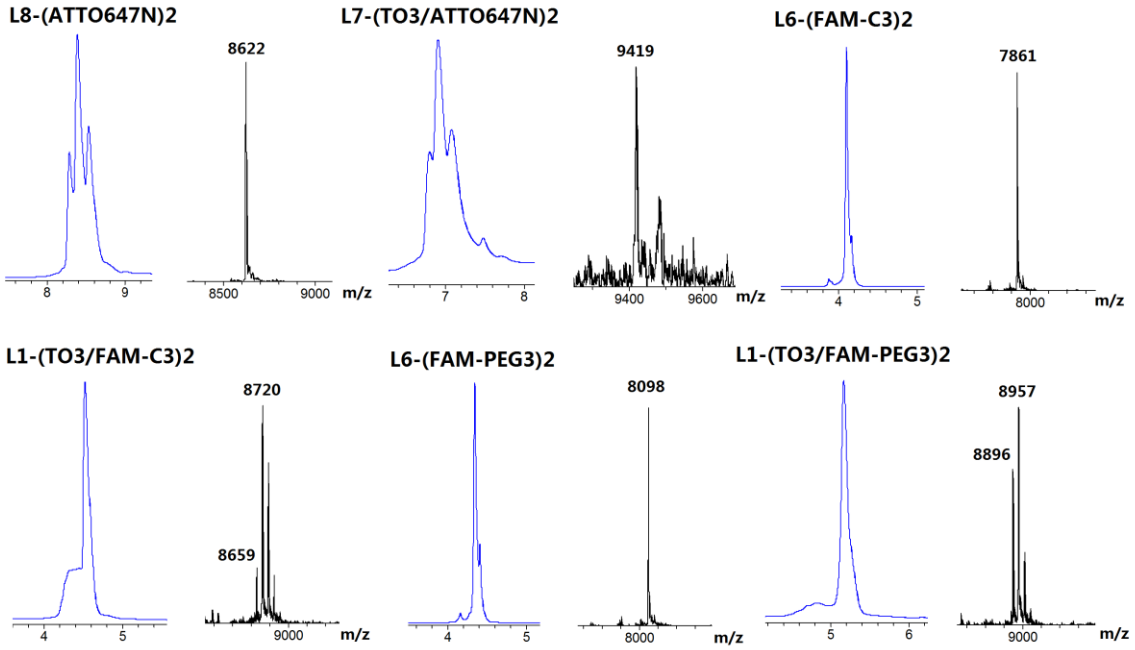
L8-(ATTO647N)2
8622
8
9
8500
9000
m/z
L7-(TO3/ATTO647N)2
9419
7
8
9400
9600
m/z
L6-(FAM-C3)2
7861
4
5
8000
m/z
L1-(TO3/FAM-C3)2
8720
8659
4
5
9000
m/z
L6-(FAM-PEG3)2
8098
4
5
8000
m/z
L1-(TO3/FAM-PEG3)2
8957
8896
5
6
9000
m/z

Figure 9.1.5. Oligonucleotide mass spectra data; sequence discussed in Chapter 6

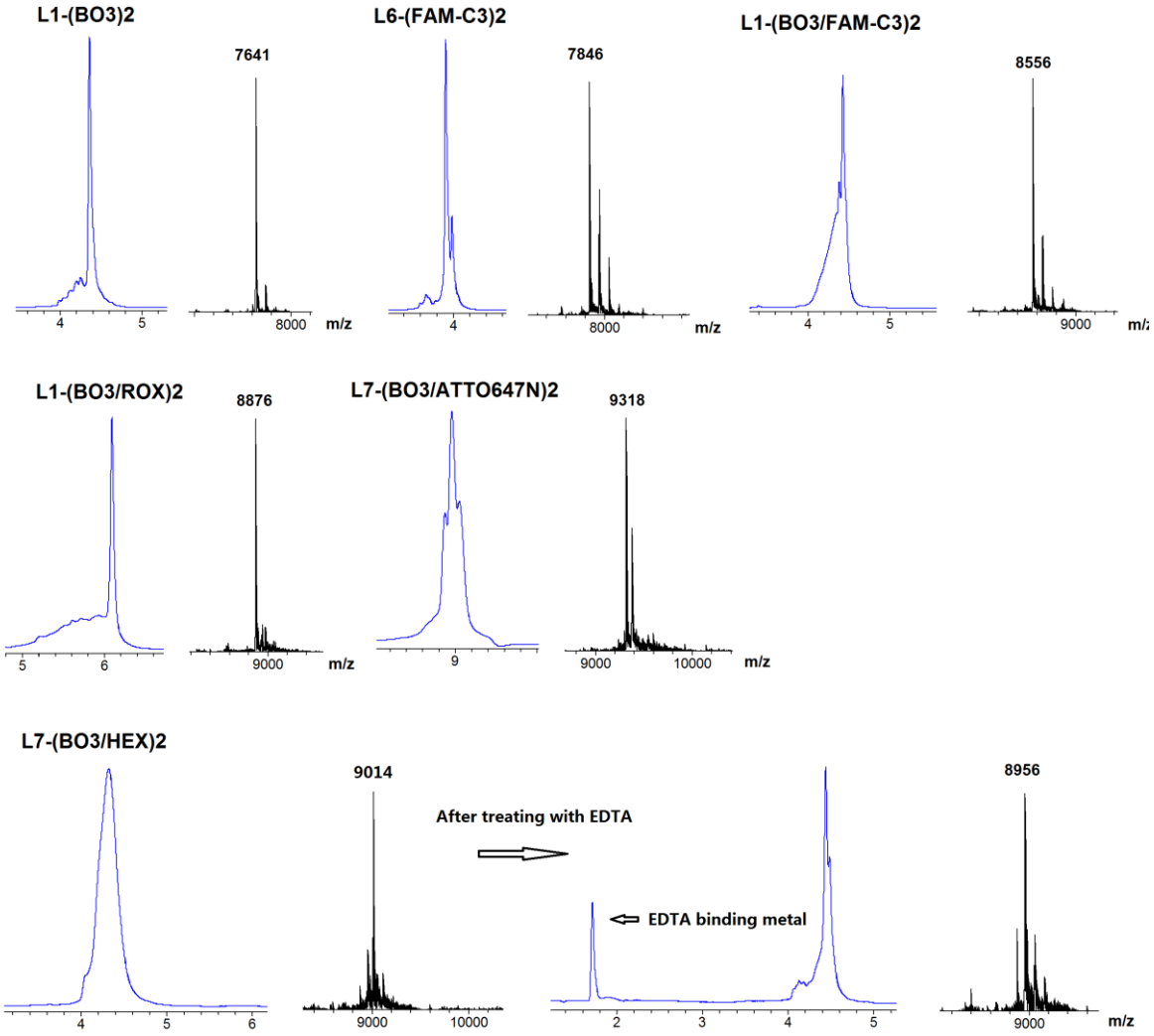

9.2 Polyacrylamide gel electrophoresis (PAGE) analysis

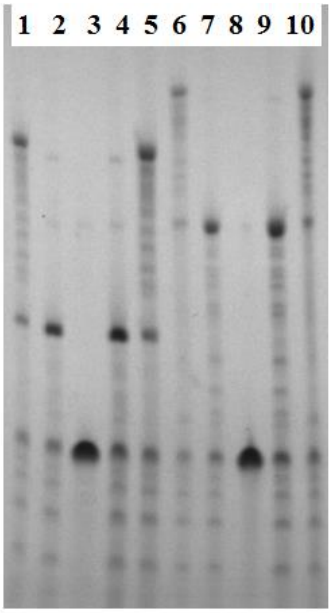

Figure 9.2.1. Denaturing PAGE analysis of crude SPAAC ligated products (all reactions were carried out in H_2O). The crude click ligation reaction mixture were analysed by 6% polyacrylamide/7 M urea gel electrophoresis at a constant power of 20 w for 1.5 h, using 1 × TBE buffer. Lane1: ODN3-22 (151-mer, 0.4 OD); lane2: ODN3-20b (85-mer, 0.4 OD); lane3: ODN3-14 (60-mer, 0.4 OD); lane4: ODN3-20b (85-mer, 0.8 OD); lane5: ODN3-22 (151-mer, 0.8 OD); lane6: ODN3-21 (186-mer, 0.4 OD); lane7: ODN3-19b (120-mer, 0.4 OD); lane8: ODN3-14 (60-mer, 0.4 OD); lane9: ODN3-19b (120-mer, 0.8 OD); lane10: ODN3-21 (186-mer, 0.8 OD).

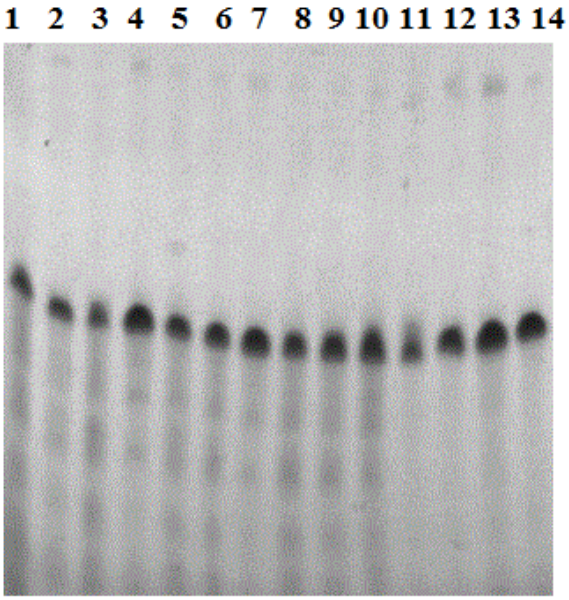

Figure 9.2.2. Denaturing PAGE analysis of starting material ODN3-14 treating with different solvents. The crude samples were analysed by 6% polyacrylamide/7 M urea gel electrophoresis at a constant power of 20 w for 1.5 h, using 1 × TBE buffer. Lane1: H_2O; lane2: 50% aq. MeCN; lane3: 50% aq. DMF; lane4: phosphate buffer (NaH_2PO_4, 10 mM; NaCl, 200 mM), pH 7.0; lane5: 50% MeCN/phosphate buffer, pH 7.0; lane6: 50% DMF/phosphate buffer, pH 7.0; lane7: phosphate buffer, pH 8.0; lane8: 50% MeCN/phosphate buffer, pH 8.0; lane9: 50% DMF/phosphate buffer, pH 8.0; lane10: 0.2M NaCl; lane11: 5% aq. TEA; lane12: 10% aq. TEA; lane13: 5% aq. pyridine; lane14: 10% aq. pyridine.

9.3 UV melting analysis

Schematic diagram	Duplexes	T_m (^oC)	ΔT_m (^oC)
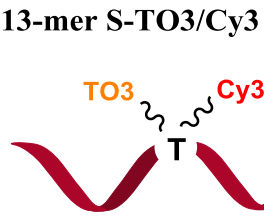	S-TO3/Cy3-ds (AT)	48.5	
	S-TO3/Cy3-3′-T	46.3	– 2.2
	S-TO3/Cy3-5′-T	43.3	– 5.2
	S-TO3/Cy3-3′-C	43.6	– 4.9
	S-TO3/Cy3-5′-C	43.9	– 4.6
	S-TO3/Cy3-CT-mis	39.4	– 9.1
	S-TO3/Cy3-TT-mis	42.5	– 6.0
	S-TO3/Cy3-GT-mis	42.0	– 6.5

Table 9.3.1. UV melting of S-TO3/Cy3 hybrided with mismatched or bulged DNA. T_m: melting temperature; ΔT_m: difference in melting temperature of S-TO3/Cy3 with mismatch sequences or bulges (an unpaired nucleobase more) compared to the complementary duplex (S-TO3/Cy3-ds). T_m values are the average of 3 separate melting and annealing curves. Melting temperatures are accurate to ± 0. 1 ^oC.

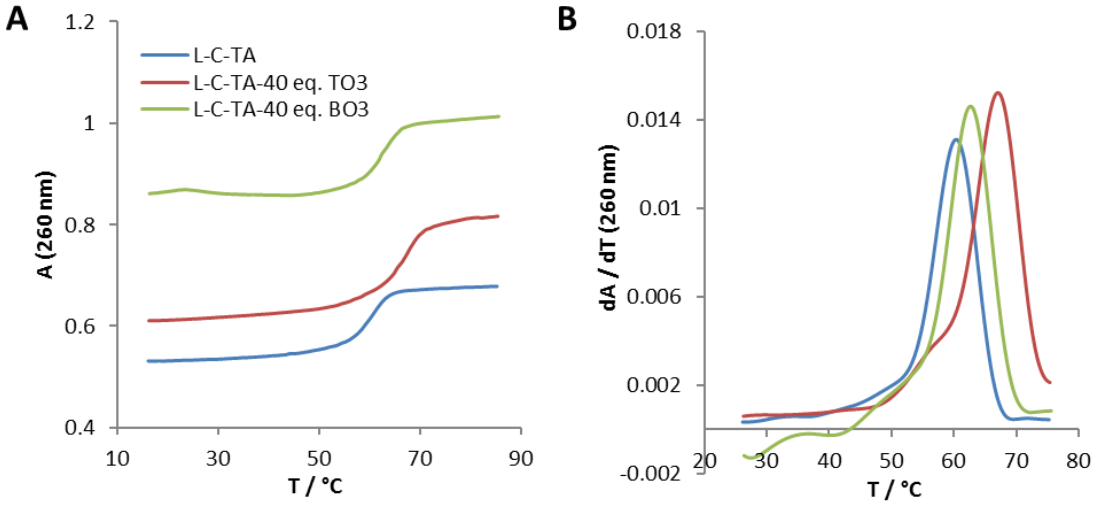

Figure 9.3.1. A: Representative UV melting curves and B: their derivatives for ODNs with the addition of unattached TO3-N3 and BO3-N3 intercalator dyes. Blue: unmodified duplex (L-C-TA-ds) as a control; red: duplex after addition of 40 eq. of TO3; green: duplex after addition of 40 eq. of BO3.

9.4 Room temperature fluorescence emission

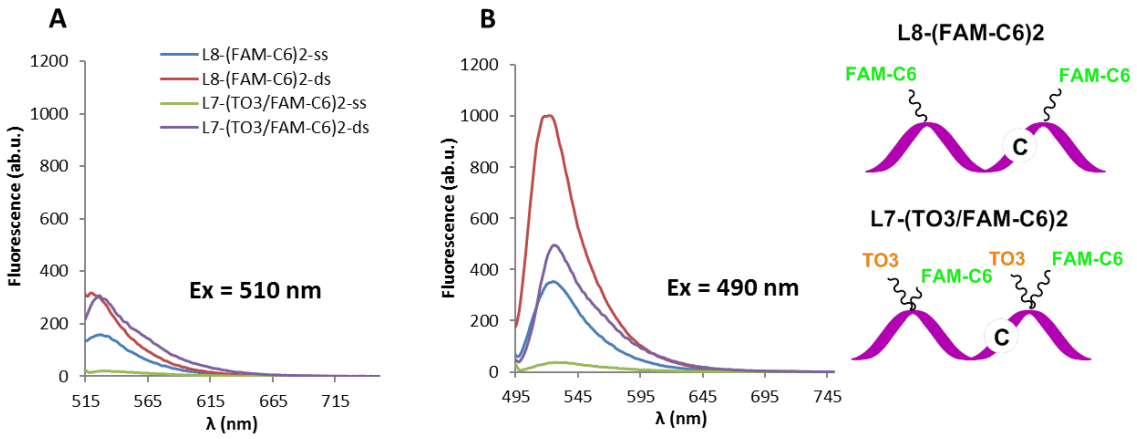

Figure 9.4.1. Comparison of room temperature steady state emission of the 22-mer probe L7-(TO3/FAM-C6)2 and its control HyBeacon probe L8-(FAM-C6)2. A: λ_{ex} = 510 nm (the excitation maximum of TO3); B: λ_{ex} = 490 nm (the excitation maximum of FAM-C6). The C in the schematic diagram highlights the position of this mutation to be detected relative to the positions of the fluorophores; ab.u .= arbitrary unit.

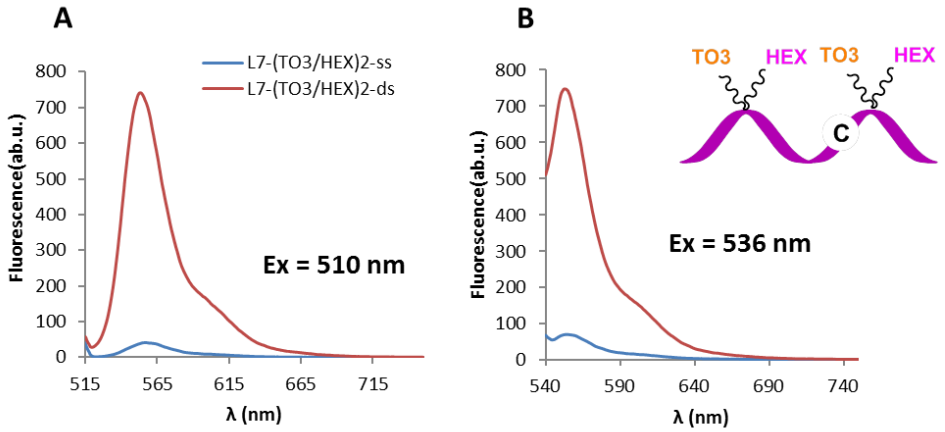

Figure 9.4.2. Room temperature steady state emission of the 22-mer probe L7-(TO3/HEX)2. A: λ_{ex} = 510 nm (the excitation maximum of TO3); B: λ_{ex} = 536 nm (the excitation maximum of HEX). The C in the schematic diagram highlights the position of this mutation to be detected relative to the positions of the fluorophores; ab.u .= arbitrary unit.

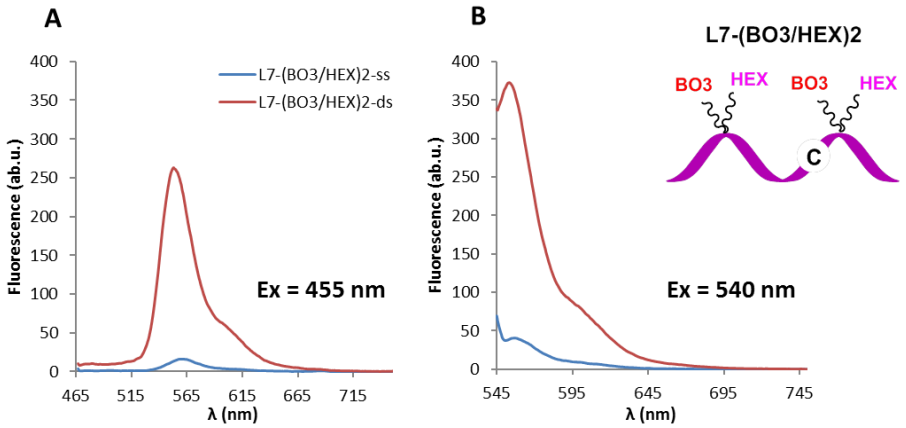

Figure 9.4.3. Room temperature steady state emission of the 22-mer probe L7-(BO3/HEX)2 in the single-stranded (ss) and double-stranded (ds) states. A: λ_{ex} = 455 nm (the excitation maximum of BO3); B: λ_{ex} = 540 nm (the excitation maximum of HEX). The C in the schematic diagram highlights the position of this mutation to be detected relative to the positions of the fluorophores; ab.u .= arbitrary unit.

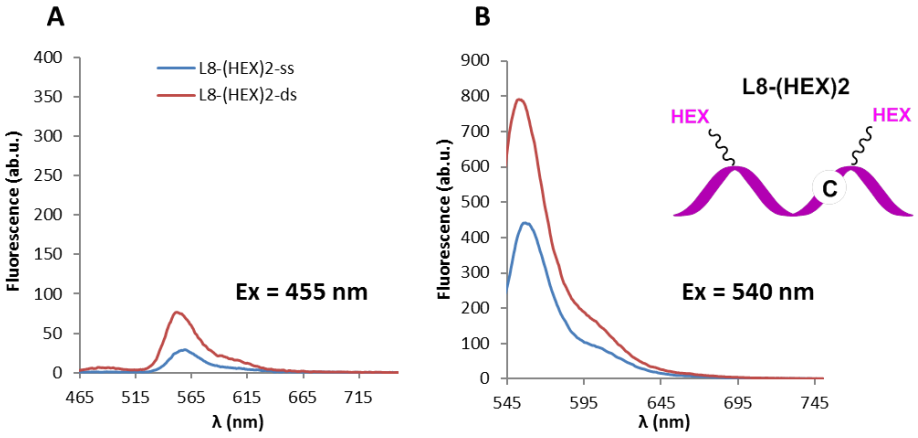

Figure 9.4.4. Room temperature steady state emission of the 22-mer control HyBeacon probe L7-(HEX)2 in the single-stranded (ss) and double-stranded (ds) states. A: λ_{ex} = 455 nm (the excitation maximum of BO3); B: λ_{ex} = 540 nm (the excitation maximum of HEX). The C in the schematic diagram highlights the position of this mutation to be detected relative to the positions of the fluorophores; ab.u .= arbitrary unit.

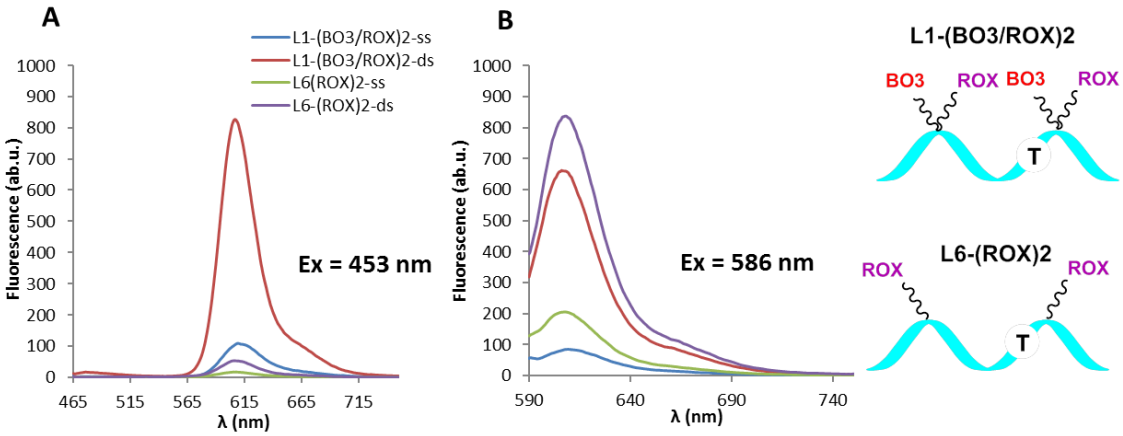

Figure 9.4.5. Comparison of room temperature steady state emission of the 22-mer probe L1-(BO3/ROX)2 and its control HyBeacon probe L6-(ROX)2. A: λ_{ex} = 453 nm (the excitation maximum of BO3); B: λ_{ex} = 586 nm (the excitation maximum of ROX). The T in the schematic diagram highlights the position of this mutation to be detected relative to the positions of the fluorophores; ab.u .= arbitrary unit.

9.5 Fluorescence melting studies in a Roche LightCycler®

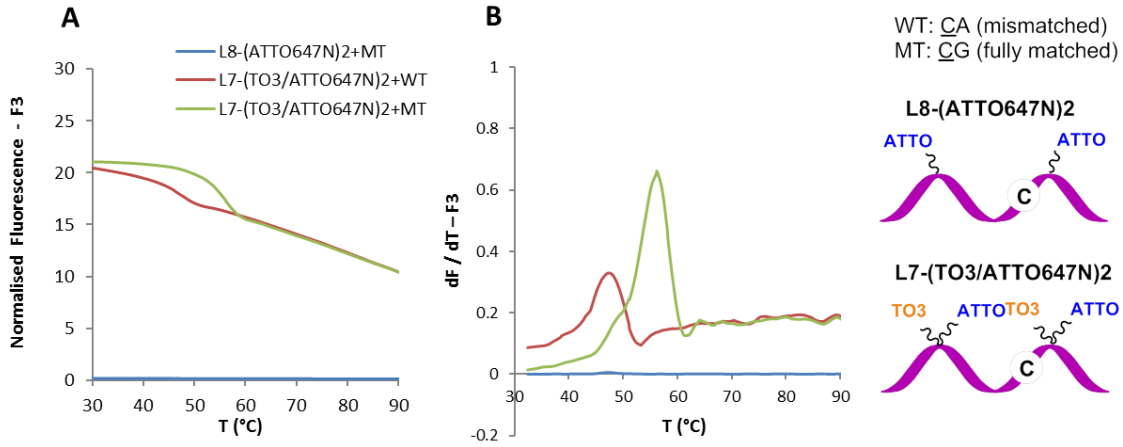

Figure 9.5.1. A: melting curves and B: melting derivatives of the 22-mer probe L7-(TO3/ATTO647N)2 and its control HyBeacon probe L8-(ATTO647N)2, based on fluorescence emission at 705 nm (F3) of the Roche LightCycler®. The C in the schematic diagram highlights the position of this mutation to be detected relative to the positions of the fluorophores.

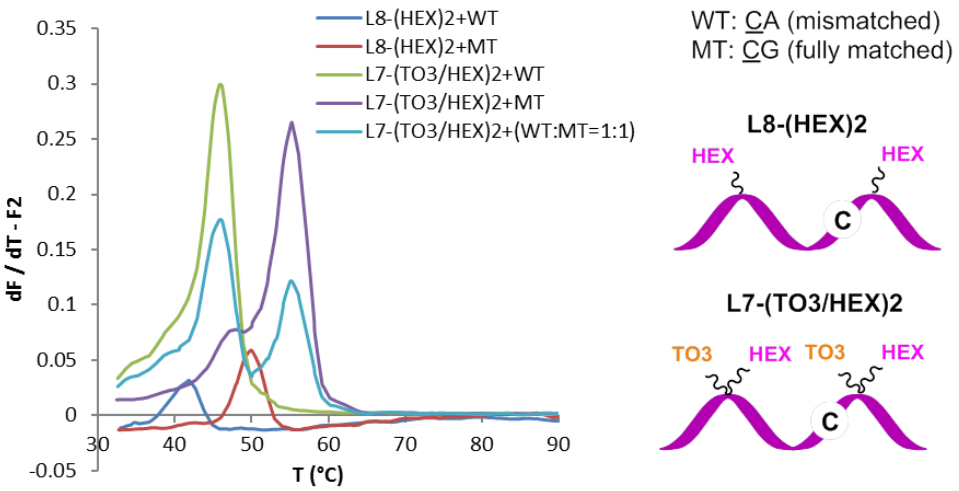

Figure 9.5.2. Melting derivatives of the 22-mer probe L7-(TO3/HEX)2 and its control HyBeacon probe L8-(HEX)2, based on fluorescence emission at 640 nm (F2) of the Roche LightCycler®. The C in the schematic diagram highlights the position of this mutation to be detected relative to the positions of the fluorophores.

9.6 Fluorescence melting studies of TO-, BO-modified probes in real-time PCR

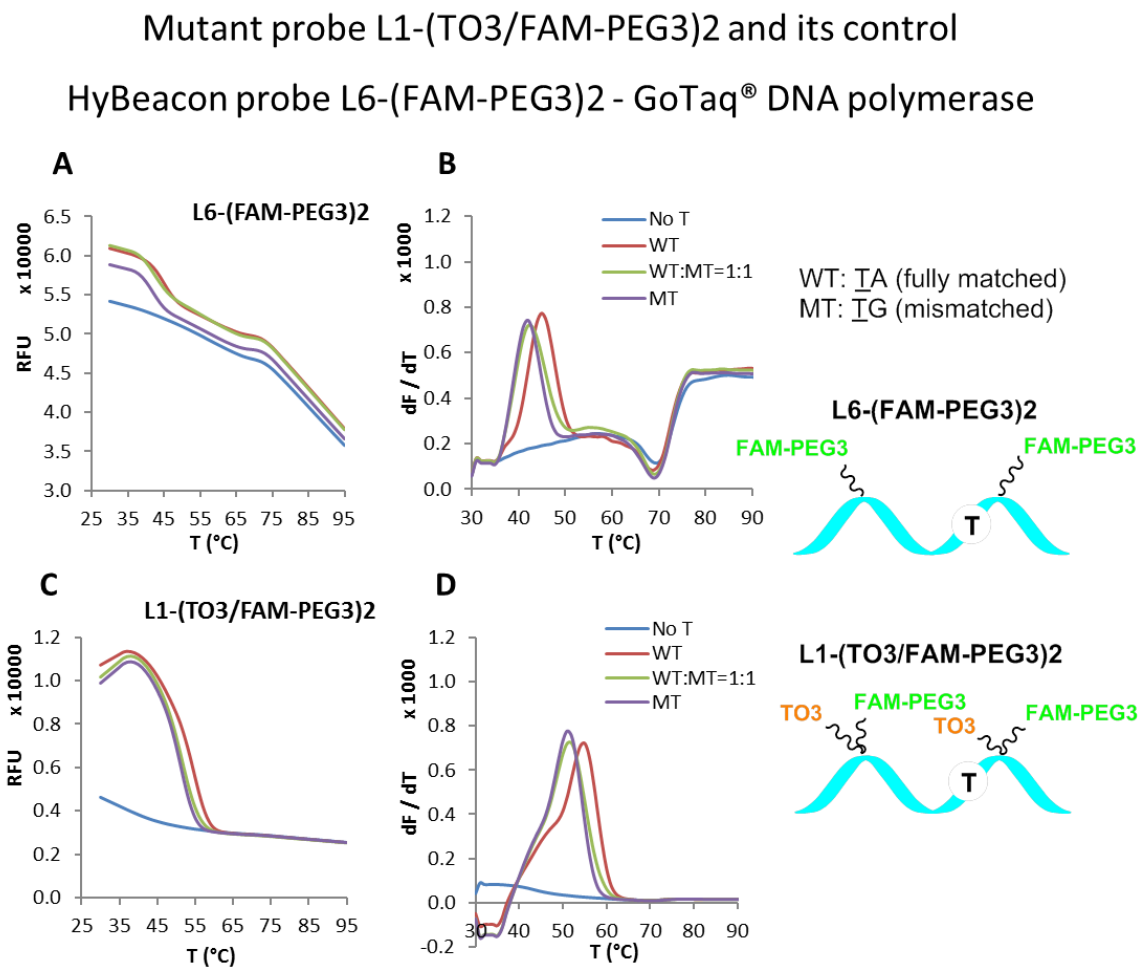

Figure 9.6.1. Fluorescence melting curves (A, C) and derivatives of post-amplification fluorescence melts (B, D) using the wild-type probe L1-(TO3/FAM-PEG3)2 (C, D) and its control HyBeacon probe L6-(FAM-PEG3)2 (A, B). Blue (No T): no template; red (WT): wild-type template; green (WT:MT = 1:1): wild-type template: mutant template, ratio = 1:1; purple (MT): mutant template. All output was monitored in the FAM channel of the CFX96™ real-time PCR instrument (excitation range 450–490 nm, detector range 510–530 nm). GoTaq® DNA polymerase, 30 cycles and 1 ng of template ODNs were used. Note: L1-(TO3/FAM-PEG3)2 is a wild-type probe that gives a fully matched duplex upon hybridization with wild-type template (WT), and forms a TG-mismatched duplex when pairs with mutant template (MT). The T in the schematic diagram highlights the position of this mutation to be detected relative to the positions of the fluorophores.

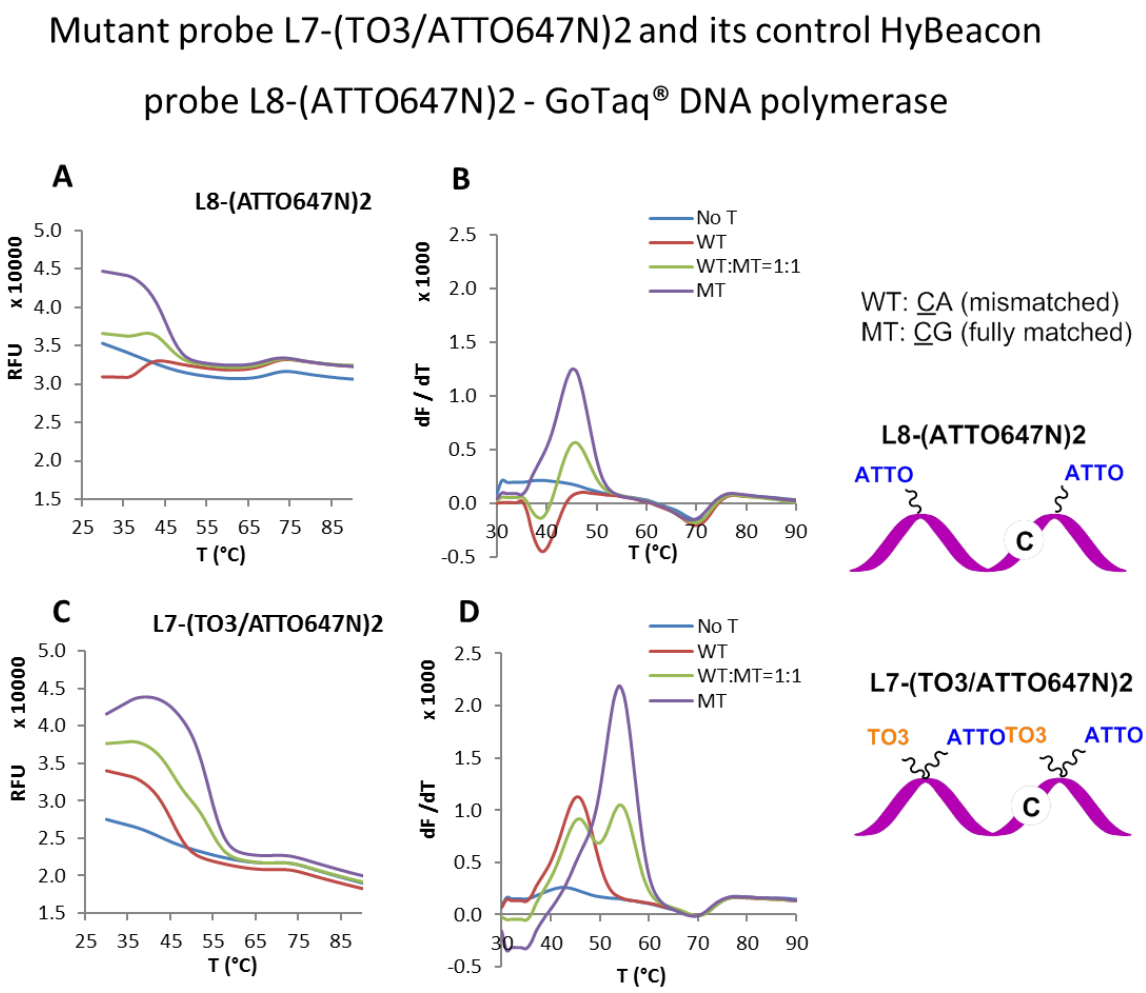

Figure 9.6.2. Fluorescence melting curves (A, C) and derivatives of post-amplification fluorescence melts (B, D) using the mutant probe L7-(TO3/ATTO647N)2 (C, D) and its control HyBeacon probe L8-(ATTO647N)2 (A, B). Blue (No T): no template; red (WT): wild-type template; green (WT:MT = 1:1): wild-type template: mutant template, ratio = 1:1; purple (MT): mutant template. All output was monitored in the Cy5 channel of the CFX96™ real-time PCR instrument (excitation range 620–650 nm, detector range 675–690 nm). GoTaq® DNA polymerase, 30 cycles and 1 ng of template ODNs were used. Note: L7-(TO3/ATTO647N)2 is a mutant probe that gives a CA-mismatched duplex upon hybridization with wild-type template (WT), and forms a fully matched duplex when pairs with mutant template (MT). The C in the schematic diagram highlights the position of this mutation to be detected relative to the positions of the fluorophores.

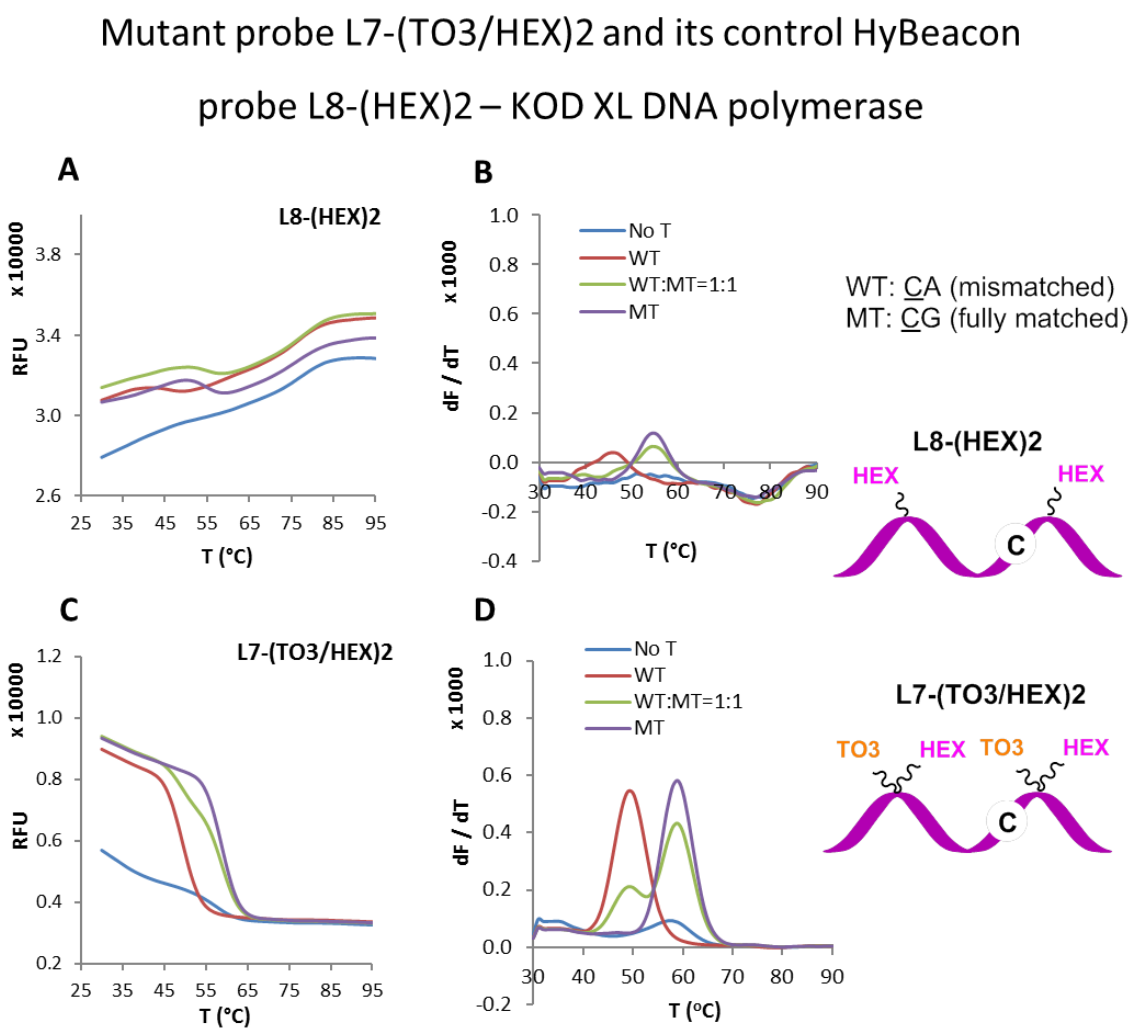

Figure 9.6.3. Fluorescence melting curves (A, C) and derivatives of post-amplification fluorescence melts (B, D) using the mutant probe L7-(TO3/HEX)2 (C, D) and its control HyBeacon probe L8-(HEX)2 (A, B). Blue (No T): no template; red (WT): wild-type template; green (WT:MT = 1:1): wild-type template: mutant template, ratio = 1:1; purple (MT): mutant template. All output was monitored in the HEX channel of the CFX96^{TM} real-time PCR instrument (excitation range 515–535 nm, detector range 560–580 nm). KOD XL DNA polymerase, 20 cycles and 1 ng of template ODNs were used. Note: L7-(TO3/HEX)2 is a mutant probe that gives a CA-mismatched duplex upon hybridization with wild-type template (WT), and forms a fully matched duplex when pairs with mutant template (MT). The C in the schematic diagram highlights the position of this mutation to be detected relative to the positions of the fluorophores.

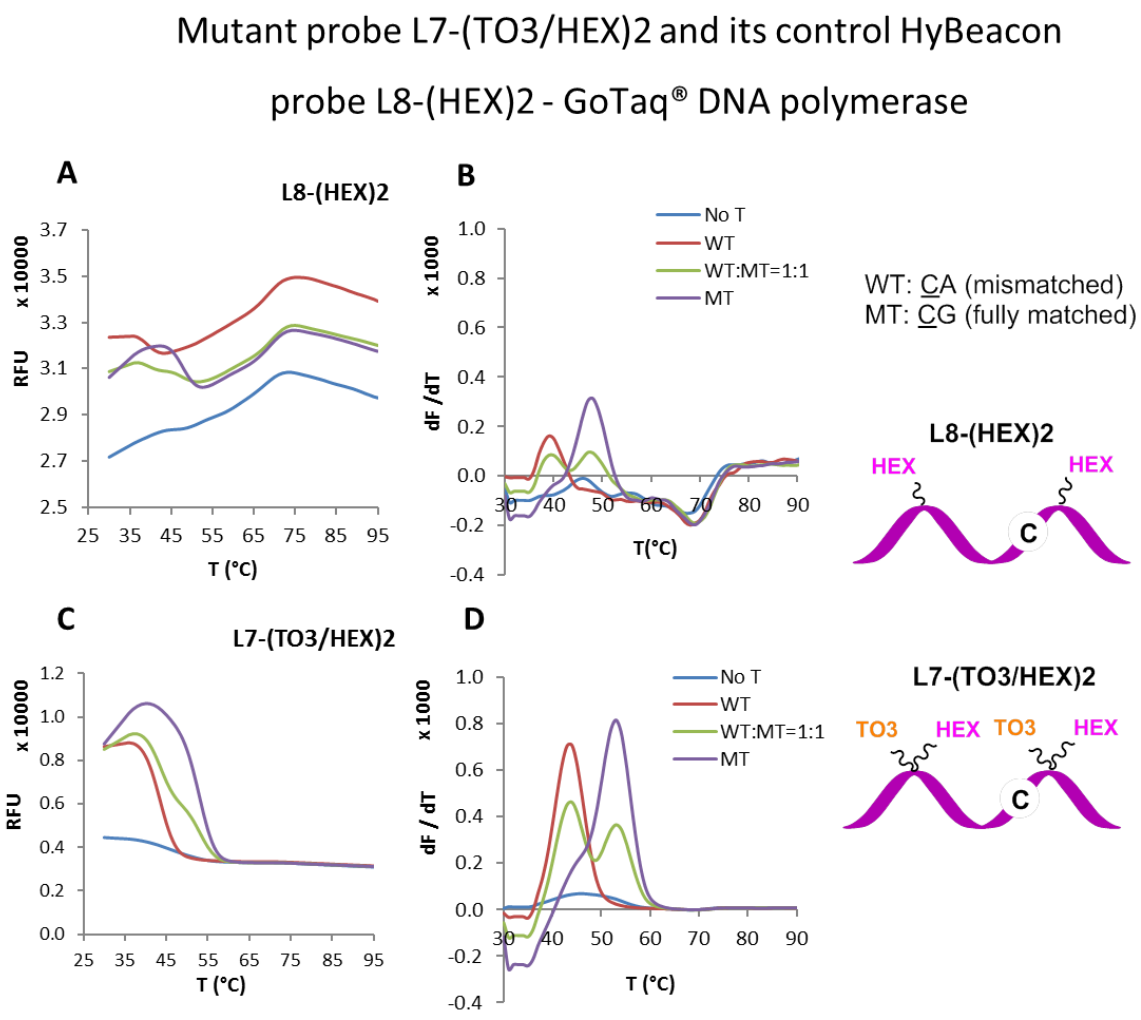

Figure 9.6.4. Fluorescence melting curves (A, C) and derivatives of post-amplification fluorescence melts (B, D) using the mutant probe L7-(TO3/HEX)2 (C, D) and its control HyBeacon probe L8-(HEX)2 (A, B). Blue (No T): no template; red (WT): wild-type template; green (WT:MT = 1:1): wild-type template: mutant template, ratio = 1:1; purple (MT): mutant template. All output was monitored in the HEX channel of the CFX96™ real-time PCR instrument (excitation range 515–535 nm, detector range 560–580 nm). GoTaq® DNA polymerase, 30 cycles and 1 ng of template ODNs were used. Note: L7-(TO3/HEX)2 is a mutant probe that gives a CA-mismatched duplex upon hybridization with wild-type template (WT), and forms a fully matched duplex when pairs with mutant template (MT). The C in the schematic diagram highlights the position of this mutation to be detected relative to the positions of the fluorophores.

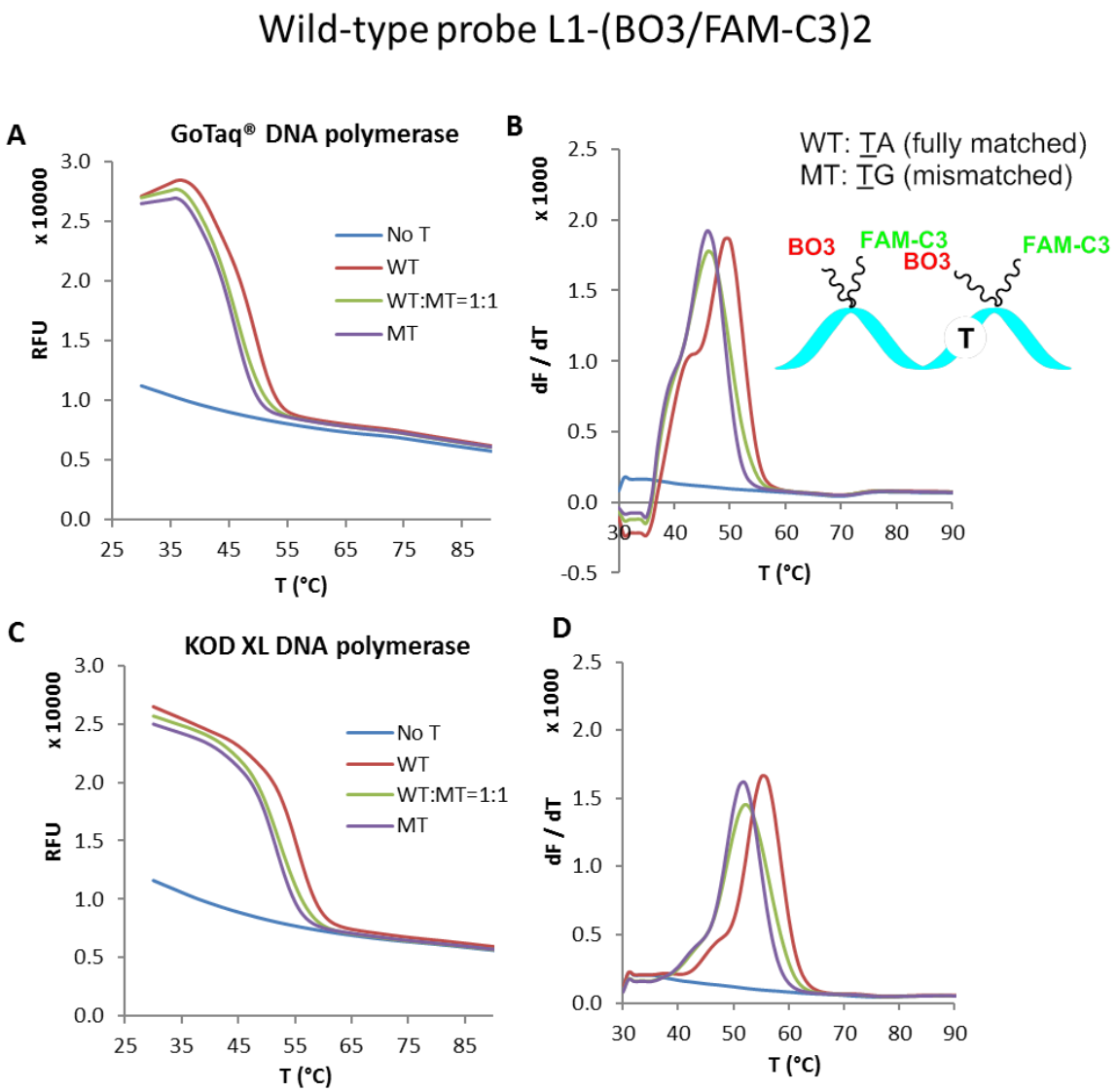

Figure 9.6.5. Fluorescence melting curves (A, C) and derivatives of post-amplification fluorescence melts (B, D) using the wild-type probe L1-(BO3/FAM-C3)2. Blue (No T): no template; red (WT): wild-type template; green (WT:MT = 1:1): wild-type template: mutant template, ratio = 1:1; purple (MT): mutant template. All output was monitored in the FAM channel of the CFX96™ real-time PCR instrument (excitation range 450–490 nm, detector range 510–530 nm). GoTaq® DNA polymerase, 30 cycles (A, B) and 1 ng of template ODNs were used; or KOD XL DNA polymerase, 20 cycles (C, D) and 1 ng of template ODNs were used. Note: L1-(BO3/FAM-C3)2 is a wild-type probe that gives a fully matched duplex upon hybridization with wild-type template (WT), and forms a TG-mismatched duplex when pairs with mutant template (MT). The T in the schematic diagram highlights the position of this mutation to be detected relative to the positions of the fluorophores.

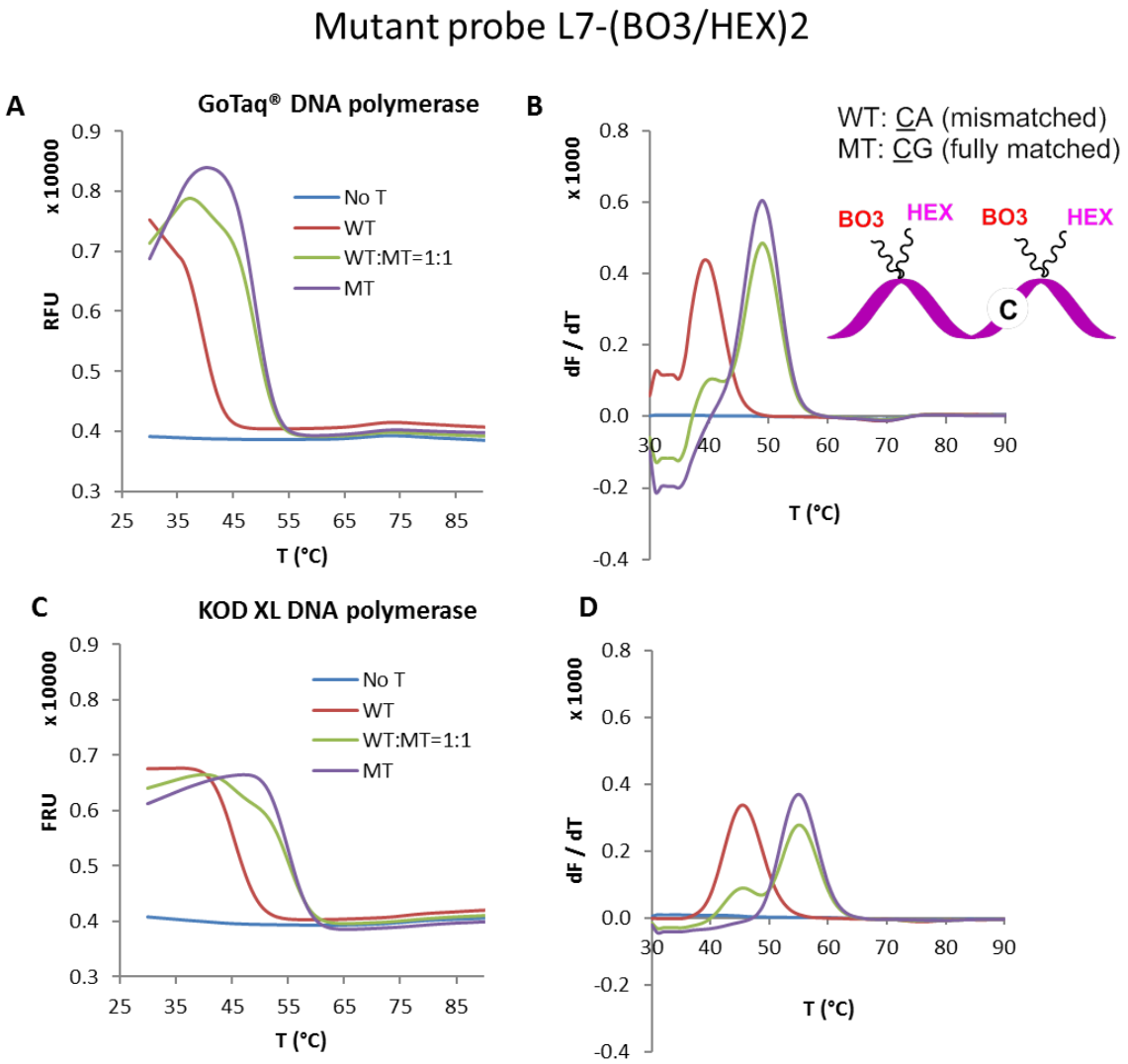

Figure 9.6.6. Fluorescence melting curves (A, C) and derivatives of post-amplification fluorescence melts (B, D) using the mutant probe L7-(BO3/HEX)2. Blue (No T): no template; red (WT): wild-type template; green (WT:MT = 1:1): wild-type template: mutant template, ratio = 1:1; purple (MT): mutant template. All output was monitored in the HEX channel of the CFX96™ real-time PCR instrument (excitation range 515–535 nm, detector range 560–580 nm). GoTaq® DNA polymerase, 30 cycles (A, B) and 1 ng of template ODNs were used; or KOD XL DNA polymerase, 20 cycles (C, D) and 1 ng of template ODNs were used. Note: L7-(BO3/HEX)2 is a mutant probe that gives a CA-mismatched duplex upon hybridization with wild-type template (WT), and forms a fully matched duplex when pairs with mutant template (MT). The C in the schematic diagram highlights the position of this mutation to be detected relative to the positions of the fluorophores.

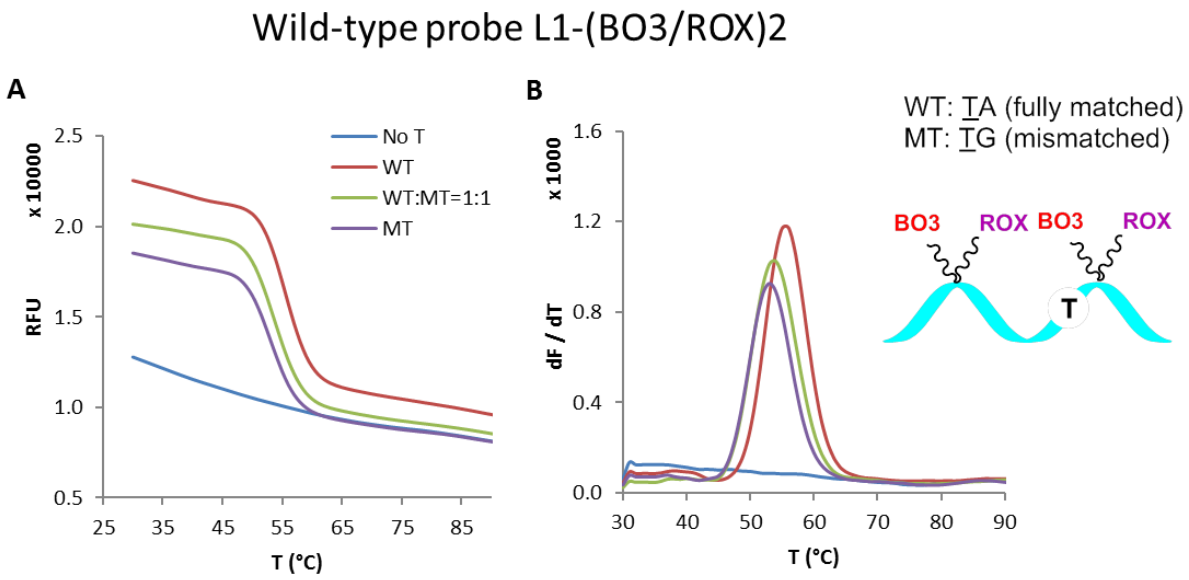

Figure 9.6.7. Fluorescence melting curves (A) and derivatives of post-amplification fluorescence melts (B) using the wild-type probe L1-(BO3/ROX)2. Blue (No T): no template; red (WT): wild-type template; green (WT:MT = 1:1): wild-type template: mutant template, ratio = 1:1; purple (MT): mutant template. All output was monitored in the ROX channel of the CFX96^{TM} real-time PCR instrument (excitation range 560–590 nm, detector range 610–650 nm). KOD XL DNA polymerase, 20 cycles and 1 ng of template ODNs were used. Note: L1-(BO3/ROX)2 is a wild-type probe that gives a fully matched duplex upon hybridization with wild-type template (WT), and forms a TG-mismatched duplex when pairs with mutant template (MT). The T in the schematic diagram highlights the position of this mutation to be detected relative to the positions of the fluorophores.

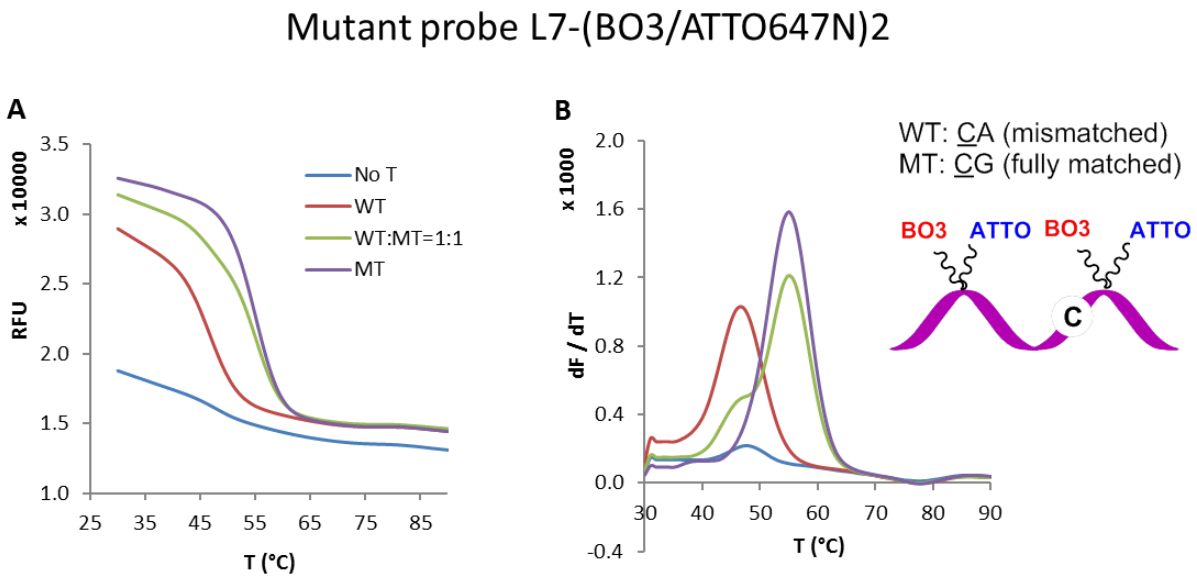

Figure 9.6.8. Fluorescence melting curves (A) and derivatives of post-amplification fluorescence melts (B) using the mutant probe L7-(BO3/ATTO647N)2. Blue (No T): no template; red (WT): wild-type template; green (WT:MT = 1:1): wild-type template: mutant template, ratio = 1:1; purple (MT): mutant template. All output was monitored in the Cy5 channel of the CFX96^{TM} real-time PCR instrument (excitation range 620–650 nm, detector range 675–690 nm). KOD XL DNA polymerase, 20 cycles and 1 ng of template ODNs were used. Note: L7-(BO3/ATTO647N)2 is a mutant probe that gives a CA-mismatched duplex upon hybridization with wild-type template (WT), and forms a fully matched duplex when pairs with mutant template (MT). The C in the schematic diagram highlights the position of this mutation to be detected relative to the positions of the fluorophores.

9.7 Fluorescence melting studies of two-probe system in real-time PCR

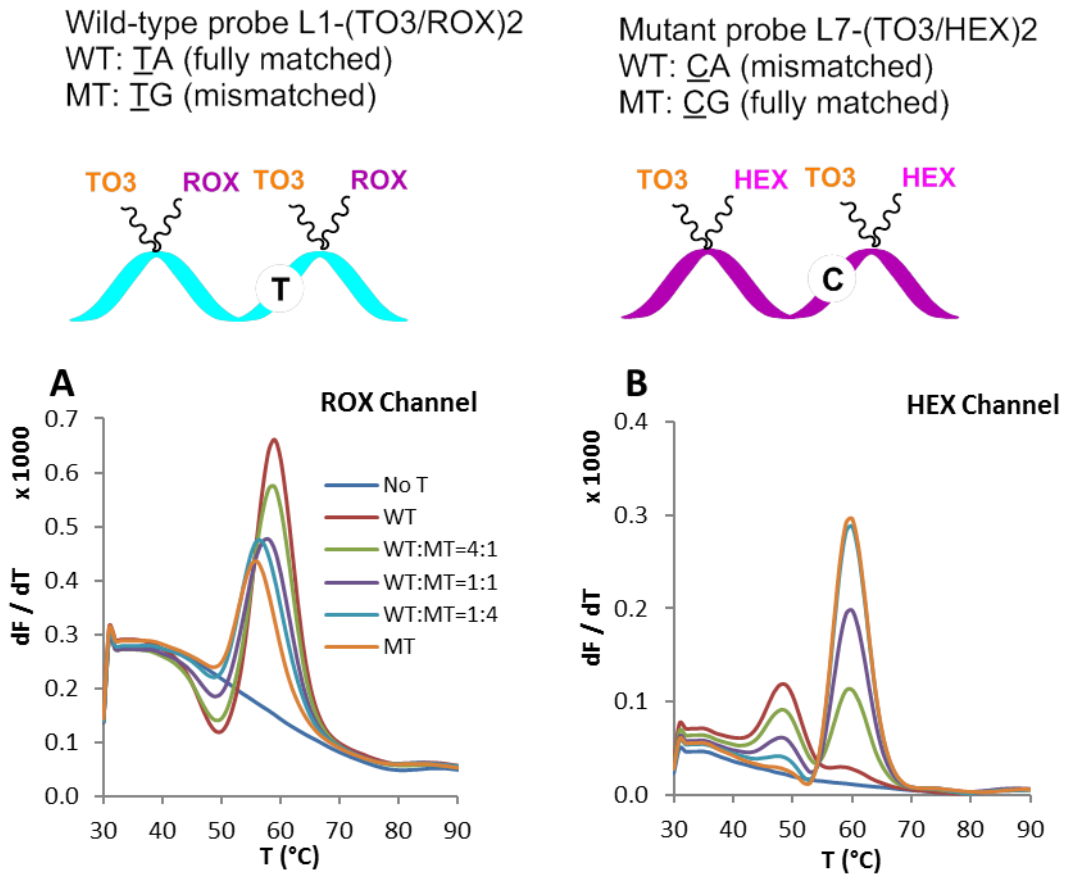

Figure 9.7.1. Fluorescence melting derivatives of mixture of the wild-type probe L1-(TO3/ROX)2 and mutant probe L7-(TO3/HEX)2. Blue (No T): no template; red (WT): wild-type template; green (WT:MT = 4:1): (wild-type: mutant template, ratio = 4:1); purple (WT:MT = 1:1): (wild-type: mutant template, ratio = 1:1); light blue (WT:MT = 1:4): (wild-type: mutant template, ratio = 1:4); orange (MT): mutant template. A was monitored in the ROX channel of the CFX96™ real-time PCR instrument (excitation range 560–590 nm, detector range 610–650 nm); B was monitored in the HEX channel of the CFX96™ real-time PCR instrument (excitation range 515–535 nm, detector range 560–580 nm). KOD XL DNA polymerase, 20 cycles and 1 ng of template ODNs were used. The position of mutation to be detected is underlined. The T or C in the schematic diagram highlights the position of this mutation to be detected relative to the positions of the fluorophores.

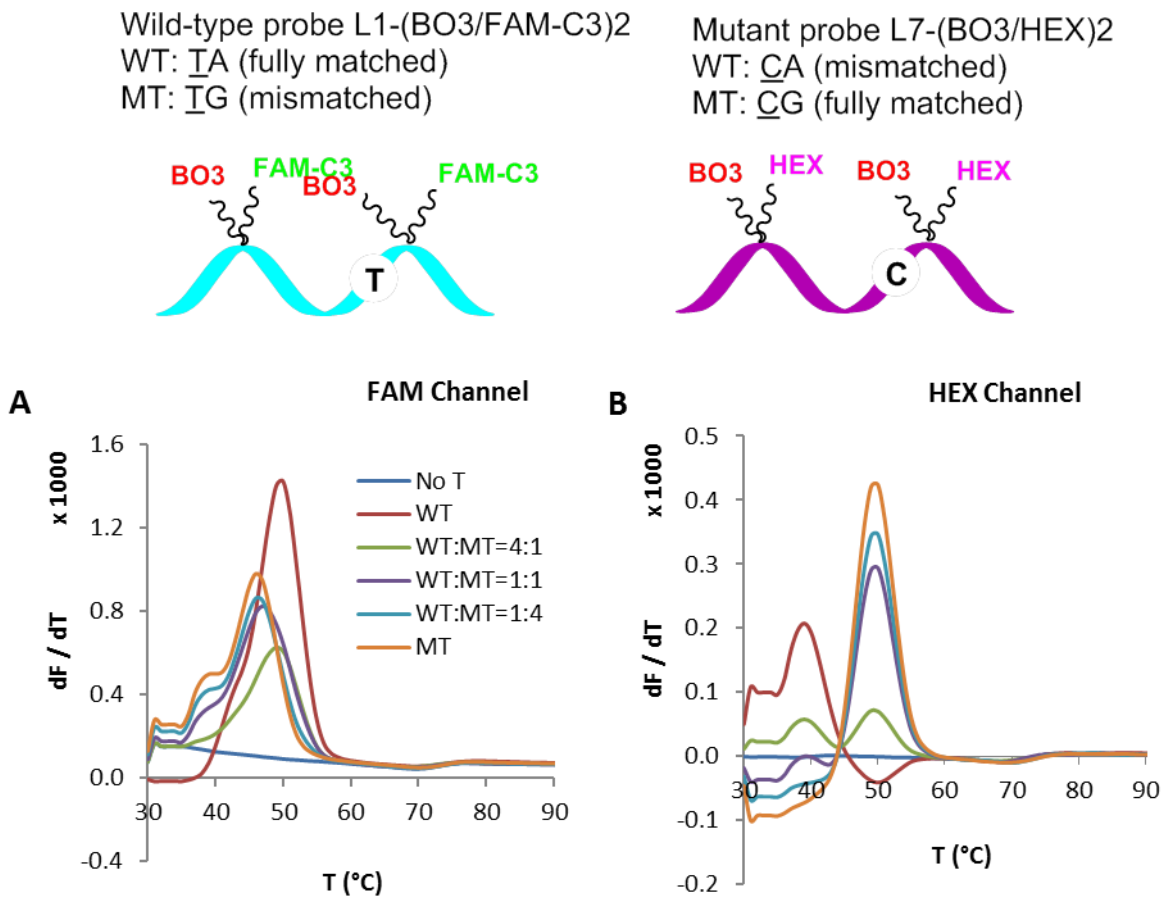

Figure 9.7.2. Fluorescence melting derivatives of mixture of the wild-type probe L1-(BO3/FAM-C3)2 and mutant probe L7-(BO3/HEX)2. Blue (No T): no template; red (WT): wild-type template; green (WT:MT = 4:1): (wild-type: mutant template, ratio = 4:1); purple (WT:MT = 1:1): (wild-type: mutant template, ratio = 1:1); light blue (WT:MT = 1:4): (wild-type: mutant template, ratio = 1:4); orange (MT): mutant template. A was monitored in the FAM channel of the CFX96™ real-time PCR instrument (excitation range 450–490 nm, detector range 510–530 nm); B was monitored in the HEX channel of the CFX96™ real-time PCR instrument (excitation range 515–535 nm, detector range 560–580 nm). Gotaq® DNA polymerase, 30 cycles and 1 ng of template ODNs were used. The position of mutation to be detected is underlined. The T or C in the schematic diagram highlights the position of this mutation to be detected relative to the positions of the fluorophores.

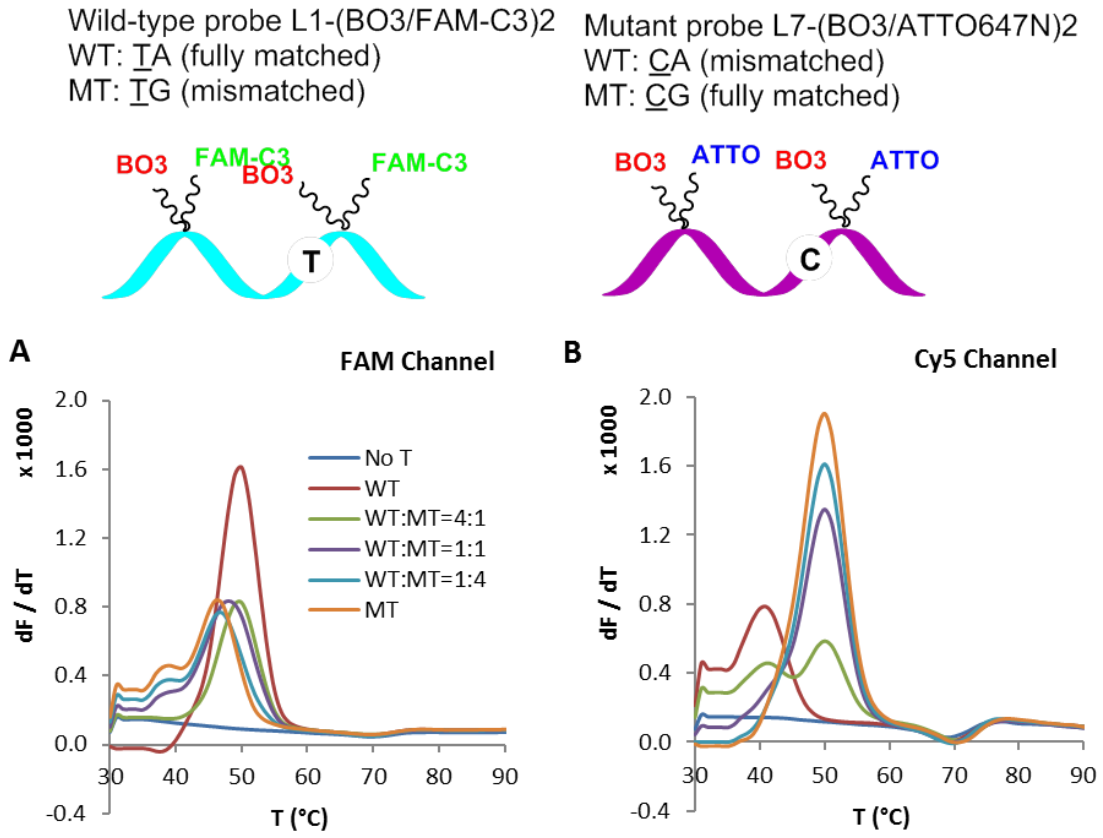

Figure 9.7.3. Fluorescence melting derivatives of mixture of the wild-type probe L1-(BO3/FAM-C3)2 and mutant probe L7-(BO3/ATTO647N)2. Blue (No T): no template; red (WT): wild-type template; green (WT:MT = 4:1): (wild-type: mutant template, ratio = 4:1); purple (WT:MT = 1:1): (wild-type: mutant template, ratio = 1:1); light blue (WT:MT = 1:4): (wild-type: mutant template, ratio = 1:4); orange (MT): mutant template. A was monitored in the FAM channel of the CFX96™ real-time PCR instrument (excitation range 450–490 nm, detector range 510–530 nm); B was monitored in the Cy5 channel of the CFX96™ real-time PCR instrument (excitation range 620–650 nm, detector range 675–690 nm). Gotaq® DNA polymerase, 30 cycles and 1 ng of template ODNs were used. The position of mutation to be detected is underlined. The T or C in the schematic diagram highlights the position of this mutation to be detected relative to the positions of the fluorophores.

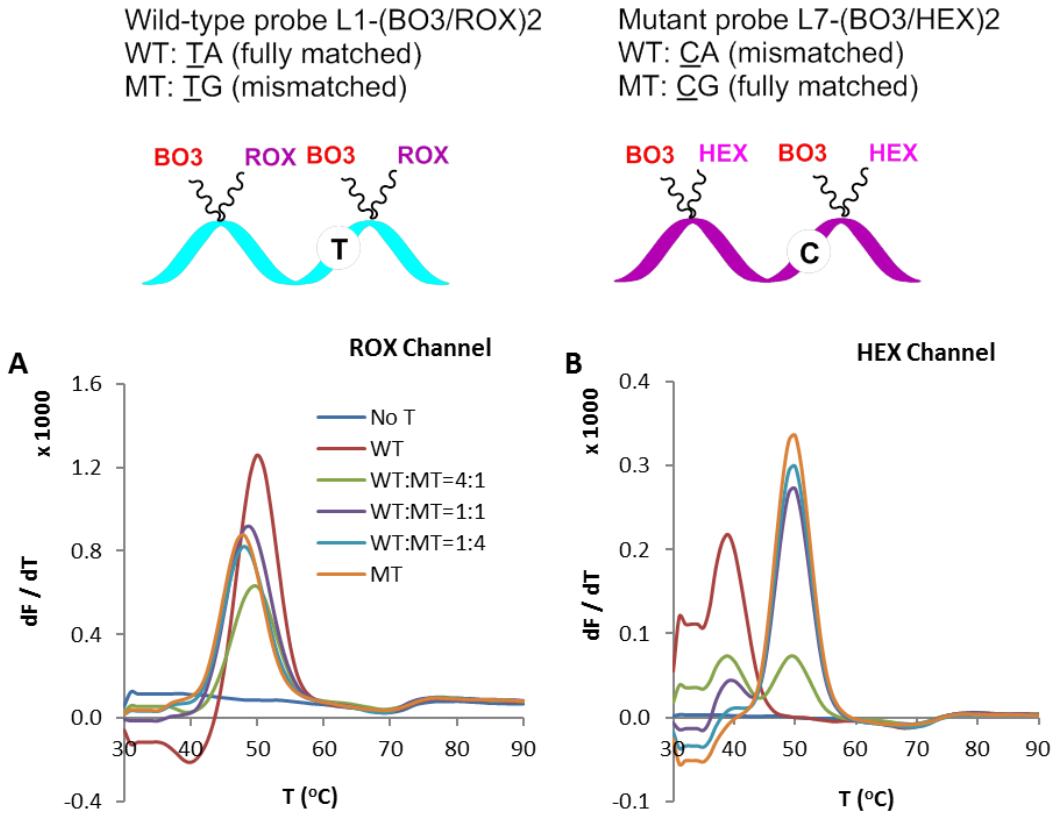

Figure 9.7.4. Fluorescence melting derivatives of mixture of the wild-type probe L1-(BO3/ROX)2 and mutant probe L7-(BO3/HEX)2. Blue (No T): no template; red (WT): wild-type template; green (WT:MT = 4:1): (wild-type: mutant template, ratio = 4:1); purple (WT:MT = 1:1): (wild-type: mutant template, ratio = 1:1); light blue (WT:MT = 1:4): (wild-type: mutant template, ratio = 1:4); orange (MT): mutant template. A was monitored in the ROX channel of the CFX96™ real-time PCR instrument (excitation range 560–590 nm, detector range 610–650 nm); B was monitored in the HEX channel of the CFX96™ real-time PCR instrument (excitation range 515–535 nm, detector range 560–580 nm). Gotaq® DNA polymerase, 30 cycles and 1 ng of template ODNs were used. The position of mutation to be detected is underlined. The T or C in the schematic diagram highlights the position of this mutation to be detected relative to the positions of the fluorophores.

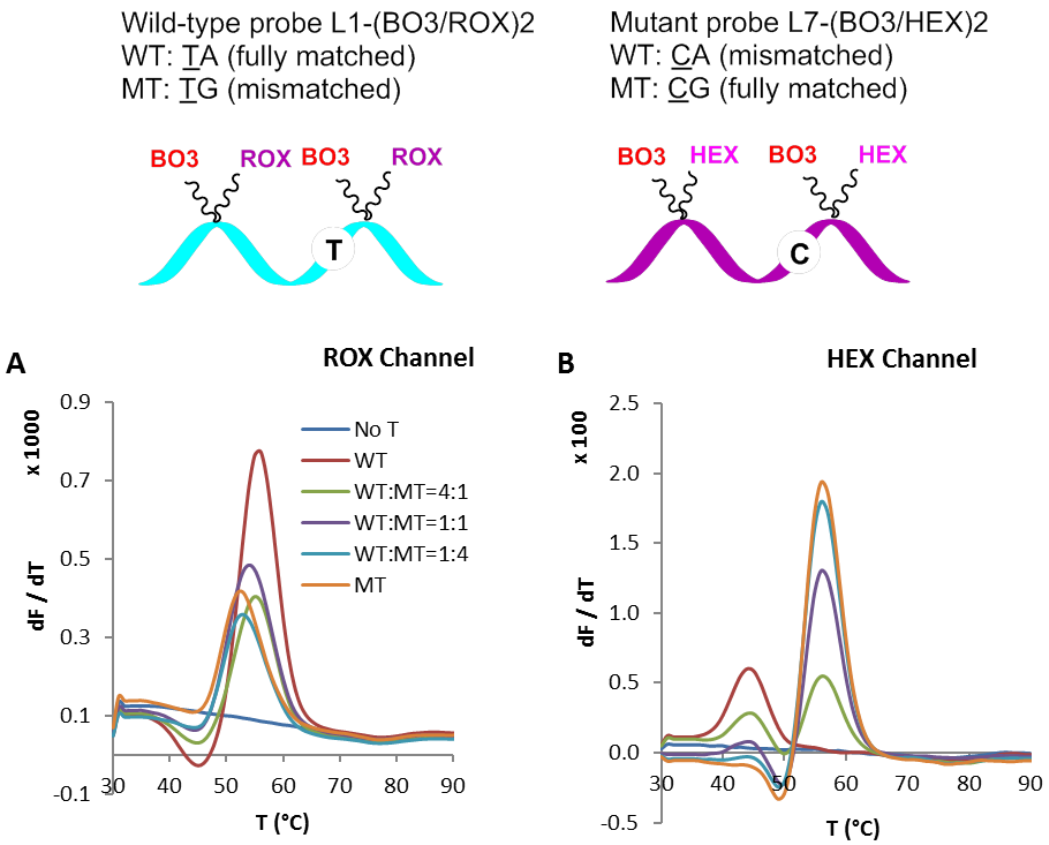

Figure 9.7.5. Fluorescence melting derivatives of mixture of the wild-type probe L1-(BO3/ROX)2 and mutant probe L7-(BO3/HEX)2. Blue (No T): no template; red (WT): wild-type template; green (WT:MT = 4:1): (wild-type: mutant template, ratio = 4:1); purple (WT:MT = 1:1): (wild-type: mutant template, ratio = 1:1); light blue (WT:MT = 1:4): (wild-type: mutant template, ratio = 1:4); orange (MT): mutant template. A was monitored in the ROX channel of the CFX96^{TM} real-time PCR instrument (excitation range 560–590 nm, detector range 610–650 nm); B was monitored in the HEX channel of the CFX96^{TM} real-time PCR instrument (excitation range 515–535 nm, detector range 560–580 nm). KOD XL DNA polymerase, 20 cycles and 1 ng of template ODNs were used. The position of mutation to be detected is underlined. The T or C in the schematic diagram highlights the position of this mutation to be detected relative to the positions of the fluorophores.

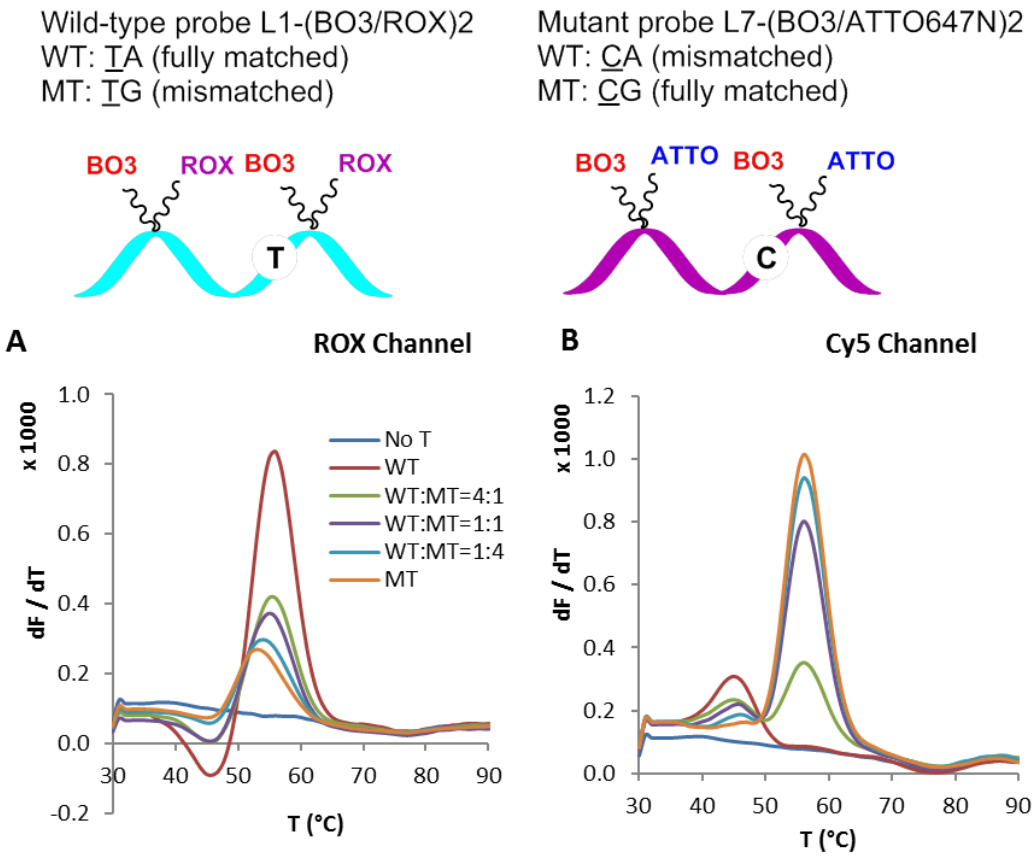

Figure 9.7.6. Fluorescence melting derivatives of mixture of the wild-type probe L1-(BO3/ROX)2 and mutant probe L7-(BO3/ATTO647N)2. Blue (No T): no template; red (WT): wild-type template; green (WT:MT = 4:1): (wild-type: mutant template, ratio = 4:1); purple (WT:MT = 1:1): (wild-type: mutant template, ratio = 1:1); light blue (WT:MT = 1:4): (wild-type: mutant template, ratio = 1:4); orange (MT): mutant template. A was monitored in the ROX channel of the CFX96™ real-time PCR instrument (excitation range 560–590 nm, detector range 610–650 nm); B was monitored in the Cy5 channel of the CFX96™ real-time PCR instrument (excitation range 620–650 nm, detector range 675–690 nm). KOD XL DNA polymerase, 20 cycles and 1 ng of template ODNs were used. The position of mutation to be detected is underlined. The T or C in the schematic diagram highlights the position of this mutation to be detected relative to the positions of the fluorophores.

References

References

(1) Blackburn, G. M.; Gait, M. J.; Loakes, D.; Williams, D. M.: *Nucleic Acids in Chemistry and Biology. Third Edition*. **2006**.

(2) Chargaff, E.; Zamenhof, S.; Green, C. Composition of human desoxypentose nucleic acid. *Nature* **1950**, *165*, 756-757.

(3) Chargaff, E. Structure and function of nucleic acids as cell constituents. *Fed. Proc.* **1951**, *10*, 654-659.

(4) Franklin, R. E.; Gosling, R. G. Evidence for 2-chain helix in crystalline structure of sodium deoxyribonucleate. *Nature* **1953**, *172*, 156-157.

(5) Franklin, R. E.; Gosling, R. G. Molecular configuration in sodium thymonucleate. *Nature* **1953**, *171*, 740-741.

(6) Watson, J. D.; Crick, F. H. Molecular structure of nucleic acids: a structure for deoxyribose nucleic acid. *Nature* **1953**, *171*, 737-738.

(7) Yakovchuk, P.; Protozanova, E.; Frank-Kamenetskii, M. D. Base-stacking and base-pairing contributions into thermal stability of the DNA double helix. *Nucleic Acids Res.* **2006**, *34*, 564-574.

(8) Ageno, M.; Dore, E.; Frontali, C. The alkaline denaturation of DNA. *Biophys. J.* **1969**, *9*, 1281-1311.

(9) Drew, H. R.; Wing, R. M.; Takano, T.; Broka, C.; Tanaka, S.; Itakura, K.; Dickerson, R. E. Structure of a B-DNA dodecamer: conformation and dynamics. *Proc. Natl. Acad. Sci. U. S. A.* **1981**, *78*, 2179-2183.

(10) Pray, L. A. Discovery of DNA structure and function: Watson and Crick. *Nature Education* **2008**, *1*, 100.

(11) Belmont, P.; Constant, J. F.; Demeunynck, M. Nucleic acid conformation diversity: from structure to function and regulation. *Chem. Soc. Rev.* **2001**, *30*, 70-81.

(12) al-Obeidi, F.; Okonya, J. F.; Austin, R. E.; Bond, D. R. Using a noncovalent protection strategy to enhance solid-phase synthesis. *Methods Mol. Biol.* **2002**, *201*, 3-14.

(13) Merrifield, R. B. Automated synthesis of peptides. *Science* **1965**, *150*, 178-185.

(14) Merrifield, R. B. Solid phase peptide synthesis. I. Synthesis of a tetrapeptide. *J. Am. Chem. Soc.* **1963**, *85*, 2149-2154.

(15) Merrifield, R. B. Solid-phase peptide synthesis. III. An improved synthesis of bradykinin. *Biochemistry* **1964**, *3*, 1385-1390.

(16) Merrified, R. B. Solid-phase peptide synthesis. *Adv. Enzymol. Relat. Areas Mol. Biol.* **1969**, *32*, 221-296.

(17) Gait, M. J.; Sheppard, R. C. Rapid synthesis of oligodeoxyribonucleotides: a new solid-phase method. *Nucleic Acids Res.* **1977**, *4*, 1135-1158.

(18) Beaucage, S. L.; Caruthers, M. H. Deoxynucleoside phosphoramidites–a new class of key intermediates for deoxypolynucleotide synthesis. *Tetrahedron Lett.* **1981**, *22*, 1859-1862.

(19) Letsinge.Rl; Mahadeva.V. Oligonucleotide synthesis on a polymer support. *J. Am. Chem. Soc.* **1965**, *87*, 3526-3527.

(20) Matteucci, M. D.; Caruthers, M. H. Synthesis of deoxyoligonucleotides on a polymer support. *J. Am. Chem. Soc.* **1981**, *103*, 3185-3191.

(21) Santini, R.; Griffith, M. C.; Qi, M. A measure of solvent effects on swelling of resins for solid phase organic synthesis. *Tetrahedron Lett.* **1998**, *39*, 8951-8954.

(22) Marsh, A.; Carlisle, S. J.; Smith, S. C. High-loading scavenger resins for combinatorial chemistry. *Tetrahedron Lett.* **2001**, *42*, 493-496.

(23) Pon, R. T.: Solid-phase supports for oligonucleotide synthesis. In *Methods in Molecular Biology; Protocols for oligonucleotides and analogs: Synthesis and properties*. **2001**, *Chapter 3*, Unit 3.1.

(24) Mcbride, L. J.; Caruthers, M. H. An investigation of several deoxynucleoside phosphoramidites useful for synthesizing deoxyoligonucleotides. *Tetrahedron Lett.* **1983**, *24*, 245-248.

(25) Sinha, N. D.; Biernat, J.; Mcmanus, J.; Koster, H. Polymer support oligonucleotide synthesis XVIII: use of beta-cyanoethyl-*N*,*N*-dialkylamino-/*N*-morpholino phosphoramidite of deoxynucleosides for the synthesis of DNA fragments simplifying deprotection and isolation of the final product. *Nucleic Acids Res.* **1984**, *12*, 4539-4557.

(26) Dorper, T.; Winnacker, E. L. Improvements in the phosphoramidite procedure for the synthesis of oligodeoxyribonucleotides. *Nucleic Acids Res.* **1983**, *11*, 2575-2584.

(27) Sojka, B.; Piunno, P. A. E.; Wust, C. C.; Krull, U. J. A novel phosphoramidite method for automated synthesis of oligonucleotides on glass supports for biosensor development. *Appl. Biochem. Biotechnol.* **2000**, *89*, 85-103.

(28) Sonveaux, E. The organic chemistry underlying DNA synthesis. *Bioorg. Chem.* **1986**, *14*, 274-325.

(29) Vongsutilers, V.; Daft, J. R.; Shaughnessy, K. H.; Gannett, P. M. A general synthesis of C8-arylpurine phosphoramidites. *Molecules* **2009**, *14*, 3339-3352.

(30) Finn, P. J.; Gibson, N. J.; Fallon, R.; Hamilton, A.; Brown, T. Synthesis and properties of DNA-PNA chimeric oligomers. *Nucleic Acids Res.* **1996**, *24*, 3357-3363.

(31) Wright, P.; Lloyd, D.; Rapp, W.; Andrus, A. Large scale synthesis of oligonucleotides *via* phosphoramidite nucleosides and a high-loaded polystyrene support. *Tetrahedron Lett.* **1993**, *34*, 3373-3376.

(32) Tornoe, C. W.; Christensen, C.; Meldal, M. Peptidotriazoles on solid phase: 1,2,3-triazoles by regiospecific copper(I)-catalyzed 1,3-dipolar cycloadditions of terminal alkynes to azides. *J. Org. Chem.* **2002**, *67*, 3057-3064.

(33) Kolb, H. C.; Finn, M. G.; Sharpless, K. B. Click chemistry: diverse chemical function from a few good reactions. *Angew. Chem. Int. Ed. Engl.* **2001**, *40*, 2004-2021.

(34) Meldal, M.; Tornoe, C. W. Cu-catalyzed azide-alkyne cycloaddition. *Chem. Rev.* **2008**, *108*, 2952-3015.

(35) Huisgen, R. Kinetics and reaction mechanisms: selected examples from the experience of 40 years. *Pure Appl. Chem.* **1989**, *61*, 613-628.

(36) Rostovtsev, V. V.; Green, L. G.; Fokin, V. V.; Sharpless, K. B. A stepwise huisgen cycloaddition process: copper(I)-catalyzed regioselective "ligation" of azides and terminal alkynes. *Angew. Chem. Int. Ed. Engl.* **2002**, *41*, 2596-2599.

(37) Appukkuttan, P.; Dehaen, W.; Fokin, V. V.; Van der Eycken, E. A microwave-assisted click chemistry synthesis of 1,4-disubstituted 1,2,3-triazoles *via* a copper(I)-catalyzed three-component reaction. *Org. Lett.* **2004**, *6*, 4223-4225.

(38) Himo, F.; Lovell, T.; Hilgraf, R.; Rostovtsev, V. V.; Noodleman, L.; Sharpless, K. B.; Fokin, V. V. Copper(I)-catalyzed synthesis of azoles. DFT study predicts unprecedented reactivity and intermediates. *J. Am. Chem. Soc.* **2005**, *127*, 210-216.

(39) Hänni, K. D.; Leigh, D. A. The application of CuAAC 'click' chemistry to catenane and rotaxane synthesis. *Chem. Soc. Rev.* **2010**, *39*, 1240-1251.

(40) Struthers, H.; Mindt, T. L.; Schibli, R. Metal chelating systems synthesized using the copper(I) catalyzed azide-alkyne cycloaddition. *Dalton Trans.* **2010**, *39*, 675-696.

(41) El-Sagheer, A. H.; Brown, T. Synthesis of alkyne- and azide-modified oligonucleotides and their cyclization by the CuAAC (click) reaction. *Current protocols in nucleic acid chemistry*. **2008**, *Chapter 4*, Unit 4.33.

(42) Bundy, B. C.; Swartz, J. R. Site-specific incorporation of *p*-propargyloxyphenylalanine in a cell-free environment for direct protein-protein click conjugation. *Bioconjugate Chem.* **2010**, *21*, 255-263.

(43) Worrell, B. T.; Malik, J. A.; Fokin, V. V. Direct evidence of a dinuclear copper intermediate in Cu(I)-catalyzed azide-alkyne cycloadditions. *Science* **2013**, *340*, 457-460.

(44) Chiou, S. H. DNA-scission and protein-scission activities of ascorbate in the presence of copper-ion and a copper-peptide complex. *J. Biochem.-Tokyo* **1983**, *94*, 1259-1267.

(45) Kumar, R.; El-Sagheer, A. H.; Tumpane, J.; Lincoln, P.; Wilhelmsson, L. M.; Brown, T. Template-directed oligonucleotide strand ligation, covalent intramolecular DNA circularization and catenation using click chemistry. *J. Am. Chem. Soc.* **2007**, *129*, 6859-6864.

(46) Imlay, J. A.; Linn, S. DNA damage and oxygen radical toxicity. *Science* **1988**, *240*, 1302-1309.

(47) Link, A. J.; Tirrell, D. A. Cell surface labeling of *Escherichia coli via* copper(I)-catalyzed [3+2] cycloaddition. *J. Am. Chem. Soc.* **2003**, *125*, 11164-11165.

(48) Jewett, J. C.; Bertozzi, C. R. Cu-free click cycloaddition reactions in chemical biology. *Chem. Soc. Rev.* **2010**, *39*, 1272-1279.

(49) El-Sagheer, A. H.; Brown, T. Factors influencing hairpin oligonucleotide cyclization by the uncatalyzed alkyne-azide cycloaddition (AAC) reaction. *Pure Appl. Chem.* **2010**, *82*, 1599-1607.

(50) Staudinger, H.; Meyer, J. Über neue organische phosphorverbindungen III. Phosphinmethylenderivate und Phosphinimine. *Helv. Chim. Acta.* **1919**, *2*, 635-646.

(51) Gololobov, Y. G.; Zhmurova, I. N.; Kasukhin, L. F. Sixty years of Staudinger reaction. *Tetrahedron* **1981**, *37*, 437-472.

(52) Gololobov, Y. G.; Kasukhin, L. F. Recent advances in the Staudinger reaction. *Tetrahedron* **1992**, *48*, 1353-1406.

(53) Saxon, E.; Bertozzi, C. R. Cell surface engineering by a modified Staudinger reaction. *Science* **2000**, *287*, 2007-2010.

(54) van Berkel, S. S.; van Eldijk, M. B.; van Hest, J. C. M. Staudinger ligation as a method for bioconjugation. *Angew. Chem. Int. Ed. Engl.* **2011**, *50*, 8806-8827.

(55) Wang, C. C. Y.; Seo, T. S.; Li, Z. M.; Ruparel, H.; Ju, J. Y. Site-specific fluorescent labeling of DNA using Staudinger ligation. *Bioconjugate Chem.* **2003**, *14*, 697-701.

(56) Prescher, J. A.; Dube, D. H.; Bertozzi, C. R. Chemical remodelling of cell surfaces in living animals. *Nature* **2004**, *430*, 873-877.

(57) Hangauer, M. J.; Bertozzi, C. R. A FRET-based fluorogenic phosphine for live-cell imaging with the Staudinger ligation. *Angew. Chem. Int. Ed. Engl.* **2008**, *47*, 2394-2397.

(58) Lin, F. L.; Hoyt, H. M.; van Halbeek, H.; Bergman, R. G.; Bertozzi, C. R. Mechanistic investigation of the Staudinger ligation. *J. Am. Chem. Soc.* **2005**, *127*, 2686-2695.

(59) Shelbourne, M.; Chen, X.; Brown, T.; El-Sagheer, A. H. Fast copper-free click DNA ligation by the ring-strain promoted alkyne-azide cycloaddition reaction. *Chem. Commun.* **2011**, *47*, 6257-6259.

(60) Groger, G.; Behrens, U.; Olbrich, F. Monomeric and dimeric cyclooctyne-stabilized complexes of copper(I). *Organometallics* **2000**, *19*, 3354-3360.

(61) Agard, N. J.; Prescher, J. A.; Bertozzi, C. R. A strain-promoted [3+2] azide-alkyne cycloaddition for covalent modification of blomolecules in living systems. *J. Am. Chem. Soc.* **2004**, *126*, 15046-15047.

(62) Agard, N. J.; Baskin, J. M.; Prescher, J. A.; Lo, A.; Bertozzi, C. R. A comparative study of bioorthogonal reactions with azides. *ACS Chem. Biol.* **2006**, *1*, 644-648.

(63) Sletten, E. M.; Bertozzi, C. R. A hydrophilic azacyclooctyne for Cu-free click chemistry. *Org. Lett.* **2008**, *10*, 3097-3099.

(64) Poloukhtine, A. A.; Mbua, N. E.; Wolfert, M. A.; Boons, G. J.; Popik, V. V. Selective labeling of living cells by a photo-triggered click reaction. *J. Am. Chem. Soc.* **2009**, *131*, 15769-15776.

(65) Ning, X. H.; Guo, J.; Wolfert, M. A.; Boons, G. J. Visualizing metabolically labeled glycoconjugates of living cells by copper-free and fast huisgen cycloadditions. *Angew. Chem. Int. Ed. Engl.* **2008**, *47*, 2253-2255.

(66) Dommerholt, J.; Schmidt, S.; Temming, R.; Hendriks, L. J.; Rutjes, F. P.; van Hest, J. C.; Lefeber, D. J.; Friedl, P.; van Delft, F. L. Readily accessible

bicyclononynes for bioorthogonal labeling and three-dimensional imaging of living cells. *Angew. Chem. Int. Ed. Engl.* **2010**, *49*, 9422-9425.

(67) Sletten, E. M.; Nakamura, H.; Jewett, J. C.; Bertozzi, C. R. Difluorobenzocyclooctyne: synthesis, reactivity, and stabilization by β-cyclodextrin. *J. Am. Chem. Soc.* **2010**, *132*, 11799-11805.

(68) Debets, M. F.; van Berkel, S. S.; Schoffelen, S.; Rutjes, F.; van Hest, J. C. M.; van Delft, F. L. Aza-dibenzocyclooctynes for fast and efficient enzyme PEGylation *via* copper-free [3+2] cycloaddition. *Chem. Commun.* **2010**, *46*, 97-99.

(69) Jewett, J. C.; Sletten, E. M.; Bertozzi, C. R. Rapid Cu-free click chemistry with readily synthesized biarylazacyclooctynones. *J. Am. Chem. Soc.* **2010**, *132*, 3688-3690.

(70) Kershner, R. J.; Bozano, L. D.; Micheel, C. M.; Hung, A. M.; Fornof, A. R.; Cha, J. N.; Rettner, C. T.; Bersani, M.; Frommer, J.; Rothemund, P. W. K.; Wallraff, G. M. Placement and orientation of individual DNA shapes on lithographically patterned surfaces. *Nat. Nanotechnol.* **2009**, *4*, 557-561.

(71) Kosuri, S.; Eroshenko, N.; LeProust, E. M.; Super, M.; Way, J.; Li, J. B.; Church, G. M. Scalable gene synthesis by selective amplification of DNA pools from high-fidelity microchips. *Nat. Biotechnol.* **2010**, *28*, 1295-1299.

(72) El-Sagheer, A. H.; Brown, T. Synthesis and polymerase chain reaction amplification of DNA strands containing an unnatural triazole linkage. *J. Am. Chem. Soc.* **2009**, *131*, 3958-3964.

(73) El-Sagheer, A. H.; Sanzone, A. P.; Gao, R.; Tavassoli, A.; Brown, T. Biocompatible artificial DNA linker that is read through by DNA polymerases and is functional in *Escherichia coli*. *Proc. Natl. Acad. Sci. U. S. A.* **2011**, *108*, 11338-11343.

(74) Isobe, H.; Fujino, T.; Yamazaki, N.; Guillot-Nieckowski, M.; Nakamura, E. Triazole-linked analogue of deoxyribonucleic acid (^{TL}DNA): design, synthesis, and double-strand formation with natural DNA. *Org. Lett.* **2008**, *10*, 3729-3732.

(75) Alvira, M.; Eritja, R. Synthesis of oligonucleotides carrying 5′-5′ linkages using copper-catalyzed cycloaddition reactions. *Chem. Biodivers.* **2007**, *4*, 2798-2809.

(76) Hall, L. M.; Gerowska, M.; Brown, T. A highly fluorescent DNA toolkit: synthesis and properties of oligonucleotides containing new Cy3, Cy5 and Cy3B monomers. *Nucleic Acids Res.* **2012**, *40*, e108.

(77) Richardson, J. A.; Gerowska, M.; Shelbourne, M.; French, D.; Brown, T. Six-colour HyBeacon probes for multiplex genetic analysis. *ChemBioChem* **2010**, *11*, 2530-2533.

(78) Kocalka, P.; El-Sagheer, A. H.; Brown, T. Rapid and efficient DNA strand cross-linking by click chemistry. *ChemBioChem* **2008**, *9*, 1280-1285.

(79) Seela, F.; Sirivolu, V. R. Nucleosides and oligonucleotides with diynyl side chains: the Huisgen-Sharpless cycloaddition "click reaction" performed on DNA and their constituents. *Nucleos. Nucleot. Nucl.* **2007**, *26*, 597-601.

(80) Gierlich, J.; Burley, G. A.; Gramlich, P. M. E.; Hammond, D. M.; Carell, T. Click chemistry as a reliable method for the high-density postsynthetic functionalization of alkyne-modified DNA. *Org. Lett.* **2006**, *8*, 3639-3642.

(81) Sivakumar, K.; Xie, F.; Cash, B. M.; Long, S.; Barnhill, H. N.; Wang, Q. A fluorogenic 1,3-dipolar cycloaddition reaction of 3-azidocoumarins and acetylenes. *Org. Lett.* **2004**, *6*, 4603-4606.

(82) Berndl, S.; Herzig, N.; Kele, P.; Lachmann, D.; Li, X. H.; Wolfbeis, O. S.; Wagenknecht, H. A. Comparison of a nucleosidic *vs.* non-nucleosidic postsynthetic "click" modification of DNA with base-labile fluorescent probes. *Bioconjugate Chem.* **2009**, *20*, 558-564.

(83) Lietard, J.; Meyer, A.; Vasseur, J. J.; Morvan, F. An efficient reagent for 5′-azido oligonucleotide synthesis. *Tetrahedron Lett.* **2007**, *48*, 8795-8798.

(84) El-Sagheer, A. H.; Brown, T. Efficient RNA synthesis by *in vitro* transcription of a triazole-modified DNA template. *Chem. Commun.* **2011**, *47*, 12057-12058.

(85) Steger, J.; Graber, D.; Moroder, H.; Geiermann, A. S.; Aigner, M.; Micura, R. Efficient access to nonhydrolyzable initiator tRNA based on the synthesis of 3′-azido-3′-deoxyadenosine RNA. *Angew. Chem. Int. Ed. Engl.* **2010**, *49*, 7470-7472.

(86) Kasha, M. Characterization of electronic transitions in complex molecules. *Discuss. Faraday Soc.* **1950**, *9*, 14-19.

(87) Lakowicz, J. R.: *Principles of Fluorescence Spectroscopy. Third Edition*. **2006**.

(88) Marras, S. A. E.: Selection of fluorophore and quencher pairs for fluorescent nucleic acid hybridization probes. In *Methods in Molecular Biology*. **2006**, *335*, 3-16.

(89) Didenko, V. V. DNA probes using fluorescence resonance energy transfer (FRET): designs and applications. *Biotechniques* **2001**, *31*, 1106-1121.

(90) Dale, R. E.; Eisinger, J.; Blumberg, W. E. The orientational freedom of molecular probes. The orientation factor in intramolecular energy transfer. *Biophys. J.* **1979**, *26*, 161-193.

(91) Lewis, F. D.; Zhang, L. G.; Zuo, X. B. Orientation control of fluorescence resonance energy transfer using DNA as a helical scaffold. *J. Am. Chem. Soc.* **2005**, *127*, 10002-10003.

(92) Iqbal, A.; Arslan, S.; Okumus, B.; Wilson, T. J.; Giraud, G.; Norman, D. G.; Ha, T.; Lilley, D. M. J. Orientation dependence in fluorescent energy transfer between Cy3 and Cy5 terminally attached to double-stranded nuclelic acids. *Proc. Natl. Acad. Sci. U. S. A.* **2008**, *105*, 11176-11181.

(93) Ranasinghe, R. T.; Brown, T. Fluorescence based strategies for genetic analysis. *Chem. Commun.* **2005**, 5487-5502.

(94) Kwok, P. Y. Methods for genotyping single nucleotide polymorphisms. *Annu. Rev. Genomics Hum. Genet.* **2001**, *2*, 235-258.

(95) Tyagi, S.; Kramer, F. R. Molecular beacons: probes that fluoresce upon hybridization. *Nat. Biotechnol.* **1996**, *14*, 303-308.

(96) Tyagi, S.; Bratu, D. P.; Kramer, F. R. Multicolor molecular beacons for allele discrimination. *Nat. Biotechnol.* **1998**, *16*, 49-53.

(97) French, D. J.; Archard, C. L.; Brown, T.; McDowell, D. G. HyBeacon™ probes: a new tool for DNA sequence detection and allele discrimination. *Mol. Cell. Probes* **2001**, *15*, 363-374.

(98) French, D. J.; Archard, C. L.; Andersen, M. T.; McDowell, D. G. Ultra-rapid DNA analysis using HyBeacon™ probes and direct PCR amplification from saliva. *Mol. Cell. Probes* **2002**, *16*, 319-326.

(99) Marras, S. A. E.; Kramer, F. R.; Tyagi, S. Multiplex detection of single-nucleotide variations using molecular beacons. *Genet. Anal. Biomol. Eng.* **1999**, *14*, 151-156.

(100) Tsourkas, A.; Behlke, M. A.; Rose, S. D.; Bao, G. Hybridization kinetics and thermodynamics of molecular beacons. *Nucleic Acids Res.* **2003**, *31*, 1319-1330.

(101) Tsourkas, A.; Behlke, M. A.; Bao, G. Structure-function relationships of shared-stem and conventional molecular beacons. *Nucleic Acids Res.* **2002**, *30*, 4208-4215.

(102) Isacsson, J.; Westman, G. Solid-phase synthesis of asymmetric cyanine dyes. *Tetrahedron Lett.* **2001**, *42*, 3207-3210.

(103) Lartia, R.; Asseline, U. New cyanine-oligonucleotide conjugates: relationships between chemical structures and properties. *Chem. -Eur. J.* **2006**, *12*, 2270-2281.

(104) Okamoto, A. ECHO probes: a concept of fluorescence control for practical nucleic acid sensing. *Chem. Soc. Rev.* **2011**, *40*, 5815-5828.

(105) Rye, H. S.; Yue, S.; Wemmer, D. E.; Quesada, M. A.; Haugland, R. P.; Mathies, R. A.; Glazer, A. N. Stable fluorescent complexes of double-stranded DNA with bis-intercalating asymmetric cyanine dyes: properties and applications. *Nucleic Acids Res.* **1992**, *20*, 2803-2812.

(106) Nygren, J.; Svanvik, N.; Kubista, M. The interactions between the fluorescent dye thiazole orange and DNA. *Biopolymers* **1998**, *46*, 39-51.

(107) Biver, T.; Boggioni, A.; Secco, F.; Turriani, E.; Venturini, M.; Yarmoluk, S. Influence of cyanine dye structure on self-aggregation and interaction with nucleic acids: a kinetic approach to TO and BO binding. *Arch. Biochem. Biophys.* **2007**, *465*, 90-100.

(108) Carreon, J. R.; Mahon, K. P.; Kelley, S. O. Thiazole orange-peptide conjugates: sensitivity of DNA binding to chemical structure. *Org. Lett.* **2004**, *6*, 517-519.

(109) Privat, E.; Asseline, U. Synthesis and binding properties of oligo-2′-deoxyribonucleotides covalently linked to a thiazole orange derivative. *Bioconjugate Chem.* **2001**, *12*, 757-769.

(110) Privat, E.; Melvin, T.; Merola, F.; Schweizer, G.; Prodhomme, S.; Asseline, U.; Vigny, P. Fluorescent properties of oligonucleotide-conjugated thiazole orange probes. *Photochem. Photobiol.* **2002**, *75*, 201-210.

(111) Jensen, L. K.; Gotfredsen, C. H.; Bondensgaard, K.; Jacobsen, J. P. Bis-intercalation of homodimeric thiazole orange dyes in selective binding sites of DNA studied by H-1 NMR spectroscopy. *Acta. Chem. Scand.* **1998**, *52*, 641-650.

(112) Stadler, A. L.; Delos Santos, J. O.; Stensrud, E. S.; Dembska, A.; Silva, G. L.; Liu, S. P.; Shank, N. I.; Kunttas-Tatli, E.; Sobers, C. J.; Gramlich, P. M. E.; Care, T.; Peteanu, L. A.; McCartney, B. M.; Armitage, B. A. Fluorescent DNA nanotags featuring covalently attached intercalating dyes: synthesis, antibody conjugation, and intracellular Imaging. *Bioconjugate Chem.* **2011**, *22*, 1491-1502.

(113) Kovaliov, M.; Segal, M.; Kafri, P.; Yavin, E.; Shav-Tal, Y.; Fischer, B. Detection of cyclin D1 mRNA by hybridization sensitive NIC-oligonucleotide probe. *Bioorg. Med. Chem.* **2014**, *22*, 2613-2621.

(114) Bethge, L.; Singh, I.; Seitz, O. Designed thiazole orange nucleotides for the synthesis of single labelled oligonucleotides that fluoresce upon matched hybridization. *Org. Biomol. Chem.* **2010**, *8*, 2439-2448.

(115) Berndl, S.; Wagenknecht, H. A. Fluorescent color readout of DNA hybridization with thiazole orange as an artificial DNA base. *Angew. Chem. Int. Ed. Engl.* **2009**, *48*, 2418-2421.

(116) Menacher, F.; Rubner, M.; Berndl, S.; Wagenknecht, H. A. Thiazole orange and Cy3: Improvement of fluorescent DNA probes with use of short range electron transfer. *J. Org. Chem.* **2008**, *73*, 4263-4266.

(117) Hovelmann, F.; Bethge, L.; Seitz, O. Single labeled DNA FIT probes for avoiding false-positive signaling in the detection of DNA/RNA in qPCR or cell media. *ChemBioChem* **2012**, *13*, 2072-2081.

(118) Holzhauser, C.; Rubner, M. M.; Wagenknecht, H. A. Energy-transfer-based wavelength-shifting DNA probes with "clickable" cyanine dyes. *Photochem. Photobiol. Sci.* **2013**, *12*, 722-724.

(119) Eriksson, M.; Karlsson, H. J.; Westman, G.; Akerman, B. Groove-binding unsymmetrical cyanine dyes for staining of DNA: dissociation rates in free solution and electrophoresis gels. *Nucleic Acids Res.* **2003**, *31*, 6235-6242.

(120) Privat, E.; Melvin, T.; Asseline, U.; Vigny, P. Oligonucleotide-conjugated thiazole orange probes as "light-up" probes for messenger ribonucleic acid molecules in living cells. *Photochem. Photobiol.* **2001**, *74*, 532-541.

(121) Ikeda, S.; Okamoto, A. Hybridization-sensitive on-off DNA probe: application of the exciton coupling effect to effective fluorescence quenching. *Chem. -Asian J.* **2008**, *3*, 958-968.

(122) Ikeda, S.; Yuki, M.; Yanagisawa, H.; Okamoto, A. Doubly thiazole orange-labeled cytidine for functional expansion of a hybridization-sensitive probe. *Tetrahedron Lett.* **2009**, *50*, 7191-7195.

(123) Kubota, T.; Ikeda, S.; Yanagisawa, H.; Yuki, M.; Okamoto, A. Hybridization-sensitive fluorescent probe for long-term monitoring of intracellular RNA. *Bioconjugate Chem.* **2009**, *20*, 1256-1261.

(124) Okamoto, A.; Kubota, T.; Ikeda, S. Design of a fluorescent probe for DNA/RNA imaging. *Nucleic Acids Symp. Ser.* **2008**, 231-232.

(125) Ikeda, S.; Kubota, T.; Kino, K.; Okamoto, A. Sequence dependence of fluorescence emission and quenching of doubly thiazole orange labeled DNA: effective design of a hybridization-sensitive probe. *Bioconjugate Chem.* **2008**, *19*, 1719-1725.

(126) Kubota, T.; Ikeda, S.; Okamoto, A. Doubly thiazole orange-labeled DNA for live cell RNA imaging. *Bull. Chem. Soc. Jpn.* **2009**, *82*, 110-117.

(127) Ikeda, S.; Kubota, T.; Yuki, M.; Okamoto, A. Exciton-controlled hybridization-sensitive fluorescent probes: multicolor detection of nucleic ccids. *Angew. Chem. Int. Ed. Engl.* **2009**, *48*, 6480-6484.

(128) Okamoto, A.; Sugizaki, K.; Yuki, M.; Yanagisawa, H.; Ikeda, S.; Sueoka, T.; Hayashi, G.; Wang, D. O. A nucleic acid probe labeled with desmethyl thiazole orange: a new type of hybridization-sensitive fluorescent oligonucleotide for live-cell RNA imaging. *Org. Biomol. Chem.* **2013**, *11*, 362-371.

(129) Hirons, G. T.; Fawcett, J. J.; Crissman, H. A. TOTO and YOYO: new very bright fluorochromes for DNA content analyses by flow cytometry. *Cytometry* **1994**, *15*, 129-140.

(130) Spielmann, H. P.; Wemmer, D. E.; Jacobsen, J. P. Solution structure of a DNA complex with the fluorescent bis-intercalator TOTO determined by NMR spectroscopy. *Biochemistry* **1995**, *34*, 8542-8553.

(131) Fei, X. N.; Gu, Y. C.; Ban, Y.; Liu, Z. J.; Zhang, B. L. Thiazole orange derivatives: synthesis, fluorescence properties, and labeling cancer cells. *Bioorg. Med. Chem.* **2009**, *17*, 585-591.

(132) Sato, Y.; Kudo, M.; Toriyabe, Y.; Kuchitsu, S.; Wang, C. X.; Nishizawa, S.; Teramae, N. Abasic site-binding ligands conjugated with cyanine dyes for "off-on" fluorescence sensing of orphan nucleobases in DNA duplexes and DNA-RNA hybrids. *Chem. Commun.* **2014**, *50*, 515-517.

(133) Jayagopal, A.; Halfpenny, K. C.; Perez, J. W.; Wright, D. W. Hairpin DNA-functionalized gold colloids for the imaging of mRNA in live cells. *J. Am. Chem. Soc.* **2010**, *132*, 9789-9796.

(134) Marti, A. A.; Li, X. X.; Jockusch, S.; Li, Z. M.; Raveendra, B.; Kalachikov, S.; Russo, J. J.; Morozova, I.; Puthanveettil, S. V.; Ju, J. Y.; Turro, N. J. Pyrene binary probes for unambiguous detection of mRNA using time-resolved fluorescence spectroscopy. *Nucleic Acids Res.* **2006**, *34*, 3161-3168.

(135) LeProust, E. M.; Peck, B. J.; Spirin, K.; McCuen, H. B.; Moore, B.; Namsaraev, E.; Caruthers, M. H. Synthesis of high-quality libraries of long (150mer) oligonucleotides by a novel depurination controlled process. *Nucleic Acids Res.* **2010**, *38*, 2522-2540.

(136) Shelbourne, M.; Brown, T.; El-Sagheer, A. H.; Brown, T. Fast and efficient DNA crosslinking and multiple orthogonal labelling by copper-free click chemistry. *Chem. Commun.* **2012**, *48*, 11184-11186.

(137) Boutorine, A. S.; Novopashina, D. S.; Krasheninina, O. A.; Nozeret, K.; Venyaminova, A. G. Fluorescent probes for nucleic acid visualization in fixed and live cells. *Molecules* **2013**, *18*, 15357-15397.

(138) Kodumal, S. J.; Patel, K. G.; Reid, R.; Menzella, H. G.; Welch, M.; Santi, D. V. Total synthesis of long DNA sequences: synthesis of a contiguous 32-kb polyketide synthase gene cluster. *Proc. Natl. Acad. Sci. U. S. A.* **2004**, *101*, 15573-15578.

(139) Villalobos, A.; Ness, J. E.; Gustafsson, C.; Minshull, J.; Govindarajan, S. Gene designer: a synthetic biology tool for constructing artificial DNA segments. *BMC Bioinformatics* **2006**, *7*, 285.

(140) Lundberg, E. P.; El-Sagheer, A. H.; Kocalka, P.; Wilhelmsson, L. M.; Brown, T.; Norden, B. A new fixation strategy for addressable nano-network building blocks. *Chem. Commun.* **2010**, *46*, 3714-3716.

(141) Norden, B.; Tumpane, J.; Sandin, P.; Kumar, R.; Powers, V. E. C.; Lundberg, E. P.; Gale, N.; Baglioni, P.; Lehn, J.-M.; Albinsson, B.; Lincoln, P.; Wilhelmsson, L. M.; Brown, T. Addressable high-information-density DNA nanostructures. *Chem. Phys. Lett.* **2007**, *440*, 125-129.

(142) Caruthers, M. H. Gene synthesis machines: DNA chemistry and its uses. *Science* **1985**, *230*, 281-285.

(143) Caruthers, M. H. Chemical synthesis of DNA and DNA analogs. *Accounts Chem. Res.* **1991**, *24*, 278-284.

(144) Gibson, D. G.; Smith, H. O.; Hutchison, C. A.; Venter, J. C.; Merryman, C. Chemical synthesis of the mouse mitochondrial genome. *Nature Methods* **2010**, *7*, 901-905.

(145) Gibson, D. G.; Glass, J. I.; Lartigue, C.; Noskov, V. N.; Chuang, R. Y.; Algire, M. A.; Benders, G. A.; Montague, M. G.; Ma, L.; Moodie, M. M.; Merryman, C.; Vashee, S.; Krishnakumar, R.; Assad-Garcia, N.; Andrews-Pfannkoch, C.; Denisova, E. A.; Young, L.; Qi, Z. Q.; Segall-Shapiro, T. H.; Calvey, C. H.; Parmar, P. P.; Hutchison, C. A.;

Smith, H. O.; Venter, J. C. Creation of a bacterial cell controlled by a chemically synthesized genome. *Science* **2010**, *329*, 52-56.

(146) Tardy-Planechaud, S.; Fujimoto, J.; Lin, S. S.; Sowers, L. C. Solid phase synthesis and restriction endonuclease cleavage of oligodeoxynucleotides containing 5-(hydroxymethyl)-cytosine. *Nucleic Acids Res.* **1997**, *25*, 553-558.

(147) Cost, G. J. Enzymatic ligation assisted by nucleases: simultaneous ligation and digestion promote the ordered assembly of DNA. *Nat. Protoc.* **2007**, *2*, 2198-2202.

(148) El-Sagheer, A. H.; Brown, T. Click chemistry with DNA. *Chem. Soc. Rev.* **2010**, *39*, 1388-1405.

(149) El-Sagheer, A. H.; Brown, T. Click nucleic acid ligation: applications in biology and nanotechnology. *Accounts Chem. Res.* **2012**, *45*, 1258-1267.

(150) Sekar, M. M. A.; Bloch, W.; St John, P. M. Comparative study of sequence-dependent hybridization kinetics in solution and on microspheres. *Nucleic Acids Res.* **2005**, *33*, 366-375.

(151) Merrified, R. B.; Stewart, J. M. Automated peptides synthesis. *Nature* **1965**, *207*, 522-523.

(152) Merrified, R. B.; Stewart, J. M.; Jernberg, N. Instrument for automated synthesis of peptides. *Anal. Chem.* **1966**, *38*, 1905-1914.

(153) Beaucage, S. L.; Iyer, R. P. Advances in the synthesis of oligonucleotides by the phosphoramidite approach. *Tetrahedron* **1992**, *48*, 2223-2311.

(154) El-Sagheer, A. H.; Brown, T. New strategy for the synthesis of chemically modified RNA constructs exemplified by hairpin and hammerhead ribozymes. *Proc. Natl. Acad. Sci. U. S. A.* **2010**, *107*, 15329-15334.

(155) Jlalia, I.; Meganem, F.; Herscovici, J.; Girard, C. "Flash" solvent-free synthesis of triazoles using a supported catalyst. *Molecules* **2009**, *14*, 528-539.

(156) Gramlich, P. M.; Warncke, S.; Gierlich, J.; Carell, T. Click-click-click: single to triple modification of DNA. *Angew. Chem. Int. Ed. Engl.* **2008**, *47*, 3442-3444.

(157) Qiu, J. Q.; El-Sagheer, A. H.; Brown, T. Solid phase click ligation for the synthesis of very long oligonucleotides. *Chem. Commun.* **2013**, *49*, 6959-6961.

(158) Gaetke, L. M.; Chow, C. K. Copper toxicity, oxidative stress, and antioxidant nutrients. *Toxicology* **2003**, *189*, 147-163.

(159) Wittig, G.; Krebs, A. Zur Existenz Niedergliedriger Cycloalkine, I. *Chem. Ber. Recl.* **1961**, *94*, 3260-3275.

(160) Wittig, G.; Pohlke, R. Zur Existenz Niedergliedriger Cycloalkine, II. *Chem. Ber. Recl.* **1961**, *94*, 3276-3286.

(161) Gutsmiedl, K.; Fazio, D.; Carell, T. High-density DNA functionalization by a combination of Cu-catalyzed and Cu-free click chemistry. *Chem. -Eur. J.* **2010**, *16*, 6877-6883.

(162) Gutsmiedl, K.; Wirges, C. T.; Ehmke, V.; Carell, T. Copper-free "click" modification of DNA *via* nitrile oxide-norbornene 1,3-dipolar cycloaddition. *Org. Lett.* **2009**, *11*, 2405-2408.

(163) Singh, I.; Heaney, F. Solid phase strain promoted "click" modification of DNA *via* [3+2]-nitrile oxide-cyclooctyne cycloadditions. *Chem. Commun.* **2011**, *47*, 2706-2708.

(164) Singh, I.; Vyle, J. S.; Heaney, F. Fast, copper-free click chemistry: a convenient solid-phase approach to oligonucleotide conjugation. *Chem. Commun.* **2009**, 3276-3278.

(165) Singh, I.; Freeman, C.; Heaney, F. Efficient synthesis of DNA conjugates by strain-promoted azide-cyclooctyne cycloaddition in the solid phase. *Eur. J. Org. Chem.* **2011**, 6739-6746.

(166) Singh, I.; Freeman, C.; Madder, A.; Vyle, J. S.; Heaney, F. Fast RNA conjugations on solid phase by strain-promoted cycloadditions. *Org. Biomol. Chem.* **2012**, *10*, 6633-6639.

(167) Krebs, A.; Wilke, J. Angle strained cycloalkynes. *Top. Curr. Chem.* **1983**, *109*, 189-233.

(168) El-Sagheer, A. H. Very stable end-sealed double stranded DNA by click chemistry. *Nucleos. Nucleot. Nucl.* **2009**, *28*, 315-323.

(169) Gibson, B.; Verkade, J. M. M.; Barta, N. S.; Hodges, J. C.; van Delft, F. L. Bicyclo[6.1.0]nonyne phoshoramidites for metal-free conjugation of oligonucleotides. *Chim. Oggi-Chem. Today* **2013**, *31*, 18-21.

(170) Vandesande, J. H.; Ramsing, N. B.; Germann, M. W.; Elhorst, W.; Kalisch, B. W.; Vonkitzing, E.; Pon, R. T.; Clegg, R. C.; Jovin, T. M. Parallel stranded DNA. *Science* **1988**, *241*, 551-557.

(171) Horne, D. A.; Dervan, P. B. Recognition of mixed-sequence duplex DNA by alternate-strand triple-helix formation. *J. Am. Chem. Soc.* **1990**, *112*, 2435-2437.

(172) Zhou, T. Y.; Chen, G. S.; Wang, Y. F.; Zhang, Q.; Yang, M.; Li, T. H. Synthesis of unimolecularly circular G-quadruplexes as prospective molecular probes. *Nucleic Acids Res.* **2004**, *32*, e173.

(173) Kandimalla, E. R.; Agrawal, S. 'Cyclicons' as hybridization-based fluorescent primer-probes: synthesis, properties and application in real-time PCR. *Bioorg. Med. Chem.* **2000**, *8*, 1911-1916.

(174) van Delft, P.; Meeuwenoord, N. J.; Hoogendoorn, S.; Dinkelaar, J.; Overkleeft, H. S.; van der Marel, G. A.; Filippov, D. V. Synthesis of oligoribonucleic acid conjugates using a cyclooctyne phosphoramidite. *Org. Lett.* **2010**, *12*, 5486-5489.

(175) Jayaprakash, K. N.; Peng, C. G.; Butler, D.; Varghese, J. P.; Maier, M.; Rajeev, K. G.; Manoharan, M. Non-nucleoside building blocks for copper-assisted and copper-free click chemistry for the efficient synthesis of RNA conjugates. *Org. Lett.* **2010**, *12*, 5410-5413.

(176) Ren, X. M.; Gerowska, M.; El-Sagheer, A. H.; Brown, T. Enzymatic incorporation and fluorescent labelling of cyclooctyne-modified deoxyuridine triphosphates in DNA. *Bioorg. Med. Chem.* **2014**, *22*, 4384-4390.

(177) El-Sagheer, A. H.; Cheong, V. V.; Brown, T. Rapid chemical ligation of oligonucleotides by the Diels-Alder reaction. *Org. Biomol. Chem.* **2011**, *9*, 232-235.

(178) Keum, J. W.; Ahn, J. H.; Bermudez, H. Design, assembly, and activity of antisense DNA nanostructures. *Small* **2011**, *7*, 3529-3535.

(179) Rosi, N. L.; Mirkin, C. A. Nanostructures in biodiagnostics. *Chem. Rev.* **2005**, *105*, 1547-1562.

(180) Kienzler, A.; Flehr, R.; Kramer, R. A.; Gehne, S.; Kumke, M. U.; Bannwarth, W. Novel three-color FRET tool box for advanced protein and DNA analysis. *Bioconjugate Chem.* **2011**, *22*, 1852-1863.

(181) Norman, D. G.; Grainger, R. J.; Uhrin, D.; Lilley, D. M. J. Location of cyanine-3 on double-stranded DNA: importance for fluorescence resonance energy transfer studies. *Biochemistry* **2000**, *39*, 6317-6324.

(182) Thomas, J. A.; Buchsbaum, R. N.; Zimniak, A.; Racker, E. Intracellular pH measurements in Ehrlich ascites tumor-cells utilizing spectroscopic probes generated *in situ*. *Biochemistry* **1979**, *18*, 2210-2218.

(183) Nakayama-Ratchford, N.; Bangsaruntip, S.; Sun, X.; Welsher, K.; Dai, H. Noncovalent functionalization of carbon nanotubes by fluorescein-polyethylene glycol:

supramolecular conjugates with pH-dependent absorbance and fluorescence. *J. Am. Chem. Soc.* **2007**, *129*, 2448-2449.

(184) Ouellet, J.; Schorr, S.; Iqbal, A.; Wilson, T. J.; Lilley, D. M. J. Orientation of cyanine fluorophores terminally attached to DNA *via* long, flexible tethers. *Biophys. J.* **2011**, *101*, 1148-1154.

(185) Weigert, R.; Porat-Shliom, N.; Amornphimoltham, P. Imaging cell biology in live animals: ready for prime time. *J. Cell Biol.* **2013**, *201*, 969-979.

(186) Kohler, O.; Seitz, O. Thiazole orange as fluorescent universal base in peptide nucleic acids. *Chem. Commun.* **2003**, 2938-2939.

(187) Doluca, O.; Hale, T. K.; Edwards, P. J. B.; Gonzalez, C.; Filichev, V. V. Assembly dependent fluorescence enhancing nucleic acids in sequence-Sspecific detection of double-stranded DNA. *ChemPlusChem* **2014**, *79*, 58-66.

(188) Wang, Q.; Chan, T. R.; Hilgraf, R.; Fokin, V. V.; Sharpless, K. B.; Finn, M. G. Bioconjugation by copper(I)-catalyzed azide-alkyne 3+2 cycloaddition. *J. Am. Chem. Soc.* **2003**, *125*, 3192-3193.

(189) Staerk, D.; Hamed, A. A.; Pedersen, E. B.; Jacobsen, J. P. Bisintercalation of homodimeric thiazole orange dyes in DNA: effect of modifying the linker. *Bioconjugate Chem.* **1997**, *8*, 869-877.

(190) Chinchilla, R.; Najera, C. The Sonogashira reaction: a booming methodology in synthetic organic chemistry. *Chem. Rev.* **2007**, *107*, 874-922.

(191) Boger, D. L.; Tse, W. C. Thiazole orange as the fluorescent intercalator in a high resolution FID assay for determining DNA binding affinity and sequence selectivity of small molecules. *Bioorg. Med. Chem.* **2001**, *9*, 2511-2518.

(192) Chan, T. R.; Hilgraf, R.; Sharpless, K. B.; Fokin, V. V. Polytriazoles as copper(I)-stabilizing ligands in catalysis. *Org. Lett.* **2004**, *6*, 2853-2855.

(193) Moreira, B. G.; You, Y.; Behlke, M. A.; Owczarzy, R. Effects of fluorescent dyes, quenchers, and dangling ends on DNA duplex stability. *Biochem. Biophys. Res. Commun.* **2005**, *327*, 473-484.

(194) Mergny, J. L. Fluorescence energy transfer as a probe for tetraplex formation: the i-motif. *Biochemistry* **1999**, *38*, 1573-1581.

(195) Jiao, G. S.; Burgess, K. Oligonucleotides with strongly fluorescent groups pi-conjugated to a nucleobase: syntheses, melting temperatures, and conformation. *Bioorg. Med. Chem. Lett.* **2003**, *13*, 2785-2788.

(196) Spiriti, J.; Binder, J. K.; Levitus, M.; van der Vaart, A. Cy3-DNA stacking interactions strongly depend on the identity of the terminal basepair. *Biophys. J.* **2011**, *100*, 1049-1057.

(197) Vankeerberghen, A.; Cuppens, H.; Cassiman, J. J. The cystic fibrosis transmembrane conductance regulator: an intriguing protein with pleiotropic functions. *J. Cyst. Fibros.* **2002**, *1*, 13-29.

(198) Darby, R. A. J.; Sollogoub, M.; McKeen, C.; Brown, L.; Risitano, A.; Brown, N.; Barton, C.; Brown, T.; Fox, K. R. High throughput measurement of duplex, triplex and quadruplex melting curves using molecular beacons and a LightCycler. *Nucleic Acids Res.* **2002**, *30*, e39.

(199) Karaman, M. W.; Groshen, S.; Lee, C. C.; Pike, B. L.; Hacia, J. G. Comparisons of substitution, insertion and deletion probes for resequencing and mutational analysis using oligonucleotide microarrays. *Nucleic Acids Res.* **2005**, *33*, e33.

(200) Sagi, J.; Perry, A.; Hang, B.; Singer, B. Differential destabilization of the DNA oligonucleotide double helix by a T·G mismatch, 3,N^4-ethenocytosine, 3,N^4-ethanocytosine, or an 8-(hydroxymethyl)-3,N^4-ethenocytosine adduct incorporated into the same sequence contexts. *Chem. Res. Toxicol.* **2000**, *13*, 839-845.

(201) Sobrino, B.; Brion, M.; Carracedo, A. SNPs in forensic genetics: a review on SNP typing methodologies. *Forensic Sci. Int.* **2005**, *154*, 181-194.

(202) Sprague, R. H.; Brooker, L. G. S. Studies in the cyanine dye series. IX. 4,4′-Pyridocyanines and 4-pyrido-4′-cyanines. *J. Am. Chem. Soc.* **1937**, *59*, 2697-2699.

(203) Gottlieb, H. E.; Kotlyar, V.; Nudelman, A. NMR chemical shifts of common laboratory solvents as trace impurities. *J. Org. Chem.* **1997**, *62*, 7512-7515.

(204) Ishizuka, T.; Kimoto, M.; Sato, A.; Hirao, I. Site-specific functionalization of RNA molecules by an unnatural base pair transcription system *via* click chemistry. *Chem. Commun.* **2012**, *48*, 10835-10837.

(205) Zhou, Y. Z.; Chladek, S.; Romano, L. J. Synthesis of oligonucleotides containing site-specific carcinogen adducts. Perparation of the 2-cyanoethyl *N*,*N*-diisopropylphosphoramidite of *N*-(2′-deoxyguanosin-8-yl)-2-(acetylamino)fluorene with Fmoc as the base-protecting group. *J. Org. Chem.* **1994**, *59*, 556-563.

(206) Lav, T. X.; Lemechko, P.; Renard, E.; Amiel, C.; Langlois, V.; Volet, G. Development of a new azido-oxazoline monomer for the preparation of amphiphilic graft copolymers by combination of cationic ring-opening polymerization and click chemistry. *React. Funct. Polym.* **2013**, *73*, 1001-1008.

(207) Shaffer, C. L.; Morton, M. D.; Hanzlik, R. P. *N*-dealkylation of an *N*-cyclopropylamine by horseradish peroxidase. Fate of the cyclopropyl group. *J. Am. Chem. Soc.* **2001**, *123*, 8502-8508.

(208) Holzhauser, C.; Berndl, S.; Menacher, F.; Breunig, M.; Gopferich, A.; Wagenknecht, H. A. Synthesis and optical properties of cyanine dyes as fluorescent DNA base substitutions for live cell imaging. *Eur. J. Org. Chem.* **2010**, 1239-1248.

(209) Kabatc, J.; Jurek, K. New two- and three-cationic polymethine dyes. Synthesis, properties and application. *Dyes Pigment.* **2015**, *112*, 24-33.

(210) Hansen, A. S.; Thalhammer, A.; El-Sagheer, A. H.; Brown, T.; Schofield, C. J. Improved synthesis of 5-hydroxymethyl-2′-deoxycytidine phosphoramidite using a 2′-deoxyuridine to 2′-deoxycytidine conversion without temporary protecting groups. *Bioorg. Med. Chem. Lett.* **2011**, *21*, 1181-1184.

(211) Sirivolu, V. R.; Chittepu, P.; Seela, F. DNA with branched internal side chains: synthesis of 5-tripropargylamine-dU and conjugation by an azide-alkyne double click reaction. *ChemBioChem* **2008**, *9*, 2305-2316.

(212) Schneider, S. K.; Roembke, P.; Julius, G. R.; Raubenheimer, H. G.; Herrmann, W. A. Pyridin-, quinolin- and acridinylidene palladium carbene complexes as highly efficient C-C coupling catalysts. *Adv. Synth. Catal.* **2006**, *348*, 1862-1873.